N° d'ordre : 2004-43 ECOLE DOCTORALE de l'ENSAM (ED-432)

Ecole Nationale Supérieure d'Arts et Métiers

Centre de Paris

THÈSE

présentée pour obtenir le grade de

DOCTEUR
de
L'ÉCOLE NATIONALE SUPÉRIEURE
D'ARTS ET MÉTIERS

Spécialité : Mécanique et Matériaux

par

Martin LÉVESQUE

MODÉLISATION DU COMPORTEMENT MÉCANIQUE DE MATÉRIAUX COMPOSITES VISCOÉLASTIQUES NON LINÉAIRES PAR UNE APPROCHE D'HOMOGÉNÉISATION

---

soutenue le 15 décembre 2004 devant le jury composé de :

MM.	D.	BAPTISTE	Professeur, ENSAM Paris	Directeur de thèse
	M.	BERVEILLER	Professeur, ENSAM Metz	Examinateur
Mme.	K.	DERRIEN	Maître de conférences, ENSAM Paris	Examinatrice
MM.	M. D.	GILCHRIST	Professeur, University College Dublin	Examinateur
	R. A.	SCHAPERY	Professeur, University of Texas, Austin	Rapporteur
	P.	SUQUET	D.R. CNRS, LMA Marseille	Rapporteur, Président

L'ENSAM est un Grand Etablissement dépendant du Ministère de l'Education Nationale, composé de huit centres :
AIX-EN-PROVENCE ANGERS BORDEAUX CHÂLONS-EN-CHAMPAGNE CLUNY LILLE METZ PARIS

Remerciements
Acknowledgements

Ce travail de thèse est issu d'une collaboration avec le Department of Mechanical Engineering de l'University College Dublin et le laboratoire LM3 de l'ENSAM de Paris. Une partie du financement de cette thèse provient du Fonds Québécois de la Recherche sur la Nature et les Technologies, une autre de Enterprise Ireland (Grant PRP00/MI/11) ainsi que des fonds propres du laboratoire LM3. Je remercie ces organisations pour m'avoir donné les moyens financiers de mener à bien mes travaux.

MM. Richard Schapery et Pierre Suquet ont accepté l'importante tâche de rapporter cette thèse tandis que Marcel Berveiller a rempli la fonction d'examinateur. Je suis conscient de la qualité exceptionnelle de ce jury et suis très reconnaissant envers ces personnes qui m'ont fait l'honneur de se pencher sur mes travaux.

Je remercie les membres du laboratoire LM3 qui ont fait que ces trois années ont passé si rapidement. J'ai eu beaucoup de plaisir à discuter avec les thésards Gregor Hug, Fahmi Bedoui, Iheb Chaieb, Zouhaier Jendli et Karen Triconnet. Je remercie particulièrement Patrick Ribot pour ses nombreux conseils et interventions lors du maniement du microscope électronique à balayage ainsi que Alain Gaudy pour les essais de traction macroscopiques. Je remercie aussi Thierry Bretheau pour ses encouragements à la fin de mon parcours. Je suis aussi reconnaissant envers les étudiants que j'ai eu l'honneur d'encadrer et qui ont apporté une contribution à ce travail : Grégory Marques, Julien Fontaine et Ferdinand Mouze, Adrien Degos et Amélie Fanica ainsi que Charles Babin.

Je tiens à remercier tous les gens qui ont collaboré avec moi sur certains aspects de ce travail : Leon Mishnaevsky Jr. pour la génération des maillages éléments finis, Nicolas Bouleau pour des discussions sur la généralisation, au sens mathématique, de la viscoélasticité linéaire et Pierre Gilormini pour de nombreux échanges sur les méthodes numériques et l'homogénéisation de matériaux non linéaires.

Je remercie Michael D. Gilchrist, co-directeur de cette thèse pour le support et la confiance qu'il m'apporte depuis déjà quelques années. Michael m'a aussi fait le grand plaisir de passer 6 mois au laboratoire LM3 où nous avons pu travailler ensemble de très près sur certains aspects de la thèse. Je suis aussi reconnaissant envers Didier Baptiste, directeur de cette thèse, de m'avoir donné la chance de poursuivre ce travail qui m'a stimulé durant ces trois années. Didier, par ses paroles et réflexions justes, a su me donner un encadrement qui m'a permis d'explorer plusieurs aspects (humains et scientifiques) du travail scientifique en plus de me permettre de me développer. Je remercie aussi Katell Derrien, co-directrice de cette thèse, pour son encadrement scientifique rapproché ainsi que nos nombreuses discussions. Katell, par sa rigueur et son exigence, m'a poussé à toujours faire mieux et par conséquent, à me dépasser. Je suis conscient de l'apport très positif de ces trois personnes sur mon développement personnel et professionnel et souhaite entretenir avec eux les relations que nous avons pris quelques années à développer.

Je remercie aussi mes parents et mes soeurs pour leur soutient inconditionnel et leur présence, malgré la distance qui nous séparait durant ces années, dans les moments heureux et moins heureux.

Finalement, et non la moindre, je suis très reconnaissant envers Yuyan Liu, mon épouse, pour son amour et son support au cours de ces trois dernières années. Elle a su m'encourager dans les moments difficiles et être patiente dans les moments d'intense travail et de stress.

⋆

⋆ ⋆

This work has been accomplished in the context of collaboration between the Department of Mechanical Engineering at University College Dublin and the Laboratoire LM3 of ENSAM - Paris. This thesis has been jointly funded by the Fonds Québécois de la Recherche sur la Nature et les Technologies, Enterprise Ireland (Grant PRP00/MI/11), and Laboratoire LM3. I am grateful to these organisations for providing the necessary support to conduct my work.

Professors Richard Schapery and Pierre Suquet accepted the important task of reviewing this thesis while Marcel Berveiller performed the task of Examiner. I am aware of the exceptional quality of this jury and am I very grateful to these people who honoured me by reading my work.

I wish to thank the Laboratoire LM3 members for their warm welcome. I had many pleasant discussions with fellow Ph.D. students, including Gregor

Hug, Fahmi Bedoui, Iheb Chaieb, Zouhaier Jendli and Karen Triconnet. I am particularly indebted to Patrick Ribot for his constant advice and assistance while using the scanning electron microscope and to Alain Gaudy for the macroscopic tensile tests. I wish also to thank Thierry Bretheau for his support at the end of the thesis. I want to acknowledge the contributions of the undergraduate students I had the honour to guide: Grégory Marques, Julien Fontaine, Ferdinand Mouze, Adrien Degos, Amélie Fanica and Charles Babin.

I wish to thank the people who collaborated with me on various aspects of this work: Leon Mishnaevsky Jr. for generating finite element meshes, Nicolas Bouleau for discussing the mathematical generalisations of linear viscoelasticity and Pierre Gilormini for many discussions and advice regarding numerical methods and the homogenisation of nonlinear materials.

I thank Michael Gilchrist, co-director of this thesis, for the support and trust he gave me over the years. It was a great pleasure for me to welcome Michael to LM3 during his sabbatical in 2003-04 when we had the chance to work closely on certain aspects of the thesis. I am also grateful to Didier Baptiste, director of my thesis, for giving me the chance to undertake this work which stimulated me for the past three years. With his relevant advice and suggestions, Didier gave me direction which allowed me to explore many aspects (human and scientific) of scientific work and also to develop myself. I am indebted to Katell Derrien, co-director of this thesis, for her very close scientific direction and our numerous discussions. With her high expectations and scientific rigor, Katell challenged me to give the very best of myself and hence, to exceed my limits. I acknowledge the very positive contribution of these people to my personal and professional development and I sincerely wish to maintain the close relations we have built over these years.

I thank my parents and sisters for their unconditional support and their presence, despite the distance separating us over the years, through both happy and less happy times.

Finally, and not least, I am indebted to my wife, Yuyan Liu, for her love and support throughout these past three years. She gave me courage in the difficult times and was patient in the times of intense stress and work.

Contents

Remerciements
Acknowledgements **i**

Résumé Étendu **ix**

Introduction **1**

1 A Nonlinear Viscoelastic Constitutive Law **5**
1.1 Introduction 5
1.2 Thermodynamics of irreversible processes 9
1.3 Linear viscoelasticity 10
1.3.1 A general representation of linear viscoelasticity 14
1.4 Schapery's constitutive theory 16
1.5 Specialisation of the constitutive theory 18
1.6 Summary 21

2 Identification of the Constitutive Law **23**
2.1 Introduction 23
2.2 Choice of the load history(ies) 27
2.3 Data reduction procedure 29
2.3.1 Definition of the problem 29
2.3.2 Procedure for calculating the material parameters . . . 31
2.4 Identifying the Constitutive Law Parameters 35
2.4.1 Experimental details 35
2.4.2 Determination of the constitutive law validity domain . 35
2.4.3 Determination of the material parameters 37
2.5 Validation of the identified behaviour law 39
2.6 Conclusion 40

3 Homogenisation Model **43**
3.1 Basics of homogenisation 43

3.1.1 Three basic steps 44
3.1.2 Bounds for the mechanical properties of linear elastic heterogeneous material 46
3.1.3 Estimation of the mechanical response 47
3.1.4 Mori-Tanaka homogenisation scheme 49
3.2 Homogenisation of linear viscoelastic materials 51
3.3 General aspects of homogenising nonlinear materials 55
3.4 Homogenisation of nonlinear non hereditary materials 57
3.4.1 Variational approaches 57
3.4.2 Empirical Approaches 58
3.5 Homogenisation of nonlinear hereditary materials 64
3.5.1 Variational approaches 64
3.5.2 Empirical approaches 64
3.5.3 Discussion 67
3.6 A new linearisation methodology 67
3.6.1 The affine model of Pouya and Zaoui [78] 68
3.6.2 A modified affine model 69
3.6.3 Limitations of the general affine linearisation 70
3.6.4 An approximate classical secant linearisation 75
3.6.5 An approximate modified secant linearisation 76
3.6.6 Limitations of the secant models 77
3.6.7 Discussion 78
3.7 Implementing the homogenisation model 82
3.8 Conclusion 84

4 Numerical Implementation 87
4.1 Solution scheme 87
4.1.1 Problem definition 87
4.1.2 Iterative procedure 88
4.1.3 Computation of the initial trial solution 89
4.1.4 Numerical integration 90
4.2 Linearisation scheme 91
4.2.1 Definition of the tangent and secant conditions 91
4.2.2 Definition of the approximate linearised material 92
4.2.3 Identification of the approximate linearised material . . 93
4.2.4 Linearised materials for a radial stress history 98
4.2.5 Linearised materials for a non radial stress history . . . 99
4.3 Numerical LCT inversion for the homogenised properties . . . 100
4.3.1 Problem definition 104
4.3.2 Case of isotropy or cubic symmetry 106

4.3.3 Transverse isotropy . . . 110
4.3.4 General anisotropy . . . 112
4.3.5 Validation for selected cases . . . 113
4.3.6 LCT inversion for the homogenisation tensors . . . 115
4.4 Simulations and comparison of the two models . . . 117
4.4.1 Variation of the glass beads volume fraction . . . 118
4.4.2 Variation of the volume fraction of spherical voids . . . 118
4.4.3 Variation of the loading rate . . . 119
4.4.4 Simulation of loading-unloading . . . 119
4.4.5 Variation of the nonlinearity and comparison of the affine and secant models . . . 119
4.5 Conclusion . . . 121

5 Validation of the Homogenisation Models 123
5.1 Generation of the FE meshes . . . 124
5.1.1 3D FE meshes of the microstructure . . . 124
5.1.2 Boundary conditions . . . 127
5.1.3 Axisymmetric meshes . . . 130
5.2 Constitutive law implementation . . . 130
5.2.1 Definition and computation of $\boldsymbol{\Delta\varepsilon}$ . . . 132
5.2.2 Computation of the Jacobian $\mathbf{N}$ . . . 134
5.2.3 Computation of the quantities required by the UMAT subroutine . . . 135
5.2.4 Execution procedure . . . 136
5.3 Validation against finite element simulations . . . 137
5.3.1 Comparisons for 10% of glass beads/voids . . . 137
5.3.2 Comparison for the 20% and 30% volume fractions of glass beads/spherical voids . . . 142
5.4 Comparisons with experimental data . . . 144
5.5 Conclusion . . . 149

Conclusion 151

A Conventions 155
A.1 Tensor, vectors and scalars . . . 155
A.2 Modified Voigt notation . . . 155
A.3 Short hand notation . . . 156

B Mori-Tanaka scheme in thermoelasticity 157

List of Figures 159

List of Tables 161

Bibliography 163

Résumé Étendu

Introduction

L'objectif principal de ce travail est la prédiction du comportement sous sollicitation mécanique d'un matériau composite viscoélastique non linéaire par une approche d'homogénéisation. Les modèles développés sont appliqués à un matériau modèle : une matrice polypropylène renforcée de billes de verre distribuées aléatoirement.

La première partie de ce mémoire est dédiée à l'écriture d'une loi de comportement viscoélastique non linéaire (chapitre 1) ainsi qu'à son identification expérimentale (chapitre 2). La deuxième partie porte sur l'écriture (chapitre 3) et l'implémentation numérique (chapitre 4) de modèles d'homogénéisation pour des matériaux viscoélastiques non linéaires. Finalement, la dernière partie (chapitre 5) s'attache à valider numériquement et expérimentalement les prédictions des modèles pour des chargements en traction uniaxiale.

Une loi de comportement viscoélastique non linéaire

Parmi les approches disponibles dans la littérature, nous avons retenu une approche thermodynamique phénoménologique pour décrire le comportement de notre matrice polymère. Nous avons retenu la théorie initialement proposée par Schapery [85, 88, 91]. Cette théorie a été développée dans le même cadre thermodynamique que celui introduit par Biot [6] et peut être interprétée comme une extension du domaine de validité d'une loi de comportement viscoélastique linéaire par l'introduction d'une dépendance non linéaire de la réponse à l'histoire du chargement. La non linéarité est introduite par le biais de fonctions scalaires du tenseur des contraintes.

Cette théorie a été largement employée par plusieurs auteurs avec succès, et ce pour différent matériaux (glace, bitume, composites organiques, etc.). Il doit être noté que la majorité des applications de cette théorie ont été réali-

sées dans le cadre unidimensionnel. Certains auteurs [33,36,104] ont proposé et utilisé des expressions tridimensionnelles de la loi de comportement en généralisant l'expression unidimensionnelle. Ce type d'approche peut conduire à des lois de comportement ne respectant pas les principes de la thermodynamique et doit donc être évité.

Face à ces difficultés, nous avons repris les développements originaux de Schapery [88] et avons écrit une loi de comportement adaptée à notre matériau. La loi de comportement ainsi obtenue est de la forme suivante :

$$\begin{aligned}\boldsymbol{\varepsilon}(t) = g_0(h(t))\mathbf{Q} : \boldsymbol{\sigma}(t) + \left(\frac{\partial g_1(h(t))}{\partial h(t)}\mathbf{Q} : \boldsymbol{\sigma}(t) \otimes \boldsymbol{\sigma}(t) + g_1(h(t))\mathbf{I}\right) : \\ \int_0^t \boldsymbol{\Delta}\tilde{\mathbf{S}}(\psi - \psi') : g_2(h(\tau))\boldsymbol{\sigma}(\tau)\mathrm{d}\tau\end{aligned} \tag{1}$$

où

$$\psi - \psi' = \int_\tau^t g_3(h(t'))\mathrm{d}t' \tag{2a}$$

$$\frac{\partial g_i}{\partial h} \geq 0 \quad \text{et} \quad g_j > 0 \quad \text{pour} \quad i = 0,1 \quad \text{et} \quad j = 0,3 \tag{2b}$$

$$h(t) = \frac{1}{2}\boldsymbol{\sigma}(t) : \mathbf{Q} : \boldsymbol{\sigma}(t) \tag{2c}$$

$$\boldsymbol{\Delta}\tilde{\mathbf{S}}(t) = \mathbf{Q}\sum_m \alpha_m\lambda_m \exp[-\lambda_m t] \tag{2d}$$

$$\begin{gathered}\mathrm{Q}_{11} = \mathrm{Q}_{22} = \mathrm{Q}_{33} = \alpha \quad \text{et} \quad \mathrm{Q}_{12} = \mathrm{Q}_{23} = \mathrm{Q}_{13} = -\alpha\nu \\ \text{et} \quad \mathrm{Q}_{44} = \mathrm{Q}_{55} = \mathrm{Q}_{66} = \alpha(1+\nu)\end{gathered} \tag{2e}$$

La non linéarité est introduite par les fonctions scalaires g_i, elles-mêmes fonctions quadratiques du tenseur des contraintes par le biais du scalaire h. La loi de comportement présente deux parties : une partie élastique non linéaire et une partie viscoélastique non linéaire. On peut remarquer que $\boldsymbol{\Delta}\tilde{\mathbf{S}}(t)$ représente une complaisance en fluage viscoélastique linéaire. Cette écriture suppose que le comportement du matériau demeure isotrope tout au long du chargement et que le coefficient de Poisson ν demeure constant lors d'un essai de traction, peu importe l'histoire du chargement.

Identification de la loi de comportement

A notre connaissance, tous les auteurs qui ont proposé des méthodes d'identification de la loi de comportement de Schapery se sont appuyés sur des essais uniaxiaux de fluage–recouvrance. De cette manière, on peut connaître

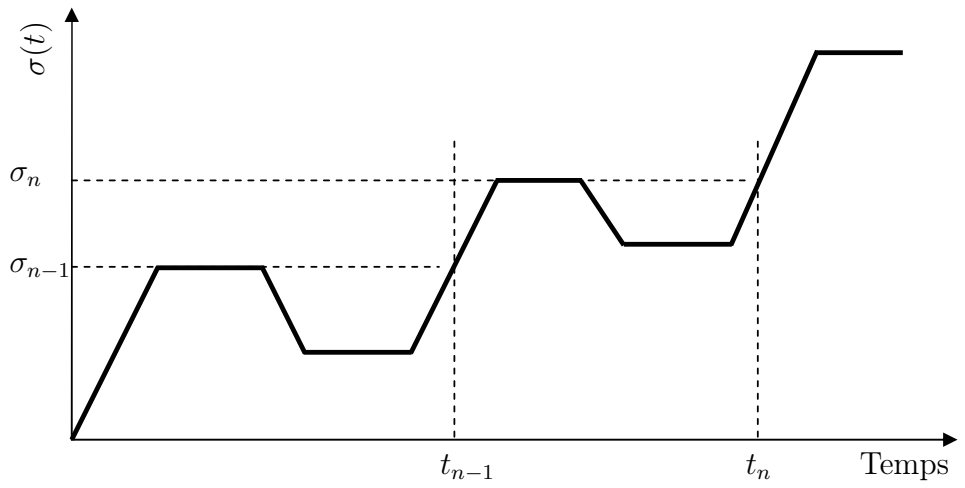


FIG. 1: Histoire de chargement typique utilisée pour l'identification de la loi de comportement

les fonctions g_i pour des valeurs ponctuelles de la contrainte appliquée σ_n. Cette approche présente deux inconvénients. Le premier est qu'il est difficile de reproduire *exactement* des essais de fluage–recouvrance théoriques. En effet, il est difficile d'appliquer ou de retirer une force instantanément. Par conséquent, si l'algorithme d'identification des paramètres utilise de l'information obtenue aux sauts de contrainte en supposant que l'essai est idéal, il est fort probable que les valeurs numériques des paramètres de la loi seront entachées d'erreurs, plus ou moins importantes. Le deuxième désavantage est lié au fait que les essais de fluage–recouvrance sont généralement traités séparément. Il est donc possible d'obtenir des $g_i(\sigma_n)$ qui oscillent en fonction de σ_n, ce qui n'a pas de sens physiquement.

Afin d'éviter ces difficultés, nous avons proposé un protocole expérimental et numérique permettant d'identifier les différentes quantités de la loi de comportement. Premièrement, nous avons réalisé des essais de traction uniaxiale où la déformation était mesurée dans la direction axiale et transverse afin d'identifier les composantes des tenseurs isotropes. Nous avons observé que le coefficient de Poisson était relativement constant, ce qui nous a permis de n'utiliser que la déformation axiale pour identifier les autres paramètres de la loi de comportement. Au lieu d'employer des chargements de fluage–recouvrance, nous avons utilisé une histoire de chargement constituée de charges et de décharges à taux de contrainte constant ainsi que des maintiens. Cette histoire de chargement typique est reproduite en figure 1. Cette histoire est décomposée en *segments* délimités par les valeurs de contraintes

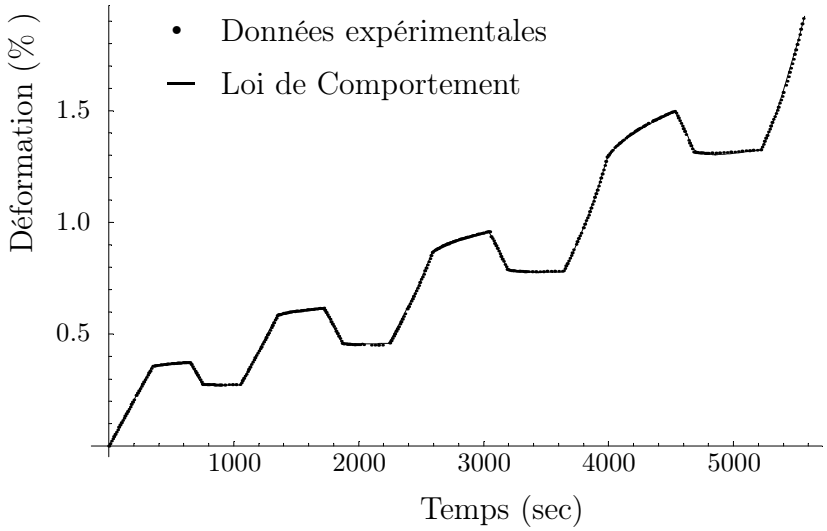


FIG. 2: Données expérimentales moyennes et prédictions théoriques de la loi de comportement pour l'histoire de contrainte utilisée pour l'identification

σ_{n-1} et σ_n. On suppose que les fonctions g_0, g_2 et g_3 varient linéairement durant un segment tandis que g_1 a une évolution quadratique. De cette manière, on pourra obtenir une expression analytique de la déformation en fonction de l'histoire des contraintes qui fera intervenir les valeurs des g_i aux bornes des segments.

Une fois cette expression analytique et les données expérimentales obtenues, il a fallu établir un algorithme minimisant la somme des carrés de la différence entre déformation théorique et expérimentale, et ce, pour tout temps. Ce problème de minimisation est non linéaire et il a fallu introduire certaines contraintes sur la valeur des paramètres (positivité, fonctions g_i monotones et strictement positives). Ces contraintes étaient nécessaires pour rencontrer les exigences de la thermodynamique et pour que la loi de comportement ait une forme réaliste (pas d'oscillations pour les g_i en fonction de la contrainte). Ce problème de minimisation sous contrainte non linéaire a été solutionné en introduisant des changements de variable appropriés pour faire disparaître les contraintes et en utilisant l'algorithme de Nelder–Mead implémenté dans Mathematica. La figure 2 compare la loi de comportement identifiée avec les données expérimentales moyennes. On peut remarquer que l'adéquation est excellente. La loi de comportement a été validée sur une autre histoire de chargement plus complexe où l'adéquation est satisfaisante.

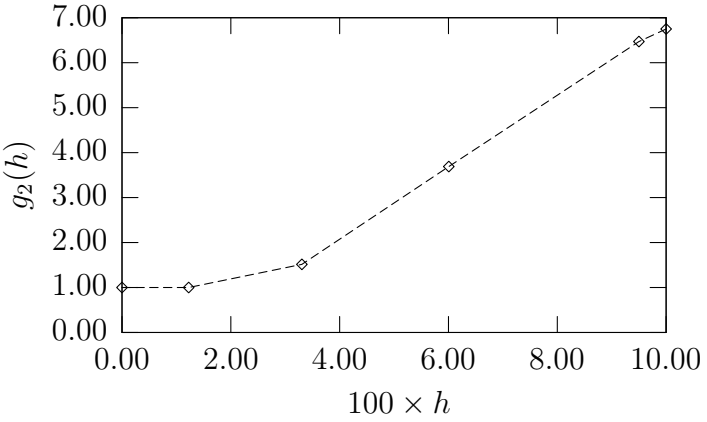


FIG. 3: g_2 en fonction de h pour notre matériau

α (MPa^{-1})	ν	λ_1	λ_2	λ_3
		$\frac{1}{100} sec^{-1}$	$\frac{1}{1000} sec^{-1}$	$\frac{1}{3162} sec^{-1}$
5×10^{-4}	0.47	α_1	α_2	α_3
		3.5×10^{-2}	1.65×10^{-3}	2.0×10^{-1}

TAB. 1: Valeurs numériques des paramètres matériau

La loi de comportement identifiée a donc la forme suivante :

$$\boldsymbol{\varepsilon}(t) = \mathbf{Q} : \boldsymbol{\sigma}(t) + \mathbf{Q} : \sum_{m=1}^{3} \left[\int_0^t \alpha_m \lambda_m \exp[-\lambda_m (t-\tau)] g_2(h(\boldsymbol{\sigma}(\tau))) \boldsymbol{\sigma}(\tau) \mathrm{d}\tau \right] \quad (3)$$

où la valeur numérique des paramètres est donnée au tableau 1 et l'évolution de g_2 est représentée à la figure 3. Il doit être noté que seul le paramètre non linéaire g_2 est différent de 1.

Modèle d'homogénéisation

Que ce soit des méthodes variationnelles ou « empiriques », l'homogénéisation de matériaux aléatoires ayant des comportements non linéaires passe habituellement par la définition d'un matériau linéaire de comparaison. Ce matériau est obtenu par une linéarisation (sécante, tangente) de la loi de comportement, autour d'un état de référence (contrainte moyenne, second moment), pour chaque phase non linéaire tout en conservant les aspects morphologiques du problème (orientation, forme des renforts par exemple).

Des propriétés mécaniques linéaires (élastiques ou viscoélastiques) homogènes sont affectées à chaque phase et le problème peut être solutionné à l'aide des outils classiques de l'homogénéisation, établis pour des matériaux linéaires. Lorsque le matériau linéaire de comparaison est viscoélastique, le principe de correspondance viscoélastique, faisant intervenir les transformées de Laplace–Carson, peut être utilisé pour résoudre le problème.

Bien que l'homogénéisation de matériaux décrits par des potentiels uniques (élasticité ou viscoplasticité non linéaires) ait reçu une grande attention, peu d'auteurs se sont intéressés à des lois comportement plus générales (plusieurs pseudo-potentiels, lois écrites sous forme fonctionnelle, etc.). Weng [100] a été parmi les premiers à aborder l'élasto-viscoplasticité non linéaire, suivi par Rougier [83], Masson et Zaoui [59] et Brenner *et coll.* [15], pour en citer quelques uns. Ces auteurs ont considéré des lois de comportement données comme une somme de pseudo-potentiels faisant intervenir, ou non, des variables internes. Des lois de comportement données sous forme fonctionnelle ont été étudiées par Pouya et Zaoui [78].

La principale difficulté associée avec les lois de comportement données sous forme fonctionnelle est que le *type* de linéarisation n'a plus de définition intuitive. En effet, la loi de comportement fait intervenir l'*histoire* du chargement et non une valeur ponctuelle, ce qui rend plus compliqué le calcul d'un module tangent (par dérivation) ou un module sécant, par exemple. Pour illustrer, considérons une loi de comportement viscoélastique non linéaire donnée sous la forme :

$$\boldsymbol{\varepsilon} = \boldsymbol{\mathfrak{F}} \circledast \boldsymbol{\sigma} \tag{4}$$

où $\boldsymbol{\sigma}$ et $\boldsymbol{\varepsilon}$ doivent être interprétées comme des histoires (i.e. fonctions du temps) et $\boldsymbol{\mathfrak{F}}$ est un opérateur non linéaire, représentant la loi de comportement, appliqué à $\boldsymbol{\sigma}$. L'équation (4) est une écriture compacte de la loi de comportement (3). Supposons une histoire particulière de contrainte $\breve{\boldsymbol{\sigma}}$ autour de laquelle on veuille effectuer la linéarisation. En utilisant la dérivée de Fréchet, Pouya et Zaoui [78] introduisent le concept de matériau tangent :

$$\boldsymbol{\mathfrak{F}} \circledast (\breve{\boldsymbol{\sigma}} + \boldsymbol{\delta\sigma}) - \boldsymbol{\mathfrak{F}} \circledast \breve{\boldsymbol{\sigma}} = \boldsymbol{\mathcal{S}}^{\mathrm{tgt}}_{\breve{\boldsymbol{\sigma}}} \circledast \boldsymbol{\delta\sigma} \tag{5}$$

où $\boldsymbol{\delta\sigma}$ est une histoire de variation de contrainte et $\boldsymbol{\mathcal{S}}^{\mathrm{tgt}}_{\breve{\boldsymbol{\sigma}}}$ l'opérateur linéaire qui représente la matériau tangent : ce matériau reproduit la variation de l'histoire de déformation autour de $\breve{\boldsymbol{\varepsilon}} = \boldsymbol{\mathfrak{F}} \circledast \breve{\boldsymbol{\sigma}}$ lorsque l'histoire de contrainte est perturbée de $\boldsymbol{\delta\sigma}$ autour de $\breve{\boldsymbol{\sigma}}$. Une fois le matériau tangent défini, une histoire de déformation libre peut être calculée pour obtenir une linéarisation affine (voir Masson *et coll.* [58] pour la définition du modèle affine). Dans leur article, Pouya et Zaoui [78] proposent d'utiliser l'histoire de contrainte

moyenne $\langle \boldsymbol{\sigma} \rangle$ comme histoire de contrainte particulière $\breve{\boldsymbol{\sigma}}$. Nous avons montré que l'on peut aussi utiliser l'histoire du second moment des contraintes $\left\langle \frac{1}{2}\boldsymbol{\sigma} \otimes \boldsymbol{\sigma} \right\rangle$ pour calculer le modèle affine, comme il l'a été proposé par Brenner *et coll.* [14] pour un matériau décrit par un potentiel.

Dans la même ligne de pensée, on peut définir un concept de matériau sécant. Un matériau sécant est un opérateur $\mathfrak{S}^{\text{sct}}_{\breve{\boldsymbol{\sigma}}}$ qui rencontre la condition suivante :

$$\mathfrak{S}^{\text{sct}}_{\breve{\boldsymbol{\sigma}}} \circledast \breve{\boldsymbol{\sigma}} = \mathfrak{F} \circledast \breve{\boldsymbol{\sigma}} \tag{6}$$

Pour notre loi de comportement, on peut montrer que cet opérateur peut avoir une définition systématique, peu importe l'histoire de chargement, et qu'il est linéaire. Nous avons aussi montré que l'on peut utiliser soit le premier ou le second moments de l'histoire des contraintes comme niveau de référence.

Ces deux approches présentent quelques désavantages. Par exemple, sauf pour des cas très particuliers, on ne peut pas obtenir d'expression analytique pour un matériau tangent. Même quand il est possible de le calculer, il n'y a aucune garantie que le matériau résultant soit un opérateur qui représente un matériau viscoélastique linéaire. Cette remarque est aussi valable pour le matériau sécant. Il est donc probable que l'on ne puisse pas résoudre le problème d'homogénéisation avec le matériau linéaire de comparaison ainsi calculé car le principe de correspondance n'est valable que pour des matériaux viscoélastiques linéaires.

Afin de contourner cette difficulté, nous introduisons une approximation. Par exemple, pour le modèle sécant, nous cherchons :

$$\hat{\boldsymbol{\mathcal{S}}}^{\text{sct}}_{\breve{\boldsymbol{\sigma}}} \circledast \breve{\boldsymbol{\sigma}} \approx \mathfrak{F} \circledast \breve{\boldsymbol{\sigma}} \tag{7}$$

où l'opérateur $\hat{\boldsymbol{\mathcal{S}}}^{\text{sct}}_{\breve{\boldsymbol{\sigma}}}$ est un matériau viscoélastique linéaire. Ce matériau doit être choisi le plus général possible, tout en rencontrant les restrictions imposées par la thermodynamique. Ce matériau viscoélastique linéaire doit donc reproduire, au mieux, l'histoire de déformation du matériau viscoélastique non linéaire lorsque qu'il est soumis à la même histoire de contrainte, et ce, pour $t \in [0, \infty[$. On peut montrer que, par causalité, si l'on désire connaître la réponse à un temps particulier t_a d'un matériau hétérogène viscoélastique linéaire, seule la connaissance du comportement mécanique des différentes phases sur $[0, t_a]$ est nécessaire. Dans la pratique, on cherchera la réponse du matériau en t_a. Par conséquent, on pourra se limiter uniquement à l'intervalle de temps $[0, t_a]$ pour calculer cette approximation. Finalement, en invoquant la caractéristique de mémoire évanescente des matériaux viscoélastiques, nous avons fait le choix de calculer $\hat{\boldsymbol{\mathcal{S}}}^{\text{sct}}_{\breve{\boldsymbol{\sigma}}}$ de manière à ce que l'approximation soit la meilleure possible sur un intervalle de temps $[t_{a-1}, t_a]$ où $t_{a-1} < t_a$.

Une fois $\hat{\boldsymbol{\mathcal{S}}}^{\text{sct}}_{\breve{\boldsymbol{\sigma}}}$ calculé, on corrigera ce défaut d'approximation par une histoire de déformation libre de sorte que :

$$\hat{\boldsymbol{\mathcal{S}}}^{\text{sct}}_{\breve{\boldsymbol{\sigma}}} \circledast \breve{\boldsymbol{\sigma}} + \boldsymbol{\varepsilon}^{\text{corr}} = \mathfrak{F} \circledast \breve{\boldsymbol{\sigma}} \tag{8}$$

Le matériau linéaire de comparaison ainsi obtenu est viscoélastique linéaire à histoire de déformation libre, ce qui peut être traité à l'aide du principe de correspondance. Une démarche similaire peut être appliquée pour le modèle affine.

Nous avons traité, jusqu'à maintenant, du schéma de linéarisation en dehors du contexte du problème d'homogénéisation. Afin d'illustrer le schéma global de l'implémentation de ces linéarisations dans une démarche d'homogénéisation, considérons le cas où l'on utilise une linéarisation sécante autour de l'histoire de contrainte moyenne dans la matrice de notre matériau composite (polypropylène chargé de billes de verre). Dans ce cas-ci, on s'intéresse à calculer la déformation macroscopique $\mathbf{E}(t_a)$ du matériau hétérogène soumis à une histoire de contrainte macroscopique $\boldsymbol{\Sigma}$. Compte tenu de la morphologie du matériau, nous avons retenu le schéma de Mori-Tanaka comme schéma d'homogénéisation. La réponse macroscopique est calculée de la manière suivante :

$$\mathbf{E}(t_a) = \int_0^{t_a} \tilde{\mathbf{S}}(t_a, t_a - \tau) : \dot{\boldsymbol{\Sigma}}(\tau) \mathrm{d}\tau + \mathbf{E}^{\mathbf{0}}(t_a) \tag{9a}$$

$$\mathbf{E}^{\mathbf{0}}(t_a) = c_0 \int_0^{t_a} \mathbf{B}_{\mathbf{0}}(t_a, t_a - \tau) : \dot{\boldsymbol{\varepsilon}}^{\mathbf{0}}(\tau) \mathrm{d}\tau \tag{9b}$$

où $\tilde{\mathbf{S}}$ et $\mathbf{B}_{\mathbf{0}}$ sont la complaisance homogénéisée et l'équivalent viscoélastique du tenseur des concentrations des contraintes, c_0 la fraction volumique de la matrice et le point représente la dérivée par rapport au temps. La première variable de $\tilde{\mathbf{S}}$ et $\mathbf{B}_{\mathbf{0}}$ a été introduite pour marquer le fait que ces fonctions tensorielles sont calculées pour le matériau linéaire de comparaison s'appuyant sur l'histoire de la contrainte moyenne dans la matrice jusqu'en t_a. La contrainte moyenne dans la matrice $\langle \boldsymbol{\sigma} \rangle_0$ en t_a peut être calculée avec des relations similaires faisant intervenir $\mathbf{B}_{\mathbf{0}}$. On peut reconnaître ainsi la nature implicite du problème : $\mathbf{B}_{\mathbf{0}}$ dépend de $\langle \boldsymbol{\sigma}(t_a) \rangle_0$ et $\langle \boldsymbol{\sigma}(t_a) \rangle_0$ dépend de $\mathbf{B}_{\mathbf{0}}$. Nous avons résolu ce problème à l'aide d'un schéma pas à pas en supposant $\langle \boldsymbol{\sigma} \rangle_0$ connue jusqu'en t_{n-1} et où l'objectif est de calculer cette quantité en t_n. Pour ce faire, une valeur de $\langle \boldsymbol{\sigma}(t_n) \rangle_0$ est calculée et la linéarisation est effectuée. Par la suite, avec ce matériau linéaire de comparaison, on calcule $\langle \boldsymbol{\sigma}(t_n) \rangle_0$. Si cette valeur calculée est voisine de la valeur supposée, la solution est atteinte. Sinon, le processus itératif continue jusqu'à ce que la solution soit atteinte.

Implémentation numérique

Ce schéma implicite a été solutionné à l'aide de la méthode de Newton et le gradient est évalué numériquement par une différence centrée.

Que ce soit du modèle sécant ou affine, le matériau linéaire de comparaison a été choisi sous la forme suivante :

$$\hat{\boldsymbol{\mathcal{S}}}_{\breve{\boldsymbol{\sigma}}} \circledast \boldsymbol{\sigma} = \int_0^t \hat{\mathbf{S}}(t-\tau) : \dot{\boldsymbol{\sigma}}(\tau) \mathrm{d}\tau \tag{10}$$

où

$$\hat{\mathbf{S}}(t) = \sum_{m=1}^{20} \left(1 - \exp[-t\kappa_m]\right) \left(\phi_m \mathbf{J} + \phi_{m+22} \mathbf{K}\right) + \left(\phi_{21}\mathbf{J} + \phi_{43}\mathbf{K}\right) t + \phi_{22}\mathbf{J} + \phi_{44}\mathbf{K} \tag{11}$$

où $\mathbf{J}$ et $\mathbf{K}$ sont les projecteurs isotropes classiques. Il peut être remarqué que nous avons choisi $\hat{\mathbf{S}}$ isotrope comme première approximation. Afin de déterminer les divers ϕ_m, nous introduisons les définitions suivantes :

$$\tilde{\boldsymbol{\varepsilon}} = \boldsymbol{\mathfrak{S}}_{\breve{\boldsymbol{\sigma}}} \circledast \tilde{\boldsymbol{\sigma}} \tag{12a}$$

$$\hat{\boldsymbol{\varepsilon}} = \hat{\boldsymbol{\mathcal{S}}}_{\breve{\boldsymbol{\sigma}}} \circledast \tilde{\boldsymbol{\sigma}} \tag{12b}$$

où $\boldsymbol{\mathfrak{S}}_{\breve{\boldsymbol{\sigma}}}$ représente soit l'opérateur *exact* sécant ou tangent, $\tilde{\boldsymbol{\sigma}}$ soit l'histoire de contrainte particulière $\breve{\boldsymbol{\sigma}}$ ou une variation $\boldsymbol{\delta\sigma}$ par rapport à celle-ci et $\hat{\boldsymbol{\mathcal{S}}}_{\breve{\boldsymbol{\sigma}}}$ représente soit l'opérateur *approximatif* sécant ou tangent. Nous introduisons la fonction coût suivante :

$$E_l^2 = \sum_{n=1}^{N} l_n [\hat{\boldsymbol{\varepsilon}}(t_n) - \tilde{\boldsymbol{\varepsilon}}(t_n)] : [\hat{\boldsymbol{\varepsilon}}(t_n) - \tilde{\boldsymbol{\varepsilon}}(t_n)] \tag{13}$$

où les $t_n \in [t_{a-1}, t_a]$ et l_n est un scalaire positif représentant le poids relatif de chaque terme dans la fonction coût. On peut de cette manière donner un poids plus important aux temps qui sont de plus en plus proches de t_a. Nous avons utilisé $t_{a-1} = 0.9t_a$, $N = 6$ avec $l_6 = 20$ et $l_1 = 1, \ldots, l_5 = 5$. Les ϕ_m formeront donc l'ensemble qui minimise E_l^2. Toutefois, pour que le matériau soit stable thermodynamiquement, il faut que $\phi_m \geq 0$. Pour ce faire, nous avons introduit le changement de variable suivant : $\phi_m = \varphi_m^2$ et la minimisation s'effectue maintenant sur les φ_m. Ce problème de minimisation non linéaire a été solutionné avec une méthode de Newton classique. Cette procédure a été utilisée pour les modèles affine et sécant.

Avec ce matériau linéaire de comparaison, il est possible de calculer la réponse effective du matériau composite. Comme le matériau est viscoélastique linéaire, le principe de correspondance viscoélastique, faisant intervenir des transformées de Laplace-Carson, est employé. La réponse effective du matériau est calculée à l'aide de la complaisance viscoélastique homogénéisée. Une étape d'inversion de la transformée de Laplace-Carson est donc nécessaire pour obtenir cette quantité. Comme la définition du matériau linéaire de comparaison est essentiellement numérique, nous avons développé un algorithme d'inversion des transformées de Laplace-Carson numérique.

L'algorithme que nous avons proposé s'appuie sur la méthode des collocations introduite par Schapery [84]. L'objectif de cette méthode est la détermination numérique des paramètres d'une fonction d'essai approximant la solution. Lorsque l'on connaît la *forme* mathématique de la solution, cette technique est très efficace. Dans notre cas, pour les propriétés homogénéisées, nous avons supposé que le matériau résultant est un matériau viscoélastique linéaire. Notre fonction d'essai est donc similaire à la relation (11).

La méthode que nous avons proposée calcule en premier lieu un ensemble de valeurs pour les temps de relaxation κ_m. Ce calcul se fait en observant le domaine où la fonction à inverser prend des valeurs significatives. Par la suite, les différents paramètres sont calculés pour que, dans l'espace de Laplace-Carson, l'erreur entre la fonction à inverser et la transformée de la fonction d'essai soit minimisée. De plus, cette minimisation se fait en s'assurant que les propriétés homogénéisées rencontrent les exigences de la thermodynamique. Nous avons proposé différents algorithmes en fonction du degré de symétrie du matériau homogénéisé. En effet, nous avons vu plus haut que l'on peut s'assurer qu'un matériau isotrope soit stable thermodynamiquement en imposant la positivité de certains scalaires. Toutefois, pour une anisotropie générale, il faut imposer que certains tenseurs d'ordre 4 symétriques (21 constantes indépendantes) soient semi-définis positifs. Imposer ce genre de contrainte est plus délicat et c'est pourquoi nous avons essayé de tirer profit des symétries matérielles.

Les modèles ainsi implémentés permettent de simuler différentes histoires de chargement et de rendre compte, par exemple, de la sensibilité du matériau composite au taux de chargement comme l'illustre la figure 4.

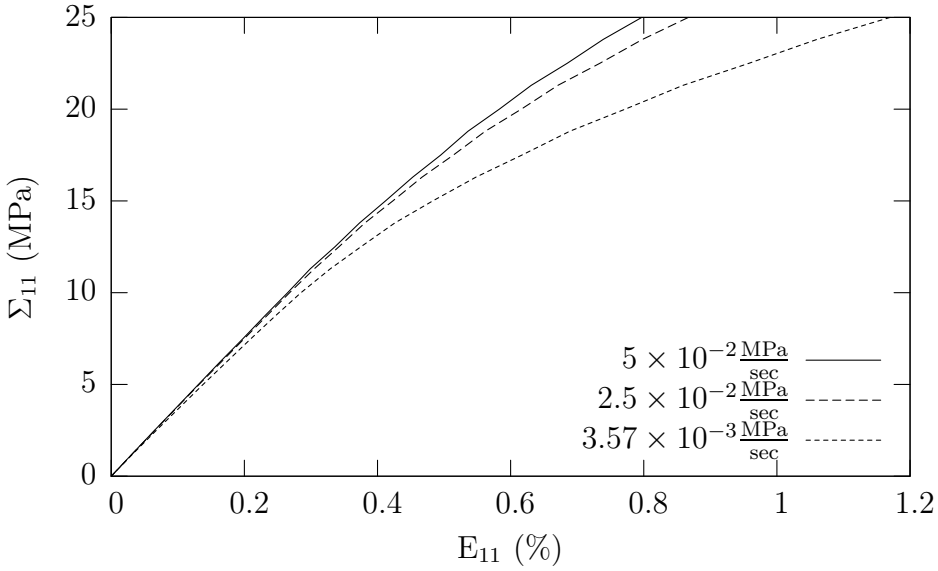


FIG. 4: Courbes de contraintes – déformations obtenues à partir du modèle sécant pour le matériau composite chargé à 20 % de billes de verre durant un essai de traction à taux de contrainte uniaxiale constant pour différents taux de contrainte uniaxiale .

Comparaison des prédictions des modèles sécant et affine avec des simulations éléments finis et des résultats expérimentaux

Nous avons implémenté les modèles affine et sécant en utilisant l'histoire de la contrainte moyenne dans la matrice comme point de fonctionnement. Afin de valider ces modèles, nous avons conduit deux types de confrontations : i) une confrontation avec des simulations éléments finis de la même microstructure et ii) une comparaison avec des données expérimentales issues d'essais de traction uniaxiale macroscopiques. Les simulations éléments finis ont été retenues afin d'obtenir une réponse théorique du matériau hétérogène dont chaque phase obéit exactement à la loi de comportement supposée. De cette manière, la confrontation avec le modèle d'homogénéisation permet de mesurer précisément l'efficacité de la procédure de linéarisation et du schéma d'homogénéisation. Les confrontations avec les données expérimentales permettent de valider les hypothèses physiques sur lesquelles se basent le modèle (i.e. parfaite cohésion de l'interface, capacités de la loi de comportement de la matrice à reproduire le comportement réel, etc.)

Nous avons utilisé des maillages tri-dimensionnels de la microstructure

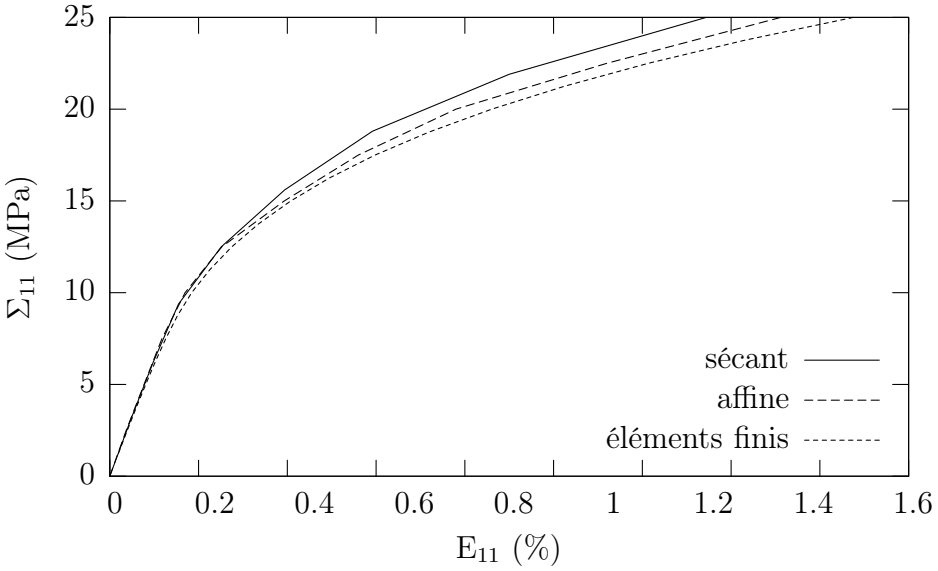


FIG. 5: Comparaison entre les prédictions des modèles affine et sécant et les simulations Éléments Finis (EF) pour un essai de traction uniaxiale à taux de contrainte constant et pour une fraction volumique de billes de 10 %.

constitués d'un cube dans lequel les positions des centres d'un certain nombre de billes sont générées aléatoirement, pour une fraction volumique de renforts de 10 %. Ces maillages nous ont été fournis par Mishnaevsky [62]. Pour des fractions volumiques de 20 et 30 %, nous avons supposé un arrangement hexagonal des positions des billes et avons utilisé une approximation axisymétrique de la cellule de base. En effet, il ne nous a pas été possible, par manque de mémoire vive, d'obtenir des maillages 3D pour ces fractions volumiques. Pour les maillages tri-dimensionnels, nous avons observé que le volume élémentaire représentatif était atteint pour 15 billes.

Les simulations ont été réalisées à l'aide du code de calcul ABAQUS. La loi de comportement de la matrice a été implémentée dans le code de calcul à l'aide de la sous-routine UMAT que nous avons développée. La figure 5 illustre le type de courbes obtenues avec les modèles affine et sécant ainsi que les simulations éléments finis pour un essai de traction à taux de contrainte constant pour une fraction volumique de renforts de 10 %. On peut remarquer de cette figure que les deux modèles conduisent à des prédictions trop raides par rapport aux simulations éléments finis. Il doit être noté que nous avons rencontré de sérieuses difficultés numériques avec le modèle affine et il n'a pas été possible de mener des simulations pour tous les cas de chargement. Ces difficultés n'ont pas été rencontrées avec le modèle sécant. Il faudrait

conduire plus de simulations pour avoir une plus grande confiance dans la comparaison entre ces deux modèles.

Des essais de traction macroscopiques ont été réalisés sur du polypropylène pur et sur des composites à 10 et 20 % de renforts. Nous avons remarqué dans un premier temps que les composites étaient plus souples que le polypropylène massif. Des essais de traction *in-situ* ont été effectués dans la chambre du Microscope Électronique à Balayage (MEB). Ces derniers ont montré qu'il y avait une faible adhésion entre les billes et la matrice et que cette dernière présentait un endommagement diffus, sous forme de craquelures, assez important. Ces phénomènes n'étant pas inclus dans nos modèles théoriques, ces observations expérimentales ne nous ont pas permis d'évaluer la capacité de nos modèles à reproduire des comportements réels.

Conclusion

En conclusion, cette étude a permis d'établir des modèles théoriques permettant de prédire le comportement macroscopique de matériaux composites viscoélastiques non linéaires à partir de la connaissance de la morphologie et du comportement de chacune des phases constituant le matériau. Les contributions spécifiques de cette étude peuvent être déclinées de la manière suivante :

1. Une écriture tri-dimensionnelle ainsi qu'une méthodologie permettant d'identifier une loi de comportement viscoélastique non linéaire.
2. Une procédure de linéarisation des lois de comportement écrites sous forme fonctionnelle pour les modèles d'homogénéisation de matériaux non linéaires basés sur le concept de matériau linéaire de comparaison.
3. Un algorithme d'inversion numérique des transformées de Laplace-Carson adapté aux problèmes d'homogénéisation.

La prochaine étape concernant l'identification de lois de comportement viscoélastique non linéaires est de traiter des champs de contrainte/déformation tri-dimensionnels afin d'avoir une plus grande confiance dans les capacités de la loi à reproduire des comportements réels. L'amélioration des prédictions théoriques des modèles d'homogénéisation pourrait se faire en considérant non plus l'histoire de la contrainte moyenne comme point de fonctionnement, mais l'histoire du second moment de cette quantité. Nous avons aussi vu qu'il est urgent de déployer des efforts sur l'écriture et l'identification de lois de comportement tri-dimensionnelles pour des polymères semi-cristallins qui incluent plusieurs phénomènes (viscoélasticité, craquelures, plasticité, etc.). Finalement, l'utilisation de fonctionnelles pour modéliser le comportement

mécanique de matériaux polymères nous a conduit à une procédure de linéarisation qui est lourde à la fois théoriquement et numériquement. Il serait souhaitable de mener une réflexion sur la nécessité d'utiliser ces lois de comportement. En effet, les lois de comportement thermodynamiques[1] ont permis récemment d'établir des procédures variationnelles donnant des résultats d'une grande qualité [46]. Il serait donc intéressant d'évaluer si des lois de comportement écrites sous cette forme peuvent bien représenter le comportement de polymères semi-cristallins. Si tel était le cas, on aurait à disposition de plus en plus d'outils pour homogénéiser des matériaux composites constitués de tels matériaux.

[1]Lois où la déformation, ou son taux, sont séparés en deux contributions : une élastique et une visqueuse où la dépendance non linéaire est introduite par des fonctions du tenseur des contraintes et de variables internes.

Introduction

Thermoplastic polymer composites have been used in industry for the past number a decades. Until recently, the applications of such materials have been limited primarily to non structural components for many different reasons. In some cases, the mechanical properties of the material do not meet the requirements of a specific application. Due to continued research into manufacturing processes, the mechanical performance of such materials has increased and such materials are used for structural applications. One other reason is that predicting the mechanical behaviour of such materials is still an open question and considerable effort is required to obtain the same degree of comprehension we have for metals.

One of the principal difficulties associated with predicting the mechanical behaviour of such materials lies in the fact that their behaviour is linear elastic/viscoelastic over a very narrow range of stresses/strains, when compared to the loads that the material can support before failure. When the loading exceeds this limited range, the material becomes nonlinear and there exist very few three-dimensional constitutive theories to predict the behaviour of such materials. Such three-dimensional constitutive theories are required in order to design three dimensional structures made of such materials.

There seems to be two approaches to modelling the behaviour of such materials. The first consists of considering the composite material as a homogeneous material and developing a phenomenological constitutive theory. This approach can lead to very accurate results but when one material parameter is changed (shape, orientation, volume fraction of reinforcements, for example) a new constitutive theory must be identified. Another approach is to consider the heterogeneous material as a structure made of homogeneous phases (i.e., the reinforcements and the matrix) and calculate the relationship between the stresses and strains applied on the boundaries of this material. This approach requires using, at some stage, some phenomenological constitutive theories to model the behaviour of each phase, but is much richer than the first alternative since it can compute, in theory, the mechanical response of any composite composed of the same basic materials. Such an approach

is called homogenisation.

There have been many interesting developments in the field of homogenisation in the last four decades. The approach has been applied successfully to many linear elastic heterogeneous materials and extended to nonlinear behaviours. In this study, we classify the nonlinear behaviour in two categories: the non hereditary and the hereditary behaviours. A non hereditary behaviour is one where the response depends only on the current loading whereas the response of a hereditary behaviour at a given time depends on the whole load history, prior to that point. Considerable progress has been achieved regarding the homogenisation of nonlinear non hereditary materials in the last decade or so. However, there are still very few approaches to the homogenisation of nonlinear hereditary materials. Nonlinear viscoelasticity is an example of nonlinear hereditary behaviour.

The objective of this present research is to develop a methodology to homogenise nonlinear viscoelastic heterogeneous materials and to apply it to a real thermoplastic composite material. The material used in this study is a glass beads reinforced polypropylene where the volume fraction of reinforcements ranges from 0 to 30%.

This thesis can be divided into three parts. The first part is concerned with the characterisation of the mechanical behaviour of polypropylene. The first chapter is dedicated to establishing a constitutive theory following the thermodynamic framework introduced by Schapery [85] many years ago. The second chapter is concerned with the identification of such nonlinear viscoelastic behaviour, within the limits of our experimental facilities.

The second section deals with developing homogenisation models to predict the mechanical behaviour of our nonlinear viscoelastic composite material. The theoretical models are presented in Chapter Three after a literature survey and a general presentation of homogenisation. Chapter Four details the numerical implementation of such models and provides a comparison between the models. The numerical implementation of our models requires numerical inversion of Laplace–Carson transforms. We have developed such a procedure for homogenisation problems; this is also presented in Chapter Four.

The final part of the thesis deals with the theoretical and experimental validation of the predictions made by the homogenisation models. In Chapter Five, we have simulated the behaviour of our composite material using the finite element technique. This allows using the same hypotheses regarding the behaviour of the local constituents for both models. This way, we can assess the relevance of our homogenisation models from a theoretical point of view. Then, such predictions are compared with limited experimental data in order to assess the relevance of the whole process and the hypotheses

regarding the local behaviour of the constituent phases.

In conclusion, we present the principal contributions of this work and give some perspectives. In addition, the notation conventions used in this thesis are presented in Appendix A.

Chapter 1

A Nonlinear Viscoelastic Constitutive Law

1.1 Introduction

Modelling the mechanical response of polymers to applied loads is a complex and difficult task. Complex since a given polymer can exhibit many *deformation regimes* over its loading history. For example, at very small strains, a polymer can be considered as a linear elastic material; at small strains, as a linear viscoelastic material[1]; at moderate strains, as a nonlinear viscoelastic material; and at large strains, as a plastic or viscoplastic material. Complex since the interactions between the various internal mechanisms (i.e., mechanisms modifying the internal structure of the material) is not yet fully understood by the scientific community. Difficult because the mathematical form of a model representing the material's behaviour must account for all of these deformation regimes. Difficult because, even if a proper mathematical model has been established, identification of the model is demanding both experimentally, theoretically and computationally. Difficult because there exist a wide range of internal parameters that can modify the mechanical behaviour of a polymer (crystallinity for a semi-crystalline material, T_g the glass-transition temperature, molecular weight, etc.). It is possible that for the same polymer, a model can be accurate for low temperatures but not for temperatures higher than the glass-transition temperature.

The mechanical response of polymers has been modelled by two schools of thought: a) mathematicians who sought general, but yet useful, expressions for the mechanical response of polymers and b) chemists and mechanicians

[1]It should be noted that if a polymer is linearly viscoelastic it usually retains this behavior down to very small strains.

who used a thermodynamic frame which incorporates information on the internal mechanisms to derive the mathematical expression of the polymer behaviour. These two topics have received considerable theoretical attention in the 50s and 60s, and more recently in the last decade due to the considerable advancements in computational mechanics [93]. We give a brief overview of these two schools of thought in the following paragraphs.

In a series of papers, Green and Rivlin [29, 30] and Green, Rivlin and Spencer [31] developed functional representations for the mechanical behaviour of nonlinear materials with memory. The functionals are *causal* (i.e., the response at t_n depends solely on the loading for $t \in [0, t_n]$). The response is a nonlinear functional of the loading (stresses or strains) history and dependence on the time derivative of the loading can be introduced. The authors developed their theory in the general case (where there is no material symmetry) and gave specialised forms for isotropy. When their constitutive relation is simplified to a uniaxial model and the response depends on the stress history, one obtains [55]:

$$\begin{aligned}\varepsilon(t) = S_0\sigma(t) &+ \int_0^t S_1(t-\tau)\dot{\sigma}(\tau)\mathrm{d}\tau \\ &+ \iint_0^t S_2(t-\tau_1, t-\tau_2)\dot{\sigma}(\tau_1)\dot{\sigma}(\tau_2)\mathrm{d}\tau_1\mathrm{d}\tau_2 \\ &+ \iiint_0^t S_3(t-\tau_1, t-\tau_2, t-\tau_3)\dot{\sigma}(\tau_1)\dot{\sigma}(\tau_2)\dot{\sigma}(\tau_3)\mathrm{d}\tau_1\mathrm{d}\tau_2\mathrm{d}\tau_3 \\ &+ \dots\end{aligned} \tag{1.1}$$

where the S_i are functions of time and stress, the dot ($\dot{}$) represents a derivative with respect to the integration variable and the τ_i are integration variables. The expression is similar in three dimensions and the response depends nonlinearly of the stress invariant histories. A dual expression can be obtained by inverting the roles of ε and σ. Such development can be interpreted as a Taylor expansion of a functional with respect to the stress *history*. In equation (1.1) the response is expanded to the third order of the stress history. Lockett [55] and later Buckley [17] have designed simple experiments involving creep and recovery tests to identify such behaviour laws. To identify the behaviour described by equation (1.1), Lockett [55] suggested performing creep – recovery tests of the following shape:

$$\sigma(t) = aH(t) + bH(t-k) + cH(t-l) \tag{1.2}$$

where $H(t)$ is the Heaviside unit step function and the other letters are constants. Such experiments allow the stress dependency of the S_i to be

determined for discrete values of σ. If the S_i are to be known for 10 levels of stress, Lockett [55] showed that 83 different load histories are required. In the three-dimensional isotropic case, this number goes up 483 (!) tests involving bi-axial, tri-axial and coupled bi-axial – shear loadings. The extensive amount of experimental work required to identify such behaviour laws has limited their application to industrial cases. The exercise is interesting, nevertheless, since it provides an estimation of the effort required to identify a general nonlinear viscoelastic behaviour law with relatively simple load histories (creep – recovery). Using more complex load histories would reduce the number of different tests but would increase the amount of computational work required to identify the material parameters.

Behaviour laws similar to equation (1.1) are quite general in nature since they are not based on material information. Using information on the internal deformation mechanisms specific to a given material could lead to simpler and more relevant behaviour laws. Amongst the most cited authors of this second school of thought, we find Schapery [85], Knauss [45] and Drozdov [24]. The works of Drozdov introduce a model where the short distance interaction between the molecules in a polymer are modelled by nonlinear springs whose laws are given by: $\sigma = \phi(\varepsilon)$, where ϕ is a function of the current strain. In his terminology, certain springs, or links, are born and others die during the deformation process. The rate of birth – death of such springs is characterised by a function X_*. The functions ϕ and X_* appear in the final expression of the behaviour law and must be identified by experiments. Using the same line of thought, Knauss introduces the concept of *free volume* which he defines as the volume available for the mobility of the polymer chains. He develops expressions for the free volume as functions of temperature, change in volume, etc. The free volume is then introduced into the calculation of a *time shift* factor which is in turn introduced into a linear viscoelastic behaviour law. The nonlinearity is therefore introduced by this time shift factor. Schapery introduced a general thermodynamic frame in which behaviour laws can be written. Such an approach is quite general and the models of Knauss [45] and Drozdov [24] (for example) can be seen as particular cases of this general context. In addition, to our knowledge, Schapery's constitutive theory is the most widely applied nonlinear viscoelastic behaviour law. Cunat [21] has used a similar thermodynamic framework to develop his Distribution of NonLinear Relaxations (DNLR) theory. This theory states that some internal events (molecular movement, etc.) happen and evolve over different relaxation times which are functions of the load history.

One other characteristic of polymers is that some of them exhibit plasticity (independent of the loading rate) as well as viscoplasticity (loading rate dependent). These phenomena are relatively well known and modelled for

polycrystals but very few 3D models exist for polymers. The mechanisms at the molecular scale are well known but their effects at the macroscopic level are not well quantified. There is a wide range of literature dealing with uniaxial plasticity. For example, Zapas and Crissman [102] have modelled the viscoplastic strains by using a functional representation while authors like Pasrischa *et al.* [72] used Schapery's model [88] in conjunction with the Zapas and Crissman model to characterise the nonlinear elasto-viscoplastic behaviour of composite laminates. Lai and Bakker [48] also used a similar model with great success to predict the behaviour of polyethylene for complex load histories. Other authors like Bardenhagen *et al.* [3] have suggested 3D plastic and viscoplastic models by arranging nonlinear springs and dashpots as functions of the strain rate and platens activated when a critical load is reached. Drozdov *et al.* [25] have also suggested a 3D viscoplasticity model where the viscoplastic strain rate is influenced by the first and second stress invariants. However, the model has only been validated on uniaxial loadings. Schapery has shown that plasticity can be included in his thermodynamics framework [91]. He also shown that his framework includes the model of Zapas and Crissman [102]. To his knowledge, in 1997, there were no well established and experimentally validated 3D viscoplasticity models in the literature. The literature we have surveyed since then shows the same deficit.

From this brief literature survey we can gauge the effort required to model adequately the mechanical behaviour of polymers. There is no well established unique constitutive law for polypropylene. In addition, the available behaviour laws model the elastic and viscoelastic behaviour of polymers in 3D but viscoplasticity and plasticity have received less attention. Therefore, we will limit ourselves in this study to viscoelastic behaviour. The validity domain of our behaviour law will then have to be identified experimentally. In addition, no attempt is made to relate the internal deformation mechanisms to the numerical values of the parameters of the constitutive law. Such study is beyond the scope of this thesis and we consider our material as a general thermodynamic system. We refer, in subsequent chapters, to some microstructural aspects in a qualitative way only.

In this study, we have decided to use Schapery's constitutive theory since it is quite general in nature and it can be customised to our specific needs. Since such a general nonlinear constitutive law has not been widely applied in homogenisation problems, the remaining sections of this chapter provides a detailed development of the theory. We insist first on basic thermodynamics concepts and notation. Then the theory of linear viscoelasticity is presented since it will be useful in future sections of this thesis. Next, we present Schapery's constitutive theory and we give an interpretation of this theory

with respect to linear viscoelastic constitutive theories. Finally, we develop the constitutive theory for our specific material.

The development we present here assumes that the material is subjected to a loading which leads to small strains (just small enough that geometrically linear theory is an acceptable approximation). It is also assumed that the material deforms at a constant temperature.

1.2 Thermodynamics of irreversible processes

It is assumed in the Thermodynamics of Irreversible Processes (TIP) that the thermodynamic state of a material is characterised by state functions of state variables (temperature, strain, molecular density, etc.). The state variables are generally divided into two categories: the observable variables (those which can be measured by experiments) and hidden variables (those that describe internal phenomena such as chain movement in polymers). The observable variables are classically denoted by q_i and the hidden variables by q_α. *Conjugate forces* are associated with the state variables. For example, if the strain is an observed variable, the stress is a conjugate force. The conjugate forces are denoted by Q_i and it is noted that the $Q_\alpha = 0$ [85]. The restrictions imposed by thermodynamics on the state functions and on the evolution of the internal variables are classically imposed by combining the first and second laws of thermodynamics (see Lemaitre and Chaboche [53]). In this study, we assume that the deformation process is isothermal and combination of the first and second laws of thermodynamics leads to the Clausius – Duhem inequality [87]:

$$T\dot{S} = \left(Q_i - \frac{\partial \Psi}{\partial q_i}\right)\dot{q}_i - \frac{\partial \Psi}{\partial q_\alpha}\dot{q}_\alpha \geq 0 \tag{1.3}$$

where T is the absolute temperature, $\dot{S}$ is the entropy production rate and $\Psi = \Psi(q_i, q_\alpha)$ is Helmholtz's free energy. In this specific case, Ψ is the state function. At this stage, the shape of the q_α has not been specified. It will be shown later that they are in fact functionals of the q_i. This result is assumed for now. Relation (1.3) must hold for any q_i history. So, imagine a history of q_i such that the q_α are constants. Furthermore, let's choose the history of q_i so that it induces a reversible process ($\dot{S} = 0$). Then:

$$Q_i = \left.\frac{\partial \Psi}{\partial q_i}\right|_{q_\alpha} \tag{1.4}$$

where the q_α are not varied when evaluating the derivative (since q_i is chosen so that $q_\alpha(t) = ct$). It should be noted that such notation is often implicit in

the literature and a certain care is required to avoid misinterpretation.

Consider $Q_i = \sigma_i$ and $q_i = \varepsilon_i$. In the absence of internal variables, we have:

$$\sigma_i = \left.\frac{\partial \Psi}{\partial \varepsilon_i}\right|_{q_\alpha} = \frac{\partial \Psi}{\partial \varepsilon_i} \tag{1.5}$$

and the following property:

$$\mathbf{M^{tgt}} = \frac{\partial^2 \Psi}{\partial \boldsymbol{\varepsilon} \partial \boldsymbol{\varepsilon}} = \frac{\partial \boldsymbol{\sigma}}{\partial \boldsymbol{\varepsilon}} \geq 0 \tag{1.6}$$

where $\mathbf{M^{tgt}}$ is the tangent modulus. $\mathbf{M^{tgt}}$ is also symmetric. If the state function Ψ meets condition (1.6) then Ψ is called a *potential*. It should be noted that a dual approach exists to express $\boldsymbol{\varepsilon} = \frac{\partial \Phi}{\partial \boldsymbol{\sigma}}$ where Φ is a different free energy.

1.3 Linear viscoelasticity

The objective of the whole approach is to end up with a mathematical *expression* of a linear viscoelastic constitutive law. The aim is also to obtain the most general shape as possible that does not violate the principles of thermodynamics. For the sake of continuity with the notation used in this manuscript, we denote the internal variables by second order tensors. It should be noted that this assumption is not required since the internal variables will be eliminated in the final results [92]. In addition, the numerical values of these quantities introduced in the analysis have no importance: ultimately, experimental investigation will be required to measure them. The tensors we introduce follow the same usual notation (i.e., bold Greek letters for second order and bold capital Roman letters for fourth order). However, their dimensions are not specified in the development, but become clear once the final result is obtained. This notation has been introduced so that the basic concepts are emphasised rather than the mathematical technicalities.

Biot [6] has suggested a general thermodynamic framework in which he developed constitutive relations for linear viscoelastic materials. He also showed the link between his constitutive theory and usual analog models (i.e., spring – dashpots). His theory led to constitutive laws where the strains are applied and the stresses measured. Schapery used similar ideas [88] to express the strains as a function of the stresses. We present here Schapery's developments by using a notation similar to his recent work [91]. In addition, the presentation allows comparision to Schapery's constitutive theory with respect to linear viscoelasticity. We recall that our development assumes

a constant temperature and therefore, temperature effects are not included here.

Suppose that the state variables are the strains $\boldsymbol{\varepsilon}$ (observable) and a set of internal variables $\boldsymbol{\xi}$ (hidden) while the conjugated forces are the stresses $\boldsymbol{\sigma}$. Then, the Clausius-Duhem inequality becomes:

$$\left(\boldsymbol{\sigma} - \frac{\partial \Psi}{\partial \boldsymbol{\varepsilon}}\right) : \dot{\boldsymbol{\varepsilon}} - \frac{\partial \Psi}{\partial \boldsymbol{\xi}} : \dot{\boldsymbol{\xi}} = \boldsymbol{\alpha} : \dot{\boldsymbol{\varepsilon}} + \boldsymbol{\beta} : \dot{\boldsymbol{\xi}} \geq 0 \tag{1.7}$$

The $\boldsymbol{\alpha}$ and $\boldsymbol{\beta}$ are called *thermodynamic forces* and they represent the irreversible component of the forces applied to the system [85]. The first hypothesis introduced in linear viscoelasticity is that there is a linear relationship between the thermodynamic forces and state variables fluxes, such that:

$$\boldsymbol{\alpha} = \mathbf{A} : \dot{\boldsymbol{\varepsilon}} \quad \text{and} \quad \boldsymbol{\beta} = \mathbf{B} : \dot{\boldsymbol{\xi}} \tag{1.8}$$

where $\mathbf{A}$ and $\mathbf{B}$ are constant tensors. In order to meet condition (1.7), $\mathbf{A}, \mathbf{B} \geq 0$ and these tensors are symmetric by virtue of Onsager's principle [88]. Combining relations (1.7,1.8) leads to the following set of equations:

$$\frac{\partial \Psi}{\partial \boldsymbol{\varepsilon}} + \mathbf{A} : \dot{\boldsymbol{\varepsilon}} = \boldsymbol{\sigma} \tag{1.9a}$$

$$\frac{\partial \Psi}{\partial \boldsymbol{\xi}} + \mathbf{B} : \dot{\boldsymbol{\xi}} = 0 \tag{1.9b}$$

The set of equations (1.9) represent the equations of motion relating the stresses, strains and hidden variables once the expression of Helmholtz's free energy is known.

So far, the development presented here assumes that the strains are applied and the stresses are obtained. In this study, we are interested in obtaining the strains when the stresses are applied[2]. Schapery has shown [88] that the set $\{\boldsymbol{\sigma}, \boldsymbol{\xi}\}$ can be considered as the state variables and $\boldsymbol{\varepsilon}$ as the

[2]This is due to the fact that for the homogenisation model we need a three dimensional constitutive law and to identify the parameters of a behaviour law where the strains are applied requires more specialised equipment than a behaviour law where the stresses are applied. For example, if we assume that our material is isotropic, applying a tensile stress and measuring the strains in the axial and transverse directions is sufficient to identify the parameters of a constitutive law where the strains are expressed as a function of stresses. On the other hand, identifying the parameters of a behaviour law where the strains are applied would require applying the strains in two different directions and measuring the stresses in these directions. For this study, we had access to a conventional tensile machine and it was thus not possible to identify such a behaviour law where the strains are applied and the stresses measured.

conjugate force when it is assumed that a sudden change in strains induces a finite stress. This leads to $\mathbf{A} = \mathbf{0}$ (see [88] for the demonstration) which implies from equation (1.9a) that $\frac{\partial \Psi}{\partial \boldsymbol{\varepsilon}} = \boldsymbol{\sigma}$.

In order to obtain a constitutive theory in a familiar form, Schapery introduces the Gibbs free energy defined as:

$$G = G(\boldsymbol{\sigma}, \boldsymbol{\xi}) = \Psi(\boldsymbol{\varepsilon}(\boldsymbol{\sigma}, \boldsymbol{\xi}), \boldsymbol{\xi}) - \boldsymbol{\sigma} : \boldsymbol{\varepsilon}(\boldsymbol{\sigma}, \boldsymbol{\xi}) \tag{1.10}$$

where we recall that the independent variables are $\{\boldsymbol{\sigma}, \boldsymbol{\xi}\}$ and the dependent variable is $\boldsymbol{\varepsilon}$. Using the fact that $\frac{\partial \Psi}{\partial \boldsymbol{\varepsilon}} = \boldsymbol{\sigma}$ leads to $\frac{\partial \Psi}{\partial \boldsymbol{\xi}} = \frac{\partial G}{\partial \boldsymbol{\xi}}$, the Clausius-Duhem inequality can be rewritten as:

$$-\frac{\partial G}{\partial \boldsymbol{\xi}} : \dot{\boldsymbol{\xi}} = \boldsymbol{\beta} : \dot{\boldsymbol{\xi}} \geq 0 \tag{1.11}$$

Partial differentiation of G with respect to $\boldsymbol{\sigma}$ leads to:

$$\left.\frac{\partial G}{\partial \boldsymbol{\sigma}}\right|_{\xi} = -\boldsymbol{\varepsilon} - \boldsymbol{\sigma} : \left.\frac{\partial \boldsymbol{\varepsilon}}{\partial \boldsymbol{\sigma}}\right|_{\xi} + \left.\frac{\partial \Psi}{\partial \boldsymbol{\varepsilon}}\right|_{\xi} : \left.\frac{\partial \boldsymbol{\varepsilon}}{\partial \boldsymbol{\sigma}}\right|_{\xi} \tag{1.12}$$

By recalling (1.5) and using (1.12) we obtain the familiar equation:

$$\boldsymbol{\varepsilon} = -\left.\frac{\partial G}{\partial \boldsymbol{\sigma}}\right|_{\xi} \tag{1.13}$$

which is the behaviour law we seek. Equation (1.13) states that, once the Gibbs free energy and the value of the hidden variables are known, the strain is obtained by differentiation of the Gibbs free energy with respect to the stresses by considering the hidden variables as constants. Our task is now to define an expression for Gibbs free energy and to express the hidden variables as functions of stresses.

Schapery [88, 91] introduced a general description of G by using a Taylor expansion with respect to the state variables. The development is done around a reference state in thermodynamic equilibrium where, by definition, $\boldsymbol{\sigma} = \boldsymbol{\xi} = \boldsymbol{\varepsilon} = \mathbf{0}$. This general description is due to the fact that we do not give any physical sense to the internal state variables. The only assumption made is that their variation around a reference state is small enough so that the Taylor expansion is valid. For convenience, he expresses G as [91]:

$$G = G_R + \boldsymbol{\rho} : \boldsymbol{\xi} + \frac{1}{2}\boldsymbol{\xi} : \mathbf{Y} : \boldsymbol{\xi} \tag{1.14}$$

where G_R, $\boldsymbol{\rho}$ and $\mathbf{Y}$ are functions of $\boldsymbol{\sigma}$. For linear viscoelasticity, we must have that $\mathbf{Y}$ is independent of $\boldsymbol{\sigma}$ and that $\boldsymbol{\rho}$ is given by:

$$\boldsymbol{\rho} = \mathbf{T} : \boldsymbol{\sigma} \tag{1.15}$$

where $\mathbf{T}$ is a constant tensor. In addition, Schapery has shown that G must be a minimum in the reference state [88] which implies that $\mathbf{Y} \geq 0$. Using definition (1.14) in (1.13) leads to the behaviour law (after neglecting some second order terms):

$$\boldsymbol{\varepsilon} = -\frac{\partial G_R}{\partial \boldsymbol{\sigma}} - \left(\frac{\partial \boldsymbol{\rho}}{\partial \boldsymbol{\sigma}}\right)^{\mathsf{T}} : \boldsymbol{\xi} \tag{1.16}$$

Combining equations (1.8,1.11,1.14) leads to the following set of differential equations imposed by thermodynamics which must be solved in order to obtain the evolution laws of the internal variables:

$$\mathbf{B} : \dot{\boldsymbol{\xi}} + \mathbf{Y} : \boldsymbol{\xi} = -\boldsymbol{\rho} \tag{1.17}$$

Biot [6] and Schapery [88] have solved such a system of equations by stating that a set of $\boldsymbol{\xi}$ can always be found so that it diagonalises $\mathbf{B}$ and $\mathbf{Y}$ simultaneously. We recall that $\mathbf{B} \geq 0$ and $\mathbf{Y} \geq 0$ since the Gibbs free energy is a minimum at the reference state.[3] Therefore, the system of equations becomes uncoupled and reads (no summation on m):

$$\mathrm{B}_m \dot{\xi}_m + \mathrm{Y}_m \xi_m = -\rho_m \tag{1.18}$$

with $\mathrm{B}_m, \mathrm{Y}_m \geq 0$. The solution of this differential equation is the familiar form:

$$\xi_m(t) = -\frac{1}{\mathrm{Y}_m} \int_0^t (1 - \exp\left[-\lambda_m (t-\tau)\right]) \frac{\mathrm{d}\rho_m}{\mathrm{d}\tau} \mathrm{d}\tau \tag{1.19}$$

with $\lambda_m = \frac{\mathrm{Y}_m}{\mathrm{B}_m}$. Substitution of the evolution law (1.19) into the behaviour law (1.16) leads to:

$$\boldsymbol{\varepsilon}(t) = -\frac{\partial G_R}{\partial \boldsymbol{\sigma}} + \int_0^t \boldsymbol{\Delta}\mathbf{S}(t-\tau) : \frac{\mathrm{d}\boldsymbol{\sigma}}{\mathrm{d}\tau} \mathrm{d}\tau \tag{1.20}$$

with

$$\Delta \mathrm{S}_{ij}(t) = \sum_m \frac{\mathrm{T}_{im}\mathrm{T}_{jm}}{\mathrm{Y}_m} (1 - \exp\left[-\lambda_m(t)\right]) \tag{1.21}$$

which is the well known linear viscoelastic behaviour law where an initial compliance has been added. Therefore, in that case, $-G_R$ is interpreted as the potential of a linear elastic material. It can be observed from equation (1.21) that $\boldsymbol{\Delta}\mathbf{S} \geq 0$ (since Y_m can be infinite). In addition, if all the sets

[3] The equality sign has been introduced for generality. In that sense, the minimum is interpreted as a stable minimum. In other words, there is a region in the space of the state variables where G is minimum and has a constant value.

$\{\mathrm{Y}_m, \mathrm{B}_m\}$ are distinct, then $\boldsymbol{\Delta}\mathbf{S}$ is anisotropic. Material symmetry will occur when there are repeated $\{\mathrm{Y}_m, \mathrm{B}_m\}$ sets (which is equivalent to repeated eigenvalues). Repeated sets lead to different tensors multiplying the same $1 - \exp[-\lambda_m t]$ term. Material symmetry will occur when some of the off diagonal terms of these tensor cancel each other. Biot [6] and Schapery [88] have shown that such a result can be interpreted as a finite arrangement of springs and dashpots, which gives a thermodynamic interpretation of the usual analog viscoelastic models. Each internal variable (i.e., each ξ_m) can be interpreted as a spring–dashpot pair. It is possible to give a more general mathematical representation of linear viscoelasticity and this is done in the next subsection. This subsection is not required for the development of our constitutive law but will be useful in the subsequent chapters. It has been inserted here for the sake of continuity.

1.3.1 A general representation of linear viscoelasticity

Bouleau [10, 11] (amongst others) has shown that, instead of considering a finite set of internal state variables, one can obtain a more general form of a linear viscoelastic constitutive law by considering the internal variables as a continuum set. In addition, when one considers the cases where $\mathrm{Y}_m = 0$ or $\mathrm{B}_m = 0$ (since these tensors are positive semi-definite) an elastic and a steady flow response are obtained. Therefore, the most general shape for a linear viscoelastic behaviour law is given by [10, 11]:

$$\begin{aligned} \boldsymbol{\varepsilon}(t) &= \int_0^t \mathbf{S}(t-\tau) : \frac{\mathrm{d}\boldsymbol{\sigma}}{\mathrm{d}\tau}\mathrm{d}\tau \quad \text{with} \\ \mathbf{S}(t) &= \int_{0^+}^{\infty} (1 - \exp[-t\lambda])\mathrm{d}\check{\mathbf{S}}(\lambda) + \mathbf{S}'t + \mathbf{S}'' \end{aligned} \tag{1.22}$$

where $\mathbf{S}'$ and $\mathbf{S}''$ are constant positive semi-definite tensors and $\check{\mathbf{S}}$ is a positive semi-definite tensor of σ-finite measures[4] on $\mathbb{R}_+^*$ such that:

$$\int_0^{\infty} \frac{\lambda}{1+\lambda}\mathrm{d}|\mathrm{S}_{ij}(\lambda)| < +\infty \tag{1.23}$$

The stresses are given as a function of strains by [10]:

$$\begin{aligned} \boldsymbol{\sigma}(t) &= \int_0^t \mathbf{C}(t-\tau) : \frac{\mathrm{d}\boldsymbol{\varepsilon}}{\mathrm{d}\tau}\mathrm{d}\tau \quad \text{with} \\ \mathbf{C}(t) &= \int_{0^+}^{\infty} \exp[-t\lambda]\mathrm{d}\check{\mathbf{C}}(\lambda) + \mathbf{C}'' \end{aligned} \tag{1.24}$$

[4] We can intepret such functions with statistical theory. The measure $\check{\mathbf{S}}(\lambda)$ can be interpreted as the cumulative distribution and $\mathrm{d}\check{\mathbf{S}}(\lambda)$ as the probability distribution.

where $\mathbf{C}''$ is a constant positive semi-definite tensor and $\check{\mathbf{C}}$ is a positive semi-definite tensor of σ-finite measures on $\mathbb{R}_+^*$ such that:

$$\int_0^\infty \frac{1}{1+\lambda} \mathrm{d}|\mathrm{C}_{ij}(\lambda)| < +\infty \tag{1.25}$$

Here, we have made the reasonable assumption that a sudden strain jump leads to a finite stress. Such relations will be useful when the numerical Laplace-Carson inversion algorithm is developed. We will now give some examples of measures to illustrate the richness of such a linear viscoelastic model.

Consider first some discrete measures. For simplicity, we consider only one-dimensional creep compliances and we set $S' = S'' = 0$. If we consider $\mathrm{d}\check{S}(\lambda)$ as a finite series of Dirac impulses, we obtain relation (1.20). Consider now a convergent series such as a geometric series:

$$\begin{gathered} \mathrm{d}\check{S}_2(\lambda) = \sum_{\lambda_n=1}^{\infty} az(1-z)^{\lambda_n}\delta(\lambda-\lambda_n) \rightarrow S_2(t) = \frac{1-\exp\left[-at\right]}{1-z\exp\left[-at\right]} \\ \text{with} \quad a>0 \quad \text{and} \quad z \in]0,1[\end{gathered} \tag{1.26}$$

or a Poisson distribution:

$$\begin{gathered} \mathrm{d}\check{S}_3(\lambda) = \sum_{\lambda_n=1}^{\infty} a\exp\left[-\gamma\right]\frac{\gamma^{\lambda_n}}{\lambda_n!}\delta(\lambda-\lambda_n) \\ \rightarrow S_3(t) = 1-\exp\left[\gamma\exp\left[-at\right]-\gamma-at\right] \\ \text{with} \quad a>0 \quad \text{and} \quad \gamma>0 \end{gathered} \tag{1.27}$$

Now, let's turn to continuous measures, where $a > 0$, $b > 0$ and $\alpha \in]0,1[$. For example:

$$\mathrm{d}\check{S}_4(\lambda) = \frac{a\alpha}{\Gamma(1-\alpha)\lambda^{\alpha+1}}\mathrm{d}\lambda \rightarrow S_4(t) = at^\alpha \tag{1.28}$$

$$\mathrm{d}\check{S}_5(\lambda) = \frac{a}{b^2}\exp\left[-\frac{\lambda}{b}\right]\mathrm{d}\lambda \rightarrow S_5(t) = \frac{at}{1+bt} \tag{1.29}$$

$$\mathrm{d}\check{S}_6(\lambda) = \frac{a}{\lambda}\exp\left[-\frac{\lambda}{b}\right]\mathrm{d}\lambda \rightarrow S_6(t) = a\log(1+bt) \tag{1.30}$$

$$\mathrm{d}\check{S}_7(\lambda) = aH[\lambda-b]\mathrm{d}\lambda \rightarrow S_7(t) = a\left(b-\frac{1-\exp[-bt]}{t}\right) \tag{1.31}$$

where H is the Heaviside unit step function and Γ the Gamma function. The functions, like the S_i, obtained in the one dimensional formula (1.22)

are called *Bernstein functions* and have the following property [11]: If φ and ψ are Bernstein and $\psi(0) = 0$ then $\varphi \circ \psi : t \to \varphi(\psi(t))$ is Bernstein. For example:

$$S_8 = S_4(S_5(t)) = a\left(\frac{at}{1+bt}\right)^{\alpha} \tag{1.32}$$

This last property shows how new behaviour laws can be created. There are a wide range of possible combinations; far more than those modelled with a finite, or even infinite, number of spring-dashpot arrangements.

Summary

To summarise, linear viscoelasticity can be interpreted in the most general case as a material for which there is a linear relationship between the thermodynamic forces (generating entropy) and the rate of change of the state variables (see equations (1.7,1.8)) and for which the state function (i.e., Gibbs free energy) is adequately approximated by a Taylor expansion, up to the second order, in the state variables. In addition, the state variables can be considered as a continuum set for more generality[5]. Therefore, linear viscoelasticity will be valid as long as the applied load does not induce large changes in the microstructure (i.e., state function). The theory introduced by Schapery [85, 88] aims at extending the domain of validity of such hypotheses by introducing nonlinear coefficients which are functionals of the loading. This is the subject of the next section.

1.4 Schapery's constitutive theory

The first hypothesis introduced by Schapery [88] is to suppose that there is no longer a linear relationship between $-\frac{\partial G}{\partial \boldsymbol{\xi}}$ and $\dot{\boldsymbol{\xi}}$ as in equation (1.8). Instead, he introduces:

$$-\frac{\partial G}{\partial \boldsymbol{\xi}} = a_1 \mathbf{B} : \dot{\boldsymbol{\xi}} \tag{1.33}$$

where $a_1 = a_1(\boldsymbol{\sigma})$ and $\mathbf{B}$ is symmetric and positive semi-definite. The second law of thermodynamics imposes that $a_1 \geq 0$ (see equations (1.7,1.8)). The other hypothesis is that:

$$\mathbf{Y} = a_2 \mathbf{Z} \tag{1.34}$$

[5]Typically, an internal variable represents an internal phenomenon. The question of a continuum set of internal variables sends us to the debate of Democritus and Aristotle on the matter. Of course, if we assume that there is a finite amount, even gigantic, of indivisible particles in a volume of material, there will be a finite amount of phenomena, and hence, a finite amount of internal variables. Physically, we can interpret a continuum set of internal variables as an approximation of a very large set of internal variables.

where $a_2 = a_2(\boldsymbol{\sigma}) \geq 0$ and $\mathbf{Z} \geq 0$ for thermodynamic stability. a_2 can be interpreted as a correction in the Gibbs free energy so that it is valid for a wider range of $\boldsymbol{\sigma}$. With these functions introduced, the set of differential equations required to identify $\boldsymbol{\xi}$ becomes:

$$\frac{a_1}{a_2}\mathbf{B} : \dot{\boldsymbol{\xi}} + \mathbf{Z} : \boldsymbol{\xi} = -\frac{\boldsymbol{\rho}}{a_2} \tag{1.35}$$

He introduced the reduced time defined by:

$$\psi = \int_0^t \frac{a_2(\boldsymbol{\sigma}(t'))}{a_1(\boldsymbol{\sigma}(t'))}\mathrm{d}t' \tag{1.36}$$

Equation (1.35) becomes:

$$\mathbf{B} : \frac{\mathrm{d}\tilde{\boldsymbol{\xi}}(\psi)}{\mathrm{d}\psi} + \mathbf{Z} : \tilde{\boldsymbol{\xi}}(\psi) = -\frac{\tilde{\boldsymbol{\rho}}(\psi)}{\tilde{a}_2(\psi)} \tag{1.37}$$

where $\tilde{\boldsymbol{\xi}}(\psi) = \boldsymbol{\xi}(t)$, $\tilde{\boldsymbol{\rho}}(\psi) = \boldsymbol{\rho}(t)$ and $\tilde{a}_2(\psi) = a_2(t)$. This is a set of differential equations with respect to ψ. The solution of this system, as before, is:

$$\tilde{\xi}_m(\psi) = -\frac{1}{\mathrm{Z}_m}\int_0^{\psi}(1 - \exp\left[-\lambda_m(\psi - \psi')\right])\frac{\mathrm{d}}{\mathrm{d}\psi'}\left(\frac{\tilde{\rho}_m}{\tilde{a}_2}\right)\mathrm{d}\psi' \tag{1.38}$$

which is equivalent to:

$$\xi_m(t) = -\frac{1}{\mathrm{Z}_m}\int_0^{t}(1 - \exp\left[-\lambda_m(\psi - \psi')\right])\frac{\mathrm{d}}{\mathrm{d}\tau}\left(\frac{\rho_m}{a_2}\right)\mathrm{d}\tau \tag{1.39}$$

where:

$$\psi' = \int_0^{\tau} \frac{a_2(\boldsymbol{\sigma}(t'))}{a_1(\boldsymbol{\sigma}(t'))}\mathrm{d}t' \tag{1.40}$$

and $\lambda_m = \frac{\mathrm{Z}_m}{\mathrm{B}_m}$. Following the same line of thought, Schapery introduced the following nonlinear parameters:

$$\boldsymbol{\rho} = a_3\mathbf{T} : \boldsymbol{\sigma} \tag{1.41}$$

and

$$G_R = G_R(\boldsymbol{\sigma}) \tag{1.42}$$

This way, all the parameters in equation (1.14) are nonlinear. Therefore, the constitutive law (1.16) becomes:

$$\boldsymbol{\varepsilon}(t) = -\frac{\partial G_R}{\partial \boldsymbol{\sigma}} + \left(\frac{\partial a_3}{\partial \boldsymbol{\sigma}} \otimes \boldsymbol{\sigma} + a_3\mathbf{I}\right) : \int_0^t \boldsymbol{\Delta}\mathbf{S}(\psi - \psi') : \frac{\mathrm{d}}{\mathrm{d}\tau}\left(\frac{a_3}{a_2}\boldsymbol{\sigma}\right)\mathrm{d}\tau \tag{1.43}$$

where the definition (1.21) has been used.

Further restrictions must now be introduced. For example, $a_3 \geq 0$ and $\frac{\partial a_3}{\partial \boldsymbol{\sigma}} \otimes \boldsymbol{\sigma} \geq 0$ in order to avoid the case where a negative viscoelastic strain would be obtained when a positive stress history has been applied. We must also have $a_1(\mathbf{0}) = a_2(\mathbf{0}) = a_3(\mathbf{0}) = 1$ since the constitutive law is a linear viscoelastic law at small strains (i.e., close to the reference state). Finally, $-G_R$ can be interpreted as a nonlinear elastic potential and must meet the conditions enumerated in section 1.2.

In summary, Schapery's constitutive theory can be interpreted as an extension of the linear viscoelastic theory to a wider range of load intensity. The nonlinearity is introduced by scalar functions which is one of the simplest ways to incorporate stress dependency. However, if the nonlinearity was introduced by tensor quantities, which are functions of the stress history, anisotropic growth could be modelled by such a behaviour law. In addition, $\boldsymbol{\Delta}\mathbf{S}$ could be given a more general interpretation such as was done in equation (1.22). Plasticity [91] and damage [92] can also be introduced in the model by incorporating special hidden variables. It should be noted that we have not given any physical interpretation for the hidden variables and the nonlinearising parameters a_1, a_2 and a_3. However, we have seen that a_1 has a direct influence on the forces creating irreversibility in the material and a_3 could be interpreted as a stress concentrator. The constitutive law could be given a more physical interpretation and a better description of the evolution of such nonlinear parameters could be achieved if such interpretations were linked with real deformation mechanisms occuring inside the polymer. Such a study is beyond the scope of this thesis and we have to make some hypothesis regarding the evolution of such parameters. Since we do not link their evolution with physical phenomena, a general mathematical shape is given to these functions so that the constitutive law adequately reproduces experimental data. In addition, our polypropylene exhibits particular behaviour and the constitutive theory could be specialised so that it reproduces these particularities. This is explained in the next section.

1.5 Specialisation of the constitutive theory

Schapery's constitutive model has been used by many investigators but mainly for one dimensional applications. When equation (1.43) is specialised in one dimension we obtain the familiar constitutive law (in a slightly different

notation):

$$\begin{aligned} \varepsilon(t) &= g_0 D_0 \sigma(t) + g_1 \int_0^t \Delta D(\psi - \psi') \frac{\mathrm{d}g_2\sigma}{\mathrm{d}\tau} \mathrm{d}\tau \\ \text{with} \quad \psi - \psi' &= \int_\tau^t g_3 \mathrm{d}t' \end{aligned} \tag{1.44}$$

where the $g_i = g_i(\sigma(t))$. Some authors, like Lai and Bakker [49], Zhang *et al.* [104] and more recently Haj-Ali and Muliana [33] have developed a 3D representation of Schapery's constitutive equation. However, these authors used equation (1.44) as a starting point and introduced tensor quantities for the material properties and preserved the scalar g_i functions. Such an approach should be avoided since there is no guarantee that the resulting constitutive behaviour law still meets the thermodynamics restrictions. For example, for all these authors, the nonlinear elastic part of the behaviour law has a nonsymmetric tangent compliance and therefore is not a potential.

We recall that the a_i are functions of the stress tensor, but so far, we have not specified the shape of such functions. Many authors [33, 41, 49, 89, 104] have suggested using a quadratic function of the stress tensor. Of course, this function must be invariant by rotation (with respect to the symmetry axes of the material) since it is a material function and does not depend on the coordinate system used. For isotropy, the a_i must be functions of the first and second stress invariants (the third invariant is not used since we seek a quadratic function of the stresses, as a first approximation). The most commonly used function is the von Mises equivalent stress, $\sigma_e = \sqrt{\frac{3}{2}\boldsymbol{s} : \boldsymbol{s}}$ where $\boldsymbol{s}$ is the deviatoric stress tensor. It is well known that the hydrostatic pressure also has an effect on the mechanical response of polymers (see Hu *et al.* [41] for example). The way the first and second invariants of the stresses are combined should then appear in the behaviour law as material constants in order to take such effects into account.

In this study, we assume that our polypropylene is isotropic and the first two stress invariants are given by the classical relations:

$$\begin{aligned} I_1 &= \sigma_1 + \sigma_2 + \sigma_3 \\ I_2 &= \sigma_1\sigma_2 + \sigma_1\sigma_3 + \sigma_2\sigma_3 - \frac{1}{2}(\sigma_4^2 + \sigma_5^2 + \sigma_6^2) \end{aligned} \tag{1.45}$$

We would then seek the tensor $\mathbf{Q}^{(\mathbf{i})}$ such that:

$$h_i = \frac{1}{2}\boldsymbol{\sigma} : \mathbf{Q}^{(\mathbf{i})} : \boldsymbol{\sigma} = \theta^{(i)} I_1^2 + \zeta^{(i)} I_2 \tag{1.46}$$

where i refers to a particular a_i parameter and the scalars $\eta^{(i)}$ and $\zeta^{(i)}$ represent the contributions of I_1 and I_2 to the nonlinearity of the model. After

some algebraic manipulations, the non zero components of $\mathbf{Q^{(i)}}$ can be calculated:

$$\begin{gathered} \mathrm{Q}_{11}^{(\mathrm{i})} = \mathrm{Q}_{22}^{(\mathrm{i})} = \mathrm{Q}_{33}^{(\mathrm{i})} = \alpha_i \quad \text{and} \quad \mathrm{Q}_{44}^{(\mathrm{i})} = \mathrm{Q}_{55}^{(\mathrm{i})} = \mathrm{Q}_{66}^{(\mathrm{i})} = \alpha_i(1+\eta_i) \\ \text{and} \quad \mathrm{Q}_{12}^{(\mathrm{i})} = \mathrm{Q}_{23}^{(\mathrm{i})} = \mathrm{Q}_{13}^{(\mathrm{i})} = -\alpha_i\eta_i \end{gathered} \tag{1.47}$$

which is an isotropic tensor and where the $\alpha^{(i)}$ and $\eta^{(i)}$ can be seen as material constants. In this study, for simplicity, we have assumed that the a_i are functions of the same tensor $\mathbf{Q}$. It should be noted that a similar approach could be applied to any anisotropic material as was done by Schapery [91].

With this definition, we can see some restrictions that must be imposed on a_3. We have stated that :

$$\frac{\partial a_3}{\partial \boldsymbol{\sigma}} \otimes \boldsymbol{\sigma} = \frac{\partial a_3}{\partial h}\mathbf{Q} : \boldsymbol{\sigma} \otimes \boldsymbol{\sigma} \geq 0 \tag{1.48}$$

Since $\boldsymbol{\sigma} \otimes \boldsymbol{\sigma} \geq 0$ and $\mathbf{Q}$ is only definite for $\eta \in \left[-1, \frac{1}{2}\right]$ (and positive for $\alpha > 0$), then we must have:

$$\eta \in \left[-1, \frac{1}{2}\right] \quad , \quad \alpha > 0 \quad \text{and} \quad \frac{\partial a_3}{\partial h} \geq 0 \tag{1.49}$$

The next step is to define the potential $-G_R$. At this stage, any thermodynamically admissible shape of $-G_R$ could be possible. We have decided to use a shape of G_R that would lead to a nonlinear elastic law similar to the one dimensional case (see equation 1.44). If we define:

$$G_R = -\int_0^h g_0(h')\mathrm{d}h' \tag{1.50}$$

which leads to:

$$-\frac{\partial G_R}{\partial \boldsymbol{\sigma}} = -\frac{\partial G_R}{\partial h}\frac{\partial h}{\partial \boldsymbol{\sigma}} = g_0\mathbf{Q} : \boldsymbol{\sigma} \tag{1.51}$$

it can be observed that g_0 must be positive. In addition, if we calculate the tangent compliance we obtain:

$$\mathbf{S^{tgt}} = \frac{\partial g_0}{\partial h}\mathbf{Q} : \boldsymbol{\sigma} \otimes \boldsymbol{\sigma} : \mathbf{Q} + g_0\mathbf{Q} \tag{1.52}$$

and therefore $\frac{\partial g_0}{\partial h} \geq 0$. In that case, and in view of equation (1.47), the initial Poisson's ratio and Young's modulus (i.e., for $t = 0$ and $\boldsymbol{\sigma} = \mathbf{0}$) will determine η and α.

In this study, we will consider that $\boldsymbol{\sigma}(\tau) = \mathbf{0}$ for $\tau \leq 0$ and smooth stress histories (i.e., no jumps). This choice leads to considerable computational

simplifications and, by corollary, considering general stress histories does not pose any theoretical difficulties. Under this assumption, the integral (1.43) can be integrated by parts and leads to:

$$\boldsymbol{\varepsilon}(t) = g_0\mathbf{Q} : \boldsymbol{\sigma}(t) + \left(\frac{\partial g_1}{\partial \boldsymbol{\sigma}} \otimes \boldsymbol{\sigma} + g_1\mathbf{I}\right) : \int_0^t \boldsymbol{\Delta}\mathbf{S}'(\psi - \psi') : g_2\boldsymbol{\sigma}(\tau)\mathrm{d}\tau \quad (1.53)$$

where:

$$\begin{gathered}\boldsymbol{\Delta}\mathbf{S}'(t) = \sum_m \lambda_m \boldsymbol{\Delta}\mathbf{S}_m^v \left(1 - \exp[-\lambda_m t]\right) \quad \text{with} \quad \boldsymbol{\Delta}\mathbf{S}_m^v \geq 0\,, \\ g_2 = \frac{a_3}{a_1} \quad \text{and} \quad \psi - \psi' = \int_\tau^t g_3 \mathrm{d}t'\end{gathered} \quad (1.54)$$

which is a proper generalisation of the one dimensional model (1.44) and the classical notation for the nonlinearising functions has been used.

Of interest is the case where the material exhibits a constant ratio, for all times, between the axial and transverse strains during a uniaxial creep test. Such observation allows further simplifications to the constitutive law. The longitudinal and transverse strains are given by (where there is a sum over m):

$$\varepsilon_{11}(t) = g_0\alpha\sigma_{11} + \left(\frac{\partial g_1}{\partial h}\alpha\sigma_{11}^2 + g_1\right)\left[\alpha_m^{\Delta\mathrm{S}}(1 - \exp[-\lambda_m t])\right]\sigma_{11} \quad (1.55a)$$

$$\begin{aligned}\varepsilon_{22}(t) = &-g_0\alpha\eta\sigma_{11} - \frac{\partial g_1}{\partial h}\alpha\eta\sigma_{11}^2\left[\alpha_m^{\Delta\mathrm{S}}(1 - \exp[-\lambda_m t])\right]\sigma_{11} \\ &- g_1\eta_m^{\Delta\mathrm{S}}\alpha_m^{\Delta\mathrm{S}}(1 - \exp[-\lambda_m t])\end{aligned} \quad (1.55b)$$

where $\alpha_m^{\Delta\mathrm{S}}$ and $\eta_m^{\Delta\mathrm{S}}$ are the Young's modulus and Poisson's ratio of each $\boldsymbol{\Delta}\mathbf{S}_m^v$. Equations (1.55) show that if we set $\eta_m^{\Delta\mathrm{S}} = \nu$ then:

$$-\frac{\varepsilon_{22}(t)}{\varepsilon_{11}(t)} = \nu(t) = \nu \quad (1.56)$$

which is the result being sought. We have observed that our material, on a first approximation, exhibited such behaviour and this simplification is introduced in our constitutive law.

1.6 Summary

In summary, the constitutive law we will use for our material is the following:

$$\begin{aligned}\boldsymbol{\varepsilon}(t) = g_0(h(t))\mathbf{Q} : \boldsymbol{\sigma}(t) + \left(\frac{\partial g_1(h(t))}{\partial h(t)}\mathbf{Q} : \boldsymbol{\sigma}(t) \otimes \boldsymbol{\sigma}(t) + g_1(h(t))\mathbf{I}\right) : \\ \int_0^t \boldsymbol{\Delta}\tilde{\mathbf{S}}(\psi - \psi') : g_2(h(\tau))\boldsymbol{\sigma}(\tau)\mathrm{d}\tau\end{aligned} \quad (1.57)$$

with

$$\psi - \psi' = \int_\tau^t g_3(h(t'))\mathrm{d}t' \tag{1.58a}$$

$$\frac{\partial g_i}{\partial h} \geq 0 \quad \text{and} \quad g_j > 0 \quad \text{for} \quad i = 0, 1 \quad \text{and} \quad j = 0, 3 \tag{1.58b}$$

$$h(t) = \frac{1}{2}\boldsymbol{\sigma}(t) : \mathbf{Q} : \boldsymbol{\sigma}(t) \tag{1.58c}$$

$$\boldsymbol{\Delta}\tilde{\mathbf{S}}(t) = \mathbf{Q}\sum_m \alpha_m \lambda_m \exp[-\lambda_m t] \tag{1.58d}$$

$$\begin{gathered} \mathrm{Q}_{11} = \mathrm{Q}_{22} = \mathrm{Q}_{33} = \alpha \quad \text{and} \quad \mathrm{Q}_{12} = \mathrm{Q}_{23} = \mathrm{Q}_{13} = -\alpha\nu \\ \text{and} \quad \mathrm{Q}_{44} = \mathrm{Q}_{55} = \mathrm{Q}_{66} = \alpha(1+\nu) \end{gathered} \tag{1.58e}$$

where α is the initial uniaxial compliance and ν the Poisson's ratio. A experimental programme is now required in order to identify the four nonlinearising functions (i.e., the g_i), the number m of exponential terms in $\boldsymbol{\Delta}\tilde{\mathbf{S}}(t)$ and the α_m and λ_m, α and ν. In total, the programme must identify 4 functions and $2m + 2$ material constants. The objective of the next chapter is then to identify experimentally all these material parameters and functions.

An alternate presentation

Some authors present nonlinear viscoelastic behaviour laws in the following form:

$$\boldsymbol{\varepsilon} = \mathbf{S} : \boldsymbol{\sigma} + \boldsymbol{\varepsilon}^{\mathrm{ve}}(\boldsymbol{\sigma}, \boldsymbol{\xi}), \quad \dot{\boldsymbol{\xi}} = \boldsymbol{f}(\boldsymbol{\sigma}, \boldsymbol{\xi}) \tag{1.59}$$

where this time the set of differential equations for the evolution of internal variables is known. The material response at a time t_n is calculated by first solving $\boldsymbol{\xi}$ as a function of $\boldsymbol{\sigma}$ and then by introducing this result in $\boldsymbol{\varepsilon}^{\mathrm{ve}}$. In our case, we would have that:

$$\mathbf{S} = g_0\mathbf{Q} \tag{1.60a}$$

$$\boldsymbol{\varepsilon}^{\mathrm{ve}} = \left(\frac{\partial g_1}{\partial \boldsymbol{\sigma}} \otimes \boldsymbol{\sigma} + g_1\mathbf{I}\right) : \mathbf{T} : \boldsymbol{\xi} \tag{1.60b}$$

$$\boldsymbol{f}(\boldsymbol{\sigma}, \boldsymbol{\xi}) = -\frac{a_2}{a_1}\mathbf{B}^{-1} : \mathbf{Z} : \boldsymbol{\xi} - \frac{g_1}{a_1}\mathbf{B}^{-1} : \mathbf{T}^{\mathsf{T}} : \boldsymbol{\sigma} \tag{1.60c}$$

where a_1 and a_2 are related to g_2 and g_3 and $\mathbf{B}$, $\mathbf{Z}$ and $\mathbf{T}$ are related to $\mathbf{Q}$, α_m and λ_m. It would be theoretically possible to calculate $\boldsymbol{f}$ from our constitutive law but this is not done here since we do not use such a result in our development. Such an alternate representation is used in Chapter Three to describe some linearisation procedures.

Chapter 2

Identification of the Constitutive Law

2.1 Introduction

In the previous chapter we have developed a constitutive theory for a nonlinear viscoelastic material. Our task now is to identify all the nonlinearising parameters so that the behaviour law can be used in the homogenisation model. As mentioned in the last chapter, Schapery's one dimensional constitutive theory has been used by many investigators, each of them suggesting his own way to interpret and identify the various parameters.

All the approaches we present here have in common that the identification is performed on creep – recovery tests. A creep – recovery test is a test where the stress history (in one dimension) is given by:

$$\sigma(t) = \begin{cases} \sigma_n & \text{for } t \in [0, t_a] \\ 0 & \text{for } t > t_a \end{cases} \tag{2.1}$$

and its response is schematically illustrated in figure 2.1. In the remainder of this section, we consider a uniaxial behaviour law for simplicity and to present the previous contributions. We recall that the constitutive law in 1D is given by:

$$\begin{gathered} \varepsilon(t) = g_0 D_0 \sigma(t) + g_1 \int_0^t \Delta D(\psi - \psi') \frac{\mathrm{d} g_2 \sigma}{\mathrm{d}\tau} \mathrm{d}\tau \\ \text{with} \quad \psi - \psi' = \int_\tau^t g_3 \mathrm{d}t' \end{gathered} \tag{2.2}$$

In that case, we have that $h = \sigma$, where σ is the uniaxial stress applied. The idea is then to identify punctual values of the various g_i functions for a given

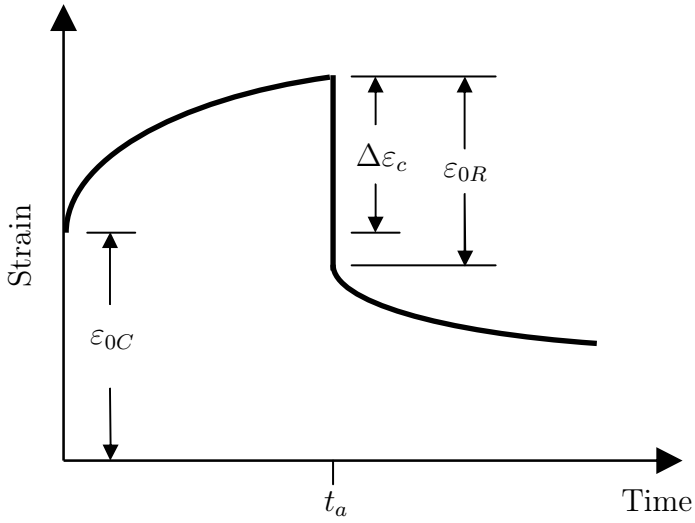


Figure 2.1: Schematic representation of the uniaxial strain evolution during a creep – recovery test

stress level. We denote by $g_i(\sigma_n)$ the value of a g_i function measured for a creep stress σ_n. Then, once enough data points are obtained, a curve is fitted or interpolated to obtain the other values of $g_i(\sigma)$, where $\sigma \neq \sigma_n$ for all n. Lou and Schapery [56] have shown that single creep tests are not sufficient to identify all the parameters, especially the g_1 function (see equation (1.57)). For this kind of loading, $g_1(\sigma_n)$ is given by [69]:

$$g_1(\sigma_n) = \frac{\Delta\varepsilon_c}{\Delta\varepsilon_c + \varepsilon_{0C} - \varepsilon_{0R}} \tag{2.3}$$

where it is obvious that a recovery test is necessary to measure its value. Such uniaxial creep experiments were conducted to identify one-dimensional as well as three-dimensional isotropic constitutive laws.

The main difference between the various identification approaches lies in the way the data reduction is accomplished in order to obtain the values of the $g_i(\sigma_n)$. Initially, Schapery [89] and Lou and Schapery [56] proposed a method where the creep and recovery curves, for each σ_n, are shifted to form a master curve. From this curve, and by assuming that ΔD is a power law, the parameters of ΔD as well as the $g_1(\sigma_n)$ and $g_3(\sigma_n)$ can be identified. The parameters of ΔD are chosen so that they best fit the master curve and $g_1(\sigma_n)$ and $g_3(\sigma_n)$ are related to the horizontal and vertical shift of their corresponding curves. $g_0(\sigma_n)$ and the initial compliance are identified by the instantaneous response of the material and $g_2(\sigma_n)$ can be identified by algebraic manipulation.

Other investigators [41, 48, 64, 69, 101, 103, 104] used a different approach. In most cases, the linear parameters (i.e., the initial compliance and ΔD) were identified from the test performed at a low stress level alone. Then, for each creep–recovery test, taken independently, a nonlinear least squares approach and some algebraic manipulations were used to identify all the $g_i(\sigma_n)$ parameters.

Such approaches have some disadvantages. The first of them is that they use creep – recovery tests to identify the various parameters. Ideal tests are almost impossible to realise in practice since it is very difficult to impose an instantaneous stress with a conventional tension machine. For example, the command given to the machine can cause the load to oveshoot σ_n (i.e., the creep stress) before reaching a stable value. Moreover, Lee and Knauss [52] have shown that, for a linear viscoelastic material, there can be a 10% difference between the real response and the idealised response of the material for short time after the application of the load. They obtained this result by theoretically calculating the initial response of a viscoelastic material to an instantaneous stress application and a load history where the stress is applied from 0 to σ_n at a constant stress rate. Therefore, one can obtain important measurement errors when identifying quantities such as $g_0(\sigma_n)$ by using the initial response (ε_{0C} on figure 2.1) or $g_1(\sigma_n)$ with equation (2.3). In addition, at low stress levels, it might be difficult to accurately measure the recovery strains since they tend towards zero as time increases. Investigators such as Zhang *et al.* [104] had to develop a method estimating the thermal drift of strain gauges in order to estimate the small recovery strains.

The second disadvantage comes from measuring the different values of the $g_i(\sigma_n)$ by a nonlinear least squares method by considering creep–recovery tests independently. By doing so, it is possible that, from one stress level to the other, the various $g_i(\sigma_n)$ oscillate as a function of σ. For example, consider figure 2.2 where $\frac{1}{g_3(\sigma)}$ is plotted by Lai and Bakker [48] as a function of the uniaxial stress σ. The tick marks represent the σ_n while the plain line represents an interpolation between the data points. It was shown in the last chapter that the only thermodynamic restriction imposed on g_3 is that it should be positive. In that sense, there is nothing wrong with the data plotted in figure 2.2. If we assume that $\Delta D(t) = \alpha_m(1 - \exp[-t\lambda_m])$, when g_3 increases, the term $1 - \exp[-t\lambda_m g_3]$ tends towards 1 more quickly. g_3 can then be seen as the parameter which controls the viscoelasticity in the model since a large value of g_3 forces ΔD to tend towards 1. Figure 2.2 shows that g_3 decreases for low stresses and begins to increase at moderate stresses, or alternatively, is more viscoelastic at low stresses than at large stresses. However, the experimental results of Lai and Bakker [48] show that the

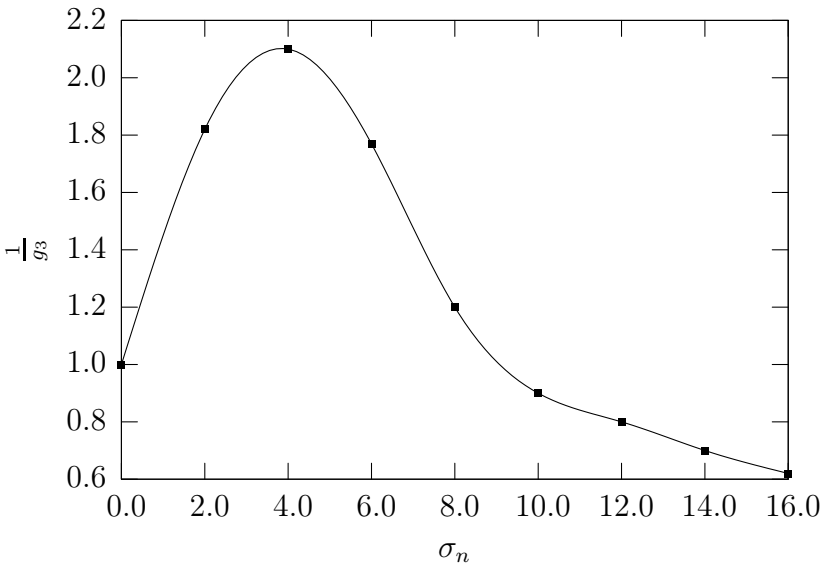


Figure 2.2: Values of $\frac{1}{g_3}$ calculed by Lai and Bakker [48] for creep–recovery tests treated individually

creep–recovery curves present more important nonlinearities as σ_n increases, which is an opposite tendency. Therefore, the other nonlinearising functions must compensate for the nonlinearity reduction induced by an increasing g_3. It should be noted that results like those shown on figure 2.2 could have been obtained for the other functions since the authors did not include any constraints in their nonlinear least squares calculation of the $g_i(\sigma_n)$. In particular, results like those in figure 2.2 could have been obtained for $g_1(\sigma_n)$. Such results would not be physically reasonable since $\frac{\partial g_1}{\partial \sigma} < 0$ for some values of σ (see section 1.4). In addition, when performing unconstrained least squares error minimisation, it is possible to obtain many sets of $g_i(\sigma_n)$ that would lead to neighbouring minima. Choosing the lowest minimum might not be the most advisable solution since a slightly higher minimum can lead to graphically acceptable results while leading to $g_i(\sigma_n)$ having a physical sense.

One other drawback of using the creep tests independently to identify the constitutive law comes from the identification of the linear parameters. At low stresses, it is possible to find a linear viscoelastic law which fits the data very well. Once the values of these linear parameters are fixed, it might be difficult to find a set of parameters which fit the data well for these high stress levels. The approach suggested by Schapery [89] and Lou and Schapery [56] avoids such difficulty since it uses all the tests to form a master curve.

In light of such observations, our task is now to establish a procedure to

identify the parameters and functions of our constitutive law. The procedure should be such that it meets the following requirements:

1. Precise measurement of the strains.
2. Accurate application of the load history.
3. Identification of the linear, as well as the nonlinear parameters, is both reasonable thermodynamically and physically.
4. All the data available is used to simultaneously identify all the parameters and nonlinear functions.

The following two sections present the methodology we have used to address these issues.

2.2 Choice of the load history(ies)

We recall, from the previous chapter, that the constitutive theory used in this study is based on a Taylor expansion of Gibbs free energy. The constitutive relation will be valid as long as there is no sudden large change in the microstructure, such as large cracks, important damage, etc[1]. In addition, our behaviour law does not take into account plasticity/viscoplasticity. Therefore, the obvious step before selecting a load history for the identification of the constitutive law is to estimate its approximate validity domain. We insist on this being an approximation since it is quite difficult to measure accurately the onset of damage, plasticity, etc., as we do not have clear or well defined criteria for these internal phenomena. In order to perform this task, we limited ourselves to macroscopic tensile tests. The validity domain was determined by performing a test where a load history up to a certain stress level is applied and the material is allowed to recover for a given period of time. If after this time there is a residual strain, we assume that we are outside the validity domain of the constitutive law. The procedure is repeated until we no longer observe any residual strains.

We also recall from Chapter One that the constitutive law has a linear viscoelastic domain. Denote by $\varepsilon_L^r(t)$ the strain history resulting from the application of a particular stress history $\sigma_L^r(t)$. The material has this linear viscoelastic property if, and only if, the following two conditions are satisfied [90]:

[1]It should be noted that Schapery [92] has suggested a constitutive relation where growing damage can be taken into consideration.

1. Proportionality:

$$\beta\varepsilon_L^0(t) = \varepsilon_L^1(t) \quad \text{with} \quad \beta\sigma_L^0(t) = \sigma_L^1(t) \quad \text{and} \quad \beta = \text{constant} \tag{2.4}$$

2. Superposition:

$$\varepsilon_L^2(t) = \varepsilon_L^0(t) + \varepsilon_L^1(t) \quad \text{with} \quad \sigma_L^2(t) = \sigma_L^0(t) + \sigma_L^1(t) \tag{2.5}$$

In this study, we assume that the material is linear viscoelastic when the proportionality condition is met (i.e. we did not check the superposition property). This property can easily be checked by first imposing a stress history at a very low level (while allowing precise measurement of the strain), say $\sigma_L^0(t)$. Then, apply a loading $\sigma_L^1 = \beta^1\sigma_L^0(t)$. If $\frac{\varepsilon_L^1(t)}{\varepsilon_L^0(t)} = \beta^1$ then the material is still in the linear viscoelastic range. β^i is increased until this relationship is not met.

Now let's turn to the stress history applied when identifying the parameters and functions of the constitutive law. We recall that our material is assumed to be isotropic. In addition, we identify the parameters and the functions with uniaxial tensile tests where the force is applied and the strains are measured in the axial and transverse directions. The stress is calculated with the initial cross section of the specimen and it was checked subsequently that this did not induce a true stress larger than 2% of this nominal stress. Therefore, in this chapter, σ should be interpreted as σ_{11}.

One of the first requirements for the load history is that the strains induced by the stress history can be measured with good accuracy. Therefore, the stress history should not be composed of segments where we impose $\sigma = 0$ for a certain duration so that we obtain strains of a measurable magnitude. The other requirement is that the tensile machine reproduces the force history we demand with good accuracy. Therefore, we exclude step changes in stress. We have chosen to create a load history composed of stress ramps at constant force rate[2] and constant force. In addition, the load history must include loading and unloading to identify all of the nonlinearising parameters. Such a history is also consistent with the work of Lockett [55] (see equation (1.2)) where the nonlinear functional is identified by a loading which presents variations with respect to time.

Figure 2.3 illustrates the typical load history we have chosen to identify the constitutive law. The stress magnitude ranges over the validity domain

[2]It was not possible to enforce a constant stress rate to our machine since it would have required a real time correction for the specimen's changing cross section. We did not have access to such equipment.

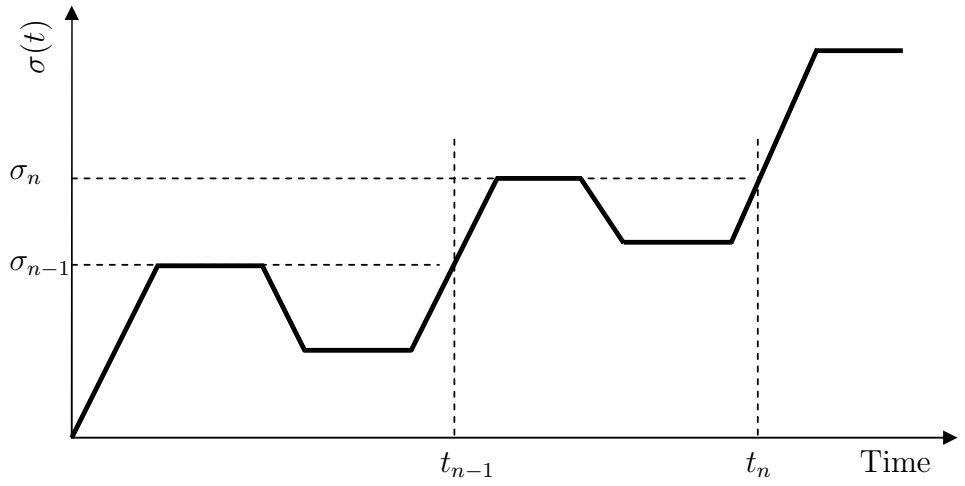


Figure 2.3: Typical stress history used to identify the constitutive law

of the behaviour law. Such a continuous stress history requires that we define a continuous expression for the g_i. Since the shape of the g_i is not known *a priori*, we will interpolate the functions between two values of g_i (this is detailed in the next section). We define as a *segment* the stress history varying from σ_{n-1} to σ_n for t varying from t_{n-1} to t_n (see figure 2.3). Therefore, we assume that the interpolation parameters are constant in a given segment. Such representation has the advantage of including the entire stress range and if the shape of the behaviour law we have chosen is the material's real behaviour law, only one test would be required to identify all the parameters. Of course, using more segments to reach the maximum stress in the validity domain leads to a more precise description of the g_i.

2.3 Data reduction procedure

2.3.1 Definition of the problem

Now that we have defined the applied stress history, we must develop the data reduction procedure leading to the relevant identification of the nonlinear viscoelastic behaviour law. We recall here our behaviour law:

$$\begin{aligned}\boldsymbol{\varepsilon}(t) = g_0(h(t))\mathbf{Q} : \boldsymbol{\sigma}(t) + \left(\frac{\partial g_1(h(t))}{\partial h(t)}\mathbf{Q} : \boldsymbol{\sigma}(t) \otimes \boldsymbol{\sigma}(t) + g_1(h(t))\mathbf{I}\right) : \\ \int_0^t \boldsymbol{\Delta}\tilde{\mathbf{S}}(\psi - \psi') : g_2(h(\tau))\boldsymbol{\sigma}(\tau)\mathrm{d}\tau\end{aligned} \tag{2.6}$$

Now define by $\hat{\boldsymbol{\varepsilon}}$ the strain *predicted* by equation 2.6 when the stress history depicted in figure 2.3 is applied and $\tilde{\boldsymbol{\varepsilon}}$ the *measured* strain obtained for the same stress history. Then, our objective here is to solve the following problem:

$$\inf_{\boldsymbol{p}\in\boldsymbol{\mathcal{Q}}} \sum_{b=1}^{B} \left([\hat{\boldsymbol{\varepsilon}}(t_b) - \tilde{\boldsymbol{\varepsilon}}(t_b)] : [\hat{\boldsymbol{\varepsilon}}(t_b) - \tilde{\boldsymbol{\varepsilon}}(t_b)] \right) \tag{2.7}$$

where $\boldsymbol{p}$ is the set of material parameters included in $\boldsymbol{\mathcal{Q}}$ which is the group of all $\boldsymbol{p}$ leading to a thermodynamically and physically admissible constitutive law, t_b is a time at which the strain is measured and B is the number of data points. This is a constrained least square minimisation problem. Since we apply a tensile stress, this equation becomes:

$$\inf_{\boldsymbol{p}\in\boldsymbol{\mathcal{Q}}} \sum_{b=1}^{B} \left([\hat{\varepsilon}_{11}(t_b) - \tilde{\varepsilon}_{11}(t_b)]^2 + 2\,[\hat{\varepsilon}_{22}(t_b) - \tilde{\varepsilon}_{22}(t_b)]^2 \right) \tag{2.8}$$

where we have assumed that our material is isotropic. The experimental results we have obtained have shown us that the material exhibited a relatively constant Poisson's ratio (in the sense of our equation (1.56)) with respect to time (within 4%). We have seen in Chapter One that this is modelled with our behaviour law. Therefore, our problem is considerably simpler and leads to:

$$\inf_{\boldsymbol{p}\in\boldsymbol{\mathcal{Q}}} \sum_{b=1}^{B} \left([\hat{\varepsilon}_{11}(t_b) - \tilde{\varepsilon}_{11}(t_b)]^2 \right) \tag{2.9}$$

We must now recall the conditions that $\boldsymbol{p}$ must meet so that it leads to a thermodynamically and physically admissible material.

We have seen in Chapter One that the tensor $\mathbf{Q}$ is isotropic and we defined it as a function of an intial compliance α and a Poisson's ratio ν. We have seen previously that ν is in fact the Poisson's ratio of the material and we assume for now that this value has been measured. Since $\mathbf{Q}$ must be positive definite, we must have that $\alpha > 0$. We have also seen that (see equation 1.58d)) $\boldsymbol{\Delta}\tilde{\mathbf{S}}$ is defined with $\mathbf{Q}$ and with the strictly positive scalars α_m and λ_m. We recall that the nonlinearising functions g_i must be positive and that $\frac{\partial g_i}{\partial h} \geq 0$ for $i = 0, 1$. We also have, for this specific loading, that $h = \frac{1}{2}\alpha\sigma^2$.

We must now specify the evolution of the g_i functions. Except for g_1, we have used a linear interpolation between two values of h for these functions. We have seen that our stress history is divided into segments and we denote by $h_{n-1} = \frac{1}{2}\alpha\sigma_{n-1}^2$ and $h_n = \frac{1}{2}\alpha\sigma_n^2$ the values of h at the beginning and at the end of a given segment. So, within a segment n, we have expressed these

functions as:

$$\begin{aligned} g_i(h) &= 1 + \sum_{s=1}^{n-1} \Delta g_i(h_s) + \frac{h - h_{n-1}}{h_n - h_{n-1}} \Delta g_i(h_n) \\ &= 1 + \sum_{s=1}^{n-1} \Delta g_i(h_s) + \frac{\sigma^2 - \sigma_{n-1}^2}{\sigma_n^2 - \sigma_{n-1}^2} \Delta g_i(h_n) \end{aligned} \tag{2.10}$$

where $\Delta g_i(h_n)$ is a variation of g_i during a given segment n. These $\Delta g_i(h_s)$ are in fact the unknowns of the problem and are the quantities to be optimised. Figure 2.4(a) illustrates the evolution of these g_i functions. We can see from such relation that α has disappeared.

Now we turn to g_1. Since the slope of g_1 appears explicitly in the behaviour law, using a linear interpolation can lead to discontinuities in the strains when we move from one segment to the next. To avoid such a problem, we have to use a quadratic expression for g_1 and enforce that the slope as well as the value of g_1 is continuous at the σ_n. Therefore, we introduce (within a segment):

$$g_1(h) = A_n(h - h_{n-1})^2 + B_n(h - h_{n-1}) + C_n \tag{2.11}$$

where:

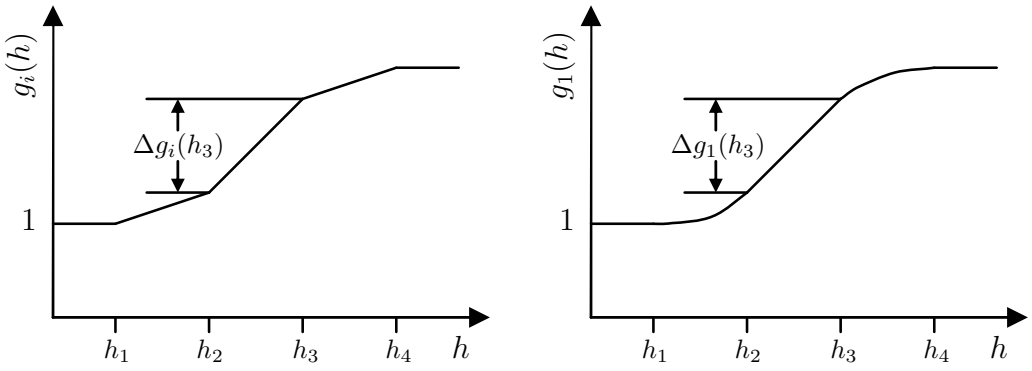
$$\begin{aligned} C_n &= 1 + \sum_{s=1}^{n-1} \Delta g_1(h_s) \\ B_n &= \sum_{s=1}^{n-1} 2B_s(h_s - h_{s-1}) \\ A_n &= \frac{\Delta g_1(h_n) - B_n(h_n - h_{n-1})}{(h_n - h_{n-1})^2} \end{aligned} \tag{2.12}$$

Figure 2.4(b) illustrates the evolution of g_1. Unlike the other functions, the parameter α must appear in the definition of g_1.

We have now defined our problem and the variables we have to optimise, namely α, the α_m, λ_m, M the number of m terms and the $\Delta g_i(h_n)$ as well as the continuous expressions for these functions. We must now solve this nonlinear constrained optimisation problem.

2.3.2 Procedure for calculating the material parameters

The optimisation problem we have to solve is difficult and we must relax some of the constraints in order to solve it. First of all, we have set the time validity domain of our constitutive law to 5500 seconds. We have decided to use



(a) g_0, g_2 and g_3 as a function of h (b) g_1 as a function of h

Figure 2.4: Examples of absolutely increasing g_i as a function of h

$M = 5$ and distribute the λ_m as follows: $\frac{1}{100}, \frac{1}{10^{2.5}}, \frac{1}{1000}, \frac{1}{10^{3.5}}, \frac{1}{10000}$. Nonlinear constrained optimisation problems are difficult to solve and we introduce a modification to the problem, through a relevant change of variables, so that the problem becomes a nonlinear unconstrained problem. For example, to set $\alpha > 0$, we introduce $\alpha = x^2$ and now, the optimisation variable becomes x. Similarly, we introduce $\alpha_m = \left(x_m^{(4)}\right)^2$.

We have seen that the slopes of g_0 and g_1 must be positive. Therefore, the $\Delta g_0(h_n)$ and $\Delta g_1(h_n)$ must be positive. We introduce $\Delta g_0(h_n) = \left(x_n^{(0)}\right)^2$ and $\Delta g_1(h_n) = \left(x_n^{(1)}\right)^2$.

Now, let's turn to the case of g_2 and g_3. The only restriction on these functions is that they must be positive. However, we introduce a physically reasonable hypothesis that these functions should be either always increasing or always decreasing. The first condition is imposed as before by setting $\Delta g_2(h_n) = \left(x_n^{(2)}\right)^2$ and $\Delta g_3(h_n) = \left(x_n^{(3)}\right)^2$. The second condition is imposed by setting $\Delta g_2(h_n) = \frac{1}{2}\left(1 - \sum_{s=1}^{n-1} \Delta g_2(h_s)\right)\left(1 - \cos x_n^{(2)}\right)$ and $\Delta g_3(h_n) = \frac{1}{2}\left(1 - \sum_{s=1}^{n-1} \Delta g_3(h_s)\right)\left(1 - \cos x_n^{(3)}\right)$. This enforces that the next variation of g_2 or g_3 is between 0 and the current value of g_2 and g_3.

If we summarise, our new optimisation problem now becomes:

$$\inf_{x, x_m^{(4)}, x_n^{(i)}} \sum_{s=1}^{S} \left([\hat{\varepsilon}_{11}(t_s) - \tilde{\varepsilon}_{11}(t_s)]^2 \right) \tag{2.13}$$

which is an unconstrained nonlinear optimisation problem. We will have $1 + M + 4N$ variables to optimise, where N is the total number of segments

and M the number of exponential terms defining $\boldsymbol{\Delta}\tilde{\mathbf{S}}$. In this study, we used 4 segments to determine our constitutive law parameters and $M = 5$. However, we know that there is a range over which the $g_i = 1$. We have chosen our first segment to be in this range, which implies that $x_1^{(i)} = 0$. Therefore, for our specific case, we have 18 unknowns to optimise.

We have seen that we have some freedom on the evolution of g_2 and g_3. Since these functions can exhibit two different behaviours, this leads to four possible combinations. Therefore, we will define 4 different expressions of $\hat{\varepsilon}_{11}(t)$ with the following variable change:

$$\begin{gathered}\alpha = x^2,\ \alpha_m = \left(x_m^{(4)}\right)^2,\ \Delta g_0(h_n) = \left(x_n^{(0)}\right)^2,\ \Delta g_1(h_n) = \left(x_n^{(1)}\right)^2,\\ \Delta g_2(h_n) = \left(x_n^{(2)}\right)^2,\\ \Delta g_3(h_n) = \left(x_n^{(3)}\right)^2\end{gathered} \tag{2.14a}$$

$$\begin{gathered}\alpha = x^2,\ \alpha_m = \left(x_m^{(4)}\right)^2,\ \Delta g_0(h_n) = \left(x_n^{(0)}\right)^2,\ \Delta g_1(h_n) = \left(x_n^{(1)}\right)^2,\\ \Delta g_2(h_n) = \frac{1}{2}\left(1 - \sum_{s=1}^{n-1} \Delta g_2(h_s)\right)\left(1 - \cos x_n^{(2)}\right),\\ \Delta g_3(h_n) = \left(x_n^{(3)}\right)^2\end{gathered} \tag{2.14b}$$

$$\begin{gathered}\alpha = x^2,\ \alpha_m = \left(x_m^{(4)}\right)^2,\ \Delta g_0(h_n) = \left(x_n^{(0)}\right)^2,\ \Delta g_1(h_n) = \left(x_n^{(1)}\right)^2,\\ \Delta g_2(h_n) = \left(x_n^{(2)}\right)^2,\\ \Delta g_3(h_n) = \frac{1}{2}\left(1 - \sum_{s=1}^{n-1} \Delta g_3(h_s)\right)\left(1 - \cos x_n^{(3)}\right)\end{gathered} \tag{2.14c}$$

$$\begin{gathered}\alpha = x^2,\ \alpha_m = \left(x_m^{(4)}\right)^2,\ \Delta g_0(h_n) = \left(x_n^{(0)}\right)^2,\ \Delta g_1(h_n) = \left(x_n^{(1)}\right)^2,\\ \Delta g_2(h_n) = \frac{1}{2}\left(1 - \sum_{s=1}^{n-1} \Delta g_2(h_s)\right)\left(1 - \cos x_n^{(2)}\right),\\ \Delta g_3(h_n) = \frac{1}{2}\left(1 - \sum_{s=1}^{n-1} \Delta g_3(h_s)\right)\left(1 - \cos x_n^{(3)}\right)\end{gathered} \tag{2.14d}$$

So, to obtain one expression of $\hat{\varepsilon}_{11}(t)$, we picked one of the variable change enumerated previously. Then, we used these in the definition of $\mathbf{Q}$, $\boldsymbol{\Delta}\tilde{\mathbf{S}}$ and the g_i functions defined by equations (2.10,2.11). This way, we have an analytical representation of the constitutive law where the parameters to be optimised appear explicitly. Then, the next step is to define an expression for $\hat{\varepsilon}_{11}(t)$. It should be noted that we have observed that the material became more compliant as the stress level increased. This would suggest that the

change of variables enumerated at equation (2.14c) is appropriate since the evolution of all the nonlinear parameters induce such a tendency. This is the variable change we have tried first. Since it led to very good results, we did not implement the other possibilities.

Since the load history is complex, it is almost impossible to obtain an analytical expression for $\hat{\varepsilon}_{11}(t)$. One alternative would be to develop a numerical integration scheme for such function. Then, we would have to implement a minimisation algorithm to solve problem (2.13). Rather than following this approach, we have used the symbolic calculation capacities of Mathematica and used the various minimisation algorithms implemented in the package. This way, we could try many different algorithms and select the most appropriate by trial and error. Since the loading is composed of relatively simple load histories, the integration of the constitutive law did not pose difficulties. It should be noted, however, that during the loading and unloading, we had to integrate a function of the type: $f(\tau) = \exp[a + b\tau + c\tau^2](d + e\tau + f\tau^2 + z\tau^3)$ due to the definition of ψ (see equation (1.58a)) and g_3. Such integration involves the *error function*, which is a numerical function.

Once we defined $\hat{\varepsilon}_{11}(t)$ and we had $\tilde{\varepsilon}_{11}(t_s)$, we could obtain an analytical expression for equation (2.13). Then, the Nelder–Mead algorithm implemented in Mathematica was used for the minimisation.

Summary

If we summarise, we have determined a stress history which allows precise measurement of the strains and an adequate load application. We have defined a minimisation problem which must be solved in order to obtain a constitutive law which matches the experimental response of the material. Then, we stated that the constitutive law parameters should lead to a physically and thermodynamically admissible constitutive law. We defined these conditions and it lead to a nonlinear constrained minimisation problem. Then, we specified the shape of the nonlinearising functions so that they are interpolated between control points. We then modified our minimisation problem, with a relevant change of variables, so that it becomes unconstrained. Next, we showed how we obtained an analytical expression of the quantity to be minimised in the commercial package Mathematica. We have seen that we can have four different physically reasonable behaviour laws and this define four different functions which must be minimised. In theory, this satisfies our objective to define a data reduction procedure which allows all the material parameters to be identified in one test while enforcing that the behaviour law meets the conditions we have imposed. We must now identify the nonlinear parameters and then validate the identification on a different load history.

This is the subject of the following sections.

2.4 Identifying the Constitutive Law Parameters

2.4.1 Experimental details

Material

Specimens used in this study were cut from plates manufactured by injection molding. The polypropylene (semi-crystalline) was supplied by the company RTP under the grade RTP100 and is a homopolymer. The plates were injected by a center gate oriented perpendicular to the plate. All the specimens were water jet cut from the plates.

Equipment

Classical tension tests were performed with an Instron 5581 machine using self-tightening grips. The specimens were cut according to the ASTM D 638 standard. Strains were measured with a knife edged extensometer to identify the validity domain and with strain gauges rosettes to determine the parameters. For the identification of the parameters and the validity domain, alignment of the specimen was checked by applying a small load and using a digital image correlation code to measure the strain field. If the strain field was that usually obtained for a tension test, the specimen was clamped rigidly. If not, the specimen position was corrected until an acceptable strain field was obtained. The load was introduced by force control by assuming that the specimen cross section remained constant throughout the test.

2.4.2 Determination of the constitutive law validity domain

Determination of the linear viscoelastic domain

The linear viscoelastic domain of the material has been determined by applying the load histories depicted in figure 2.5.

As can be seen, the stress was ramped at a constant stress rate from 0 to σ_i, maintained at this level and unloaded to zero and maintained at zero. The subscript i refers to the magnitude in MPa of the holding stress. The minimum stress applied was 3 MPa and it is assumed that the material is linear viscoelastic for stress magnitudes below this level. It was found that

$\frac{3}{5}\varepsilon_5(t)$ superimposed very well with $\varepsilon_3(t)$. It was found that scaling ε_7 by $\frac{2.75}{7} \sim \frac{3}{7}$ led to an acceptable strain history superposition (see figure 2.5). This value lies within 8.33% of the theoretical value. Therefore, we assume that our material is well approximated by a linear viscoelastic model up to 7 MPa. It should be noted that only one test run was performed per σ_i level due to the limited amount of specimens available.

Determination of the viscoelastic domain

The viscoelastic domain has been established by classical tensile tests. The stress histories applied for the macroscopic tests were ramps from 0 to σ_{max} at a constant stress rate of 0.03 MPa/sec followed by an unloading to 0 MPa at the same stress rate and maintained at 0 MPa for up to 6 hours. It was found that the strains were recovered for the test where $\sigma_{max} = 20\,\text{MPa}$ while there was still a residual strain for the test where $\sigma_{max} = 25\,\text{MPa}$. This suggests that the material is viscoelastic up to 20 MPa and therefore, we assume that our constitutive law is valid up to 20 MPa. It should be noted that only one test run was performed per maximum stress level due to the limited amount of specimens available.

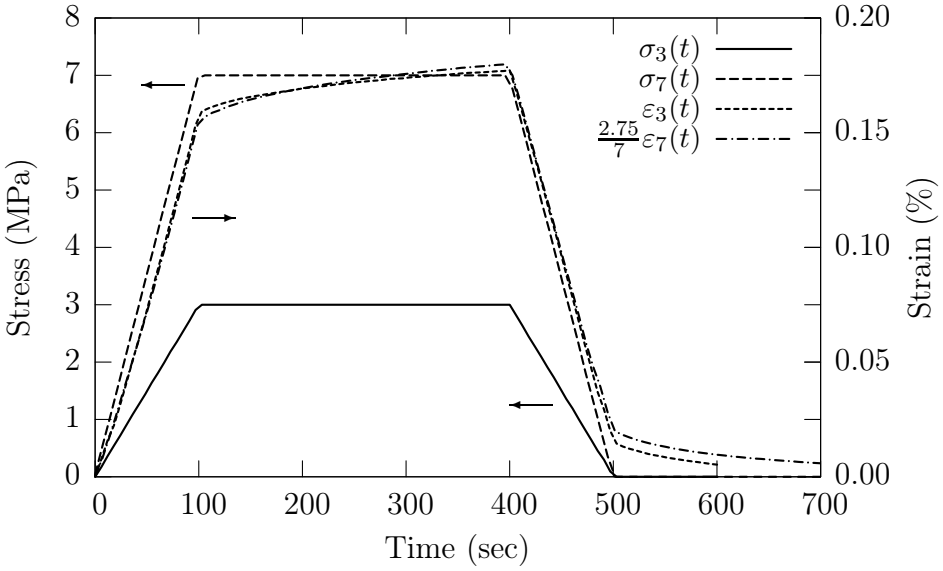


Figure 2.5: Stress histories and material responses used to determine the linear viscoelasticity domain of the polypropylene

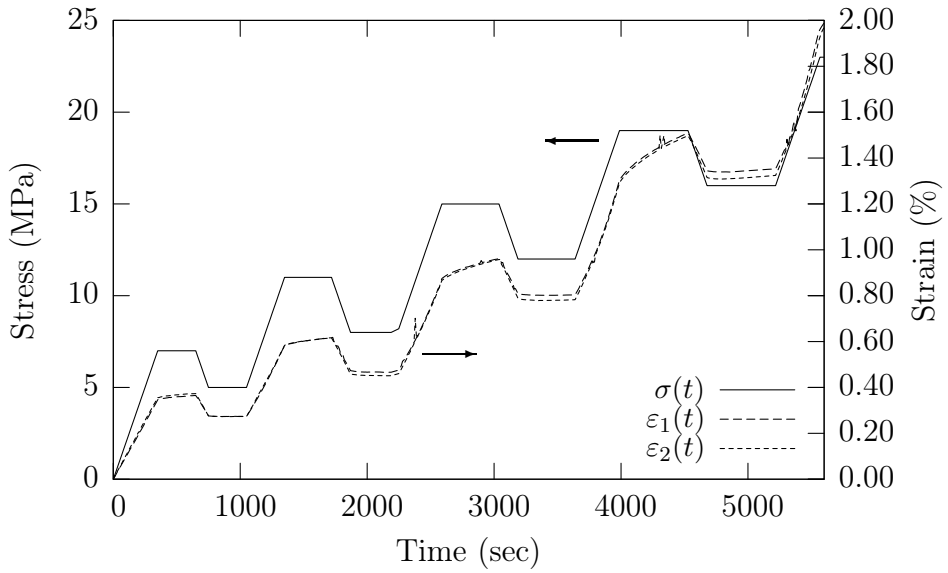


Figure 2.6: Stress history ($\sigma(t)$) and material's response ($\varepsilon_1(t)$ and $\varepsilon_2(t)$) used for the identification of the material's parameters

2.4.3 Determination of the material parameters

The material parameters were determined according to the procedure described previously. The stress history $\sigma(t)$ imposed on the material is plotted in figure 2.6. Two test runs, denoted $\varepsilon_1(t)$ and $\varepsilon_2(t)$, were performed and their responses are also plotted on figure 2.6. Only the axial strains are reported here since the material Poisson's ratio is approximately constant. As mentioned previously, the optimisation problem (2.13) was solved, for the change of variables described in equation (2.14c) by the Nelder-Mead algorithm implemented in Mathematica. The strain response of the material as predicted by the constitutive law with the optimal set of parameters is plotted in figure 2.7[3]. It can be observed that the model fits the data adequately over the range previously identified. It should be noted that the constitutive law was fitted to the average of the material responses plotted on figure 2.6. The numerical values for the various material parameters can be found in table 2.1. It was found that, when setting $g_3 = 1$, the numerical algorithm led to: $g_0(h) = g_1(h) \approx 1$ and $g_2(h)$ given by the function plotted in figure 2.8. We can see that, for low stresses and relatively short times, the material response is dominated by an elastic response due to the relatively small values of the α_m and λ_m. However, as the stress level increases (in the sense

[3]This curve was obtained by introducing the numerical values of the parameters and the functions thus identified in equations (1.57,1.58).

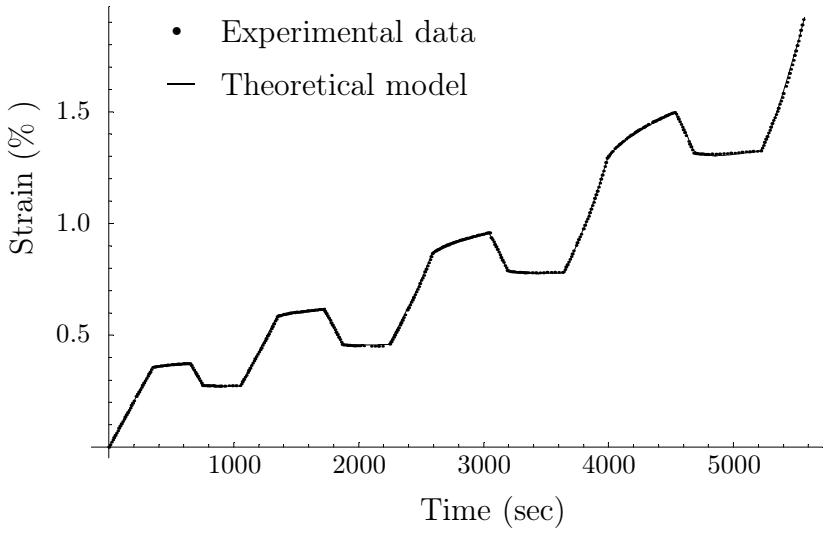


Figure 2.7: Experimental data and theoretical predictions of the constitutive law

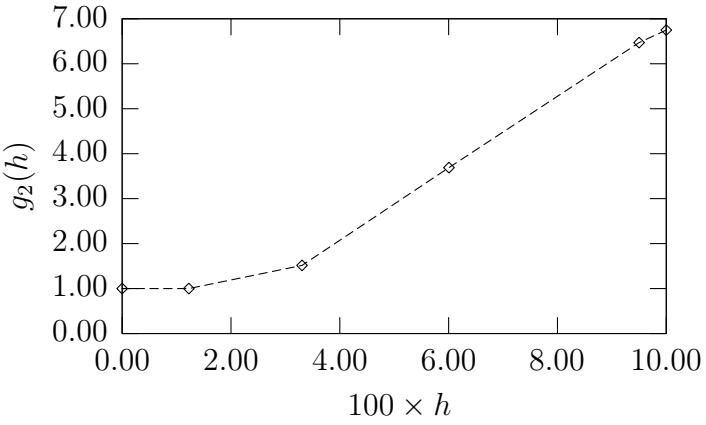


Figure 2.8: g_2 as a function of h for our material

α (MPa^{-1})	ν	λ_1	λ_2	λ_3
		$\frac{1}{100} sec^{-1}$	$\frac{1}{1000} sec^{-1}$	$\frac{1}{3162} sec^{-1}$
5×10^{-4}	0.47	α_1	α_2	α_3
		3.5×10^{-2}	1.65×10^{-3}	2.0×10^{-1}

Table 2.1: Numerical values of the various material's properties

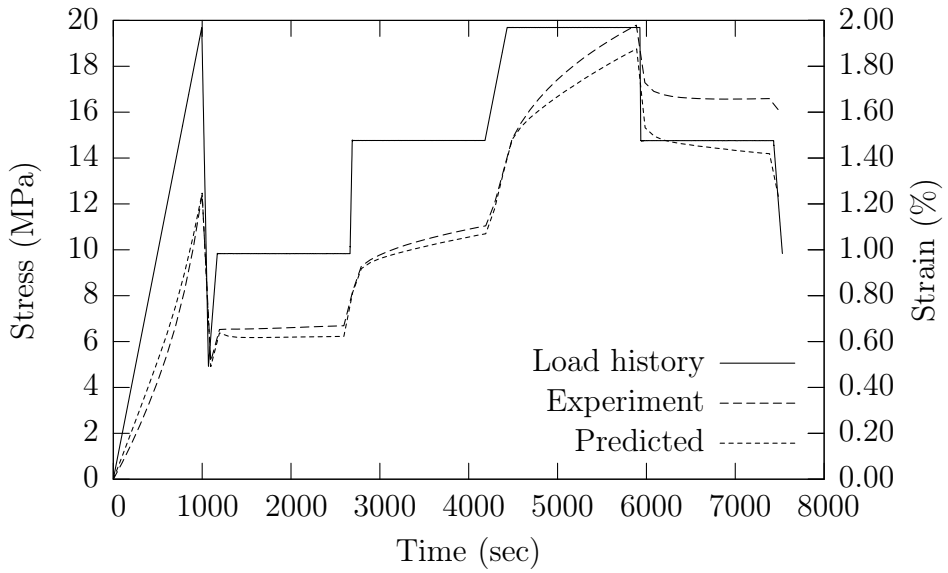


Figure 2.9: Validation of the identified behaviour law for a load history different than the one used for the identification.

of our parameter h), the viscoelastic strains become more important. In that respect, the g_2 parameter can be seen as the parameter which controls the viscoelastic response of the material.

2.5 Validation of the identified behaviour law

In order to validate the identified behaviour law, we have designed a load history which is different from the one used for identification. For the identification process, we used a stress history which was globally increasing and all the loading and unloading were done at the same stress rate. The history we have chosen for validation is a history where the loading and unloading are at different stress rates and for which there are large stress variations over short periods of time. We have performed a single test run and the strains were measured with an extensometer. Figure 2.9 shows the load history we have used as well as the experimental and predicted strains obtained from such a load history. The predictions of the model were obtained by calculating the strains obtained from the stress history as measured by the load cell of the tensile machine. Figure 2.9 shows that there is relatively good agreement between the experimental and predicted values up to approximately 6000 sec-

onds[4]. We recall that we have fixed the validity domain of our constitutive law up to 5500 seconds. However, after 6000 seconds, there is a considerable discrepancy between the predicted and observed strains when the material is unloaded. It is difficult to formulate an explanation for this discrepancy at this stage. One possibility would be that we are simply outside the valid time domain of the constitutive law. However, the discrepancy occurred close to the limit of the validity domain and it would be surprising if the adequacy is good up to 5500 and is lost suddenly after. One other alternative would be to suggest that there is plasticity in the material so that some part of the deformation is not fully recovered at the quasi-sudden stress jump at 6000 seconds. This would suggest then that the validity domain of the constitutive law has not been adequately determined. On the other hand, it is also possible that we have found a load history for which the constitutive law is not adequate. We recall that our constitutive theory has been developed without regard of the physical nature of the internal phenomena and it is possible that, for this load history, the representation we have used for the Gibbs free energy is no longer valid. In other words, our constitutive theory might not describe some internal phenomena. Answering this challenging and very interesting problem is outside the scope we have set for this study.

2.6 Conclusion

In conclusion, we have reached our objective of obtaining the parameters of our constitutive law. The data reduction procedure and the experimental programme we have suggested led to a constitutive law which is both physically and thermodynamically admissible. The final behaviour law is:

$$\begin{aligned}\boldsymbol{\varepsilon}(t) = \mathbf{Q} : \boldsymbol{\sigma}(t) \\ + \mathbf{Q} : \sum_{m=1}^{3} \left[\int_0^t \alpha_m \lambda_m \exp[-\lambda_m (t-\tau)] g_2(h(\boldsymbol{\sigma}(\tau))) \boldsymbol{\sigma}(\tau) \mathrm{d}\tau \right]\end{aligned} \quad (2.15)$$

It was observed that the behaviour law fitted the experimental results used for its identification very well. In addition, the identified behaviour law behaved relatively well when predicting the material response to a different load history. However, the identification we have done relies on very few observations. Even though the response to quite a different load history was modelled with reasonable accuracy, it is our belief that a more extensive

[4]The discrepancy between the experimental and predicted data is less than 7% of the experimental strain for $t \in [1050, 5950]$.

experimental programme should be undertaken in order to obtain a more relevant identification. This could be done, for example, by generating other load histories where the stress varies over the whole validity range of the constitutive law. This way, a more important statistical volume representing the response to many different load histories could be generated. Finding the set of parameters minimising the square of the error between the predicted and observed strains of such a large statistical volume would lead to a behaviour law more adequate for different load histories. This would require conducting more experiments but would not change the data reduction technique or the code used to perform this task. In addition, in this study we only relied on macroscopic observations to evaluate the limits of our constitutive theory. It would be advisable to combine these macroscopic observations with microscopic observations to define a more elaborate criterion for the validity range of the constitutive theory.

In light of such observations, we will consider our identification as a first approximation of the material behaviour. In addition, we have made the hypothesis that the behaviour is isotropic and that the Poisson's ratio remained constant for all loadings. Verifying such hypotheses would require performing experiments where the stress/strain fields are two or three dimensional. This would require developing an accurate measurement of the strain field (this can be achieved by optical methods such as digital image correlation or grid methods) and a proper way to estimate the strain field obtained from the load application (by finite elements for example). Then, load histories which present variations with respect to time and space could be generated and an approach similar to our data reduction procedure could be used to identify all the material parameters. It should be noted that this topic has received very little attention so far [44] and it is of prime importance that efforts be undertaken in such a direction so that we can get more confidence on the theoretical constitutive laws developed.

Chapter 3

Homogenisation Models for Nonlinear Viscoelastic Materials

The objective of this chapter is to develop theoretical models for the homogenisation of nonlinear viscoelastic materials, the numerical implementation being presented in Chapter Four. We present first a general introduction on homogenisation of linear elastic, as well as linear viscoelastic, materials. Then, we present some of the results available in the literature regarding the homogenisation of nonlinear materials. In the presentation, we make a clear difference between *hereditary* and *non hereditary* materials. We define a hereditary material as a material for which the response at $t = t_a$ depends on the whole load history for $t \in [0, t_a]$ as opposed to a non hereditary material where the response at $t = t_a$ depends only on the loading at $t = t_a$. This distinction is made since hereditary materials require specific treatment. A new general methodology is then suggested for generating homogenisation models for hereditary materials. We give some examples of the type of models that can be thus generated and discuss and illustrate some of the limitations of the approach. Finally, we discuss the general numerical algorithm required for the homogenisation.

3.1 Basics of homogenisation

Homogenisation is a discipline which aims at predicting the overall, or *average* properties of a heterogeneous material by using information regarding its microstructure. Electrical, magnetic, mechanical and thermal properties can be predicted by such an approach. In this study, we deal exclusively with mechanical properties and the word homogenisation should be interpreted in this context throughout this thesis. Homogenisation is sometimes referred as

micromechanics or multi-scale modelling.

Homogenisation is a relatively old discipline since the well known *rule of mixtures* dates back to 1889 with Voigt. However, much theoretical work has been accomplished in the 1960s and numerical work in the mid 1980s which make this discipline a quite young and active discipline. Good literature on the subject exists in French (see for example the books from Bornert *et al.* [8, 9]) and English (see the book of Christensen [20] and the course notes of Böhm [7] for example) and the reader should refer to these books for a rigorous and detailed presentation of the theory.

In this section, we give first the general guidelines of homogenisation, divided in three basic steps, for completeness and to introduce the notation. We then focus on the homogenisation scheme we have used in this study. The presentation we give here assumes that the heterogeneous material is composed of linear elastic *phases*, which we define subsequently, and on which the loading leads to small deformations.

3.1.1 Three basic steps

Representation

It is necessary in this first step to define the scales to which the homogenisation is applied. The smallest scale is, of course, the scale above which the heterogeneous material can be considered as an assemblage of homogeneous and continuous phases. This is required since homogenisation relies on continuum mechanics. The next dimension to identify is the characteristic scale of the study. For example, will we consider a semi-crystalline polymer as homogeneous or composed of an assemblage of spherulites, themselves made of crystalline and amorphous phases? The choice is made by the modeller and will depend on his objectives. Once this has been determined, the last dimension to identify is the size of the Representative Volume Element (RVE). For example, this could be the number of grains in a polycrystal that must be taken into account so that the model represents adequately the macroscopic response of the metal. The definition of the RVE has received a lot of attention and has, until recently, been defined qualitatively. For example, Kanit *et al.* [43] have given a quantitative description of the RVE as the size for which a given material property, for a given microstructure, can be evaluated within a given relative precision for a given number of representations. Therefore, the RVE definition is not unique and depends on the property being estimated, the precision required and the number of measurements (numerical or experimental) which will be performed.

The representation aims also at collecting morphological information. For

example, in a short fibre reinforced plastic, the aspect ratio of the fibres, their volume fractions and their angles with respect to the specimen's axes will be sought; in a periodic material, the geometrical parameters of the base pattern will be identified. Other information collected is concerned with the mechanical properties of the constituents *in-situ* (i.e., inside) the heterogeneous material. It is well known for reinforced plastics that the matrix can be different in its bulk form and inside the composite due to the manufacturing process. Since it is difficult to measure the mechanical response of the matrix *in-situ* the composite, this question is still open. In this study, we assumed that the bulk and *in-situ* properties are the same.

In light of such information, the notion of a *phase* can be introduced. For the remainder of this document, a phase will be defined as a volume of material where the morphological and mechanical properties are constant. For example, two short glass fibres oriented at two different angles form two different phases (same material, same shape but different orientation) while two short glass fibres oriented at the same angle belong to the same phase. A particular phase is referred to by the subscript r.

Localisation

Before we treat the subject of localisation, we must introduce some notation. We define by $\boldsymbol{\sigma}_r(\boldsymbol{x})$ and $\boldsymbol{\varepsilon}_r(\boldsymbol{x})$ the stresses and strains in a given phase at position $\boldsymbol{x}$. We denote by capital Greek letters $\boldsymbol{\Sigma}$ and $\mathbf{E}$ the macroscopic stresses and strains. These quantities are assumed to be homogeneous on the boundaries of the RVE.

The aim of localisation is to find a relationship between the microscopic and macroscopic quantities so that:

$$\boldsymbol{\sigma}_r(\boldsymbol{x}) = \mathbf{B}_r(\boldsymbol{x}) : \boldsymbol{\Sigma} \tag{3.1a}$$

$$\boldsymbol{\varepsilon}_r(\boldsymbol{x}) = \mathbf{A}_r(\boldsymbol{x}) : \mathbf{E} \tag{3.1b}$$

where $\mathbf{A}$ is the so-called strain localisation tensor and $\mathbf{B}$ the stress concentration tensor. These tensors can be approximated by analytical solutions or evaluated by numerical methods, such as the finite elements. Such techniques used to calculate these tensors are called homogenisation schemes. For linear elastic materials, the principal differences in the various theories lie in the way they compute such quantities. Of course, in the general case, analytical methods will approximate such tensors due to the inherent complexity of the problem.

Homogenisation

In what follows, the volume average $\langle . \rangle$ operator is defined as:

$$\langle f(\boldsymbol{x}) \rangle = \frac{1}{V} \int_V f(\boldsymbol{x}) \mathrm{d}V \tag{3.2}$$

where V is the volume of the RVE. It can be shown, by using simple equilibrium equations that:

$$\boldsymbol{\Sigma} = \langle \boldsymbol{\sigma}(\boldsymbol{x}) \rangle = c_r \langle \boldsymbol{\sigma}_r(\boldsymbol{x}) \rangle_r \tag{3.3a}$$

$$\mathbf{E} = \langle \boldsymbol{\varepsilon}(\boldsymbol{x}) \rangle = c_r \langle \boldsymbol{\varepsilon}_r(\boldsymbol{x}) \rangle_r \tag{3.3b}$$

where c_r is the volume fraction and $\langle . \rangle_r$ must be interpreted as the volume average over phase r. If the behaviour law is inserted in these formulas, we obtain:

$$\boldsymbol{\Sigma} = \langle \mathbf{C}(\boldsymbol{x}) : \boldsymbol{\varepsilon}(\boldsymbol{x}) \rangle = c_r \mathbf{C}_r : \langle \boldsymbol{\varepsilon}_r(\boldsymbol{x}) \rangle_r \tag{3.4a}$$

$$\mathbf{E} = \langle \mathbf{S}(\boldsymbol{x}) : \boldsymbol{\sigma}(\boldsymbol{x}) \rangle = c_r \mathbf{S}_r : \langle \boldsymbol{\sigma}_r(\boldsymbol{x}) \rangle_r \tag{3.4b}$$

where $\mathbf{C}$ is a stiffness and $\mathbf{S}$ a compliance. We have assumed that the mechanical properties of phase r are spacewise constant. When equations (3.1) are inserted into these equations we obtain:

$$\boldsymbol{\Sigma} = c_r \mathbf{C}_r : \langle \mathbf{A}_r(\boldsymbol{x}) : \mathbf{E} \rangle_r = c_r \mathbf{C}_r : \langle \mathbf{A}_r \rangle_r : \mathbf{E} = \tilde{\mathbf{C}} : \mathbf{E} \tag{3.5a}$$

$$\mathbf{E} = c_r \mathbf{S}_r : \langle \mathbf{B}_r(\boldsymbol{x}) : \boldsymbol{\Sigma} \rangle_r = c_r \mathbf{S}_r : \langle \mathbf{B}_r \rangle_r : \boldsymbol{\Sigma} = \tilde{\mathbf{S}} : \boldsymbol{\Sigma} \tag{3.5b}$$

where $\tilde{\mathbf{C}}$ and $\tilde{\mathbf{S}}$ are the homogenised stiffness and compliances and are the results being sought. It can be observed from equations (3.4) that only the average values of the microscopic stress and strain fields are required. This simplifies the problem considerably and facilitates subsequent analytical treatment, which can be of two types: bounds or estimates of the homogenised properties. These are discussed in the following two sections.

3.1.2 Bounds for the mechanical properties of linear elastic heterogeneous material

Variational principles can be used to bound the mechanical properties of a heterogeneous material. The idea is to define a continuum mechanics problem and the minimum potential energy theorems to solve it. For example, consider a heterogeneous material where a uniform strain field $\mathbf{E}$ is applied on its boundaries. Then, the minimum potential energy theorem states that [9]:

$$\langle \boldsymbol{\varepsilon}(\boldsymbol{u}) : \mathbf{C} : \boldsymbol{\varepsilon}(\boldsymbol{u}) \rangle = \inf_{\boldsymbol{v} \in \mathcal{K}(\mathbf{E})} \langle w(\boldsymbol{\varepsilon}(\boldsymbol{v})) \rangle \leq \langle \boldsymbol{\varepsilon}(\boldsymbol{v}) : \mathbf{C} : \boldsymbol{\varepsilon}(\boldsymbol{v}) \rangle \tag{3.6}$$

where $\mathcal{K}(\mathbf{E})$ represents the set of kinematically admissible displacement fields leading to $\mathbf{E}$ on the material boundaries, $\boldsymbol{u}$ is the solution of the problem and $w(\boldsymbol{\varepsilon}) = \frac{1}{2}\boldsymbol{\varepsilon} : \mathbf{C} : \boldsymbol{\varepsilon}$ is the potential describing the behaviour of a given phase. It can also be shown that:

$$W(\mathbf{E}) = \frac{1}{2}\mathbf{E} : \tilde{\mathbf{C}} : \mathbf{E} = \inf_{\boldsymbol{v} \in \mathcal{K}(\mathbf{E})} \langle w(\boldsymbol{\varepsilon}(\boldsymbol{v})) \rangle \tag{3.7}$$

where W is the homogenised potential and where $\boldsymbol{\Sigma} = \frac{\partial W}{\partial \mathbf{E}}$ is the homogenised behaviour law. Equation (3.6) shows that any $\boldsymbol{v} \in \mathcal{K}(\mathbf{E}) \neq \boldsymbol{u}$ leads to an upper bound for W. Since in practice $\boldsymbol{u}$ is too complex to be determined by analytical means, trial displacement fields $\boldsymbol{v}$ will be sought so that they decrease the value of W as much as possible. One obvious trial field to choose is $\boldsymbol{v} = \mathbf{E} \cdot \boldsymbol{x}$ which implies that the strain field is homogeneous in the material. Such a bound is known as the Voigt bound and is an upper bound. This bound coincides with the rule of mixtures. It can also be shown that [9]:

$$\frac{1}{2}\boldsymbol{\Sigma} : \tilde{\mathbf{C}}^{-1} : \boldsymbol{\Sigma} = \inf_{\boldsymbol{\tau} \in \mathcal{S}(\boldsymbol{\Sigma})} \langle l(\boldsymbol{\tau}) \rangle \tag{3.8}$$

where $l(\boldsymbol{\tau}) = \frac{1}{2}\boldsymbol{\tau} : \mathbf{S} : \boldsymbol{\tau}$ is the potential energy associated with the stresses and $\mathcal{S}$ is the set the statically admissible stress fields for which $\langle \boldsymbol{\tau} \rangle = \boldsymbol{\Sigma}$. The solution of such a problem is $\boldsymbol{\sigma}$ and any field $\boldsymbol{\tau} \neq \boldsymbol{\sigma}$ will lead to a higher potential energy. One trial stress field would be a constant stress field where $\boldsymbol{\tau} = \boldsymbol{\Sigma}$ and would lead to an upper bound for $\tilde{\boldsymbol{C}}^{-1}$. This bound is known as the Reuss bound. In the end, we have that:

$$\langle \mathbf{S} \rangle^{-1} \leq \tilde{\mathbf{C}} \leq \langle \mathbf{C} \rangle \tag{3.9}$$

which bounds the homogenised stiffness $\tilde{\mathbf{C}}$. A similar approach can be used to bound the homogenised compliance.

It should be noted that equation (3.9) has been obtained using only the volume fraction and the mechanical properties of each phase. The shape, the arrangement, etc., of the various phases are not taken into account. It is not surprising that such bounds are generally quite wide and have limited use. Using the same basic ideas, other variational principles can be used to obtain tighter bounds. This topic is mathematically involved and will not be discussed in this thesis.

3.1.3 Estimation of the mechanical response

Instead of bounding the homogenised properties, another approach consists of estimating the material response by using solutions of continuum mechanics

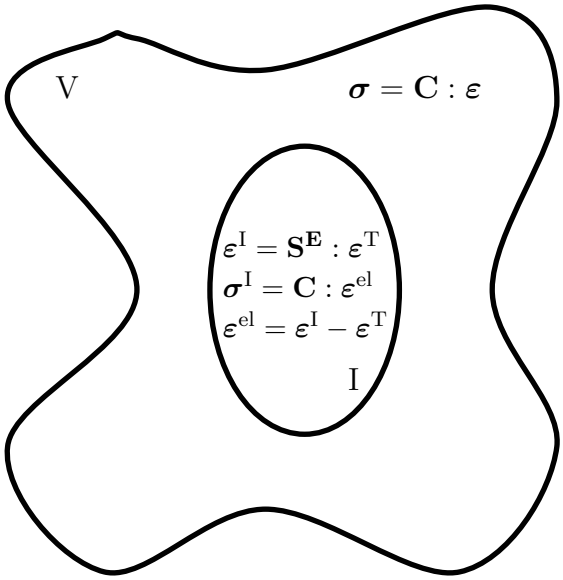


Figure 3.1: Eshelby's ellipsoidal inclusion problem [27]. An ellipsoidal subdomain I of V is subjected to a stress-free strain $\boldsymbol{\varepsilon}^{\mathrm{T}}$. The resulting strain in the inclusion, $\boldsymbol{\varepsilon}^{\mathrm{I}}$ is given by $\boldsymbol{\varepsilon}^{\mathrm{I}} = \mathbf{S}^{\mathbf{E}} : \boldsymbol{\varepsilon}^{\mathrm{T}}$, where $\mathbf{S}^{\mathbf{E}}$ Eshelby's tensor.

problems. Most of the analytical homogenisation schemes are based upon Eshelby's ellipsoidal inclusion problem [27]. Eshelby solved the problem of an infinite media free of strains and stresses, to which a uniform stress-free strain $\boldsymbol{\varepsilon}^{\mathrm{T}}$ is applied in an ellipsoidal domain denoted I (see figure 3.1). Since the inclusion is embedded in the surrounding domain V, there is an elastic accommodation between the inclusion and its surroundings. Eshelby has shown that the resulting strain in the inclusion is given by $\boldsymbol{\varepsilon}^{\mathrm{I}} = \mathbf{S}^{\mathbf{E}} : \boldsymbol{\varepsilon}^{\mathrm{T}}$ where $\mathbf{S}^{\mathbf{E}}$ is known as Eshelby's tensor. This tensor is a function of the material stiffness $\mathbf{C}$ and the shape of the inclusion. His other finding was that the resulting strain field in the inclusion is also homogeneous. This result is valid regardless of the material symmetry.

Such a result can be used to derive the expression of the strain field inside an inclusion with different mechanical properties from the surroundings when domain V is subjected to a uniform loading at infinity [9]. In that case, the inclusion with different mechanical properties is called heterogeneity. In addition, since thermal strains are stress-free strains, the development can be extended to thermomechanical loadings.

For real materials, the assumption of an infinite surrounding, or matrix, can become less relevant as the volume fraction of heterogeneities increases. In addition, as the volume fraction of heterogeneities increases, a single heterogeneity "sees" not only the matrix around it but the other heterogeneities.

Therefore, different theories must be developed to take into account such perturbations in the stress/strain fields. Various homogenisation schemes have been adapted to specific morphologies. The reader is referred to the general text books mentioned in the introduction for an exhaustive list. In this study, we have used the Mori-Tanaka scheme [66] and this is the topic of the next section. The scheme is well suited to our microstructure (i.e., spherical particles randomly distributed within a homogeneous matrix for volume fractions up to 30%).

3.1.4 Mori-Tanaka homogenisation scheme

The theory originally introduced by Mori and Tanaka [66] has been applied to many materials, especially those where there is a dominant phase (i.e., matrix) in which heterogeneities are embedded. This theory has been given many physical interpretations (see Bourgeois [12] or Tucker and Liang [97] for a list and comparisons). In addition, for a two phase material where the matrix is the soft phase and the heterogeneity is spherical and is the hard phase, the model corresponds to the lower Hashin-Shtrikman bound (see [4] for the details). Benveniste [4] has observed that in the Mori-Tanaka scheme, the average strain in the reinforcement, in the case of a two phase material, is approximated by:

$$\bar{\boldsymbol{\varepsilon}}_1 = \mathbf{A}^{\mathrm{E}} : \bar{\boldsymbol{\varepsilon}}_0 \tag{3.10}$$

where $\bar{\boldsymbol{\varepsilon}}_0$ and $\bar{\boldsymbol{\varepsilon}}_1$ are the average strains in the matrix and in the reinforcement and $\mathbf{A}^{\mathrm{E}}$ is the strain localisation tensor associated with Eshelby's ellipsoidal heterogeneity problem. Therefore, the calculation of the strain field inside a heterogeneity can be interpreted as Eshelby's heterogeneity problem where this time, the matrix is not subjected to $\mathbf{E}$ but to $\bar{\boldsymbol{\varepsilon}}_0$. However, $\bar{\boldsymbol{\varepsilon}}_0$ depends on the heterogeneities inside the material. So, a single heterogeneity does not "see" the others but "sees" a matrix around itself where the effect of the strain perturbation of the other heterogeneities has been incorporated. In practice, for a two phase composite with spherical heterogeneities, and depending on the contrast between the various phases, the theory leads to acceptable results for volume fractions up to 20 – 30%.

Thermomechanical loadings

The theory can also be used to derive the thermomechanical response of the heterogeneous material. Since we deal with linear materials, the superposition principle applies and various alternate problems can be combined to obtain the results sought. For example, if we assume that each phase

undergoes a uniform stress-free deformation $\boldsymbol{\varepsilon^0}$ (like a thermal strain) the homogenised properties are classically given by:

$$\mathbf{E} = \langle \mathbf{S}(\boldsymbol{x}) : \mathbf{B}(\boldsymbol{x}) \rangle : \boldsymbol{\Sigma} + \langle \mathbf{B}^{\mathrm{T}}(\boldsymbol{x}) : \boldsymbol{\varepsilon^0}(\boldsymbol{x}) \rangle = \tilde{\mathbf{S}} : \boldsymbol{\Sigma} + \mathbf{E^0} \tag{3.11}$$

Suppose for now that there is no loading applied to the material but that each phase undergoes a stress-free deformation. Since each phase is embedded in a surrounding material, residual stresses will develop in each phase, but their volume average cancels. Using again the superposition principle, these "residual" stresses can be calculated (see below).

Specific results used in this study

In this study, the composite material is a glass beads reinforced polypropylene. The glass beads are distributed randomly within the composite so that its behaviour is isotropic. We give here the theoretical results we have used (Appendix B gives a more detailed list). Since all the tensors involved in the calculations are isotropic, they are given in short hand notation (see Appendix A). The subscript 0 refers to the matrix and the subscript 1 refers to the reinforcement. The homogenised compliance is given by:

$$\tilde{\mathbf{S}} = \left(\frac{(1-c_1)(k_0 + \alpha_0(k_1 - k_0)) + c_1 k_0}{3k_0[(1-c_1)(k_0 + \alpha_0(k_1 - k_0)) + c_1 k_1]}, \right. \\ \left. \frac{(1-c_1)(\mu_0 + \beta_0(\mu_1 - \mu_0)) + c_1 \mu_0}{2\mu_0[(1-c_1)(\mu_0 + \beta_0(\mu_1 - \mu_0)) + c_1 \mu_1]} \right) \tag{3.12}$$

where k and μ are bulk and shear moduli,

$$\alpha_0 = \frac{3k_0}{3k_0 + 4\mu_0} \quad \text{and} \quad \beta_0 = \frac{6(k_0 + 2\mu_0)}{5(3k_0 + 4\mu_0)} \tag{3.13}$$

are the components of Eshelby's tensor. The stress concentration tensor *for the matrix* is given by:

$$\mathbf{B}_0 = \left(\frac{k_0 + \alpha_0(k_1 - k_0)}{(1-c_1)(k_0 + \alpha_0(k_1 - k_0)) + c_1 k_1}, \right. \\ \left. \frac{\mu_0 + \beta_0(\mu_1 - \mu_0)}{(1-c_1)(\mu_0 + \beta_0(\mu_1 - \mu_0)) + c_1 \mu_1} \right) \tag{3.14}$$

The residual stresses $\boldsymbol{\sigma}_0^{\mathrm{res}}$, as discussed above, are given by [12]:

$$\boldsymbol{\sigma}_0^{\mathrm{res}} = \mathbf{R}_0 : \left(\boldsymbol{\varepsilon}_{\mathbf{1}}^{\mathbf{0}} - \boldsymbol{\varepsilon}_{\mathbf{0}}^{\mathbf{0}} \right) \tag{3.15}$$

where:

$$\mathbf{R}_0 = \left(\frac{3c_1 k_0 k_1 (1-\alpha_0)}{(1-c_1)(k_0 + \alpha_0(k_1 - k_0)) + c_1 k_1}, \right. \\ \left. \frac{2c_1 \mu_0 \mu_1 (1-\beta_0)}{(1-c_1)(\mu_0 + \beta_0(\mu_1 - \mu_0)) + c_1 \mu_1} \right) \quad (3.16)$$

In our case, the treatment of the nonlinear problem will induce stress-free strains in the matrix but none in the spherical particles. For this particular condition, the average stress in the matrix is given by:

$$\bar{\boldsymbol{\sigma}}_{\mathbf{0}} = \mathbf{B_0} : \boldsymbol{\Sigma} - \mathbf{R}_0 : \boldsymbol{\varepsilon}^{\mathbf{0}}_{\mathbf{o}} \quad (3.17)$$

3.2 Homogenisation of linear viscoelastic materials

The results presented so far are valid for linear elastic materials. It is possible to calculate the homogenised creep compliance or relaxation modulus of linear viscoelastic materials by using the previous results and the viscoelastic correspondence principle. The application and limitations of this principle to homogenisation problems has been formally demonstrated by Laws and McLaughlin [51] for the self-consistent scheme. We assume here that the same results apply to the Mori-Tanaka scheme.

Before describing this principle, we recall the definition of the well known Laplace–Carson transform:

$$f^*(p) = p \int_{-\infty}^{\infty} f(t) \exp[-pt] \mathrm{d}t \quad (3.18)$$

where $f^*(p)$ is the Laplace–Carson transform of $f(t)$. When this transform is applied to a linear viscoelastic behaviour law, we obtain (for example) the following result:

$$\boldsymbol{\varepsilon}^*(p) = \mathbf{S}^*(p) : \boldsymbol{\sigma}^*(p) \quad (3.19)$$

which is analogous to a linear elastic behaviour law in the Laplace–Carson space.

The correspondence principle states that if a viscoelastic continuum mechanics problem has time varying boundary conditions where the types of boundary conditions applied over a given surface do not change with time (i.e. an applied traction condition cannot change to a prescribed displacement), its Laplace–Carson transformed solution can be obtained by solving

the corresponding elastic problem. In other words, if the solution to an elastic problem is known, the transformed solution of the viscoelastic problem is obtained by replacing the elastic constants by their Laplace–Carson transforms. Once this solution has been obtained, the time domain solution is obtained by Laplace–Carson inversion. For simple cases, the inversion can be carried out analytically, but for most situations it has to be evaluated numerically. It is noted that other correspondence principles exist (for example using Fourier transforms, considering steady state harmonic sollicitations, etc.).

In our case, the viscoelastic equivalent of equation (3.11) is given by:

$$\mathbf{E}(t) = \int_0^t \tilde{\mathbf{S}}(t-\tau) : \dot{\boldsymbol{\Sigma}}(\tau)\mathrm{d}\tau + \mathbf{E^0}(t) \tag{3.20}$$

where the dot ($\dot{}$) indicates the first derivative and:

$$\mathbf{E^0}(t) = \left\langle \int_0^t \mathbf{B}(\boldsymbol{x}, t-\tau) : \dot{\boldsymbol{\varepsilon}}^{\mathbf{0}}(\boldsymbol{x}, \tau)\mathrm{d}\tau \right\rangle \tag{3.21}$$

and the equivalent of relation (3.15) is given by:

$$\boldsymbol{\sigma}_{\mathbf{0}}^{\mathbf{res}} = -\int_0^t \mathbf{R_0}(t-\tau) : \dot{\boldsymbol{\varepsilon}}_{\mathbf{0}}^{\mathbf{0}}(\tau)\mathrm{d}\tau \tag{3.22}$$

For convenience, we have chosen to evaluate the material response by first calculating the time domain expressions of the tensors involved in homogenisation ($\tilde{\mathbf{S}}(t)$, $\mathbf{B}(t)$ ...) and then calculate the convolutions of equations (3.20,3.21,3.22). For example, calculating the inverse Laplace-Carson transform of $\mathbf{E}^* = \tilde{\mathbf{S}}^* : \boldsymbol{\Sigma}^*$ requires defining $\boldsymbol{\Sigma}(t)$ for $t \in [0, \infty]$. Using the convolution products only requires defining $\boldsymbol{\Sigma}(t)$ up the time where the response is sought.

The correspondence principle applied to homogenisation problems has been used by many investigators. For example, Hashin [34, 35] considered unidirectionally reinforced materials, Christensen [18] developed bounds for the complex modulus of isotropic materials, Wang and Weng [99] compared some theoretical results with experiments and obtained relatively good results. Turner and Tomé [98] have applied it to polycrystalline aggregates. Brinson and Lin [16] compared the results of various theories and recently Allen *et al.* [1] implemented the homogenised creep compliance of a glass mat reinforced plastic into a finite element package to predict the response of a structure.

Causality

As pointed out by Laws and McLaughlin [51], the solution of the homogenisation problem should preserve the *causality* nature of the material. In other words, the response of the homogenised material for times included in $[0, t_a]$ depends on the mechanical responses of the constituent materials over the same time interval. Consider, for example, our material where the reinforcements are linear elastic and the matrix is linear viscoelastic. Suppose in addition that we seek the homogenised material response over $[0, t_a]$. Now, introduce the following behaviour laws for the matrix:

$$k_0(t) = \hat{\hat{k}}_0(t)H(t) + \hat{k}_0(t - t_a)H(t - t_a) \tag{3.23a}$$

$$\mu_0(t) = \hat{\hat{\mu}}_0(t)H(t) + \hat{\mu}_0(t - t_a)H(t - t_a) \tag{3.23b}$$

where $H(t)$ is the Heaviside unit step function and $\hat{\hat{k}}_0(t)$, $\hat{k}_0(t)$, $\hat{\hat{\mu}}_0(t)$ and $\hat{\mu}_0(t)$ are different functions of time. Equation (3.23) expresses the behaviour law in two parts: before and after t_a. The Laplace-Carson transform of such a function is given by:

$$k_0^*(p) = p\big(\hat{\hat{k}}_0^*(p) + \exp[-t_a p]\hat{k}_0^*(p)\big) \tag{3.24a}$$

$$\mu_0^*(p) = p\big(\hat{\hat{\mu}}_0^*(p) + \exp[-t_a p]\hat{\mu}_0^*(p)\big) \tag{3.24b}$$

When equations (3.24) are inserted in equations (3.12,3.14,3.16) the spherical or deviatoric parts (denoted by a) of such tensors are of the form (after some algebraic manipulations):

$$\begin{aligned} a^*(p) &= \frac{A(p) + \exp[-t_a p]B(p)}{D(p) + \exp[-t_a p]E(p)} \\ &= \frac{A(p)}{D(p)} + \exp[-t_a p]\frac{B(p) - \frac{A(p)E(p)}{D(p)}}{D(p) + \exp[-t_a p]E(p)} \end{aligned} \tag{3.25}$$

where $A(p)$ and $D(p)$ are functions of c_1, k_1, μ_1, $\hat{\hat{k}}_0$ and $\hat{\hat{\mu}}_0$ only. Inversion of equation (3.25) leads to:

$$a(t) = \hat{\hat{a}}(t) + \hat{a}(t - t_a)H(t - t_a) \tag{3.26}$$

where, of course, $\hat{\hat{a}}$ is a function of c_1, k_1, μ_1, $\hat{\hat{k}}_0$ and $\hat{\hat{\mu}}_0$ only. This shows that the expression of the tensors described in equations (3.12,3.14,3.16) for $t \in [0, t_a]$ depends on the material properties for $t \in [0, t_a]$. Such a result will be useful when we define the linearisation of the nonlinear material.

Thermodynamically acceptable homogenised materials

In the remainder of this chapter, we insist on the fact that the constituent materials must be thermodynamically acceptable in order to lead to a thermodynamically acceptable homogenised material. In reality, the materials are thermodynamically admissible since they exist and this question does not have much sense. However, the treatment we use to perform the homogenisation of our nonlinear viscoelastic material introduces a linearisation of the local constituents (see section 3.6). We show here, as an example, what kind of behaviour can be obtained if the linearisation leads to a material which is not thermodynamically admissible.

We recall that we have given general expressions for the relaxation and compliance of a linear viscoelastic material in section 1.3.1. For illustration, consider the following example of a two phase composite, where the reinforcements are spherical particles and their volume fraction is 30%. Assume further that the behaviour of the phases obeys a Maxwell law, so that $\mathbf{S_0}(t) = \{a_0 + b_0 t, f_0 + l_0 t\}$ and $\mathbf{S_1}(t) = \{a_1 + b_1 t, f_1 + l_1 t\}$. When all the constants are positive, the homogenisation of such material leads to a thermodynamically admissible material (according to the Mori-Tanaka scheme). However, if we have that $l_0 < 0$, then the homogenised shear compliance of such material is not thermodynamically admissible. Figure 3.2 plots this property where we have set all the parameters to 1 except l_0 which we set equal to -1. In a different context, the issue a thermodynamic stability of non hereditary materials has been studied by Lakes and Drugan [50]. The authors have simulated the homogenised properties of composite materials where the reinforcements had negative stiffness. The negative stiffness the authors introduced is in fact the equivalent stiffness of a structure (the authors give some examples of negative stiffness structures). They have shown that under certain conditions, the resulting material is stiffer than the two phases. In that context, our example shows that using a material which is not thermodynamically admissible *can* lead to unacceptable results. It does not show, however, that all heterogeneous materials, where at least one material does not meet the requirements of thermodynamics, lead to an unacceptable homogenised material. On the other hand, it was not possible to show that homogenisation (according to the Mori-Tanaka scheme) of all heterogeneous materials made of thermodynamically admissible constituents leads to a thermodynamically admissible linear viscoelastic material. Therefore, we have to assume that it is the case.

In summary, this exercise has shown that homogenisation of materials that do not meet the requirements of thermodynamics can lead to unacceptable homogenised behaviours. In this study, we deal with real materials

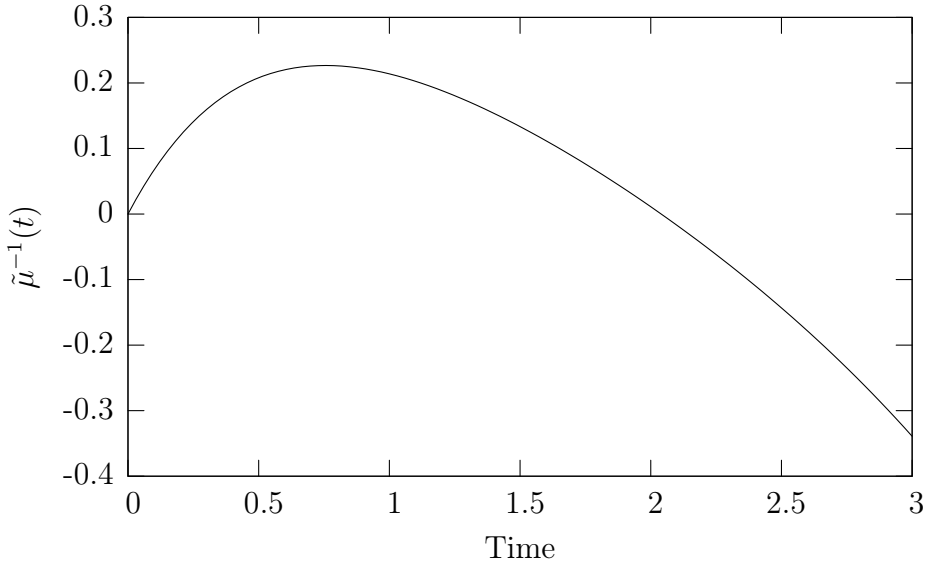


Figure 3.2: Homogenised shear creep compliance (denoted by $\tilde{\mu}^{-1}(t)$) of a two phase composite material where the reinforcements are spherical and where the matrix and the reinforcements obey a Maxwell law. All the material parameters, except the viscous shear compliance of the matrix, are positive.

exhibiting positive stiffness (in a general sense). Therefore, we enforce, in what follows, that the treatment of our nonlinear viscoelastic homogenisation problem leads to a thermodynamically admissible material.

3.3 General aspects of homogenising nonlinear materials

The presentation we have made so far applies to linear, elastic or viscoelastic, materials. To our knowledge, for random media, there is no exact homogenisation solution for predicting of the global behaviour of nonlinear materials. The theories we present here rely on linearisation of the nonlinear materials so that the well known results of homogenisation can be applied to this new linearised material. The choice of the proper type of linearisation is still an open question since this problem is quite complex. Consider, for example, our problem with a nonlinear matrix and elastic heterogeneities. Suppose that a macroscopic stress is applied on the boundary of the RVE. This induces a stress field which is heterogeneous in the matrix and possibly heterogeneous in the beads, so that we have $\boldsymbol{\sigma_0} = \boldsymbol{\sigma_0}(\boldsymbol{x})$. Then, one alternative would be to

reach the solution by a series of increments where the problem is linear within each increment. The linearisation could be to take the tangent modulus (in the case of a non hereditary material) evaluated at the $\boldsymbol{\sigma_0}(\boldsymbol{x})$. This would, of course, lead to an elastic material but the phase definition would have been considerably changed since we would have approximately one different linearised material at each position $\boldsymbol{x}$. So, our problem would then be linearised but would be too complex to be solved by analytical means. Therefore, we have to restrict the linearisation spatially so that we end up with a linearised material compatible with the homogenisation schemes available.

One classical hypothesis is to consider that the morphology remains unchanged and the mechanical properties of each phase are spacewise constant within the phase. This way, we can use a homogenisation scheme to predict the overall response of this linearised material. Of course this linearised material does not reproduce the response of the nonlinear material for all loadings but aims at reproducing the same response as the nonlinear material for a specific applied load. This raises two issues to address:

1. The reference level. Since we assume uniform properties within the phase, the linearised material will be calculated from its constitutive law for a given value of the stress/strain. Classically, the average stress/strain field (i.e. $\langle\boldsymbol{\sigma}(\boldsymbol{x})\rangle_r$ or $\langle\boldsymbol{\varepsilon}(\boldsymbol{x})\rangle_r$) has been used but recent applications used the second moments of these fields (namely $\langle\boldsymbol{\sigma}(\boldsymbol{x})\otimes\boldsymbol{\sigma}(\boldsymbol{x})\rangle_r$ or $\langle\boldsymbol{\varepsilon}(\boldsymbol{x})\otimes\boldsymbol{\varepsilon}(\boldsymbol{x})\rangle_r$) which incorporate some of the spatial fluctuations of the stress/strain field.

2. The type of linearisation. We have mentioned earlier a tangent linearisation, but this choice is not unique. We could imagine a secant linearisation or a linearisation which incorporates a stress-free strain or its dual since we know how to homogenise such materials.

From these considerations, we can see that we can generate many different linearisation procedures which will lead to different estimates of the same problem. It is difficult to determine *a priori* which approach is the most relevant. The presentation we make in the next two sections details some of the existing models.

As was stated in the introduction, we make a clear difference between non hereditary and hereditary materials. This is motivated by the fact that it makes physical sense that the linearised material shares some of the particularities of the nonlinear material. For example, it would not make much physical sense to linearise a nonlinear elastic material with a linear viscoelastic material. So, generally, nonlinear non hereditary materials are linearised by linear non hereditary materials and, in our case, our nonlinear viscoelastic

material is linearised with a linear viscoelastic material. We also introduce this difference because the treatment of hereditary materials involves more abstract concepts than non hereditary materials (in general). As much as possible, we try to interpret the developments for hereditary materials with respect to those of non hereditary materials so that an intuitive representation of the mathematical developments can be obtained. In addition, we also make a clear difference between variational approaches and empirical approaches. By empirical we mean that the linearisation does not rely on an energy formulation or any other physical/mathematical grounds. Finally, we wish to point out that the homogenisation of nonlinear materials has received a lot of attention in the last decades and there is good French (see, for example, the book by Bornert *et al.* [9] and the theses of Masson [57] and Brenner [13]) as well as English (see the review of Ponte Castañeda and Suquet [76]) literature on the subject.

3.4 Homogenisation of nonlinear non hereditary materials

3.4.1 Variational approaches

We have seen in section 3.1 that the mechanical response of heterogeneous linear elastic materials can be bounded or estimated. When the mechanical response of the constituent materials can be described by a single potential (see section 1.2), their special properties can be used to deliver variational estimates or bounds for the homogenised potential. The aim of the variational approaches is then to estimate or to bound the effective potential of the nonlinear material. Then, the response (in theory) is calculated by differentiation of this homogenised potential.

Using such ideas, Ponte Casteñada [73] introduces a comparison material which has the same morphology[1] as the nonlinear material. However, the behaviour of each phase is no longer a nonlinear potential, but a linear elastic potential. Then he writes a variational principle where its optimisation with respect to the materials constants of this comparison material leads to bounds or estimates of the nonlinear material. These bounds or estimations are based on the bounds and estimations available in linear elasticity. In a sense, this variational procedure makes it possible to *translate* linear bounds and estimates to nonlinear materials for which the behaviour is described by a

[1]By morphology we refer to the geometrical aspects of the microstructure. We see each phase as a domain for which we do not yet know the mechanical properties.

potential.

Ponte Castañada has introduced a second order procedure [74], which was given a variational interpretation by Ponte Castañada and Willis [77] using the same concept of a comparison material. However, this time, the nonlinear potential of each phase is approximated by a Taylor expansion with a remainder and the linear comparison material can be interpreted as a thermoelastic material. In this procedure, a stationary point is obtained when the modulus of the linear comparison material is set to the tangent modulus of the nonlinear material evaluated for the mean loading (for example $\langle \boldsymbol{\sigma} \rangle$ or $\langle \boldsymbol{\varepsilon} \rangle$) in this phase. Since this choice leads to a stationary point (i.e., a point where the gradient of the function to be optimised is equal to zero), as opposed to an extremum, the procedure can only provide an estimate. Ponte Castañada [74] shows that other stationary points can be obtained by using *second moments* (related to the field fluctuations of the stress/strain field) information. In a recent paper, Ponte Castañada [75] uses such information to develop variational estimates. Using first and second moments information is believed to lead to better estimates of the global response since much more information is known about the stress/strain field inside the material than just using the mean values of these fields.

Even though variational approaches are powerful (because they can deliver bounds) and formal, their application has been limited, so far, to materials for which the behaviour is described by a single potential (except for the very recent works of Lahellec and Suquet [46]). In our case, the behaviour law we use is more general and such approaches cannot be used. However, the concept of a comparison material introduced by Ponte Castañada is useful to compare *empirical* approaches with variational approaches because the linearised comparison material corresponds to a well defined variational problem. This is the subject of the next section.

3.4.2 Empirical Approaches

The concept of a comparison material is powerful since it allows use of the well known results of homogenisation of linear elastic materials. The macroscopic response is calculated by using the homogenised stiffness of this comparison material. For example, $\mathbf{E} = \tilde{\mathbf{S}} : \boldsymbol{\Sigma}$ where $\tilde{\mathbf{S}}$ is the homogenised compliance of this linearised material. This comparison material is obtained by a *linearisation* (tangent, secant, etc.) of the local constituent. Since constant properties are assumed for each phase, this linearisation must be accomplished for a *reference* level. Variational approaches like those listed in the previous section can give some insight for choosing the best linearisation type/reference level combination.

We recall that we have emphasised the linearisation procedure rather than the whole homogenisation and numerical implementation process. In addition, we treat compliances and moduli indifferently and it should be kept in mind that a similar approach exists for the dual quantity. It should be noted that the presentation we make here is not exhaustive.

Classical secant model

In this model, the mechanical properties of the comparison material phases are their secant properties evaluated at the average stress/strain field in the given phase. We denote the secant modulus of phase r by $\mathbf{C}_r^{\mathbf{sct}}$. The secant modulus is calculated so that the following relation is met:

$$\bar{\boldsymbol{\sigma}}_r(\bar{\boldsymbol{\varepsilon}}_r) = \mathbf{C}_r^{\mathbf{sct}} : \bar{\boldsymbol{\varepsilon}}_r \tag{3.27}$$

where $\bar{\boldsymbol{\sigma}}_r(\bar{\boldsymbol{\varepsilon}}_r)$ is interpreted as the behaviour law. In the case of a potential, $\bar{\boldsymbol{\sigma}}_r = \frac{\partial w(\bar{\boldsymbol{\varepsilon}}_r)}{\partial \boldsymbol{\varepsilon}}$ where the derivative is interpreted as the derivative of w with respect to $\boldsymbol{\varepsilon}$ evaluated at $\bar{\boldsymbol{\varepsilon}}_r$. In general, this problem is ill posed since we seek the 21 unknowns of $\mathbf{C}_r^{\mathbf{sct}}$ for six equations. There can therefore be an infinity of solutions. In addition, it is not guaranteed the each of the possibilities lead to $\mathbf{C}_r^{\mathbf{sct}} > 0$, which is required for thermodynamic stability. For example, consider the case of a nonlinear isotropic material loaded in tension. This results in a positive strain in one direction and two negative strains in the other directions. One obvious choice of $\mathbf{C}_r^{\mathbf{sct}}$ would be to set all the off diagonal terms to zero and choose the diagonal terms so that the secant condition is met. This would lead to negative diagonal terms and hence, to a modulus which is not positive definite. One alternative would be to restrict ourselves to solutions where $\mathbf{C}_r^{\mathbf{sct}} > 0$. However, we do not know if a solution exists within this set and even if it exists, we do not know if it is unique. On the other hand, if the behaviour is described by a potential so that [76]:

$$w(\boldsymbol{\varepsilon}) = F(\mathbf{L}) \tag{3.28}$$

where $\mathbf{L} = \frac{1}{2}\boldsymbol{\varepsilon} \otimes \boldsymbol{\varepsilon}$, then we can define:

$$\boldsymbol{\sigma} = \frac{\partial F(\mathbf{L})}{\partial \boldsymbol{\varepsilon}} = \frac{\partial F(\mathbf{L})}{\partial \mathbf{L}} : \boldsymbol{\varepsilon} = \mathbf{C}^{\mathbf{sct}}(\mathbf{L}) : \boldsymbol{\varepsilon} \tag{3.29}$$

which leads to a systematic definition of $\mathbf{C}_r^{\mathbf{sct}}$ (but we have to prove that it leads to $\mathbf{C}_r^{\mathbf{sct}} > 0$). An example of such a potential, would be, for example, an elastic potential where: $2w(\boldsymbol{\varepsilon}) = \boldsymbol{\varepsilon} : \mathbf{C} : \boldsymbol{\varepsilon} = 2F(\mathbf{L}) = \mathbf{C} :: \boldsymbol{\varepsilon} \otimes \boldsymbol{\varepsilon}$. Alternatively, our equivalent stress h can also be expressed as: $2h = \mathbf{Q} ::$

$\boldsymbol{\sigma} \otimes \boldsymbol{\sigma}$. For the classical secant approach, the secant modulus for a material described by a potential is expressed as:

$$\mathbf{C}_r^{\mathbf{sct}} = \frac{\partial F(\frac{1}{2}\bar{\boldsymbol{\varepsilon}} \otimes \bar{\boldsymbol{\varepsilon}})}{\partial \mathbf{L}} \tag{3.30}$$

Authors like Berveiller and Zaoui [5] and Bourgeois [12] developed models with the classical secant linearisation. One clear limitation of the secant approach is that it fails to produce a relevant material when there is unloading. For example, when a polycrystal is strained beyond its elastic limit, there is plastic flow and the behaviour is no longer linear. However, when there is unloading, the material is linear and using a secant modulus does not make sense.

Modified secant model

Following the same line of thought, the modified secant model $\mathbf{C}^{\mathbf{sct_2}}$ is calculated with:

$$\mathbf{C}_r^{\mathbf{sct_2}} = \mathbf{C}_r^{\mathbf{sct_2}}(\langle \mathbf{L} \rangle_r) = \mathbf{C}_r^{\mathbf{sct_2}} \left(\frac{1}{2} \langle \boldsymbol{\varepsilon} \otimes \boldsymbol{\varepsilon} \rangle_r \right) \tag{3.31}$$

where $\langle \boldsymbol{\varepsilon} \otimes \boldsymbol{\varepsilon} \rangle$ is the second moment of the strain field and the subscript 2 has been introduced to illustrate that the secant material is calculated by using the second moments of the strains. The equations involved in the determination of the second moments are beyond the scope of this study.

Authors like Hu [40] and Derrien *et al.* [23] have used such an approach to predict plasticity in porous materials. It is well known that if a hydrostatic pressure is applied to a voided material that the average stress in the matrix is also hydrostatic. Since plasticity is activated by the deviatoric part of the stress tensor, using the mean stress as the reference level, does not the plasticity of the matrix to be taken into account. However, when the second moments are used, some plasticity can develop and the model leads to more realistic predictions.

It should be noted that Suquet [95] has shown that using this modified secant approach leads to the same results as Ponte Castañada's variational procedure [73] when the phases are nonlinear and incompressible. In that case, such an empirical model can be given a variational interpretation.

Incremental formulation

The original incremental formulation is due to Hill [38]. The idea of the incremental procedure is to reach the final load by a series of load increments.

During a load increment, the stiffness (or compliance) of phase r is given by its tangent modulus (or compliance) evaluated at its average stress/strain field. For example:

$$\mathbf{C}_r^{\mathbf{tgt}} = \frac{\partial^2 w(\bar{\boldsymbol{\varepsilon}}_r)}{\partial \boldsymbol{\varepsilon} \partial \boldsymbol{\varepsilon}} = \frac{\partial \bar{\boldsymbol{\sigma}}_r(\bar{\boldsymbol{\varepsilon}}_r)}{\partial \boldsymbol{\varepsilon}} \tag{3.32}$$

In the case of a material described by a potential or a sum of potentials, the definition of a tangent modulus poses no particular problem since we are guaranteed that the resulting tangent modulus is symmetric and positive definite. However, when the material is described by a general state function there is no guarantee that the tangent modulus as defined by the last term of equation (3.32) can be assimilated to a linear elastic material and therefore, the linear elastic homogenisation solutions cannot be used. Such an approach is then limited to materials described by potential(s). Even with such limitation, this approach has been widely applied to polycrystals where the behaviour is well described by potential(s).

Classical affine procedure

Inspired by the works of Rougier [81], Masson [57], Masson *et al.* [58] and Masson and Zaoui [59] introduced their affine procedure. Like the second order procedure of Ponte Castañada [74], the comparison material is composed of thermoelastic phases. The modulus of such phases is the tangent modulus calculated in equation (3.32) and the polarisation stress $\boldsymbol{\sigma}_{\boldsymbol{r}}^{\mathbf{0}}$ (dual of a stress free strain) is calculated by :

$$\frac{\partial w(\bar{\boldsymbol{\varepsilon}}_r)}{\partial \boldsymbol{\varepsilon}} - \mathbf{C}_r^{\mathbf{tgt}} : \bar{\boldsymbol{\varepsilon}}_r = \boldsymbol{\sigma}_{\boldsymbol{r}}^{\mathbf{0}} \tag{3.33}$$

and the behaviour law of the linearised phase is given by:

$$\boldsymbol{\sigma} = \mathbf{C}_r^{\mathbf{tgt}} : \boldsymbol{\varepsilon} + \boldsymbol{\sigma}_{\boldsymbol{r}}^{\mathbf{0}} \tag{3.34}$$

The problem then becomes a problem similar to a thermoelastic problem and can be solved, as we have seen previously, by an homogenisation approach. Masson *et al.* [58] showed for power law materials that the affine formulation leads to estimates that were softer than the classical secant approach but stiffer than the second order procedure of Ponte Castañada. So far, the affine procedure seems the most adequate empirical procedure when only phase averages are used for the linearisation. However, in certain cases, the affine procedure is known to violate some nonlinear bounds [58].

It should be noted that the idea of using a thermoelastic comparison material has been first introduced by Molinari *et al.* [65] in a different context.

Modified affine procedure

Following the same line of thought as in the modified secant approach, Brenner [13] and Brenner *et al.* [14] introduced a modified affine procedure where this time the tangent modulus is calculated for the second moments of the stress/strain field. If the material behaviour is described by a potential $F(\mathbf{L})$ then the tangent modulus is calculated by:

$$\mathbf{C}_r^{\mathbf{tgt_2}} = \frac{\partial^2 F(\langle \mathbf{L} \rangle_r)}{\partial \mathbf{L} \partial \mathbf{L}} :: \langle \boldsymbol{\varepsilon} \otimes \boldsymbol{\varepsilon} \rangle_r + \frac{\partial F(\langle \mathbf{L} \rangle_r)}{\partial \mathbf{L}} \tag{3.35}$$

and the polarisation is calculated by:

$$\hat{\boldsymbol{\sigma}}_r(\langle \bar{\mathbf{L}} \rangle_r, \bar{\boldsymbol{\varepsilon}}_r) - \mathbf{C}_r^{\mathbf{tgt_2}} : \bar{\boldsymbol{\varepsilon}}_r = \boldsymbol{\sigma}_r^{\mathbf{0}} \tag{3.36}$$

where $\hat{\boldsymbol{\sigma}}_r$ is evaluated by the constitutive law using the second moments and the average strain in phase r [14]. The behaviour law of this linearised material then becomes:

$$\boldsymbol{\sigma} = \mathbf{C}_r^{\mathbf{tgt_2}} : \boldsymbol{\varepsilon} + \boldsymbol{\sigma}_r^{\mathbf{0}} \tag{3.37}$$

For the load cases they have simulated, Brenner *et al.* [14] have shown that their modified affine procedure leads to softer estimates than the classical affine and the modified secant procedures. Implementing such a linearisation procedure is more involved than the classical affine procedure because the first and second moments of the stresses/strains in each phases are unknown *a priori*.

It should be noted that Brenner [13] has introduced another linearisation where the linearised material reproduces at best (in the least squares sense) the local behaviour in a given phase r. This approach introduces moments of order higher than two and some assumptions must be made regarding the spatial distribution of the strain/stress field in order to estimate these higher order moments. In addition, the author enforced that the material thus obtained is symmetric for the minimisation of the least squares problem. However, he did not require that the linearised material be definite positive, which could lead to odd results for the homogenised material.

Ponte Castañada [75] has also introduced a modified affine procedure where the linearised material is related to the second moments of the loading. In addition, Lahellec and Suquet [47] have suggested another affine procedure where this time the polarisation $\boldsymbol{\sigma}^{\mathbf{0}}$ depends on the first and second moments and the tangent modulus is evaluated with respect to the first moment. Their procedure has the advantage that it gives the same results as a variational formulation when the potential is approximated by an approximate Taylor expansion[2].

[2]The third order terms in the expansion are linearised.

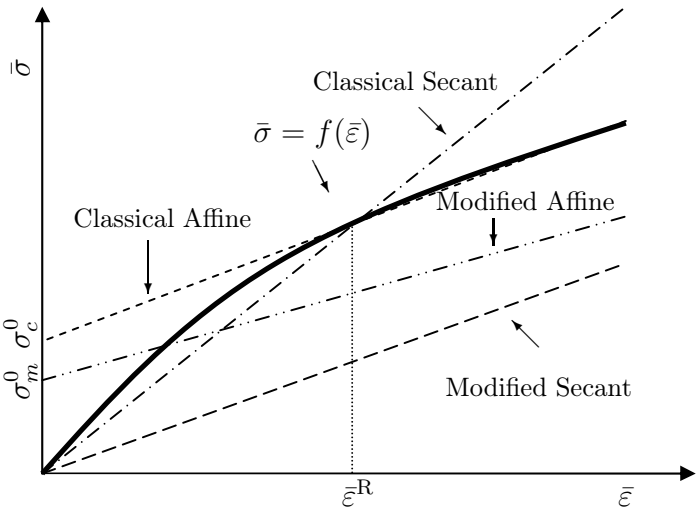


Figure 3.3: Schematic representation of the various empirical linearisation procedures expressed for the phase averages around a given reference strain level $\bar{\varepsilon}^{\mathrm{R}}$. The thick line represents the actual behaviour of the nonlinear material and σ_m^0 and σ_c^0 are the polarisations for the modified and affine procedures, respectively.

Discussion

The various linearisation procedures mentioned previously are illustrated in figure 3.3 so that a graphical interpretation can be given. We recall that the apparent magnitude of the slopes depicted on the picture is only an indication and a comparison of the linearised stiffness is not possible since the first and second moments have different values for the same macroscopic loading, when different linearisations schemes are used.

In most situations, all these linearisation procedures are known to overestimate the overall response of nonlinear composites. For the same type of reference level, it would seem that the affine procedures lead to softer estimates than the secant procedures. For the same type of linearisation, using second moments leads to more compliant estimates than those obtained when using first moments. It would seem, with the limited experience so far, that the modified affine procedures lead to the most accurate estimates (in the context of empirical approaches). On the other hand, we have seen that when the material is not described by a potential, the definition of a secant modulus is not necessarily unique and a tangent modulus can be non symmetric.

The presentation we have made so far has been concerned with non hereditary materials where the response can be predicted by the instantaneous value

of the stress/strain. In our case, the mechanical response depends on the load history and now time is the independent variable. Therefore, we actually deal with behaviour laws that are no longer functions (in the general case) but are functionals of the load. Functional analysis is much more involved than function analysis and in most situations, it is not possible to give an intuitive representation (as it is done in figure 3.3) of the developments. We will see in the following section how some of these linearisation procedures, inspired by variational principles, can be translated to the homogenisation of nonlinear hereditary materials.

3.5 Homogenisation of nonlinear hereditary materials

3.5.1 Variational approaches

Up to very recently, there were no variational estimates for the homogenised behaviour of hereditary materials. The recent work of Lahellec and Suquet [46] use a forward difference to approximate the evolution rate of the internal variables $\dot{\boldsymbol{\xi}}$ (see chapter 1, equation (1.59)) so that: $\dot{\boldsymbol{\xi}}(t_{n+1}) \approx \frac{\boldsymbol{\xi}(t_{n+1})-\boldsymbol{\xi}(t_n)}{\Delta t}$. This way, they obtain a variational problem for a time increment Δt similar to the second order procedure of Ponte Castañada [74]. They have obtained very accurate results when their predictions are compared with numerical simulations of the microstructure.

3.5.2 Empirical approaches

The behaviour of most of the materials used in the empirical approaches available in the literature are described by the following constitutive law:

$$\boldsymbol{\varepsilon} = \mathbf{S} : \boldsymbol{\sigma} + \boldsymbol{\varepsilon}^{\mathrm{ve}}(\boldsymbol{\sigma}, \boldsymbol{\xi}), \quad \dot{\boldsymbol{\xi}} = \boldsymbol{f}(\boldsymbol{\sigma}, \boldsymbol{\xi}) \tag{3.38}$$

or alternatively when the strain rate is expressed:

$$\dot{\boldsymbol{\varepsilon}} = \mathbf{S} : \dot{\boldsymbol{\sigma}} + \dot{\boldsymbol{\varepsilon}}^{\mathrm{ve}}(\boldsymbol{\sigma}, \boldsymbol{\xi}), \quad \dot{\boldsymbol{\xi}} = \boldsymbol{f}(\boldsymbol{\sigma}, \boldsymbol{\xi}) \tag{3.39}$$

In some cases the internal variables are fixed and in other cases they can evolve.

Weng's [100] and Li and Weng's [54] contributions

One of the first contributions was suggested by Weng [100] where he expresses the behaviour law as a function of strain rates. Weng regarded $\dot{\boldsymbol{\varepsilon}}^{\mathrm{ve}}$

as a stress-free strain rate and considered the linearised material as a thermoelastic material. Such an approach has been criticised by many authors (see for example Masson and Zaoui [59]) because $\dot{\boldsymbol{\varepsilon}}^{\mathrm{ve}}$ is not a "true" stress-free strain rate. In addition, this treatment does not preserve the nature of the nonlinear material since the viscoelastic aspect of the constitutive law is lost in the linearisation. Such approaches usually lead to very stiff estimates of the behaviour. Later, Li and Weng [54] proposed a linearisation where the nonlinear material is replaced by a Maxwell material where the elastic part is $\mathbf{S}$ and where the viscous part is such that it leads to the same strain rate as $\dot{\boldsymbol{\varepsilon}}^{\mathrm{ve}}(t)$ evaluated for the effective stress calculated by Qiu and Weng theory [80]. Since the linearised material is linear viscoelastic, the homogenisation is carried out using the correspondence principle and the comparison material has the same nature (i.e., viscoelastic) as the nonlinear material.

The model of Paquin [70] and Paquin *et al.* [71]

We have seen that the homogenisation of viscoelastic materials involves a coupling between time and space. One way to remove this coupling is to use the Laplace-Carson transform so that, in the Laplace-Carson space, we only need to solve the spatial problem, the time solution being obtained by inversion. This requires knowing the whole load history, or at least, up to time t_a, where the solution is sought. One other alternative would be to rewrite the behaviour law with new internal state variables which incorporate, or represent, the stress history. Then, if we seek the solution at time t_a through a series of increments, the solution of each increment only requires the storage of the internal variables at the end of the previous increment. This has the advantage of reducing the computational burden, in comparison with the use of the correspondence principle. On the other hand, it requires a reformulation of the homogenisation problem [71]. The authors have applied their model to linear viscoelastic materials and compared their results with analytical solutions, with good agreement.

Masson's [57] and Masson and Zaoui's [59] linearisation procedure

Rougier [81, 83] initially introduced two linearisations, where the internal state variables evolve or when they are fixed in an incremental context. He also assumed that $\mathbf{S}$ is constant. Later, Masson [57] and Masson and Zaoui [59] clarified his procedures and those are the procedures we present here. The linearisation they suggest in the first case is (where the constitutive law

expresses the strain rate):

$$\begin{aligned}\dot{\boldsymbol{\varepsilon}}(t) = \mathbf{S} : \dot{\boldsymbol{\sigma}}(t) + \frac{\partial \boldsymbol{\varepsilon}^{\mathrm{ve}}}{\partial \boldsymbol{\sigma}}(\boldsymbol{\sigma}(t_a)) : \boldsymbol{\sigma}(t) + \Bigg(\boldsymbol{\varepsilon}^{\mathrm{ve}}(\boldsymbol{\sigma}(t)) \\ - \frac{\partial \boldsymbol{\varepsilon}^{\mathrm{ve}}}{\partial \boldsymbol{\sigma}}(\boldsymbol{\sigma}(t_a)) \Bigg) : \boldsymbol{\sigma}(t) \\ = \mathbf{S} : \dot{\boldsymbol{\sigma}}(t) + \mathbf{S}' : \boldsymbol{\sigma}(t) + \dot{\boldsymbol{\varepsilon}}^{\mathbf{0}}(t) \quad \text{for } t \in [0, t_a]\end{aligned} \tag{3.40}$$

where t_a is the time at which the solution is sought. They also defined the linearisation for $t > t_a$ but we do not need it for our calculations since we seek the response at t_a and we have shown that our homogenisation scheme preserves the causality (see section 3.2). The material described by equation (3.40) is a Maxwell material with a history of stress-free deformation. The history of stress-free deformation is calculated so that the nonlinear material and the linearised material (not the composite material but the material of phase r) have the same response for $t \in [0, t_a]$.

When the internal state variables are active, the linearisation becomes more complex. The authors first made a Taylor expansion of the constitutive law so that it leads to:

$$\begin{aligned}\boldsymbol{\varepsilon}(t) = \mathbf{S} : \boldsymbol{\sigma}(t) + \boldsymbol{\varepsilon}^{\mathrm{ve}}(t_a) + \frac{\partial \boldsymbol{\varepsilon}^{\mathrm{ve}}}{\partial \boldsymbol{\sigma}}(t_a) : [\boldsymbol{\sigma}(t) - \boldsymbol{\sigma}(t_a)] \\ + \frac{\partial \boldsymbol{\varepsilon}^{\mathrm{ve}}}{\partial \boldsymbol{\xi}}(t_a) : [\boldsymbol{\xi}(t) - \boldsymbol{\xi}(t_a)]\end{aligned} \tag{3.41a}$$

$$\dot{\boldsymbol{\xi}} = \boldsymbol{f}(t_a) + \frac{\partial \boldsymbol{f}}{\partial \boldsymbol{\sigma}}(t_a) : [\boldsymbol{\sigma}(t) - \boldsymbol{\sigma}(t_a)] + \frac{\partial \boldsymbol{f}}{\partial \boldsymbol{\xi}}(t_a) : [\boldsymbol{\xi}(t) - \boldsymbol{\xi}(t_a)] \tag{3.41b}$$

where $\boldsymbol{\varepsilon}^{\mathrm{ve}}(t_a) = \boldsymbol{\varepsilon}^{\mathrm{ve}}(\boldsymbol{\sigma}(t_a), \boldsymbol{\xi}(t_a))$ and $\boldsymbol{f}(t_a) = \boldsymbol{f}(\boldsymbol{\sigma}(t_a), \boldsymbol{\xi}(t_a))$. This linearisation defines an entirely new material. They have obtained, in equation (3.41b), a new evolution law for the internal state variables. We have seen in Chapter One that such a system of equations can be solved to obtain the evolution of the state variables as a function of the stress history. However, in the present work, we have assumed that the set of $\boldsymbol{\xi}$ was the one which diagonalised the system. Here, if we were to apply this linearisation to our constitutive law, we would first have to write it in the form of equation (3.38) and then solve this set of differential equations. In addition, this linearised evolution law was calculated irrespective of thermodynamic considerations and there is no guarantee that, when we solve this system of differential equations (as was done by the authors), the linearised material would be thermodynamically valid. When the solution of the differential equations leads to a thermodynamically admissible material, their linearisation leads

also to a linear viscoelastic material with a stress-free strain history. In addition, this stress-free strain is calculated so that the responses of the nonlinear and the linearised materials are identical for all $t \in [0, t_a]$.

It should be noted that Brenner *et al.* [15] have implemented such a model in the case where the internal state variables are fixed. Rather than using the correspondence principle to solve the homogenisation problem, the authors introduce a computationally efficient quasi-elastic approximation of the viscoelastic problem.

3.5.3 Discussion

In this study, we have decided to use an empirical approach to model the behaviour of our nonlinear viscoelastic material. Clearly, our linearised material must share the same characteristics as the nonlinear material (being viscoelastic) so that the nature of the problem is preserved. Masson [57] and Masson and Zaoui [59] have introduced a relevant linearisation procedure but since the behaviour of our material is not expressed as in equation (3.38), but as a functional of stress, their approach might not be practicable. On the other hand, this affine linearisation was given a more formal and general interpretation by Pouya and Zaoui [78]. There, instead of considering the evolution of the state variables, the authors considered a functional representation of the behaviour law. They considered the strain history as a functional of stress and derived a linearised model. In other words, they addressed the exact same issue but from a different perspective. In our case, the constitutive law is also given as a functional of stress and their developments would appear to be more suitable than the one suggested in the last subsection.

3.6 A new general methodology to generate empirical linearisations of nonlinear viscoelastic materials

In this section we use some of the basic ideas of Pouya and Zaoui [78] to develop a general methodology to derive empirical linearisations. We show that, in fact, we can generate a wide range of models, as was done for non hereditary materials by using similar concepts. We give first the affine model generated by Pouya and Zaoui [78]. Then we derive three new models: a modified affine model, a classical secant model and a modified secant model. In the developments, we identify the limitations of such approaches. In addi-

tion, we present the linearisations outside the general context of homogenisation for clarity. We discuss in section 3.7 how the models are implemented using materials linearised following these procedures.

3.6.1 The affine model of Pouya and Zaoui [78]

The development introduced by Pouya and Zaoui [78] relies on functional analysis. As much as possible, we adopt a notation, as was done by Pouya and Zaoui [78], which is illustrative and can be related to the empirical approaches discussed previously. In our notation, a bold capital gothic letter represents a nonlinear functional while a bold capital calligraphic roman letter represents a linear functional. In the sequel, we assume that the stress and strain histories are as smooth as we want (i.e., their derivatives do not present discontinuities) and they are bounded.

In this section, unless it is specified otherwise, $\boldsymbol{\sigma}$ and $\boldsymbol{\varepsilon}$ should be interpreted as $\boldsymbol{\sigma}(t)$ and $\boldsymbol{\varepsilon}(t)$ repectively. They are no longer instantaneous values, but histories, functions of time. We recall that our main objective is to calculate the homogenised response of a nonlinear viscoelastic material up to a given time t_a. We have seen in section 3.2 that calculating the response up to t_a only requires knowing the constitutive material responses up to t_a only. In other words, we do not need the histories of the quantities involved in the homogenisation process over the interval $[t_a, \infty[$.

In the most general case, we have that the stress history, up to a time t is related to the strain history by a functional, namely:

$$\boldsymbol{\varepsilon} = \boldsymbol{\mathfrak{F}}\left[\boldsymbol{\sigma}\right]_{\tau=0}^{\tau=t} = \boldsymbol{\mathfrak{F}} \circledast \boldsymbol{\sigma} \tag{3.42}$$

where $\boldsymbol{\mathfrak{F}}$ is a causal functional or operator. The notation $\boldsymbol{\mathfrak{F}} \circledast \boldsymbol{\sigma}$ means that this operator is applied to the stress history. This notation is analogous to a contracted product and has been introduced so that a conceptual link can be established with elasticity. This renders the interpretation of the results easier. More formally, $\boldsymbol{\varepsilon}$, $\boldsymbol{\sigma} \in \boldsymbol{\mathcal{M}}_{3\times3}$ where $\boldsymbol{\mathcal{M}}_{3\times3}$ is the vectorial space of symmetric second order tensors of continuous functions and $\boldsymbol{\mathfrak{F}}$ is an operator from $\boldsymbol{\mathcal{M}}_{3\times3}$ to $\boldsymbol{\mathcal{M}}_{3\times3}$.

Now consider a given stress history $\breve{\boldsymbol{\sigma}}$ and its associated response given by $\breve{\boldsymbol{\varepsilon}} = \boldsymbol{\mathfrak{F}} \circledast \breve{\boldsymbol{\sigma}}$. We suppose that $\boldsymbol{\mathfrak{F}}$ is differentiable in the sense of Fréchet so that:

$$\boldsymbol{\mathfrak{F}} \circledast (\breve{\boldsymbol{\sigma}} + \boldsymbol{\Delta\sigma}) = \boldsymbol{\mathfrak{F}} \circledast \breve{\boldsymbol{\sigma}} + \boldsymbol{\mathcal{S}} \circledast \boldsymbol{\Delta\sigma} + ||\boldsymbol{\Delta\sigma}||\boldsymbol{\mathfrak{A}} \circledast \boldsymbol{\Delta\sigma} \tag{3.43}$$

where $||\cdot||$ is a norm (i.e., a scalar),

$$\lim_{||\boldsymbol{\Delta\sigma}||\to0} ||\boldsymbol{\mathfrak{A}} \circledast \boldsymbol{\Delta\sigma}|| = 0 \tag{3.44}$$

and $\boldsymbol{\mathcal{S}}$ is unique, linear and causal [78]. Now suppose that $\breve{\boldsymbol{\sigma}}$ is close to $\boldsymbol{\sigma}$ so that $||\boldsymbol{\sigma} - \breve{\boldsymbol{\sigma}}|| = ||\boldsymbol{\delta\sigma}|| \ll 1$. The last term in equation (3.43) can then be neglected and we obtain:

$$\boldsymbol{\mathfrak{F}} \circledast (\breve{\boldsymbol{\sigma}} + \boldsymbol{\delta\sigma}) - \boldsymbol{\mathfrak{F}} \circledast \breve{\boldsymbol{\sigma}} = \boldsymbol{\varepsilon} - \breve{\boldsymbol{\varepsilon}} = \boldsymbol{\delta\varepsilon} = \boldsymbol{\mathcal{S}} \circledast \boldsymbol{\delta\sigma} \tag{3.45}$$

where $\boldsymbol{\mathcal{S}}$ can be interpreted as a linear functional linking the variation of the strain history when a variation of the stress history occurs around a reference level of $\breve{\boldsymbol{\sigma}}$. $\boldsymbol{\mathcal{S}}$ can then be interpreted as the tangent material to the material described by $\boldsymbol{\mathfrak{F}}$ around $\breve{\boldsymbol{\sigma}}$. We denote this material by $\boldsymbol{\mathcal{S}}^{\mathbf{tgt}}_{\breve{\boldsymbol{\sigma}}}$. Since $\boldsymbol{\mathcal{S}}$ is a linear operator, equation (3.45) can be rewritten in the form:

$$\boldsymbol{\varepsilon} = \boldsymbol{\mathcal{S}}^{\mathbf{tgt}}_{\breve{\boldsymbol{\sigma}}} \circledast \boldsymbol{\sigma} + \boldsymbol{\varepsilon}^{\mathbf{0}} \tag{3.46}$$

where $\boldsymbol{\varepsilon}^{\mathbf{0}} = \breve{\boldsymbol{\varepsilon}} - \boldsymbol{\mathcal{S}}^{\mathbf{tgt}}_{\breve{\boldsymbol{\sigma}}} \circledast \breve{\boldsymbol{\sigma}}$. It is evident that $\boldsymbol{\varepsilon}^{\mathbf{0}}$ is a stress free strain history since it does not depend on the load history $\boldsymbol{\sigma}$. It can also be observed that the affine and nonlinear material have the same response when $\breve{\boldsymbol{\sigma}}$ is applied. In the classical affine model, the tangent material is calculated so that:

$$\boldsymbol{\mathfrak{F}} \circledast \langle \breve{\boldsymbol{\sigma}} + \boldsymbol{\delta\sigma} \rangle - \boldsymbol{\mathfrak{F}} \circledast \langle \breve{\boldsymbol{\sigma}} \rangle = \boldsymbol{\mathcal{S}}^{\mathbf{tgt}}_{\langle \breve{\boldsymbol{\sigma}} \rangle} \circledast \langle \boldsymbol{\delta\sigma} \rangle \tag{3.47}$$

and the linearised constitutive law is:

$$\boldsymbol{\varepsilon} = \boldsymbol{\mathcal{S}}^{\mathbf{tgt}}_{\langle \breve{\boldsymbol{\sigma}} \rangle} \circledast \boldsymbol{\sigma} + \boldsymbol{\varepsilon}^{\mathbf{0}} \tag{3.48}$$

where $\boldsymbol{\varepsilon}^{\mathbf{0}} = \boldsymbol{\mathfrak{F}} \circledast \langle \breve{\boldsymbol{\sigma}} \rangle - \boldsymbol{\mathcal{S}}^{\mathbf{tgt}}_{\langle \breve{\boldsymbol{\sigma}} \rangle} \circledast \langle \breve{\boldsymbol{\sigma}} \rangle$. We can see the similarity of this general affine model to the classical affine model obtained for non hereditary materials.

3.6.2 A modified affine model

A modified affine model, similar to that of Brenner [13] can also be given such an interpretation. For example:

$$\begin{aligned} \boldsymbol{\mathfrak{F}} \circledast \left(\boldsymbol{\mathcal{K}} \circledast \breve{\mathbf{M}} + \boldsymbol{\delta\mathcal{K}} \circledast \mathbf{M} \right) - \boldsymbol{\mathfrak{F}} \circledast \left(\boldsymbol{\mathcal{K}} \circledast \breve{\mathbf{M}} \right) &= \boldsymbol{\mathcal{S}}^{\mathbf{tgt_2}} \circledast (\boldsymbol{\delta\mathcal{K}} \circledast \mathbf{M}) \\ &= \boldsymbol{\mathcal{S}}^{\mathbf{tgt_2}} \circledast \boldsymbol{\delta\sigma_2} \end{aligned} \tag{3.49}$$

where $\mathbf{M} = \boldsymbol{\sigma} \otimes \boldsymbol{\sigma}$ and $\boldsymbol{\mathcal{K}}$ is a functional which projects the fourth order tensor $\mathbf{M}$ to a second order tensor $\boldsymbol{\delta\sigma_2}$, where again the subscript 2 is included to mark the fact that this quantity is calculated from $\mathbf{M}$. In addition, we set that $\boldsymbol{\delta\sigma_2}(t_i)$ is calculated by using only the values of $\mathbf{M}$ evaluated at $t = t_i$. For example, we can have that $\delta\sigma_{2_{ij}}(t) = \sqrt{M_{ijij}(t)}$. This operator is introduced

since the final objective is to obtain a linear viscoelastic constitutive law and such laws usually have as input the history of a second order tensor. The tangent material is calculated so that the following relation is satisfied:

$$\boldsymbol{\mathfrak{F}} \circledast \left(\boldsymbol{\mathcal{K}} \circledast \left\langle \breve{\mathbf{M}} \right\rangle + \boldsymbol{\delta\sigma_2} \right) - \boldsymbol{\mathfrak{F}} \circledast \left(\boldsymbol{\mathcal{K}} \circledast \left\langle \breve{\mathbf{M}} \right\rangle \right) = \boldsymbol{\mathcal{S}}^{\mathbf{tgt_2}}_{\left\langle \breve{\mathbf{M}} \right\rangle} \circledast \boldsymbol{\delta\sigma_2} \tag{3.50}$$

The final behaviour law of the linearised material is:

$$\boldsymbol{\varepsilon} = \boldsymbol{\mathcal{S}}^{\mathbf{tgt_2}}_{\left\langle \breve{\mathbf{M}} \right\rangle} \circledast \boldsymbol{\sigma} + \boldsymbol{\varepsilon}^0 \tag{3.51}$$

where:

$$\boldsymbol{\varepsilon}^0 = \boldsymbol{\mathfrak{F}} \circledast \left(\boldsymbol{\mathcal{K}} \circledast \left\langle \breve{\mathbf{M}} \right\rangle \right) - \boldsymbol{\mathcal{S}}^{\mathbf{tgt_2}}_{\left\langle \breve{\mathbf{M}} \right\rangle} \circledast \left(\boldsymbol{\mathcal{K}} \circledast \left\langle \breve{\mathbf{M}} \right\rangle \right) \tag{3.52}$$

Other variants of this modified affine model can be obtained by using the first and second moments differently.

3.6.3 Limitations of the general affine linearisation

We are satisfied that we have obtained, in theory, general affine models for nonlinear viscoelasticity. However, there are some major practical difficulties with this linearisation.

1. Except for very specific cases (a simple behaviour law or simple loading), it is not possible to obtain a closed form expression for the tangent material.

2. Although $\boldsymbol{\mathcal{S}}$ is a linear causal functional, there is no guarantee that it is similar to a linear viscoelastic material. We have seen in section 1.3 and in equations (1.22,1.24) that linear viscoelasticity can be given a quite general functional representation. However, linear viscoelastic materials are a specific group of linear functionals and there is no way to impose that $\boldsymbol{\mathcal{S}}$ falls within this group. This can be problematic because if $\boldsymbol{\mathcal{S}}$ is not a linear viscoelastic material, there is no guarantee that the correspondence principle can be used to perform the homogenisation.

To illustrate this second difficulty, consider our behaviour law described at equation (1.58). Suppose the various $g_i = g_i(h_i)$ where $h_i = \frac{1}{2}\boldsymbol{\sigma} : \mathbf{Q}^{(\mathbf{i})} : \boldsymbol{\sigma}$ for generality. Suppose that a creep load (i.e., $\boldsymbol{\sigma}(t) = \boldsymbol{\sigma}^{\mathbf{cr}} = ct$) is applied to this material. The creep response of such a material is given by:

$$\boldsymbol{\varepsilon}(t) = g_0 \mathbf{Q}^{(\mathbf{0})} : \boldsymbol{\sigma}^{\mathbf{cr}} + g_2' \left(\frac{\partial g_1}{\partial h_1} \mathbf{Q}^{(\mathbf{1})} : \boldsymbol{\sigma}^{\mathbf{cr}} \otimes \boldsymbol{\sigma}^{\mathbf{cr}} + g_1 \mathbf{I} \right) : \boldsymbol{\Delta}\mathbf{S}(g_3 t) : \boldsymbol{\sigma}^{\mathbf{cr}} \tag{3.53}$$

In that case, if we suppose that $\boldsymbol{\mathcal{S}}$ is a convolution operator similar to a linear viscoelastic behaviour law, the expression of the kernel of $\boldsymbol{\mathcal{S}}$ (i.e., the tangent creep compliance) is simply given by $\frac{\partial \boldsymbol{\varepsilon}(t)}{\partial \boldsymbol{\sigma}^{\mathbf{cr}}}$ which leads to (after tedious calculations):

$$\begin{aligned}
\frac{\partial \boldsymbol{\varepsilon}(t)}{\partial \boldsymbol{\sigma}^{\mathbf{cr}}} = & \frac{\partial g_0}{\partial h_0}\mathbf{Q}^{(\mathbf{0})} : \boldsymbol{\sigma}^{\mathbf{cr}} \otimes \boldsymbol{\sigma}^{\mathbf{cr}} : \mathbf{Q}^{(\mathbf{0})} + g_0 \mathbf{Q}^{(\mathbf{0})} \\
& + \frac{\partial^2 g_1}{\partial h_1^2} g_2' A(t) \mathbf{Q}^{(\mathbf{1})} : \boldsymbol{\sigma}^{\mathbf{cr}} \otimes \boldsymbol{\sigma}^{\mathbf{cr}} : \mathbf{Q}^{(\mathbf{1})} \\
& + \frac{\partial g_1}{\partial h_1} g_2' \Big[A(t) \mathbf{Q}^{(\mathbf{1})} + \mathbf{Q}^{(\mathbf{1})} : \boldsymbol{\sigma}^{\mathbf{cr}} \otimes \boldsymbol{\sigma}^{\mathbf{cr}} : \boldsymbol{\Delta}\mathbf{S}(g_3 t) \Big] \\
& + \frac{\partial g_1}{\partial h_1} g_2' \frac{\partial g_3}{\partial h_3} t \mathbf{Q}^{(\mathbf{1})} : \boldsymbol{\sigma}^{\mathbf{cr}} \otimes \boldsymbol{\sigma}^{\mathbf{cr}} : \frac{\partial \boldsymbol{\Delta}\mathbf{S}(g_3 t)}{\partial (g_3 t)} : \boldsymbol{\sigma}^{\mathbf{cr}} \otimes \boldsymbol{\sigma}^{\mathbf{cr}} : \mathbf{Q}^{(\mathbf{3})} \\
& + \frac{\partial g_1}{\partial h_1} \frac{\partial g_2'}{\partial h_2} \mathbf{Q}^{(\mathbf{1})} : \boldsymbol{\sigma}^{\mathbf{cr}} \otimes \boldsymbol{\sigma}^{\mathbf{cr}} : \boldsymbol{\Delta}\mathbf{S}(g_3 t) : \boldsymbol{\sigma}^{\mathbf{cr}} \otimes \boldsymbol{\sigma}^{\mathbf{cr}} : \mathbf{Q}^{(\mathbf{2})} \\
& + 2 \frac{\partial g_1}{\partial h_1} g_2' \mathbf{Q}^{(\mathbf{1})} : \boldsymbol{\sigma}^{\mathbf{cr}} \otimes \boldsymbol{\sigma}^{\mathbf{cr}} : \boldsymbol{\Delta}\mathbf{S}(g_3 t) \\
& + g_1 \frac{\partial g_2'}{\partial h_2} \mathbf{Q}^{(\mathbf{2})} : \boldsymbol{\sigma}^{\mathbf{cr}} \otimes \boldsymbol{\sigma}^{\mathbf{cr}} : \boldsymbol{\Delta}\mathbf{S}(g_3 t) \\
& + g_1 g_2' \frac{\partial g_3}{\partial h_3} \frac{\partial \boldsymbol{\Delta}\mathbf{S}(g_3 t)}{\partial (g_3 t)} : \boldsymbol{\sigma}^{\mathbf{cr}} \otimes \boldsymbol{\sigma}^{\mathbf{cr}} : \mathbf{Q}^{(\mathbf{3})} + g_1 g_2' \boldsymbol{\Delta}\mathbf{S}(g_3 t)
\end{aligned} \tag{3.54}$$

where:

$$A(t) = \boldsymbol{\sigma}^{\mathbf{cr}} : \boldsymbol{\Delta}\mathbf{S}(g_3 t) : \boldsymbol{\sigma}^{\mathbf{cr}} \tag{3.55}$$

It can easily be seen from equation (3.54) that setting $\mathbf{Q}^{(\mathbf{i})} = \mathbf{Q}$ and $\boldsymbol{\Delta}\mathbf{S}(t) = f(t)\mathbf{Q}$ leads to a symmetric creep compliance (which is also our hypothesis). However, even if this specific choice is made, there is no guarantee that $\frac{\partial \boldsymbol{\varepsilon}(t)}{\partial \boldsymbol{\sigma}} \geq 0$ for all t. This comes from the fact that there is no restriction for the sign of the slopes of g_2' and g_3 and the second derivative of g_1. If these were all set greater than zero, then a symmetric and definite semi-positive tangent creep compliance would be obtained. This exercise shows that, when calculable, unless very specific loading and constitutive laws are used, the tangent material calculated exactly by this general linearisation procedure will not be consistent with the resolution technique we have chosen for the homogenisation problem.

Another example of calculating a tangent material in this way is given in Pouya and Zaoui [78]. The authors have considered a behaviour law of the type:

$$\dot{\boldsymbol{\varepsilon}}(t) = \mathbf{S} : \dot{\boldsymbol{\sigma}}(t) + \dot{\boldsymbol{\varepsilon}}^{\mathrm{ve}}(\boldsymbol{\sigma}(t)) \tag{3.56}$$

where there are no internal state variables. They define the following tangent model:

$$\boldsymbol{\delta\dot{\varepsilon}} = \mathbf{S} : \boldsymbol{\delta\dot{\sigma}} + \frac{\partial \dot{\boldsymbol{\varepsilon}}^{\mathrm{ve}}(\breve{\boldsymbol{\sigma}}(t))}{\partial \boldsymbol{\sigma}} : \boldsymbol{\delta\sigma} \tag{3.57}$$

which leads to the following affine model (after time integration):

$$\begin{aligned} \boldsymbol{\varepsilon}(t) &= \mathbf{S} : \boldsymbol{\sigma}(t) + \int_0^t \frac{\partial \dot{\boldsymbol{\varepsilon}}^{\mathrm{ve}}(\breve{\boldsymbol{\sigma}}(\tau))}{\partial \boldsymbol{\sigma}} : \boldsymbol{\sigma}(\tau)\mathrm{d}\tau \\ &\quad + \int_0^t \left[\dot{\boldsymbol{\varepsilon}}^{\mathrm{ve}}(\breve{\boldsymbol{\sigma}}(\tau)) - \frac{\partial \dot{\boldsymbol{\varepsilon}}^{\mathrm{ve}}(\breve{\boldsymbol{\sigma}}(\tau))}{\partial \boldsymbol{\sigma}} : \breve{\boldsymbol{\sigma}}(\tau)\right]\mathrm{d}\tau \\ &= \mathbf{S} : \boldsymbol{\sigma}(t) + \int_0^t \mathbf{N}_{\breve{\boldsymbol{\sigma}}}(\tau) : \boldsymbol{\sigma}(\tau)\mathrm{d}\tau + \boldsymbol{\varepsilon}^{\mathbf{0}}(t) \end{aligned} \tag{3.58}$$

If $\breve{\boldsymbol{\sigma}}$ is a creep loading, then equation (3.58) leads to a Maxwell model since $\mathbf{N}_{\breve{\boldsymbol{\sigma}}}(t_a) = ct$ (under the condition that $\mathbf{N}_{\breve{\boldsymbol{\sigma}}}(t_a) > 0$). However, for a more complicated loading, it does not lead to a Maxwell model. Consider, for illustrative purposes, the following example. We have seen in section 1.3 that a general viscoelastic material is not limited to a Maxwell model. It is possible to manipulate equation (3.58) so that we obtain a form similar to a linear viscoelastic constitutive law. For simplicity, consider a one-dimensional behaviour law. In addition, assume that $\dot{\varepsilon}^{\mathrm{ve}} = \alpha\sigma^n$ where $0 \leq n \leq 1$ and that $\breve{\sigma} = \beta t$, with $\beta > 0$. With this choice, the integral in equation (3.58) becomes:

$$\int_0^t \frac{\partial \dot{\varepsilon}^{\mathrm{ve}}(\breve{\sigma}(\tau))}{\partial \sigma}\sigma(\tau)\mathrm{d}\tau = \int_0^t n\alpha\beta^{n-1}\tau^{n-1}\sigma(\tau)\mathrm{d}\tau \tag{3.59}$$

Integration by parts leads to:

$$\int_0^t n\alpha\beta^{n-1}\tau^{n-1}\sigma(\tau)\mathrm{d}\tau = \frac{\alpha}{\beta}\beta^n t^n\sigma(t) - \int_0^t \frac{\alpha}{\beta}\beta^n\tau^n\frac{\mathrm{d}\sigma}{\mathrm{d}\tau}\mathrm{d}\tau \tag{3.60}$$

If we define:

$$\tilde{S}(t,x) = \frac{\alpha}{\beta}\beta^n\left[t^n - (t-x)^n\right] \tag{3.61}$$

equation (3.59) becomes:

$$\int_0^t n\alpha\beta^{n-1}\tau^{n-1}\sigma(\tau)\mathrm{d}\tau = \int_0^t \tilde{S}(t,t-\tau)\frac{\mathrm{d}\sigma}{\mathrm{d}\tau}\mathrm{d}\tau \tag{3.62}$$

which has the same shape as a linear viscoelastic behaviour law. However, it is not. The first reason is that $\tilde{S}(t,x)$ depends on the time t at which the

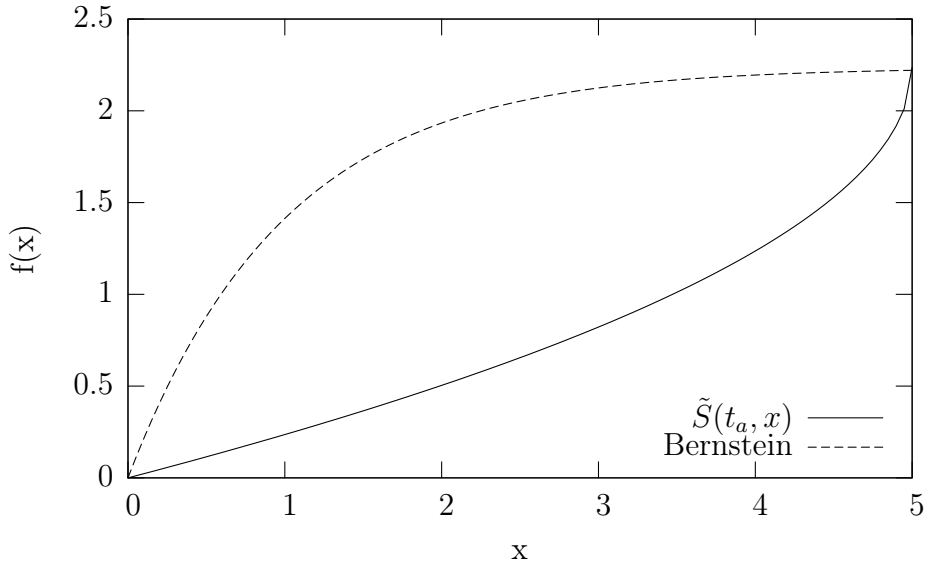


Figure 3.4: Comparison between a typical Bernstein function and the pseudo creep compliance $\tilde{S}$ calculated in equation (3.61) where $\alpha = \beta = t_a = 5$ and $n = 0.5$.

response is sought. In other words, the material parameters of the creep compliance are different for different values of t. Such material can be interpreted as an ageing material[3].

One alternative would be to use an approximate expression of $\tilde{S}(t, x)$ which is similar to a linear viscoelastic behaviour law. Suppose that the approximation we make is the following: $\tilde{S}(t, x) \approx \tilde{S}(t_a, x)$. This way, the approximate material has a similar shape to a linear viscoelastic material. We recall from section 1.3 that a creep compliance must be a Bernstein function. By definition, a Bernstein function is such that $f(x) \geq 0$ and $(-1)^p D^p f(x) \leq 0$ for all x [10] (and where D^p is the differentiation operator). It can be seen that successive differentiation of $\tilde{S}(t_a, x)$ with respect to x leads to $D^p \tilde{S}(t_a, x) \geq 0$, which does not meet the definition of a Bernstein function. Figure 3.4 compares $\tilde{S}(t_a, x)$ with a typical Bernstein function. It can be seen that such approximation will fail to generate a thermodynamically admissible linear viscoelastic material. Other load cases can be found where the same problem is encountered. Therefore, except for very particular loadings, we can expect that the affine model used for the homogenisation will be an

[3]We would like to point out that Schapery has developed a correspondence principle (see the appendix of [92]) for linear viscoelastic materials with ageing in the context of crack growth. The application of this correspondence principle to our problem has not been studied here.

approximation of the exact affine model.

Pouya and Zaoui [78] introduce the following approximation for the tangent material (see equation (3.57)):

$$\boldsymbol{\delta}\dot{\boldsymbol{\varepsilon}} = \mathbf{S} : \boldsymbol{\delta}\dot{\boldsymbol{\sigma}} + \mathbf{N}_{\breve{\boldsymbol{\sigma}}}(t_a) : \boldsymbol{\delta}\boldsymbol{\sigma} \tag{3.63}$$

where we recall that $\mathbf{N}_{\breve{\boldsymbol{\sigma}}}(t_a)$ is a constant. Such a treatment leads to a Maxwell model (under the assumption that $\mathbf{N}_{\breve{\boldsymbol{\sigma}}}(t_a) > 0$) where the constants are such that $\boldsymbol{\delta}\dot{\boldsymbol{\varepsilon}}(t_a)$ is equal to the strain rate of the Maxwell model, evaluated at t_a, when subjected to the same $\boldsymbol{\delta}\boldsymbol{\sigma}$. After integration, the approximate affine model becomes:

$$\boldsymbol{\varepsilon}(t) = \mathbf{S} : \boldsymbol{\sigma}(t) + \mathbf{N}_{\breve{\boldsymbol{\sigma}}}(t_a) : \int_0^t \boldsymbol{\sigma}(\tau)\mathrm{d}\tau + \boldsymbol{\varepsilon}^{\mathbf{0}}(t) \quad \text{for} \quad t \in [0, t_a] \tag{3.64}$$

This is exactly the linearisation introduced by Rougier [83] and used by Masson [57] and Masson and Zaoui [59] (see equation (3.40)). Their linearisation can then be interpreted as an approximate affine linearisation in this general context.

Pouya and Zaoui [78] also introduced a general procedure to improve the latter approximation. The approach involves higher order time differentiation of the constitutive law and leads to a viscoelastic model where the compliance is expressed as a polynomial of time. Brenner [13] has used this procedure and, for the cases he simulated, obtained a slight difference between the first and second order approximations. If we consider a "second order" approximation, in one dimension, the creep compliance is given by (see appendix D in the thesis of Brenner [13]):

$$S(t) = a_0 + a_1 t + a_2 \frac{t^2}{2} \tag{3.65}$$

where there is no *a priori* thermodynamic restrictions on the a_i constants. It can readily be seen, if we have all $a_i > 0$, that equation (3.65) is not a Bernstein function and therefore it does not represent the constitutive law of a thermodynamically admissible material. There is therefore no guarantee that the homogenised compliance of this comparison material is physically reasonable. One other alternative would be generating the following system of equations:

$$\begin{aligned} \boldsymbol{\delta}\boldsymbol{\varepsilon}(t_a) &= \hat{\boldsymbol{\mathcal{S}}} \circledast \boldsymbol{\delta}\boldsymbol{\sigma} \\ \tfrac{\mathrm{d}\boldsymbol{\delta}\boldsymbol{\varepsilon}}{\mathrm{d}t}(t_a) &= \tfrac{\mathrm{d}}{\mathrm{d}t}\left(\hat{\boldsymbol{\mathcal{S}}} \circledast \boldsymbol{\delta}\boldsymbol{\sigma}\right) \\ &\vdots \\ \tfrac{\mathrm{d}^n\boldsymbol{\delta}\boldsymbol{\varepsilon}}{\mathrm{d}t^n}(t_a) &= \tfrac{\mathrm{d}^n}{\mathrm{d}t^n}\left(\hat{\boldsymbol{\mathcal{S}}} \circledast \boldsymbol{\delta}\boldsymbol{\sigma}\right) \end{aligned} \tag{3.66}$$

where the unknowns are the parameters of $\hat{\boldsymbol{\mathcal{S}}}$. This forces the approximate and exact tangent materials to have similar responses (i.e., $\boldsymbol{\delta\varepsilon}$ as a consequence of $\boldsymbol{\delta\sigma}$) for $t \in [t_{a-1}, t_a]$ where $t_{a-1} < t_a$. This problem is ill posed because even if we set the shape of $\hat{\boldsymbol{\mathcal{S}}}$, there is no guarantee that there is a solution or that the solution is unique. In addition, if there are solutions, there is no guarantee that they lead to materials that are thermodynamically admissible. The question of the approximation is discussed further in section 3.6.7.

In light of these observations, the linearised behaviour law used in the homogenisation process resulting from the affine formulation is:

$$\boldsymbol{\varepsilon} = \hat{\boldsymbol{\mathcal{S}}}^{\mathbf{tgt}}_{\langle\breve{\boldsymbol{\sigma}}\rangle} \circledast \boldsymbol{\sigma} + \boldsymbol{\varepsilon}^{\mathbf{0}} \tag{3.67}$$

where $\boldsymbol{\varepsilon}^{\mathbf{0}} = \mathfrak{F} \circledast \langle\breve{\boldsymbol{\sigma}}\rangle - \hat{\boldsymbol{\mathcal{S}}}^{\mathbf{tgt}}_{\langle\breve{\boldsymbol{\sigma}}\rangle} \circledast \langle\breve{\boldsymbol{\sigma}}\rangle$ and where $\hat{\boldsymbol{\mathcal{S}}}^{\mathbf{tgt}}_{\langle\breve{\boldsymbol{\sigma}}\rangle}$ is an approximation of the exact tangent material $\boldsymbol{\mathcal{S}}^{\mathbf{tgt}}_{\langle\breve{\boldsymbol{\sigma}}\rangle}$. Again, it is clear that $\boldsymbol{\varepsilon}^{\mathbf{0}}$ is a stress free strain since it does not depend on $\boldsymbol{\sigma}$. In addition, we also set that $\hat{\boldsymbol{\mathcal{S}}}^{\mathbf{tgt}}_{\langle\breve{\boldsymbol{\sigma}}\rangle}$ must represent a thermodynamically admissible linear viscoelastic material so that the correspondence principle can be used to solve the homogenisation problem. In other words, $\hat{\boldsymbol{\mathcal{S}}}^{\mathbf{tgt}}_{\langle\breve{\boldsymbol{\sigma}}\rangle} \circledast \boldsymbol{\sigma}$ should be interpreted as: $\int_0^t \hat{\boldsymbol{\mathcal{S}}}^{\mathbf{tgt}}_{\langle\breve{\boldsymbol{\sigma}}\rangle}(t-\tau) : \dot{\boldsymbol{\sigma}}(\tau)\mathrm{d}\tau$.

3.6.4 An approximate classical secant linearisation

Following a procedure similar to the one used in the development of the affine models, we introduce a secant material $\mathfrak{S}^{\mathbf{sct}}_{\breve{\boldsymbol{\sigma}}}$ which is calculated so that:

$$\breve{\boldsymbol{\varepsilon}} = \mathfrak{S}^{\mathbf{sct}}_{\breve{\boldsymbol{\sigma}}} \circledast \breve{\boldsymbol{\sigma}} = \mathfrak{F} \circledast \breve{\boldsymbol{\sigma}} \tag{3.68}$$

As in the case of non hereditary materials, $\mathfrak{S}^{\mathbf{sct}}_{\breve{\boldsymbol{\sigma}}}$ might not be uniquely defined. In addition, it is most likely that $\mathfrak{S}^{\mathbf{sct}}_{\breve{\boldsymbol{\sigma}}}$ is not a linear functional and therefore there is no guarantee that $\mathfrak{S}^{\mathbf{sct}}_{\breve{\boldsymbol{\sigma}}}$ describes a linear viscoelastic material.

Consider now our behaviour law which is subjected to a given load history $\breve{\boldsymbol{\sigma}}$. Then, we have:

$$\breve{\boldsymbol{\varepsilon}} = \mathbf{Q} : \breve{\boldsymbol{\sigma}}(t) + \int_0^t \boldsymbol{\Delta}\tilde{\mathbf{S}}(t-\tau) : g_2(h(\breve{\boldsymbol{\sigma}}(\tau)))\breve{\boldsymbol{\sigma}}(\tau)\mathrm{d}\tau \tag{3.69}$$

where we recall that $\boldsymbol{\Delta}\tilde{\mathbf{S}}(t) = \sum_{m=1}^{3} \mathbf{Q}\alpha_m\lambda_m \exp[-\lambda_m t]$. For simplicity, denote $g_2(h(\breve{\boldsymbol{\sigma}}(\tau)))$ by $\breve{g}_2(\tau)$. Now define:

$$\breve{\mathbf{S}}(t,x) = \boldsymbol{\Delta}\tilde{\mathbf{S}}(t)\breve{g}_2(t-x) + \mathbf{Q}\delta(t-\Delta) \tag{3.70}$$

where $\Delta \ll 1$ and positive and $\delta(t)$ is a Dirac impulse centered on t. This leads to:

$$\breve{\boldsymbol{\varepsilon}} = \int_0^t \breve{\mathbf{S}}(t, t-\tau) : \breve{\boldsymbol{\sigma}}(\tau)\mathrm{d}\tau \tag{3.71}$$

which defines a secant operator. Then, the secant model would be:

$$\begin{aligned} \boldsymbol{\varepsilon} &= \int_0^t \breve{\mathbf{S}}(t, t-\tau) : \boldsymbol{\sigma}(\tau)\mathrm{d}\tau \\ &= \boldsymbol{\mathcal{S}}^{\mathbf{sct}}_{\breve{\boldsymbol{\sigma}}} \circledast \boldsymbol{\sigma} \end{aligned} \tag{3.72}$$

In this particular case, $\breve{\mathbf{S}}$ is a linear functional since it does not depend on $\boldsymbol{\sigma}$. For this specific behaviour law, we can see that $\breve{\mathbf{S}}$ has the same symmetries as $\mathbf{Q}$[4]. However, it is not a linear viscoelastic behaviour law since the definition of the pseudo creep compliance depends on the time where the response is sought. So, as was done previously, we introduce an approximation of $\boldsymbol{\mathcal{S}}^{\mathbf{sct}}_{\breve{\boldsymbol{\sigma}}} \approx \hat{\boldsymbol{\mathcal{S}}}^{\mathbf{sct}}_{\breve{\boldsymbol{\sigma}}}$ and our approximate secant model becomes:

$$\boldsymbol{\varepsilon} = \hat{\boldsymbol{\mathcal{S}}}^{\mathbf{sct}}_{\breve{\boldsymbol{\sigma}}} \circledast \boldsymbol{\sigma} + \boldsymbol{\varepsilon}^{\mathbf{cor}} \tag{3.73}$$

where $\boldsymbol{\varepsilon}^{\mathbf{cor}} = \breve{\boldsymbol{\varepsilon}} - \hat{\boldsymbol{\mathcal{S}}}^{\mathbf{sct}}_{\breve{\boldsymbol{\sigma}}} \circledast \breve{\boldsymbol{\sigma}}$ is a correction strain to the approximate secant material which ensures that the secant condition is met for all times. Since $\boldsymbol{\varepsilon}^{\mathbf{cor}}$ does not depend on $\boldsymbol{\sigma}$ it is a stress-free strain. The approximate secant material is calculated so that:

$$\hat{\boldsymbol{\mathcal{S}}}^{\mathbf{sct}}_{\langle\breve{\boldsymbol{\sigma}}\rangle} \circledast \langle\breve{\boldsymbol{\sigma}}\rangle \approx \boldsymbol{\mathfrak{F}} \circledast \langle\breve{\boldsymbol{\sigma}}\rangle \tag{3.74a}$$

$$\boldsymbol{\varepsilon}^{\mathbf{cor}} = \boldsymbol{\mathfrak{F}} \circledast \langle\breve{\boldsymbol{\sigma}}\rangle - \hat{\boldsymbol{\mathcal{S}}}^{\mathbf{sct}}_{\langle\breve{\boldsymbol{\sigma}}\rangle} \circledast \langle\breve{\boldsymbol{\sigma}}\rangle \tag{3.74b}$$

which leads to the linearised thermo-viscoelastic material:

$$\boldsymbol{\varepsilon} = \hat{\boldsymbol{\mathcal{S}}}^{\mathbf{sct}}_{\langle\breve{\boldsymbol{\sigma}}\rangle} \circledast \boldsymbol{\sigma} + \boldsymbol{\varepsilon}^{\mathbf{cor}} \tag{3.75}$$

3.6.5 An approximate modified secant linearisation

In a similar manner, we could define a modified secant material. We introduce $\breve{\boldsymbol{\sigma}}_{\mathbf{2}} = \boldsymbol{\mathcal{K}} \circledast \breve{\mathbf{M}}$ and $\breve{g}_{2_2}(\tau) = g_2(\frac{1}{2}\mathbf{Q} :: \breve{\mathbf{M}}(\tau))$. Then introduce:

$$\breve{\mathbf{S}}_{\mathbf{2}}(t, x) = \boldsymbol{\Delta}\tilde{\mathbf{S}}(t)\breve{g}_{2_2}(t-x) + \mathbf{Q}\delta(t-\epsilon) \tag{3.76}$$

[4]It should be noted that the same conclusion could be drawn if g_0 and g_3 are different to 1. On the other hand, having $g_1 \neq 1$ would introduce a tensor $\mathbf{Q} : \boldsymbol{\sigma} \otimes \boldsymbol{\sigma} : \mathbf{Q}$ (see the definition of the behaviour law at equation (1.57)) which does not necessarily have the same symmetries as $\mathbf{Q}$.

and this leads to:

$$\breve{\boldsymbol{\varepsilon}} = \int_0^t \breve{\mathbf{S}}_{\mathbf{2}}(t, t-\tau) : \breve{\boldsymbol{\sigma}}_{\mathbf{2}}(\tau)\mathrm{d}\tau \tag{3.77}$$

and the behaviour law is simply:

$$\begin{aligned} \boldsymbol{\varepsilon} &= \int_0^t \breve{\mathbf{S}}_{\mathbf{2}}(t, t-\tau) : \boldsymbol{\sigma}(\tau)\mathrm{d}\tau \\ &= \boldsymbol{\mathcal{S}}_{\breve{\mathbf{M}}}^{\mathbf{sct_2}} \circledast \boldsymbol{\sigma} \end{aligned} \tag{3.78}$$

As in the case of the classical secant model developed previously, $\boldsymbol{\mathcal{S}}_{\breve{\mathbf{M}}}^{\mathbf{sct_2}}$ has the same material symmetries as $\mathbf{Q}$. As previously, this does not represent a linear viscoelastic constitutive law and we must introduce the approximation $\boldsymbol{\mathcal{S}}_{\breve{\mathbf{M}}}^{\mathbf{sct_2}} \approx \hat{\boldsymbol{\mathcal{S}}}_{\breve{\mathbf{M}}}^{\mathbf{sct_2}}$, which is calculated so that:

$$\begin{aligned} \hat{\boldsymbol{\mathcal{S}}}_{\left\langle\breve{\mathbf{M}}\right\rangle}^{\mathbf{sct_2}} \circledast \left(\boldsymbol{\mathcal{K}} \circledast \left\langle\breve{\mathbf{M}}\right\rangle\right) \approx \mathbf{Q} : \left(\boldsymbol{\mathcal{K}} \circledast \left\langle\breve{\mathbf{M}}\right\rangle\right)(t) \\ + \int_0^t \boldsymbol{\Delta}\tilde{\mathbf{S}}(t-\tau) : \tilde{\breve{g}}_{2_2}(\tau) \left(\boldsymbol{\mathcal{K}} \circledast \left\langle\breve{\mathbf{M}}\right\rangle\right)(\tau)\mathrm{d}\tau \end{aligned} \tag{3.79}$$

where $\tilde{\breve{g}}_{2_2}(\tau) = g_2\left(\frac{1}{2}\mathbf{Q} :: \left\langle\breve{\mathbf{M}}(\tau)\right\rangle\right)$. Then, the behaviour law of the linearised material would be:

$$\boldsymbol{\varepsilon} = \hat{\boldsymbol{\mathcal{S}}}_{\left\langle\breve{\mathbf{M}}\right\rangle}^{\mathbf{sct_2}} \circledast \boldsymbol{\sigma} + \boldsymbol{\varepsilon}^{\mathbf{cor}} \tag{3.80}$$

where:

$$\begin{aligned} \boldsymbol{\varepsilon}^{\mathbf{cor}} = \mathbf{Q} : \left(\boldsymbol{\mathcal{K}} \circledast \left\langle\breve{\mathbf{M}}\right\rangle\right)(t) \\ + \int_0^t \boldsymbol{\Delta}\tilde{\mathbf{S}}(t-\tau) : \tilde{\breve{g}}_{2_2}(\tau) \left(\boldsymbol{\mathcal{K}} \circledast \left\langle\breve{\mathbf{M}}\right\rangle\right)(\tau)\mathrm{d}\tau \\ - \hat{\boldsymbol{\mathcal{S}}}_{\left\langle\breve{\mathbf{M}}\right\rangle}^{\mathbf{sct_2}} \circledast \left(\boldsymbol{\mathcal{K}} \circledast \left\langle\breve{\mathbf{M}}\right\rangle\right) \end{aligned} \tag{3.81}$$

Other variants of this modified secant model can be imagined by using the first and second moments differently.

3.6.6 Limitations of the secant models

The first limitation of the secant models we have defined is that the problem is ill defined as for classical secant models. This is due to the fact that there can be an infinity of functionals $\boldsymbol{\mathfrak{S}}_{\breve{\boldsymbol{\sigma}}}^{\mathbf{sct}}$ that meet condition (3.68). The second limitation is that we have to approximate this unknown functional by

a functional $\hat{\boldsymbol{\mathcal{S}}}^{\mathbf{sct}}_{\breve{\boldsymbol{\sigma}}}$ which describes a linear viscoelastic material because we solve the homogenisation problem with the correspondence principle. So, in the general case, there are no systematic way to generate $\mathfrak{S}^{\mathbf{sct}}_{\breve{\boldsymbol{\sigma}}}$ and therefore to generate $\hat{\boldsymbol{\mathcal{S}}}^{\mathbf{sct}}_{\breve{\boldsymbol{\sigma}}}$. The same reasoning applies to the modified secant models.

However, our behaviour law allowed us to define a linear secant operator. In addition, the procedure for defining this operator is systematic, as in the case of the secant modulus of a material described by a potential $F(\mathbf{L})$ (see section 3.4.2). In addition, we have seen that this secant material has the same symmetries as $\mathbf{Q}$, which is isotropic in our case.

3.6.7 Discussion

The preceding survey suggests that we face two major difficulties. On the one hand, we have seen that it is possible, under special conditions, to systematically define tangent and secant materials and their approximations. However, there is no guarantee that these approximations are compatible with the solution technique we have chosen for the homogenisation problem. On the other hand, we have seen that trying to find an admissible linear viscoelastic material approximating the tangent (see equation (3.47)) or the secant (see equation 3.68)) conditions does not lead to a systematic definition of a linearised material. Then, it might be difficult to compare two different models if each of them is not systematically defined.

At this stage, we must make a choice between a linearisation which could possibly lead to a material which is not thermodynamically admissible and a procedure which leads to thermodynamically admissible materials but not in a systematic way. Neither approach is optimal. In this thesis, we have chosen the second option since we are guaranteed that the linearised comparison material leads to a homogenised material which has a realistic behaviour (in the thermodynamic sense). The issue to address now is which type of approximation is the most relevant and realistic.

The first step in defining the procedure leading to the linearised material is to define the sense of the approximation. We can see that the tangent and secant materials can be summarised as a functional $\mathfrak{S}$ which reproduces a certain stress history denoted by $\tilde{\boldsymbol{\varepsilon}}$ when a particular stress history $\tilde{\boldsymbol{\sigma}}$ is applied, so that $\tilde{\boldsymbol{\varepsilon}} = \mathfrak{S} \circledast \tilde{\boldsymbol{\sigma}}$. We have seen that $\tilde{\boldsymbol{\varepsilon}}$ and $\tilde{\boldsymbol{\sigma}}$ have different expressions for the tangent and secant materials. Now, we have seen that we seek an approximate material, denoted by $\hat{\boldsymbol{\mathcal{S}}}$ which approximates $\mathfrak{S}$ so that $\hat{\boldsymbol{\varepsilon}} = \hat{\boldsymbol{\mathcal{S}}} \circledast \tilde{\boldsymbol{\sigma}} \approx \mathfrak{S} \circledast \tilde{\boldsymbol{\sigma}}$. In other words, we seek $\hat{\boldsymbol{\varepsilon}} \approx \tilde{\boldsymbol{\varepsilon}}$. We recall that these functions are functions of time and that in fact we imply: $\hat{\boldsymbol{\varepsilon}}(t) \approx \tilde{\boldsymbol{\varepsilon}}(t)$ for $t \in [0, t_a]$. Since it will most likely be impossible to meet the condition for all times, we have to determine the time interval on which the approximation

should be the most accurate. For example, if we consider that each $t_i \in [0, t_a]$ has the same weight, then we could define an approximate material so that $\sum_i (\hat{\boldsymbol{\varepsilon}}(t_i) - \tilde{\boldsymbol{\varepsilon}}(t_i)) : (\hat{\boldsymbol{\varepsilon}}(t_i) - \tilde{\boldsymbol{\varepsilon}}(t_i))$ is minimised. To guide the choice, we can also invoke the *fading memory* characteristic exhibited by linear viscoelastic materials. By fading memory we imply that the response at time t_a depends more on the load history close to t_a than the load history far away from t_a (see for example Christensen [19]). Following this line of thought, it would make more sense that our linearised material meets the tangent/secant conditions close to t_a, the time at which the response is sought, than close to 0, for example.

For illustration purposes, consider the following case. Suppose that we applied a given loading and we have obtained the secant strain history that our linearised material must reproduce when subjected to the same stress history. Then, we seek a linear viscoelastic material best reproducing this strain history, in the sense we have just defined, when the same stress history is applied. We have considered a two phase material with spherical reinforcements in 30% volume fraction where each phase is isotropic and used the Mori-Tanaka scheme for predicting the overall mechanical properties. We have assumed that $k_0^{-1}(t) = k_1^{-1}(t) = \mu_1^{-1}(t) = 1$ so that the only viscoelastic part is $\mu_0^{-1}(t)$. $k_i^{-1}(t)$ and $\mu_i^{-1}(t)$ are to be interpreted as the bulk and shear creep compliances of phase i. Now suppose that $\boldsymbol{\Sigma}$ leads to a average stress field in the matrix of pure shear, constant with respect to time. Asumme further that $\mu_0^{-1}(t) = \alpha(1 - \exp[-\lambda(t-\tau)])g_2(h(\boldsymbol{\sigma}(\tau)))$. In that case, the exact secant condition leads to a linear viscoelastic material because g_2 is constant with respect to time. Now, consider that the secant condition, up to $t = 3$, is given by the curve labelled as "exact" on figure 3.5.

Now consider that we approximate the shear compliance of this linearised material by linear viscoelastic materials having approximately the same response over $[3-\Delta, 3]$ (where $\Delta \in [0, 3[$), as in figure 3.5. In addition, we use a Maxwell model which has the same response at time $t = 3$ as the exact secant material. This is equivalent to the first order approximation introduced by Pouya and Zaoui [78]. Since we know that the exact secant condition is met with a known linear viscoelastic material, we can compute the exact response of this secant material. Next, compute the homogenised shear compliance of these approximate linear viscoelastic comparison materials with the Mori-Tanaka scheme. These homogenised shear compliances are reported in figure 3.6. It can be observed that calculating the creep response with these models at $t = 3$ give almost the exact same value, except with the Maxwell model. In that sense, the approximations introduced (except for the Maxwell material) are relevant approximations since they lead to almost the same response as the exact secant material. In itself, this example, although it is not a formal

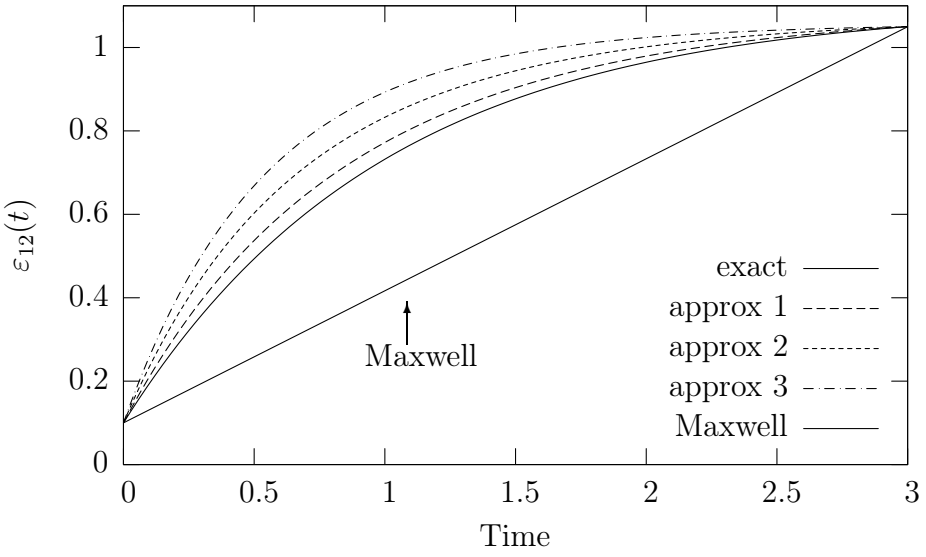


Figure 3.5: Comparison of the approximate and exact secant conditions for the shear compliance of the linear viscoelastic comparison material. The load history is a shear creep.

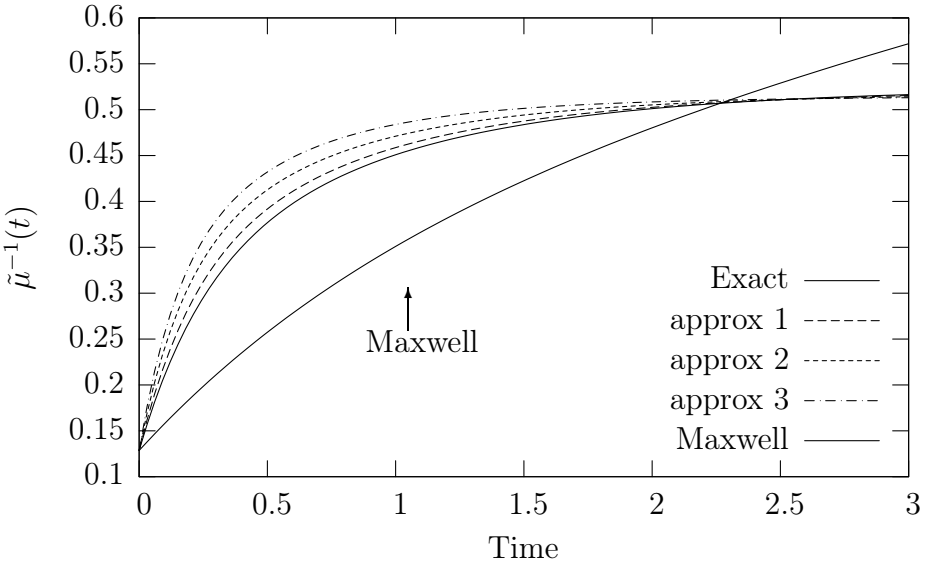


Figure 3.6: Comparison of the homogenised creep compliances ($\tilde{\mu}^{-1}(t)$) of the linear viscoelastic comparison materials calculated in figure 3.5

proof, suggests that the linearisation procedure we discussed is relevant (i.e., the approximate linearised material approximately meets the tangent/secant conditions for $t \in [t_{a-1}, t_a]$, where $t_{a-1} < t_a$) and this is the procedure we have implemented numerically in the next chapter.

Now that we have defined the sense of our approximation, we must detail the generic shape that will be given to $\hat{\boldsymbol{\mathcal{S}}}$. We have seen in Chapter One the general definition of a creep compliance (see equation (1.22)). According to this definition, the linearised material will have an elastic and a viscous part. However, we will have to find a relevant approximation of $\mathrm{d}\check{\mathbf{S}}(\lambda)$ since we use a numerical algorithm to determine $\hat{\boldsymbol{\mathcal{S}}}$. In addition, we have to determine the material symmetries, if any, of $\hat{\boldsymbol{\mathcal{S}}}$.

For the affine model, it is most likely that $\mathfrak{F}$ and $\mathfrak{S}$ do not have the same material symmetries. Then, it would make sense to define $\hat{\boldsymbol{\mathcal{S}}}$ as a general anisotropic material. On the other hand, we have seen that in the case of the classical secant model we defined for our material that $\mathfrak{F}$ and $\mathfrak{S}$ share the same material symmetries. Then, as a first approximation, we have approximated the exact secant material with an isotropic linear viscoelastic material.

Consider now our behaviour law:

$$\tilde{\boldsymbol{\varepsilon}} = \mathbf{Q} : \tilde{\boldsymbol{\sigma}} + \mathbf{Q} : \sum_{m=1}^{3} \int_0^t \alpha_m \lambda_m \exp[-\lambda_m (t-\tau)] g_2(h(\tilde{\boldsymbol{\sigma}}(\tau))) \tilde{\boldsymbol{\sigma}}(\tau) \mathrm{d}\tau \quad (3.82)$$

In this behaviour law, the only nonlinear parameter is the scalar function $g_2(h(\breve{\boldsymbol{\sigma}}(\tau)))$. We could imagine the approximate secant behaviour law in the form:

$$\hat{\boldsymbol{\varepsilon}} = \mathbf{Q} : \tilde{\boldsymbol{\sigma}} + \mathbf{Q} : \int_0^t \hat{s}(t-\tau) \dot{\tilde{\boldsymbol{\sigma}}}(\tau) \mathrm{d}\tau \approx \tilde{\boldsymbol{\varepsilon}} \quad (3.83)$$

Then, we would seek $\hat{s}(t)$ as a Bernstein function so that $\hat{\boldsymbol{\varepsilon}} \approx \boldsymbol{\varepsilon}$. In that case, the unknown quantity is a scalar function, which is a considerable simplification from the general problem. We define a radial load history as: $\tilde{\boldsymbol{\sigma}}^R = f(t)\boldsymbol{\sigma}^{\mathbf{ct}}$, where $\boldsymbol{\sigma}^{\mathbf{ct}}$ is a constant stress tensor, where it is noted that $f(t)$ is not necessarily monotonous. In this specific case, we can expect the approximation (3.83) to be very good since the problem reduces to a unidimensional problem. However, if the load history is not radial, there is no guarantee that the approximation is good for all the components of $\hat{\boldsymbol{\varepsilon}}$. For this reason, we introduce instead:

$$\hat{\boldsymbol{\varepsilon}} = \int_0^t (\hat{s}_h(t-\tau)\mathbf{J} + \hat{s}_d(t-\tau)\mathbf{K}) : \dot{\tilde{\boldsymbol{\sigma}}}(\tau) \mathrm{d}\tau \approx \tilde{\boldsymbol{\varepsilon}} \quad (3.84)$$

where $\hat{s}_h(t)$ and $\hat{s}_d(t)$ are the hydrostatic and deviatoric creep compliances, which are taken as Bernstein functions and $\mathbf{J}$ and $\mathbf{K}$ are the classic spherical

and deviatoric projection tensors. This approximation has more flexibility than the previous isotropic approximation since we identify two different functions instead of one.

It should be noted that an isotropic approximation of the exact secant material might not be the best approximation for all loadings. It might be possible that a general anisotropic material would lead to a better approximation. In that sense, our approximation should be interpreted as the isotropic approximation of the general approximate linear viscoelastic material.

In the next chapter, we have implemented this approximation for the classical secant model we have defined. In addition, we have also implemented this approximation for the classical affine model.

3.7 General implementation of the homogenisation model

We have presented thus far some of the various empirical linearisations available and introduced a general approach to generate new linearisations for non hereditary materials. However, this was outside the context of a homogenisation problem. In such a problem, we recall that the objective is to find the link between the applied stresses and the resulting strains, or vice-versa. This link is obtained by considering the local behaviour of the phases constituting the heterogeneous material. When the various phases are nonlinear, one way to estimate the solution of such a problem is to introduce a linearisation of the local behaviour of the various phases. This linearisation is accomplished around a reference load level which we have discussed previously. We have seen, for example, that the average stress or strain in a given phase of a linear elastic heterogeneous material can be related to the macroscopic quantities through the tensors $\mathbf{A}_r$ and $\mathbf{B}_r$. These tensors are function of the mechanical properties of the linear phases. We can readily see the implicit nature of the problem we face: the linearisation depends of the average stress (for example) while the average stress depends on $\mathbf{B}_r$ which in turn depends on the linearisation. Therefore, an implicit procedure is required to determine the linear comparison material.

Consider that we apply $\boldsymbol{\Sigma}(t)$ (the same reasoning is valid if we apply $\mathbf{E}$) and where the reference level is $\bar{\boldsymbol{\sigma}}_r$. For a non hereditary material, the iterative process is only on the $\bar{\boldsymbol{\sigma}}_r(t_a)$, where again, t_a is the time at which the solution is sought. However, for hereditary materials, we have seen that linearisation of the material requires knowing not only the $\bar{\boldsymbol{\sigma}}_r(t_a)$, but also the $\bar{\boldsymbol{\sigma}}_r(t)$ for $t \in [0, t_a]$. Therefore, the iterative procedure must be applied

to the $\bar{\boldsymbol{\sigma}}_r(t_i)$ where the $t_i \in [0, t_a]$. In other words, the iterative procedure is no longer on a punctual values but applied to functions.

This discussion brings us to the following paradox. Suppose we have a problem where we apply $\boldsymbol{\Sigma}(t)$ and we seek the response of the material in t_a and t_{a-1}, with $t_{a-1} < t_a$. The linearised materials we define with our approach will have different expressions, namely $\hat{\boldsymbol{\mathcal{S}}}(t_{a-1}, t)$ and $\hat{\boldsymbol{\mathcal{S}}}(t_a, t)$, where we have used the same notation as Masson and Zaoui [59]. The first variable refers to the upper boundary of the time interval considered for linearisation. Since the two materials are linearised for two different stress histories, they are different. Now, for our problem, if we compute the average stress in the matrix for these two models, at t_{a-1}, we have:

$$\bar{\boldsymbol{\sigma}}_0(t_{a-1}, t_{a-1}) = \int_0^{t_{a-1}} \mathbf{B}_0(t_{a-1}, t_{a-1} - \tau) : \dot{\boldsymbol{\Sigma}}(\tau) \mathrm{d}\tau - \int_0^{t_{a-1}} \mathbf{R}_0(t_{a-1}, t_{a-1} - \tau) : \dot{\boldsymbol{\varepsilon}}_{\mathbf{0}}^{\mathbf{0}}(t_{a-1}, \tau) \mathrm{d}\tau \quad (3.85a)$$

$$\bar{\boldsymbol{\sigma}}_0(t_a, t_{a-1}) = \int_0^{t_{a-1}} \mathbf{B}_0(t_a, t_{a-1} - \tau) : \dot{\boldsymbol{\Sigma}}(\tau) \mathrm{d}\tau - \int_0^{t_{a-1}} \mathbf{R}_0(t_a, t_{a-1} - \tau) : \dot{\boldsymbol{\varepsilon}}_{\mathbf{0}}^{\mathbf{0}}(t_a, \tau) \mathrm{d}\tau \quad (3.85b)$$

which, in the general case, will not be equal. We could ask ourselves what would be the "real" value of $\bar{\boldsymbol{\sigma}}_0(t_{a-1})$? As pointed out by Masson [57] the answer lies in physical arguments related to the causality. Clearly, $\bar{\boldsymbol{\sigma}}_0(t_a, t_{a-1})$ depends on t_a since the linearised material is calculated up to this point. In other words, the stress $\bar{\boldsymbol{\sigma}}_0(t_{a-1})$ depends also on the stress history $\bar{\boldsymbol{\sigma}}_0(t)$ for $t \in [t_{a-1}, t_a]$, which does not make physical sense. Therefore, our models will only evaluate the quantities $\mathbf{E}$ and $\bar{\boldsymbol{\sigma}}_r$ at t_a.

Using such arguments, Masson [57] and Masson and Zaoui [59] suggest a step-by-step resolution of the problem. The problem consists of discretizing the calculation at intermediate times t_i between 0 and t_a. Then, the objective is to calculate, for increasing values of t_i, the "real" $\bar{\boldsymbol{\sigma}}_0(t_i)$. Since we require the entire stress history and not only the punctual values, we assume a linear variation of this stress tensor with respect to the time between two consecutive values of $\bar{\boldsymbol{\sigma}}_r$. Now, suppose that we have determined $\bar{\boldsymbol{\sigma}}_0(t)$ for $t \in [0, t_i]$ and that we want to compute $\bar{\boldsymbol{\sigma}}_0(t_{i+1})$. We will establish an iterative procedure where the value of $\bar{\boldsymbol{\sigma}}_0(t_{i+1})$ is first assumed. With this value, and our linear interpolation to generate the stress history, we can calculate our linearised material. This allows us to calculate a new value of $\bar{\boldsymbol{\sigma}}_0(t_{i+1}, t_{i+1})$

according to equation (3.85a). If this calculated value is approximately equal to the one we have assumed, we have reached the solution. Otherwise, a new trial value for $\bar{\boldsymbol{\sigma}}_0(t_{i+1}, t_{i+1})$ is assumed and the loop is repeated until we have reached the solution. This procedure is described in the next chapter. When we have reached t_a, the macroscopic response of the material $\mathbf{E}(t_a)$ can be computed. It should be noted that $\mathbf{E}(t_i)$ can also be computed at each intermediate time with the linearised material defined at this intermediate time. We have implemented such an algorithm.

So far, we have overlooked a major difficulty which we now introduce: the numerical inversion of Laplace-Carson Transforms. We have seen in section 3.2 that the homogenisation tensors are first calculated in the Laplace-Carson (LC) space by using the Laplace-Carson Transform (LCT) of the linearised behaviour laws and the results of the homogenisation scheme obtained for linear elastic materials. To obtain the time domain expression of these tensors, we must apply the inverse LCT. We have seen in section 3.6 that the linearisation process requires a numerical procedure and it is most likely that the linearised material will be only known numerically. Therefore, it will not be possible to obtain an analytical expression for the time domain expression of these tensors and a numerical procedure is required for the LCT inversion. This procedure is developed in the next chapter. Since this procedure is used in an iterative process, it is critical that it leads to very accurate results. Once the time expressions of the homogenisation tensors are calculated, their application is computed by the convolution integrals presented in equations (3.20,3.21,3.22). Figure 3.7 represent the general algorithm within a time interval.

3.8 Conclusion

This chapter allowed us to define a general procedure to apply empirical linearisation schemes obtained for non hereditary materials to empirical linearisation schemes for hereditary materials. The different models introduced present some limitations:

1. The affine models lead to unique tangent materials but the closed form expressions of these materials can only be calculated analytically in the most general case.

2. It is possible that there is a large number of secant operators that meet the secant condition we have defined. In addition, some of these secant materials can be nonlinear operators. Therefore, in the general case,

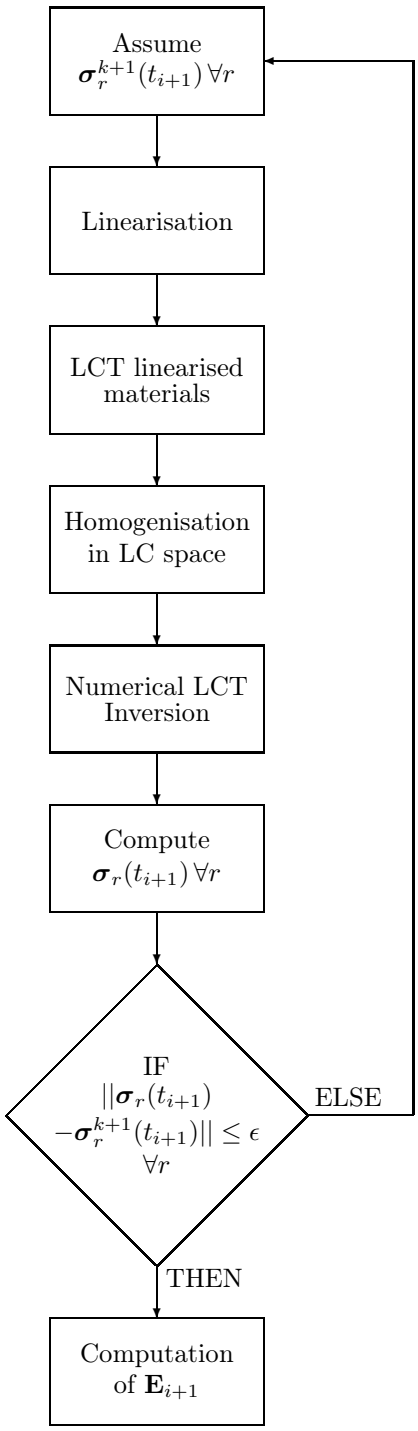


Figure 3.7: General solution algorithm for the homogenisation model during a time interval. r refers to a specific phase, LCT is the Laplace-Carson Transform and the subscript $i+1$ refers to the quantity evaluated at $t = t_{i+1}$, ϵ is the accuracy of the solution and k refers to the k^{th} iteration. This algorithm is repeated for $i = 1 \ldots a - 1$.

it is not possible to give a systematic definition of the secant material. However, in our specific case, it was possible to give a systematic definition of a secant operator, irrespectively of the applied loading.

3. Since these exact secant and tangent materials do not meet the conditions of thermodynamics in the most general situation, there is no guarantee that the correspondence principle can be used to solve the homogenisation problem with the comparison materials generated by such procedures. We must, therefore, introduce an approximation of the exact treatment.

4. There is a wide range of approximations that can be generated. However, for most of them, unless very specific conditions are met, the resulting linearised material is not a thermodynamically admissible linear viscoelastic material.

In this study, we have decided to use an approximation of the exact treatment which leads to a thermodynamically admissible linear viscoelastic comparison material. The linearised material is an isotropic approximation of the exact secant or tangent material.

We have seen that the homogenisation problem thus defined is an implicit problem. The general solution algorithm is a step-by-step and iterative procedure. This requires defining a relevant accuracy goal for the solution and a proper updating scheme for the trial solutions. In addition, since the linearisation procedure leads to a numerical linear viscoelastic material, a numerical Laplace-Carson transform inversion algorithm is required. The next chapter aims to develop and implement the solution scheme, the linearisation procedure and the numerical inverse Laplace-Carson transforms.

Chapter 4

Numerical Implementation of the Homogenisation Models

This chapter details the numerical procedures used to compute the homogenisation model as described in figure 3.7. First, we present the solution scheme we have used for the iterative procedure when computing the various $\bar{\boldsymbol{\sigma}}_0(t_i)$. Then, we present the numerical procedure leading to the linearised materials according to the affine and secant procedures. Next, we present the algorithms we have developed to numerically invert the Laplace-Carson transforms involved in applying the correspondence principle to solve the homogenisation problem. These three topics are treated completely independently. Finally, we present and discuss some of the results we have obtained with the classical affine and secant models.

4.1 Solution scheme

4.1.1 Problem definition

Our objective is to homogenise a two phase composite constituted of a nonlinear viscoelastic matrix and reinforced by linear elastic spherical particles, distributed randomly. The behaviour law of our matrix (identified in chapter 2) is given by:

$$\boldsymbol{\varepsilon}(t) = \mathbf{Q} : \boldsymbol{\sigma}(t) + \mathbf{Q} : \int_0^t S(t-\tau) g_2(\boldsymbol{\sigma}(\tau)) \boldsymbol{\sigma}(\tau) \mathrm{d}\tau \tag{4.1}$$

with:

$$S(t) = \sum_{m=1}^{3} \alpha_m \lambda_m \exp[-\lambda_m t] \tag{4.2}$$

where $\mathbf{Q}$ is an isotropic tensor and λ_m and α_m are positive constants (see table 2.1 for the numerical values). The reinforcements are made of glass and are assumed to be also isotropic. The mechanical properties of the glass were assumed to be: $k_1 = 57500\,\text{MPa}$ and $\mu_1 = 26538.46\,\text{MPa}$. Therefore, the composite is isotropic and the homogenisation scheme of Mori-Tanaka is used to solve the linear elastic homogenisation problem.

For now, suppose that the macroscopic response $\mathbf{E}$ is sought at $t = t_a$ and that we apply a stress history $\mathbf{\Sigma}$. We have seen in the last chapter that computing $\mathbf{E}(t_a)$ requires the computation of $\bar{\boldsymbol{\sigma}}_{\mathbf{0}}$ for $[0, t_a]$. We have also seen that this stress history is computed by a step-by-step algorithm where $\bar{\boldsymbol{\sigma}}_{\mathbf{0}}$ is calculated for increasing values of t_i. It was shown that the $\bar{\boldsymbol{\sigma}}_{\mathbf{0}}(t_i)$ are calculated by an iterative process and this is what we detail here. Our task is to establish the system of nonlinear equations to be solved and the appropriate solution scheme.

Now, suppose that $\bar{\boldsymbol{\sigma}}_{\mathbf{0}}(t)$ is known up to t_i and that we seek its value at t_{i+1}. We know that:

$$\int_0^{t_{i+1}} \mathbf{B}_0(t_{i+1}, t_{i+1} - \tau) : \dot{\mathbf{\Sigma}}(\tau)\mathrm{d}\tau - \int_0^{t_{i+1}} \mathbf{R}_0(t_{i+1}, t_{i+1} - \tau) : \dot{\boldsymbol{\varepsilon}}^{\mathbf{0}}_{\mathbf{0}}(t_{i+1}, \tau)\mathrm{d}\tau - \bar{\boldsymbol{\sigma}}_0(t_{i+1}, t_{i+1}) = \mathbf{0} \quad (4.3)$$

where $\mathbf{B}_0(t_{i+1}, t)$, $\mathbf{R}_0(t_{i+1}, t)$ and $\boldsymbol{\varepsilon}^{\mathbf{0}}_{\mathbf{0}}(t_{i+1}, t)$ depend on the known quantities $\bar{\boldsymbol{\sigma}}_{\mathbf{0}}(t)$ for $t \in [0, t_i]$ and the unknown $\bar{\boldsymbol{\sigma}}_0(t_{i+1}, t_{i+1})$, which shows the implicit nature of the problem. We can rewrite equation (4.3) as:

$$\mathbf{\Omega}(\bar{\boldsymbol{\sigma}}_0(t_{i+1}, t_{i+1})) = \mathbf{0} \quad (4.4)$$

which is the nonlinear system of equations to be solved and whose solution is $\bar{\boldsymbol{\sigma}}_0(t_{i+1}, t_{i+1})$.

4.1.2 Iterative procedure

We have solved this system of equations by the Newton method. In the Newton method, one has to compute the gradient of $\mathbf{\Omega}$ (usually called Jacobian), $\mathbf{N} = \nabla\mathbf{\Omega} = \frac{\partial \mathbf{\Omega}}{\partial \bar{\boldsymbol{\sigma}}_0(t_{i+1}, t_{i+1})}$, at $\bar{\boldsymbol{\sigma}}_{\mathbf{0}}(t_{i+1}, t_{i+1})$. In the Newton method the objective is to obtain $\mathbf{\Omega} = \mathbf{0}$ by a series of trial solution vectors (i.e., in our case $\bar{\boldsymbol{\sigma}}_{\mathbf{0}}(t_{i+1}, t_{i+1})$) which are obtained by a specific procedure. So, an initial value is assumed and it is first checked if $\mathbf{\Omega} = \mathbf{0}$. If this is not the case, the next trial solution is obtained by:

$$\bar{\boldsymbol{\sigma}}^{k+1}_{\mathbf{0}}(t_{i+1}, t_{i+1}) = \bar{\boldsymbol{\sigma}}^{k}_{\mathbf{0}}(t_{i+1}, t_{i+1}) + \boldsymbol{\delta\sigma} \quad (4.5)$$

where the exponent k refers to the k^{th} trial solution and where:

$$\boldsymbol{\delta\sigma} = -\mathbf{N}^{-1} : \boldsymbol{\Omega}(\bar{\boldsymbol{\sigma}}_0^k(t_{i+1}, t_{i+1})) \tag{4.6}$$

This iterative procedure is repeated until $\boldsymbol{\Omega}(\bar{\boldsymbol{\sigma}}_{\mathbf{0}}^{k+1}(t_{i+1}, t_{i+1}))$ becomes small, the sense of which we define later.

Since a numerical procedure is used to linearise the nonlinear viscoelastic matrix, $\mathbf{N}$ cannot be calculated analytically. We have calculated $\mathbf{N}$ with a centred difference so that (in the modified Voigt notation):

$$\mathrm{N}_{MP} \approx \frac{H_M\left[\bar{\boldsymbol{\sigma}}_{\mathbf{0}}^k(t_{i+1}, t_{i+1}) + \boldsymbol{\Delta\sigma}_{\mathbf{0}}\right] - H_M\left[\bar{\boldsymbol{\sigma}}_{\mathbf{0}}^k(t_{i+1}, t_{i+1}) - \boldsymbol{\Delta\sigma}_{\mathbf{0}}\right]}{2\Delta\sigma_{0_P}} \tag{4.7}$$

where $\Delta\sigma_{0_I} = 0$ for $I \neq P$ and $\Delta\sigma_{0_I} = \epsilon$ for $I = P$, where $\epsilon \ll 1$. Typically, we have used $\epsilon = 10^{-2}$.

In order to accept a solution, we must introduce a norm for $\boldsymbol{\Omega}$. We have used:

$$||\boldsymbol{\Omega}(\bar{\boldsymbol{\sigma}}_0(t_{i+1}, t_{i+1}))|| = \sqrt{\boldsymbol{\Omega}(\bar{\boldsymbol{\sigma}}_0(t_{i+1}, t_{i+1})) : \boldsymbol{\Omega}(\bar{\boldsymbol{\sigma}}_0(t_{i+1}, t_{i+1}))} = \gamma \tag{4.8}$$

The solution was accepted when $\gamma \leq 1 \times 10^{-3}$. For the cases where the solution was not reached in 10 iterations, we accepted the solution when $\gamma \leq 5 \times 10^{-3}$. If the solution was not attained with this relaxed convergence criterion, we introduced an alternate convergence criteria. We defined $\theta = \sqrt{\boldsymbol{\Sigma}(t_{i+1}) : \boldsymbol{\Sigma}(t_{i+1})}$. We accepted the solution when $\frac{\gamma}{\theta} < \frac{1}{100}$.

It should be noted that the affine model usually required more iterations than the secant model. In addition, there were some cases where it was not possible to simulate the whole loading path we have imposed with the affine model.

4.1.3 Computation of the initial trial solution

Suppose that the solution is known up to t_i. In the Newton method, we need a first initial solution to start the iterative procedure. When this trial solution is close to the real solution, the Newton method converges very rapidly to the solution. Since we imposed quite smooth loadings, we have decided to compute the first trial vector with:

$$\bar{\boldsymbol{\sigma}}_{\mathbf{0}}^1(t_{i+1}, t_{i+1}) = \int_0^{t_{i+1}} \mathbf{B}_0(t_i, t_{i+1} - \tau) : \dot{\boldsymbol{\Sigma}}(\tau)\mathrm{d}\tau - \int_0^{t_{i+1}} \mathbf{R}_0(t_i, t_{i+1} - \tau) : \dot{\boldsymbol{\varepsilon}}_{\mathbf{0}}^{\mathbf{0}}(t_i, \tau)\mathrm{d}\tau \tag{4.9}$$

where we use the results of the previous time interval. In addition, we set that $\dot{\boldsymbol{\varepsilon}}_{\mathbf{0}}^{\mathbf{0}}(t_i, t_{i+1}) = \dot{\boldsymbol{\varepsilon}}_{\mathbf{0}}^{\mathbf{0}}(t_i, t_i)$.

4.1.4 Numerical integration

The constitutive law of our matrix is given by a convolution integral, as well as the homogenisation solutions. In addition, the linearisations will also require additional integrations (see the next section). Rather than using a general numerical integration scheme, we preferred to take advantage of the particularities of the quantities we have to integrate. We recall that $\boldsymbol{\sigma_0}(t)$ was assumed to vary linearly within a step.

Consider the integral in our constitutive law presented by equation (4.1). We define as $\boldsymbol{\rho}_{i+1}^m$ the integral in equation (4.1) associated with the term m from 0 to t_{i+1} as:

$$\boldsymbol{\rho}_{i+1}^m = \int_0^{t_{i+1}} \alpha_m \lambda_m \exp[-\lambda_m(t_{i+1}-\tau)] g_2(\boldsymbol{\sigma}(\tau))\boldsymbol{\sigma}(\tau)\mathrm{d}\tau \tag{4.10}$$

Due to the nature of the exponential, this integral can be expressed in recursive form as:

$$\begin{aligned}\boldsymbol{\rho}_{i+1}^m = \exp[-\lambda_m(t_{i+1}-t_i)]\boldsymbol{\rho}_i^m \\ + \int_{t_i}^{t_{i+1}} \alpha_m \lambda_m \exp[-\lambda_m(t_{i+1}-\tau)] g_2(\boldsymbol{\sigma}(\tau))\boldsymbol{\sigma}(\tau)\mathrm{d}\tau\end{aligned} \tag{4.11}$$

Since we know the expression of $\boldsymbol{\sigma}$ during the step, an analytical expression for the second integral in equation (4.11) can be obtained as a function of the parameters α_m, λ_m, the time increment $t_{i+1}-t_i$, the parameters of g_2 and the value of $\boldsymbol{\sigma}(t_{i+1})$. We recall that when we seek the material response at t_{i+1}, we know the value of $\boldsymbol{\rho}_i^m$. Therefore, the value of $\boldsymbol{\rho}_{i+1}^m$ can be calculated by very few operations. In a classical integration scheme, we would have to execute many operations and make sure that the integration has converged. This recurrence relation is very useful when implementing the constitutive law in the finite element package (see next chapter for the detailed calculation of these quantities). In addition, this integration scheme computes the integral over $[0, t_{i+1}]$ for all t_i up to t_a. Therefore, much information can be obtained in very few computational operations.

The other convolution integrals can be calculated in a similar manner. It will be shown in section 4.3 that the numerical inversion of the LCT leads to homogenisation tensors functions constituted of exponentials. If the second member of the convolution integral is not $\boldsymbol{\sigma_0}$ then the integration is divided in n increments and the second member is interpolated linearly with respect to time. It was found by trial and errors that $n = 100$ lead to accurate integration. In addition, the second integral in equation (4.3) involves the time derivative of the stress free strain $\boldsymbol{\varepsilon_0^0}$. We recall that $\boldsymbol{\varepsilon_0^0}$ is only known

numerically and therefore, its time derivative must be evaluated numerically. Numerical differentiation is a delicate operation that can lead to significant error. Integration by parts of the second term of equation (4.3) leads to:

$$\int_0^{t_{i+1}} \dot{\mathbf{B}}_{\mathbf{0}}(t_{i+1}, t_{i+1}-\tau) : \boldsymbol{\Sigma}(\tau)\mathrm{d}\tau - \int_0^{t_{i+1}} \dot{\mathbf{R}}_{\mathbf{0}}(t_{i+1}, t_{i+1}-\tau) : \boldsymbol{\varepsilon}_{\mathbf{0}}^{\mathbf{0}}(t_{i+1}, \tau)\mathrm{d}\tau + \dot{\mathbf{B}}_{\mathbf{0}}(t_{i+1}, 0) : \boldsymbol{\Sigma}(t_{i+1}) + \dot{\mathbf{R}}_{\mathbf{0}}(t_{i+1}, 0) : \boldsymbol{\varepsilon}_{\mathbf{0}}^{\mathbf{0}}(t_{i+1}, t_{i+1}) - \bar{\boldsymbol{\sigma}}_0(t_{i+1}, t_{i+1}) = 0 \quad (4.12)$$

where the actual value of $\boldsymbol{\varepsilon}_{\mathbf{0}}^{\mathbf{0}}$ appears explicitly. Due to the fact that $\mathbf{B}_{\mathbf{0}}(t_{i+1}, t)$ and $\mathbf{R}_{\mathbf{0}}(t_{i+1}, t)$ are a sum of exponentials and constants, an analytical shape of the integral between t_{i-1} and t_i can be obtained as a function of the numerical values of the exponential parameters and $\boldsymbol{\varepsilon}_{\mathbf{0}}^{\mathbf{0}}(t_i)$ and $\boldsymbol{\varepsilon}_{\mathbf{0}}^{\mathbf{0}}(t_{i+1})$.

4.2 Linearisation scheme

We have implemented the classical secant and affine models as described in the previous chapter. Even though these models are quite different in nature, their numerical approximations share many similarities. The approximate material must be such that it meets a certain condition (secant or tangent), and this condition is different for the two models. However, the approximate material, for both cases, has the same mathematical shape (specified below) and is evaluated in the same way. In addition, the stress-free strain for both materials is calculated in the same way. We present the main differences between the two models first and then present the common steps with a general notation.

4.2.1 Definition of the tangent and secant conditions

For this section, we assume that $\bar{\boldsymbol{\sigma}}_0$ inside the matrix is known up to t_a. As was done in the previous chapter, we denote by $\boldsymbol{\mathfrak{F}}$ the nonlinear viscoelastic constitutive law. We denote by $\tilde{\boldsymbol{\varepsilon}}$ the response that the linearised material must reproduce and by $\tilde{\boldsymbol{\sigma}}$ the loading that leads to this response so that: $\tilde{\boldsymbol{\varepsilon}} = \boldsymbol{\mathfrak{S}} \circledast \tilde{\boldsymbol{\sigma}}$, where $\boldsymbol{\mathfrak{S}}$ is the material which meets the secant/tangent condition.

Classical secant condition

We recall that the secant condition is defined by:

$$\boldsymbol{\mathfrak{F}} \circledast \bar{\boldsymbol{\sigma}}_0 = \tilde{\boldsymbol{\varepsilon}} = \boldsymbol{\mathfrak{S}} \circledast \bar{\boldsymbol{\sigma}}_0 = \boldsymbol{\mathfrak{S}} \circledast \tilde{\boldsymbol{\sigma}} \quad (4.13)$$

where the definition of $\tilde{\boldsymbol{\varepsilon}}$ and $\tilde{\boldsymbol{\sigma}}$ are obvious.

Classical tangent condition

We recall that the classical tangent condition is defined by (see section 3.6.1):

$$\mathfrak{F} \circledast (\bar{\boldsymbol{\sigma}}_0 + \boldsymbol{\delta\sigma}) - \mathfrak{F} \circledast \bar{\boldsymbol{\sigma}}_0 = \mathfrak{S} \circledast \boldsymbol{\delta\sigma} \tag{4.14}$$

where the norm of $\boldsymbol{\delta\sigma}$, $||\boldsymbol{\delta\sigma}||$, is small. The norm, as in a classical Cartesian system, represents the intensity of a vector. The norm operation has the following property:

$$||\eta\boldsymbol{\delta\sigma}|| = |\eta|||\boldsymbol{\delta\sigma}||, \quad \eta \in \mathbb{R} \tag{4.15}$$

We have chosen to define $||\boldsymbol{\delta\sigma}|| \ll ||\bar{\boldsymbol{\sigma}}_0||$. With the last property, we can define $\boldsymbol{\delta\sigma} = \eta\bar{\boldsymbol{\sigma}}_0$ where $\eta \ll 1$. Therefore, $\boldsymbol{\delta\sigma}$ can be as small as we want, with respect to any norm. Then, with this result, we have the following definitions:

$$\tilde{\boldsymbol{\varepsilon}} = \mathfrak{F} \circledast ([1+\eta]\bar{\boldsymbol{\sigma}}_0) - \mathfrak{F} \circledast \bar{\boldsymbol{\sigma}}_0 \tag{4.16a}$$

$$\tilde{\boldsymbol{\sigma}} = \eta\bar{\boldsymbol{\sigma}}_0 \tag{4.16b}$$

For the load cases we have simulated, we have used $\eta = 10^{-2}$. This choice of η was obtained by successively decreasing η until very small variations were obtained in the definition of the approximate tangent material.

4.2.2 Definition of the approximate linearised material

In order to carry out the homogenisation by the correspondence principle, the linearised material must be a thermodynamically admissible linear viscoelastic material. In our case, the linearised material must link a strain response to an applied stress history. We recall the definition of a general creep compliance as defined in equation (1.22):

$$\begin{aligned} \boldsymbol{\varepsilon}(t) &= \int_0^t \mathbf{S}(t-\tau) : \frac{\mathrm{d}\boldsymbol{\sigma}}{\mathrm{d}\tau}\mathrm{d}\tau \quad \text{with} \\ \mathbf{S}(t) &= \int_{0^+}^{\infty} (1 - \exp[-t\lambda])\mathrm{d}\check{\mathbf{S}}(\lambda) + \mathbf{S}'t + \mathbf{S}'' \end{aligned} \tag{4.17}$$

where:

$$\int_0^{\infty} \frac{\lambda}{1+\lambda}\mathrm{d}|\mathrm{S}_{ij}(\lambda)| < +\infty \tag{4.18}$$

and $\mathrm{d}\check{\mathbf{S}}(\lambda)$, $\mathbf{S}'$ and $\mathbf{S}''$ are definite semi-positive. There is no doubt that the approximate creep compliance, $\hat{\mathbf{S}}(t)$, will be composed of an elastic $\hat{\mathbf{S}}''$ and a viscous $\hat{\mathbf{S}}'$ parts. We must, however, define an approximate expression for $\mathrm{d}\check{\mathbf{S}}(\lambda)$.

As was done in Chapter Two, we could try to find an expression for $\check{\mathbf{S}}$ that would lead to a $\mathrm{d}\check{\mathbf{S}}(\lambda) = \acute{\mathbf{S}}(\lambda)\mathrm{d}\lambda$, where $\acute{\mathbf{S}}(\lambda)$ is a continuous tensor function. This function would be defined by interpolation between various control points. We recall that the LCT of this linearised behaviour law will be used to solve the homogenisation problem. Therefore, using such a general description might require numerical integration to calculate the LCT of such a creep compliance. It is shown in section 4.3 that a finite amount of Dirac masses can be a very good approximation for the creep compliance, even if $\mathrm{d}\check{\mathbf{S}}$ is a continuous function. Such a choice has the advantage of leading to an analytical LCT of the linearised material, which allows efficient computations.

We have used 20 such Dirac impulses. This number was obtained by trial and errors and it was found that adding more impulses did not change the final result significantly. Although the intensity of the impulses were not set, their distribution (i.e., their position on the λ axis) was fixed. It was found by trial and errors that a logarithmic distribution, between $\frac{\lambda_3}{2} = \frac{1}{6324}$ and $2\lambda_1 = \frac{1}{50}$ (see table 2.1), lead to acceptable results and widening this range further did not change the final result significantly.

With these choices, the creep compliance of our approximate linearised material is defined by:

$$\hat{\mathbf{S}}(t) = \sum_{m=1}^{20} \left(1 - \exp[-t\kappa_m]\right) \acute{\mathbf{S}}_m + \hat{\mathbf{S}}' t + \hat{\mathbf{S}}'' \tag{4.19}$$

where the κ_m are distributed on a log scale between $\frac{1}{6324}$ and $\frac{1}{50}$ and represent the position of the Dirac masses defining $\mathrm{d}\check{\mathbf{S}}$ on the λ axis. We must now specify the material symmetry of this approximate linearised material. We have chosen, in the previous chapter, to use isotropic approximate materials so that:

$$\hat{\mathbf{S}}(t) = \sum_{m=1}^{20} \left(1 - \exp[-t\kappa_m]\right) \left(\phi_m \mathbf{J} + \phi_{m+22} \mathbf{K}\right) + \left(\phi_{21}\mathbf{J} + \phi_{43}\mathbf{K}\right) t + \phi_{22}\mathbf{J} + \phi_{44}\mathbf{K} \tag{4.20}$$

where $\mathbf{J}$ and $\mathbf{K}$ are the classical spherical and deviatoric projection tensors and the various ϕ_m are the material constants to be determined.

4.2.3 Identification of the approximate linearised material

We have seen in Chapter Three the various ways in which the approximate linearised material can be calculated. We have chosen that $\hat{\mathbf{S}}(t)$ should be

such so that the tangent/secant condition is met over an interval $[t_{a-1}, t_a]$ (with $t_{a-1} < t_a$), *at best*. If we denote by $\hat{\boldsymbol{\varepsilon}}$ the response associated with $\hat{\mathbf{S}} \circledast \tilde{\boldsymbol{\sigma}}$, we introduce the weighted square of error E_l^2:

$$E_l^2 = \sum_{n=1}^{N} l_n [\hat{\boldsymbol{\varepsilon}}(t_n) - \tilde{\boldsymbol{\varepsilon}}(t_n)] : [\hat{\boldsymbol{\varepsilon}}(t_n) - \tilde{\boldsymbol{\varepsilon}}(t_n)] \tag{4.21}$$

where $t_n \in [t_{a-1}, t_a]$ and l_n is a positive scalar representing the weight of the term n in the total square of error. The various parameters of $\hat{\mathbf{S}}(t)$ are chosen so that E_l^2 is minimised. Typically, we have chosen $t_{a-1} = 0.9t_a$, used $N = 6$ with $l_6 = 20$ (associated with t_a) and $l_1 = 1, l_2 = 2, \ldots, l_5 = 5$.

There are many algorithms available in the literature for the numerical optimisation of functions. The book of Press *et al.* [79] lists and explains some of them. Each approach has its own advantage (using or not using gradient information, requiring more or less computational operations, etc.). We have tried most of the algorithms suggested and implemented in [79]. We have also tried to cancel the gradient of E_l^2 by a Newton method. Far from being the most computationally efficient approach, for most of the cases we have tried, this method led to the lowest value of E_l^2. For that reason, we used this approach to minimise E_l^2.

In order to have all the tensors in relation (4.20) definite semi-positive, all the unknowns must be greater than or equal to zero. Normally, without this constraint, the minimisation of E_l^2 with respect to the material parameters would lead to a linear set of equations. However, our problem is a constrained optimisation problem and the function to minimise is not a linear function. Such constrained optimisation problems are still open problems. Rather than following this approach, we have chosen to modify the definition of our approximate linearised material so that it still meets the thermodynamics requirements, but leads to an unconstrained optimisation problem. As was done in Chapter Two we introduce $\phi_m = (\varphi_m)^2$ where the optimisation variables are now the φ_m.

The definition of $\hat{\mathbf{S}}$ involves 44 unknowns that must be determined. Computing $\frac{\partial E_l^2}{\partial \boldsymbol{\varphi}} = \mathbf{0}$ leads to 44 equations. One component of this system of equations is given by:

$$\frac{\partial E_l^2}{\partial \varphi_m} = 2 \sum_{n=1}^{6} l_n [\hat{\boldsymbol{\varepsilon}}(t_n) - \tilde{\boldsymbol{\varepsilon}}(t_n)] : \left[\frac{\partial \hat{\boldsymbol{\varepsilon}}(t_n)}{\partial \varphi_m} \right] \tag{4.22}$$

As we have seen before, we must also compute the Jacobian of this system

of equation to calculate the next trial solution vector. This leads to:

$$\frac{\partial^2 E_l^2}{\partial\varphi_m\partial\varphi_p} = 2\sum_{n=1}^{6} l_n \left[\frac{\partial\hat{\boldsymbol{\varepsilon}}(t_n)}{\partial\varphi_p}\right] : \left[\frac{\partial\hat{\boldsymbol{\varepsilon}}(t_n)}{\partial\varphi_m}\right] + 2\sum_{n=1}^{6} l_n[\hat{\boldsymbol{\varepsilon}}(t_n) - \tilde{\boldsymbol{\varepsilon}}(t_n)] : \left[\frac{\partial^2\hat{\boldsymbol{\varepsilon}}(t_n)}{\partial\varphi_m\partial\varphi_p}\right] \quad (4.23)$$

We must now detail the explicit values of the terms involving differentiation with respect to the φ_m. The response of our linearised material is given by:

$$\hat{\boldsymbol{\varepsilon}} = \int_0^t \hat{\mathbf{S}}(t-\tau) : \dot{\tilde{\boldsymbol{\sigma}}}(\tau)\mathrm{d}\tau \quad (4.24)$$

As was done previously, integration by parts leads to:

$$\begin{aligned}\hat{\boldsymbol{\varepsilon}} &= \int_0^t \dot{\hat{\mathbf{S}}}(t-\tau) : \tilde{\boldsymbol{\sigma}}(\tau)\mathrm{d}\tau \\ &= \int_0^t \sum_{m=1}^{20} \left[\kappa_m \exp[-\kappa_m(t-\tau)] \left((\varphi_m)^2\mathbf{J} + (\varphi_{m+22})^2\mathbf{K}\right) : \tilde{\boldsymbol{\sigma}}(\tau)\right] \mathrm{d}\tau \\ &\quad + \left((\varphi_{21})^2\mathbf{J} + (\varphi_{43})^2\mathbf{K}\right) : \int_0^t \tilde{\boldsymbol{\sigma}}(\tau)\mathrm{d}\tau \\ &\quad + \left((\varphi_{22})^2\mathbf{J} + (\varphi_{44})^2\mathbf{K}\right) : \tilde{\boldsymbol{\sigma}}(t)\end{aligned} \quad (4.25)$$

where it is assumed that $\tilde{\boldsymbol{\sigma}}(0) = \mathbf{0}$. We can rewrite this equation in the following form:

$$\hat{\boldsymbol{\varepsilon}}(t_n) = \sum_{m=1}^{44} (\varphi_m)^2 \boldsymbol{\zeta}_m^n \quad (4.26)$$

where, for $m \in [1, 20]$ (for example),

$$\boldsymbol{\zeta}_m^n = \int_0^{t_n} \kappa_m \exp[-\kappa_m(t_n - \tau)]\mathbf{J} : \tilde{\boldsymbol{\sigma}}(\tau)\mathrm{d}\tau \quad (4.27)$$

$\boldsymbol{\zeta}_m^n$ can be computed for the other components of m in a similar way. When $\boldsymbol{\zeta}_m^n$ is in the form of the previous equation, the recurrence relation defined previously can be used for the integration. We recall that $\tilde{\boldsymbol{\sigma}}$ varies linearly within each time step used to compute $\mathbf{E}(t_a)$ (see figure 3.7). $\int_0^t \tilde{\boldsymbol{\sigma}}(\tau)\mathrm{d}\tau$ can then be calculated easily. Then, the gradient of E_l^2 becomes:

$$\frac{\partial E_l^2}{\partial\varphi_m} = 4\varphi_m \sum_{n=1}^{6} \left(l_n \left[\sum_{m=1}^{44} (\varphi_m)^2 \boldsymbol{\zeta}_m^n - \tilde{\boldsymbol{\varepsilon}}(t_n)\right] : \boldsymbol{\zeta}_m^n \right) \quad (4.28)$$

and the Jacobian is:

$$\frac{\partial^2 E_l^2}{\partial\varphi_m\varphi_p} = 8\varphi_m\varphi_p \sum_{n=1}^{6} l_n \boldsymbol{\zeta}_m^n : \boldsymbol{\zeta}_p^n + 4\delta_{mp} \sum_{n=1}^{6} \left(l_n \left[\sum_{m=1}^{44} \left(\varphi_m\right)^2 \boldsymbol{\zeta}_m^n - \tilde{\boldsymbol{\varepsilon}}(t_n) \right] : \boldsymbol{\zeta}_m^n \right) \tag{4.29}$$

where δ_{mp} is the Kronecker Delta. This shows that, if we store the values of the various $\boldsymbol{\zeta}_m^n$, the most computationally expensive evaluation of the gradient and the Jacobian is the first one. Subsequent evaluations require very few operations.

We can introduce a simplification to the problem. We can write $\hat{\boldsymbol{\varepsilon}}$ as:

$$\hat{\boldsymbol{\varepsilon}}(t_n) = \mathbf{J} : \hat{\boldsymbol{\sigma}}_{\boldsymbol{h}}(t_n) + \mathbf{K} : \hat{\boldsymbol{\sigma}}_{\boldsymbol{d}}(t_n) \tag{4.30}$$

where $\hat{\boldsymbol{\sigma}}_{\boldsymbol{h}} = \hat{\boldsymbol{\sigma}}_{\boldsymbol{h}}(\varphi_1, \ldots, \varphi_{22})$ and $\hat{\boldsymbol{\sigma}}_{\boldsymbol{d}} = \hat{\boldsymbol{\sigma}}_{\boldsymbol{d}}(\varphi_{23}, \ldots, \varphi_{44})$. If we write $\tilde{\boldsymbol{\varepsilon}}$ as:

$$\tilde{\boldsymbol{\varepsilon}}(t_n) = \mathbf{J} : \tilde{\boldsymbol{\sigma}}_{\boldsymbol{h}}(t_n) + \mathbf{K} : \tilde{\boldsymbol{\sigma}}_{\boldsymbol{d}}(t_n) \tag{4.31}$$

then we obtain:

$$\begin{aligned} E_l^2 &= \sum_{n=1}^{N} l_n \mathbf{J} : [\tilde{\boldsymbol{\sigma}}_{\boldsymbol{h}}(t_n) - \hat{\boldsymbol{\sigma}}_{\boldsymbol{h}}(t_n)] : \mathbf{J} : [\tilde{\boldsymbol{\sigma}}_{\boldsymbol{h}}(t_n) - \hat{\boldsymbol{\sigma}}_{\boldsymbol{h}}(t_n)] \\ &\quad + \sum_{n=1}^{N} l_n \mathbf{K} : [\tilde{\boldsymbol{\sigma}}_{\boldsymbol{d}}(t_n) - \hat{\boldsymbol{\sigma}}_{\boldsymbol{d}}(t_n)] : \mathbf{K} : [\tilde{\boldsymbol{\sigma}}_{\boldsymbol{d}}(t_n) - \hat{\boldsymbol{\sigma}}_{\boldsymbol{d}}(t_n)] \\ &= f(\varphi_1, \ldots, \varphi_{22}) + g(\varphi_{23}, \ldots, \varphi_{44}) \end{aligned} \tag{4.32}$$

Since f and g are two functions of different independent variables, the minimisation of E_l^2 can be accomplished by minimising f and g independently. The number of variables of each independent problem is then divided by two which is generally more computationally efficient than solving the whole problem. Equations (4.28,4.29) can be easily modified to define the problems associated with f and g. This is the minimisation algorithm we have used.

This minimisation technique suffers a limitation. Cancelling the gradient is a necessary, but insufficient, condition to define a local minimum. The gradient can also vanish at a saddle point or at a local maximum. As with most other minimisation algorithms, once a local minimum is reached, there is no way to check if this is the absolute minimum. Even with the techniques described in [79] it is possible to end up with a local minimum which has a larger value than a local maximum. So, in order to find the best solution, one

alternative is to restart the minimisation but with a different initial solution vector. Once the gradient is cancelled with this initial starting point, compare it with the previous solution and keep the lowest minima. Of course, the more starting points are tried, the greater is the probability of reaching an absolute minimum. There is then a trade-off between the permissible computation time and the quality of the minimum sought. It was found by trial and error that doing this 10 times, with different starting points, the minimisation lead to good results. All the initial components of the trial vectors were obtained by a uniform random number generator between $\pm 50 \times 10^{-4}$, which is ten times the largest value of the material parameters (see table 2.1).

For the cases we have simulated, it was found that including or not including a viscous term in the definition of the comparison material had little influence on the approximation quality. For this reason, in addition to the fact that it led to computational simplifications when performing the Laplace-Carson transform inversion, we did not include a viscous term in the comparison material (i.e. $\varphi_{21} = \varphi_{43} = 0$).

Summary

So far, we have defined the general algorithm we have used to calculate our secant and tangent materials. We have first given the definition of the secant and tangent conditions that our linearised material must meet. Then, we have defined the type of linear viscoelastic material we will use for the approximation. It can be interpreted as a Maxwell model in series with many Voigt models. Next, we have explicitly defined the sense of the approximation we make of the exact secant/tangent materials. We used a weighted least squares where much importance was given to the value of $\hat{\boldsymbol{\varepsilon}}(t_a)$ and decreasingly less to the other values of $\hat{\boldsymbol{\varepsilon}}(t_n)$, as we go from t_a to 0. This causes the linearised material to meet at best the secant or tangent conditions at t_a and then, if possible, at the anterior times. Next, we have shown how we minimised our weighted square of error by cancelling the gradient of this quantity with the Newton method. Due to the nature of the equations involved, we have shown that the system of equations and the Jacobian leads to analytical expressions which are also computationally efficient. Now we present some linearised materials that we have obtained with this general algorithm. As mentioned in section 3.6.7, we expect the secant condition to be approximated well by our isotropic material under radial loadings. So, for comparison purposes, we present some linearised materials for radial and non radial load histories.

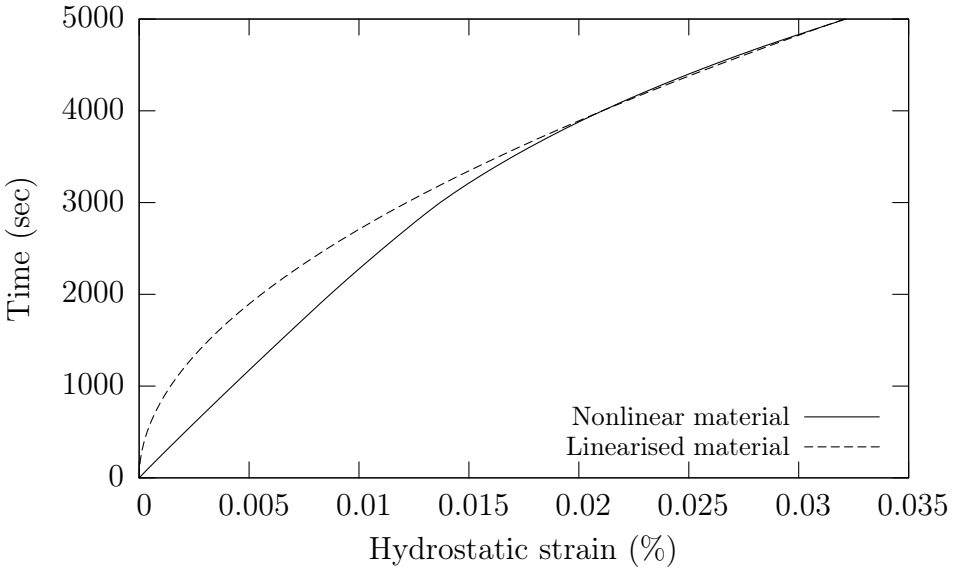


Figure 4.1: Hydrostatic component of strain associated with the secant condition for the linearised secant and nonlinear material (i.e., $\mathbf{J} : \hat{\boldsymbol{\varepsilon}}$ and $\mathbf{J} : \tilde{\boldsymbol{\varepsilon}}$) as a function of time for $\breve{\boldsymbol{\sigma}} = \breve{\sigma}_{11}(t)$

4.2.4 Linearised materials for a radial stress history

We present here approximate linearised secant and affine materials where the load history was $\breve{\boldsymbol{\sigma}} = \breve{\sigma}_{11}(t) = \beta t$, where $\beta = \frac{20\,\mathrm{MPa}}{5000\,\mathrm{sec}}$. It should be noted that we have simulated other radial histories but the tendencies we report here were the same. For conciseness, such plots are not repeated here.

Secant condition

Figure 4.1 shows the hydrostatic component of the strains associated with the secant condition for the approximate affine and nonlinear viscoelastic materials. Similar plots are obtained for the other components of the strain tensor. We can see from the picture that the secant approximation in that case is very accurate over a wide time interval to the left of t_a.

Tangent condition

Figure 4.2 shows the hydrostatic component of the strains associated with the tangent condition for the approximate affine and nonlinear viscoelastic materials. Similar plots are obtained for the other components of the strain tensor. Unlike the secant condition, the tangent condition is approximately met at t_a but is not met over a large time interval $[t_{a-1}, t_a]$.

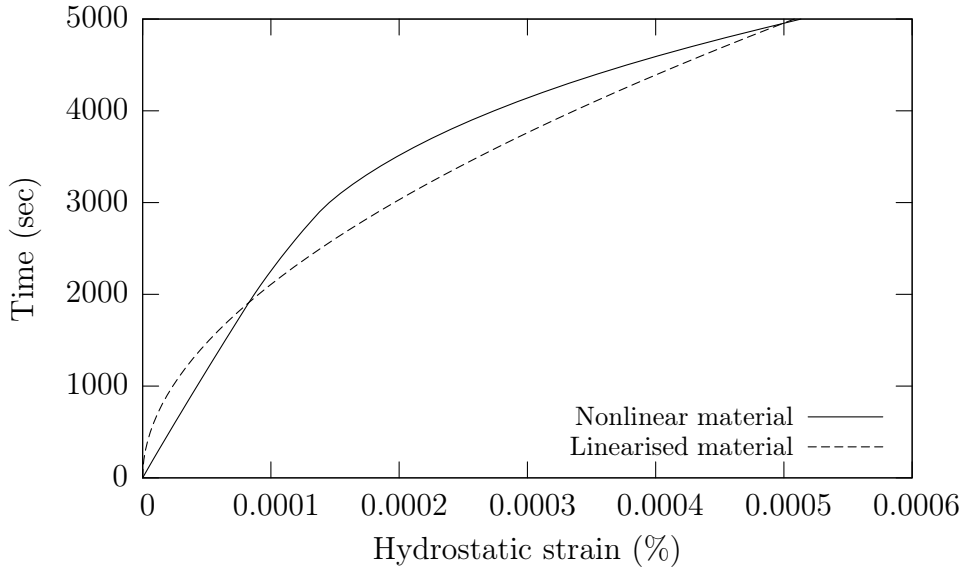


Figure 4.2: Hydrostatic component of strain associated with the tangent condition for the linearised affine and nonlinear material (i.e., $\mathbf{J} : \hat{\boldsymbol{\varepsilon}}$ and $\mathbf{J} : \tilde{\boldsymbol{\varepsilon}}$) as a function of time for $\breve{\boldsymbol{\sigma}} = \breve{\sigma}_{11}(t)$

Comparision of the two linearised materials

Figure 4.3 shows the hydrostatic part of creep compliances and the stress-free strains of the approximate secant and affine materials for a reference stress history $\breve{\boldsymbol{\sigma}} = \breve{\sigma}_{11}(t)$. In that case, as for the non hereditary materials, the affine model leads to a more compliant linear viscoelastic model than the secant material for the same average stress. The history of $\boldsymbol{\varepsilon}_{\mathbf{0}}^{\mathbf{0}}$ for the secant material is small in comparison to the mechanical response associated with its creep compliance. On the other hand, $\boldsymbol{\varepsilon}_{\mathbf{0}}^{\mathbf{0}}$ is considerable with respect to the response associated with the creep compliance of the affine material. We recall that the average stress in the matrix will depend on the mechanical properties and the stress-free strain of the linearised materials and there is no indication, *a priori*, that a linearisation procedure, as implemented here, will lead to softer or stiffer estimates.

4.2.5 Linearised materials for a non radial stress history

We have simulated some non radial load histories in order to assess the accuracy of our approximate linearised materials. As expected, for the secant material, the approximation is less accurate than for a radial stress history. As an example consider $\breve{\sigma}_{11} = \beta t$ for $t \in [0, 5000]$, $\breve{\sigma}_{22} = \beta t$ for $t \in [0, 2500]$,

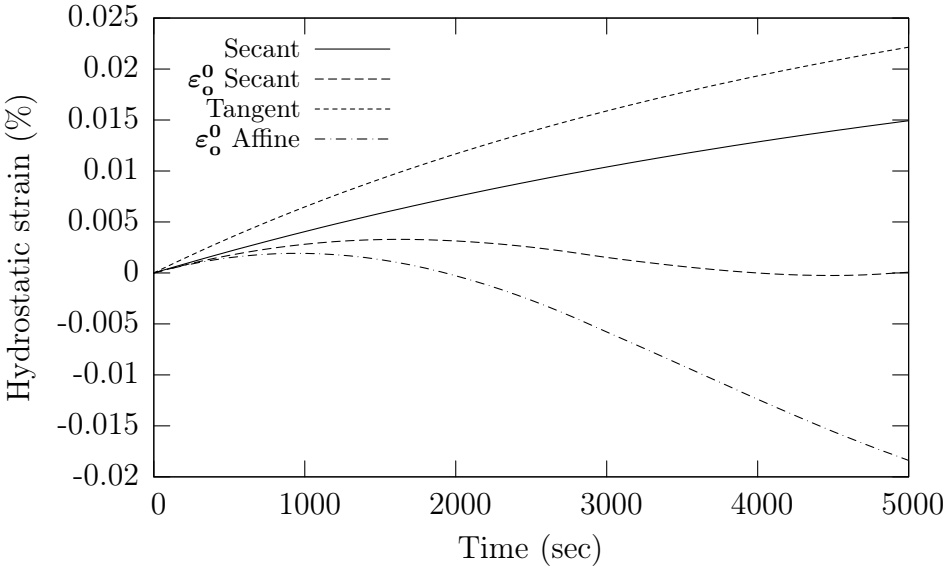


Figure 4.3: Hydrostatic components of the creep compliances and the stress free strains for the approximate secant and affine models for a reference stress history $\breve{\boldsymbol{\sigma}} = \breve{\sigma}_{11}(t)$

and $\breve{\sigma}_{22} = 10 - \beta(t - 2500)$ for $t \in [2500, 5000]$ and where $\beta = \frac{20\,\mathrm{MPa}}{5000\,\mathrm{sec}}$. Figure 4.4 shows the comparison for some components of the strain history of the exact and approximate secant materials when subjected to this defined stress history. As can be seen, the approximation is relatively accurate at $t = 5000$ (in other words at t_a) for all the non zero components of the strain tensors but is less accurate for times prior to $t = 5000$. The same tendencies were observed for the affine model and they are not presented here.

4.3 Numerical inversion of Laplace – Carson Transforms for the homogenised properties

The Laplace or Laplace–Carson Transforms have been used to solve many engineering problems in many disciplines (electrical, chemical and mechanical engineering) where phenomena are described by functions depending on physical time. The advantage of the LCT, as we have seen in Chapter Three, is that the initial problem is transformed into a corresponding problem where the time-dependency has disappeared and where a corresponding solution is easily obtained. The critical operation is then to obtain the time solution from the corresponding solution with an appropriate inversion procedure. In

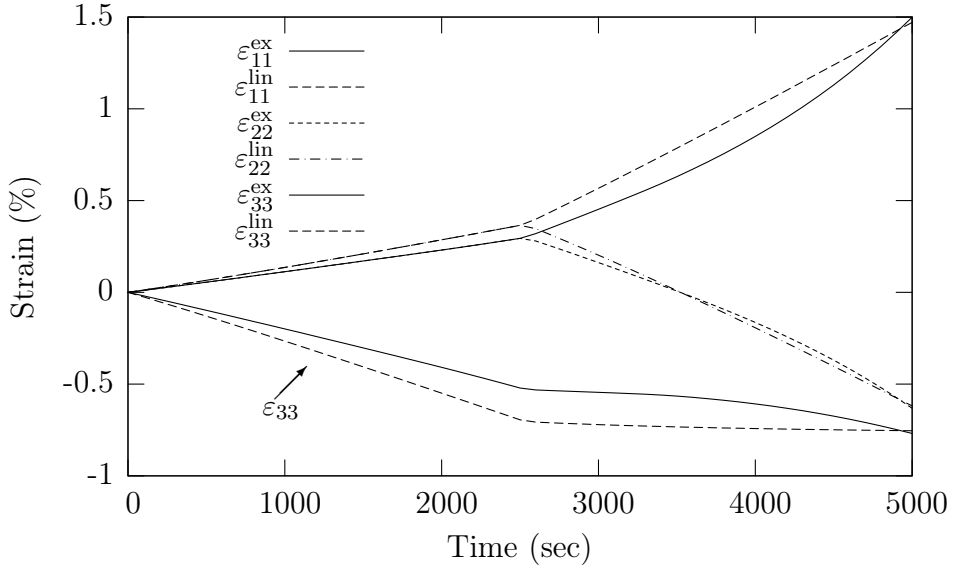


Figure 4.4: Comparison between some components of the strain history of the exact and approximate secant materials when subjected to the same non radial stress history. On the figure, exponent "ex" refers to the exact secant material and exponent "lin" refers to the approximate linearised material.

very specific cases, an analytical solution can be obtained, but in most cases, the solution has to be obtained numerically.

We recall that the LCT of a function g is given by:

$$g^* = p \int_{-\infty}^{t} g(t) \exp[-pt] \mathrm{d}t \tag{4.33}$$

The exact inversion formula is given by the Browhich integral:

$$g(t) = \frac{1}{2\pi i} \int_{c-i\infty}^{c+i\infty} \frac{1}{p} g^*(p) \exp[pt] \mathrm{d}p \tag{4.34}$$

where p is a complex variable. As pointed out by Davies and Martin [22], Duffy [26] and Taiwo *et al.* [96] there seems to be two approaches to calculating the inverse LCT, namely i)those where the integration in equation (4.34) is carried out numerically and ii)those where $g(t)$ is approximated by an appropriate series of functions $\hat{g}(t) = \sum \bar{g}_n(t)$ and where the parameters are calculated so that the error between $g(t)$ and $\hat{g}(t)$ is minimised. The advantage of the first approach is that it is quite general in nature and can be used for many problems. However, knowing different values of t requires another integration of equation (4.34). On the other hand, the second alternative leads to an approximate analytical expression of $g(t)$ which allows

rapid computation of the time response for different values of t. However, this approach is less general than the first one and the series of functions must be chosen so that they are a good approximation to $g(t)$. When information is known *a priori* on $g(t)$ such an approach can be very useful.

Many other authors (see [51, 59, 99], for example) have used such an approach to obtain the homogenised properties of heterogeneous viscoelastic materials. We have seen in equations (1.22,1.24) the most general shape of a linear viscoelastic material. If we assume that the homogenisation process leads to a thermodynamically admissible material, then we know a lot of information regarding the shape of the homogenised material. From these relations, it can be instinctively guessed that the approximate solution should be a series of functions involving decaying exponentials.

Before presenting the theory, we would like to point out the work of Brenner *et al.* [15] where the authors developed a direct method for the inversion of the LCT. Their method allows calculation of $g(t_i) \approx g^*(p_i)$, where the key issue is to define the proper p_i. For their particular problem, the authors obtained very good results. Even though such an approach is computationally efficient, we have chosen to develop a method where the quality of the solution can be controlled, to a certain extent.

We recall here our equations (1.22,1.24):

$$\begin{aligned} \boldsymbol{\varepsilon}(t) &= \int_0^t \mathbf{S}(t-u) : \frac{\mathrm{d}\boldsymbol{\sigma}}{\mathrm{d}\tau}\mathrm{d}u \quad \text{with} \\ \mathbf{S}(t) &= \int_{0^+}^{\infty} (1-\exp[-t\tau])\mathrm{d}\check{\mathbf{S}}(\tau) + \mathbf{S}'t + \mathbf{S}'' \end{aligned} \tag{4.35a}$$

$$\begin{aligned} \boldsymbol{\sigma}(t) &= \int_0^t \mathbf{C}(t-u) : \frac{\mathrm{d}\boldsymbol{\varepsilon}}{\mathrm{d}u}\mathrm{d}\tau \quad \text{with} \\ \mathbf{C}(t) &= \int_{0^+}^{\infty} \exp[-t\tau]\mathrm{d}\check{\mathbf{C}}(\tau) + \mathbf{C}'' \end{aligned} \tag{4.35b}$$

Assume for now that all the constant quantities are included in S''_{ij} or C''_{ij} and that S'_{ij}, S''_{ij} and C''_{ij} are known. Therefore, we only have to deal with the integral part of the compliance/modulus of the behaviour law. The following definitions are introduced for notational simplicity:

$$g(t) = \int_{0^+}^{\infty} (-1)^z \exp\left[-t\tau\right] \mathrm{d}\check{\mathrm{G}}_{\mathrm{ij}}(\tau) = \int_{0^+}^{\infty} (-1)^z \exp\left[-t\tau\right] \mathrm{d}\check{g}(\tau) \tag{4.36a}$$

$$\hat{g}(t) = \int_{0^+}^{\infty} (-1)^z \exp\left[-t\tau\right] \mathrm{d}\bar{\mathrm{G}}_{\mathrm{ij}}(\tau) = \int_{0^+}^{\infty} (-1)^z \exp\left[-t\tau\right] \mathrm{d}\bar{g}(\tau) \tag{4.36b}$$

where $z = 0$ for a relaxation modulus and $z = 1$ for a creep compliance and $\mathrm{d}\check{\mathrm{G}}_{ij}(\tau)$ is either $\mathrm{d}\check{\mathrm{S}}_{ij}(\tau)$ or $\mathrm{d}\check{\mathrm{C}}_{ij}(\tau)$. We seek the approximate function $\hat{g}(t)$ so that:

$$\inf_{\bar{g}} E^2 = \inf_{\bar{g}} \int_0^\infty \left[g(t) - \hat{g}(t)\right]^2 \mathrm{d}t \tag{4.37}$$

It can be observed in equation (4.37) that the approximate function should match the real function only on the real positive time axis. We recall that, *a priori*, $\bar{g}$ is a function and this minimisation problem is difficult to solve. Schapery [84, 86], amongst others, introduces:

$$\bar{g}(t) = \sum_{n=1}^{N} \bar{g}_n \delta(t - \tau_n) \tag{4.38}$$

where $\tau_n > 0$ and $\delta(t - \tau_n)$ is a Dirac impulse centered on τ_n. This leads to:

$$\hat{g}(t) = \sum_{n=1}^{N} \bar{g}_n \exp\left[-t\tau_n\right] \tag{4.39}$$

where $\bar{g}_n$ is no longer a function but a scalar quantity. Combining equations (4.37) and (4.39) leads to:

$$\inf_{\bar{g}_n, \tau_n} \int_0^\infty \left[g(t) - \hat{g}(t)\right] \left[\int_{0^+}^\infty \exp\left[-t\tau\right] \mathrm{d}\check{g}(\tau) - \sum_{n=1}^{N} \bar{g}_n \exp\left[-t\tau_n\right]\right] \mathrm{d}t \tag{4.40}$$

Assuming that the order of integration can be changed [84] and the Laplace transform definition, equation (4.40) becomes:

$$\inf_{\bar{g}_n, \tau_n} \int_{0^+}^\infty \left[\underset{\sim}{g}(\tau) - \underset{\sim}{\hat{g}}(\tau)\right] \mathrm{d}\check{g}(\tau) - \sum_{n=1}^{N} \bar{g}_n \left[\underset{\sim}{g}(\tau_n) - \underset{\sim}{\hat{g}}(\tau_n)\right] \tag{4.41}$$

where $\underset{\sim}{g}$ is the Laplace transform of $g(t)$. Equation (4.41) shows that if $\underset{\sim}{g}(\Re(p)) = \underset{\sim}{\hat{g}}(\Re(p))$ for $\Re(p) > 0$ then $g(t) = \hat{g}(t)$ for $t \geq 0$. This result is very useful since it shows that, for our approximate function, we only need to consider the real positive p axis. In his collocation method, Schapery [84] used this concept to find the $\bar{g}_n$ so that $\underset{\sim}{g}(\tau_n) = \underset{\sim}{\hat{g}}(\tau_n)$ for all n, for a range of predefined τ_n. This leads to a linear system of equations which can be easily solved to obtain the $\bar{g}_n$. Such an approach has two main disadvantages:

1. So far, we have considered only one component G_{ij} of $\mathbf{G}$, but the previous section showed that conditions for thermodynamic stability

are over the interaction of the various components of $\mathbf{G}$ (i.e., $\mathbf{G}(t)$ must be positive semi-definite). For some applications (e.g., plotting the time response), it can be sufficient to treat each of the components of $\mathbf{G}$ individually. This reduces the inversion problem to a set of many simple problems. However, there are situations where it is necessary to find a solution which leads to a thermodynamically admissible material as, for example, when the resulting homogenised material is used in subsequent calculations, as in a FE code. The inversion problem then becomes a single complicated problem.

2. There is no way to determine if the sets of $\bar{g}_n$ and τ_n lead to an *acceptable* solution. Masson *et al.* [59] have determined that $n \approx 20$ is a good choice for a particular type of application. This number has been determined by comparing the approximate results with analytical ones for a similar kind of problem. However, if a problem is encountered where no analytical solution is available, n might be greater that 20 but there will be no way to validate this. Authors such as Laws and MacLaughlin [51] used more than 30 τ_n.

The algorithm which we suggest attempts to improve Schapery's collocation method by addressing these issues. We also suggest additional algorithms for approximate inversion (where thermodynamic conditions are not enforced) and algorithms where the solution satisfies the thermodynamics requirements.

4.3.1 Problem definition

So far, the general approach to identifying the transient part of the relaxation modulus or the creep compliance has been presented. However, in order to identify the stationary parts, these two quantities must be treated differently. If we deal with a creep compliance, it can readily be seen from equation (4.35a) that:

$$\mathbf{S}(0) = \mathbf{S}'' = \mathbf{S}^*(\infty) \tag{4.42a}$$

$$\dot{\mathbf{S}}(\infty) = \mathbf{S}' = \lim_{p\to 0} p\mathbf{S}^*(p) - p\mathbf{S}'' \tag{4.42b}$$

$$\lim_{t\to\infty} \mathbf{S}(t) - \mathbf{S}'t - \mathbf{S}'' = \lim_{p\to 0} \mathbf{S}^*(p) - \frac{\mathbf{S}'}{p} - \mathbf{S}'' = \int_{0^+}^{\infty} \mathrm{d}\check{\mathbf{S}}(\tau) \tag{4.42c}$$

where the limit value theorem has been used. For a relaxation modulus, it can be observed from equation (4.35b) that:

$$\mathbf{C}(\infty) = \mathbf{C}^*(0) = \mathbf{C}'' \tag{4.43a}$$

$$\mathbf{C}(0) - \mathbf{C}'' = \mathbf{C}^*(\infty) - \mathbf{C}'' = \int_{0^+}^{\infty} \mathrm{d}\check{\mathbf{C}}(\tau) \tag{4.43b}$$

where the limit value theorem has also been used. Combining equations (4.35a,4.35b,4.42,4.43) leads to:

$$\left[\int_{0^+}^{\infty} \exp\left[-t\tau\right] \mathrm{d}\check{\mathbf{S}}(\tau)\right]^* = \mathbf{S}'' + \int_{0^+}^{\infty} \mathrm{d}\check{\mathbf{S}}(\tau) + \frac{\mathbf{S}'}{p} - \mathbf{S}^* = \check{\mathbf{S}}^* \tag{4.44a}$$

$$\left[\int_{0^+}^{\infty} \exp\left[-t\tau\right] \mathrm{d}\check{\mathbf{C}}(\tau)\right]^* = \mathbf{C}^* - \mathbf{C}'' = \check{\mathbf{C}}^* \tag{4.44b}$$

As was done previously, let $\check{\mathbf{G}}$ denote either $\check{\mathbf{S}}$ or $\check{\mathbf{C}}$. Equations (4.44) give the transient part of the behaviour law that must be approximated if it is a creep compliance or a relaxation modulus. The approximate function becomes:

$$\hat{\mathbf{G}}(t) = \sum_{n=1}^{N} \bar{\mathbf{G}}^{\mathbf{n}} \exp\left[-t\tau_n\right] \approx \check{\mathbf{G}}(t) \tag{4.45}$$

Equation 4.41 has shown that if the Laplace transforms of f and $\hat{f}$ are equal on the real positive p axis, then their time domain function (for $t > 0$) are equal. By the definition of the LCT, this also holds for the LCT. Then, our problem becomes:

$$\inf_{\bar{\mathbf{G}}^{\mathbf{n}},\tau_n} \int_0^{\infty} \left[\hat{\mathbf{G}}^*(p) - \check{\mathbf{G}}^*(p)\right]^2 \mathrm{d}p \quad \text{with} \quad \bar{\mathbf{G}}^{\mathbf{n}} \geq 0 \quad \text{and} \quad \tau_n > 0 \tag{4.46}$$

This a problem is difficult to implement numerically. We have used a least squares approximation and a relaxed form of equation (4.46), so that it becomes:

$$\inf_{\bar{\mathbf{G}}^{\mathbf{n}}} \sum_{s=1}^{S} \left[\hat{\mathbf{G}}^*(p_s) - \check{\mathbf{G}}^*(p_s)\right]^2 \text{with} \quad \bar{\mathbf{G}}^{\mathbf{n}} \geq 0 \quad \text{and} \quad \sum_{n=1}^{N} \bar{\mathbf{G}}^{\mathbf{n}} = \check{\mathbf{G}}^*(\infty) \tag{4.47}$$

where the τ_n have been carefully chosen. Equation (4.47) is in fact the constrained optimisation problem to be solved in order to obtain our Laplace–Carson inversion. The last constraint of equation (4.47) imposes that $\hat{\mathbf{G}}(0) = \check{\mathbf{G}}(0)$. It was found that the quality of the inversion is greatly improved when the last constraint is added. Therefore, the minimisation problem of equation (4.47) can be seen to be a curve fit where one end of the curve is fixed. Statistical tools can then be used to assess the adequacy of $\hat{\mathbf{G}}$. Then, problem (4.47) requires that the following procedures be developed:

1. Choose the τ_n properly and refine them if necessary.

2. Choose the p_s appropriately so that the statistical tests used to check the accuracy of the inversion are meaningful.

3. Impose the two constraints properly, especially in the case where there is no material symmetry.

These three procedures are described in the remainder of this section. In addition, we present the various algorithms which are function of the material symmetry, since some very useful simplifications can be introduced to reduce the computational burden.

4.3.2 Case of isotropy or cubic symmetry

Any isotropic tensor can be expressed as $\mathbf{G} = \alpha\mathbf{J} + \beta\mathbf{K}$ where $\mathbf{J}$ and $\mathbf{K}$ are the spherical and deviatoric projection tensors (see Appendix A). In the case of cubic symmetry, we have:

$$\begin{aligned} \mathbf{G} = \alpha\mathbf{J} + \beta\mathbf{K_a} + \gamma\mathbf{K_b} \quad \text{with} \quad \Lambda_{iiii} = 1, \quad \mathbf{K_a} = \mathbf{\Lambda} - \mathbf{J} \\ \text{and} \quad \mathbf{K_b} = \mathbf{I} - \mathbf{\Lambda} \end{aligned} \tag{4.48}$$

Simple calculation rules follow from these definitions which means that the result of homogenisation is given in terms of $\{\alpha, \beta, \gamma\}$. For these material symmetries, having $\mathbf{G} \geq 0$ implies that $\alpha, \beta, \gamma \geq 0$. Therefore, the multidimensional problem (4.47) becomes two or three one-dimensional problems, which present no difficulties. Let α be any of $\{\alpha, \beta, \gamma\}$. Problem (4.47) then becomes:

$$\inf_{\bar{\alpha}^n} \sum_{s=1}^{S} [\hat{\alpha}^*(p_s) - \breve{\alpha}^*(p_s)]^2 \quad \text{with} \quad \bar{\alpha}^n \geq 0 \quad \text{and} \quad \sum_{n=1}^{N} \bar{\alpha}^n = \breve{\alpha}^*(\infty) \tag{4.49}$$

It will be seen later how this constrained quadratic programming problem is simplified and solved after the procedure for choosing the τ_n and p_s has been described. For these symmetries, treating α, β and γ separately is sufficient to enforce the thermodynamic stability of the inversion procedure.

Procedure for choosing the p_s for $\bar{\alpha}^n \geq 0$

Due to the definition of the Laplace transform, if g is a monotonous function, then g^* is also monotonous. A good set of p_s would be one where the values of $\breve{\alpha}^*(p)$ are equally distributed over $]0, (1-\epsilon)\breve{\alpha}^*(\infty)]$ where $\epsilon \ll 1$. This ensures that no portion of the curve in the LC space is given more importance than

any other in the least squares calculation. Suppose that the number of p_s is S. Then, the set of p_s is defined by:

$$\breve{\alpha}^*(p_s) = \frac{s}{S}(1-\epsilon)\breve{\alpha}^*(\infty) \quad \text{for } s = 1, \ldots, S \tag{4.50}$$

The solutions of this nonlinear equation were obtained by an algorithm which combines a Newton-Raphson and a bisection method as implemented in [79]. For the cases simulated, it was found that $S = 50$ and $\epsilon = 10^{-3}$ were acceptable choices.

Procedure for choosing the τ_n

Most real materials found in the literature are modelled by an arrangement of spring-dashpot pairs. If E denotes the elastic constant of a spring and η the damping coefficient of a dashpot, it is classical to define a relaxation time by $\varphi_n = \frac{\eta_n}{E_n} = \frac{1}{T_n}$. It was found by Rougier [82] that applying the self-consistent homogenisation scheme to two isotropic incompressible Maxwell materials leads to a homogenised shear relaxation modulus, $\mu(t)$, where $\mathrm{d}\breve{\mu}(\tau)$ is defined by two Dirac impulses at T_1 and T_2 and a continuous function between $[\theta_1, \theta_2]$, with θ_1, θ_2 lying between T_1 and T_2. Homogenisation of the same materials in accordance with the Mori-Tanaka scheme leads to $\mathrm{d}\breve{\mu}(\tau)$ being composed of two Dirac impulses, one in T_0 (associated with the matrix phase) and the other in θ_1 which lies between T_0 and T_1. This suggests, for materials where $\breve{\mathbf{G}}$ is non zero over a given interval, that the τ_n be distributed within the bounds of this interval. Masson [57] suggested the use of bounds $[10^{-4} \min T_n, 10^2 \max T_n] = [T_{min}, T_{max}]$ which might be safer. When the domain over which the spectra is non zero cannot be bounded (for example, in an elastic material where $T_n = \infty$) then the choice of an interval for the τ_n can be difficult. In the case of a homogenised material which is made of elastic and viscoelastic phases, the choice $[\rho^{-1} \min T_n, \rho \max T_n]$ has been used with success, where $\rho \approx 10^4$.

Another alternative would be to take advantage of the p_s evaluated previously. The collocation method of Schapery [84, 86] suggests finding the parameters of the approximate solution (i.e., the α, β, etc.) so that the following system of N equations:

$$\alpha^*(\tau_n) = \hat{\alpha}^*(\tau_n) \tag{4.51}$$

is solved. We recall that $\alpha(\infty) = \hat{\alpha}(\infty) = 0$ (see equation (4.45)) which implies that $\alpha^*(0) = \hat{\alpha}^*(0) = 0$. We also have, from the problem definition (see equation (4.47)), that $\alpha^*(\infty) = \hat{\alpha}^*(\infty)$. Therefore, we are guaranteed that the approximate and exact solutions are equal at zero and at infinity.

We also require that the approximate solution matches the exact solution for the other intermediate values of p. The set of p_s we have calculated represents the variation of α^* over almost all the interval $[0, \alpha^*(\infty)]$. So, in the collocation method, distributing the τ_n over the range $[p_1, p_S]$ would force the approximate and exact solutions to match at points distributed on almost all the variation domain of α^*. So, in our case, a good choice for the interval over which the τ_n are distributed would be $[p_1, p_S]$. For safety, we have used the interval $[10^{-1}p_1, 10p_s]$. This choice has the advantage that it does not require that we know the relaxation times of the constituent materials.

We have implemented these two approaches. For the cases we have simulated, the most accurate and computationally efficient inversions were obtained with the second procedure.

Now that the interval over which the τ_n are distributed has been chosen, it only remains to choose the number of τ_n and and distribute them within the interval. For the cases we have simulated, it was found that approximately ten τ_n are sufficient. However, if the inversion does not provide an acceptable accuracy, more terms can be included. As for the distribution of the τ_n, Masson *et al.* [59] used a logarithmic distribution between $[T_{min}, T_{max}]$ while Laws *et al.* [51] used uniformly spaced τ_n. It should be noted that for most real materials found in the literature, $\check{\mathbf{G}}$ is a series of Dirac impulses on a log scale (i.e., one per decade). It would then seem natural to distribute the τ_n on a log scale between $[T_{min}, T_{max}]$. We have used such a distribution. However, other choices of distributions are possible and should be chosen according to the type of materials being homogenised.

Determination of approximate function $\hat{\alpha}(t)$

The constrained optimisation problem (4.47) has been solved with the Lagrange multiplier technique and by setting $\bar{\alpha}^n = (x^n)^2$. The least squares equation becomes:

$$E^2 = \sum_{s=1}^{S} \left[\breve{\alpha}^*(p_s) - \sum_{n=1}^{N} \frac{(x^n)^2 p_s \tau_n}{1 + p_s \tau_n} \right]^2 - \lambda \left[\sum_{n=1}^{N} (x^n)^2 - \breve{\alpha}^*(\infty) \right] \tag{4.52}$$

where λ is the Langrange multiplier and the LCT of $\hat{\alpha}(t)$ has been explicitly calculated. The gradient and Jacobian of equation (4.52) can be calculated easily. The Lagrange multiplier technique consists of cancelling the gradient of E^2 where λ is considered as an independent variable. Cancellation of the gradient was accomplished by the Newton method. Since $|x^n| \in \left[0, \sqrt{\breve{\alpha}^*(\infty)}\right]$ (due to the constraint), the initial values of x^n were chosen randomly within the interval $\left[-\sqrt{\breve{\alpha}^*(\infty)}, \sqrt{\breve{\alpha}^*(\infty)}\right]$.

In order to assess the adequacy of the model , statistical tests can be used. We have used the *adjusted multiple coefficient of determination* defined by:

$$\begin{aligned} R^2 &= 1 - \frac{S-1}{S-N-1} \frac{\sum_{s=1}^{S} \left[\hat{\alpha}^*(p_s) - \breve{\alpha}^*(p_s)\right]^2}{\sum_{s=1}^{S} \left[\breve{\alpha}^*(p_s) - \langle \breve{\alpha}^*(p_s) \rangle\right]^2} \\ &= 1 - \nu \frac{1}{\mathrm{SSE}} \sum_{s=1}^{S} \left[\hat{\alpha}^*(p_s) - \breve{\alpha}^*(p_s)\right]^2 \end{aligned} \tag{4.53}$$

where $\langle f \rangle$ is the average of f. In the cases we have simulated, an accurate inversion was judged to have been obtained when $R^2 > 0.999$. Since the Lagrange multiplier technique does not ensure that the solution is a minimum, the analysis has to be repeated with different starting points. Typically, approximately ten different starting points were used. It should be noted that for some simulated cases, some saddle points lead to larger R^2 than local minima.

In some situations, the algorithm did not lead to an acceptable value of R^2. In other situations, the Jacobian of the system was nearly singular and it was not possible to cancel the gradient within the maximum number of iterations we allowed. For these two situations, we have implemented an algorithm which first tried to run the minimisation with less terms in the approximate function (i.e., fewer exponentials). The smallest number of terms was set to 5. If an acceptable solution was not achieved within 10 minimisations, this number of terms was incremented by one and the procedure was repeated until an acceptable solution was attained or the number of terms exceeded 16. Then, if this happened, the range over which the t_n were distributed was increased to $[10^{-2}p_1, 10^2 p_S]$ and the procedure described previously was repeated. If an acceptable solution was not obtained after such procedure, the objective value of $R^2 = 0.999$ was relaxed to $R^2 = 0.995$ and an error message was issued. The minimisation leading to the largest value of $R^2 > 0.995$ out of the previous minimisations was chosen as the solution. If no acceptable solution was obtained after this procedure, the simulation was stopped. For all the simulations we have run, such algorithm led to a solution.

4.3.3 Transverse isotropy

As with isotropy or cubic symmetry, a transversely isotropic tensor can be written using a short hand notation [9]. We introduce:

$$\begin{aligned} \boldsymbol{i_T} &= \boldsymbol{i} - \boldsymbol{h}\otimes\boldsymbol{h}, \quad \mathbf{E_L} = \boldsymbol{h}\otimes\boldsymbol{h}\otimes\boldsymbol{h}\otimes\boldsymbol{h}, \quad \mathbf{J_T} = \frac{1}{2}\boldsymbol{i_T}\otimes\boldsymbol{i_T}, \\ \mathbf{K_E} &= \frac{1}{6}(2\boldsymbol{h}\otimes\boldsymbol{h} - \boldsymbol{i_T})\otimes(2\boldsymbol{h}\otimes\boldsymbol{h} - \boldsymbol{i_T}), \quad \mathbf{K_T} = \mathbf{I_T} - \mathbf{J_T}, \\ \mathbf{K_L} &= \mathbf{K} - \mathbf{K_T} - \mathbf{K_E}, \quad \text{and} \quad \mathbf{F} = \frac{1}{\sqrt{2}}\boldsymbol{i_T}\otimes\boldsymbol{h}\otimes\boldsymbol{h} \end{aligned} \tag{4.54}$$

where $\boldsymbol{h}$ is a vector along the axis of transverse isotropy and $\mathbf{I_T}$ is the fourth order identity tensor in the transverse plane[1]. Then, a fourth order, symmetric, transverse isotropic tensor is given by:

$$\mathbf{A} = \alpha\mathbf{E_L} + \beta\mathbf{J_T} + \gamma(\mathbf{F} + \mathbf{F}^{\mathsf{T}}) + \delta\mathbf{K_T} + \delta'\mathbf{K_L} \tag{4.55}$$

In order to have $\mathbf{A} \geq 0$, it is necessary that $\alpha, \beta, \delta, \delta' \geq 0$ and $\gamma^2 \leq \alpha\beta$. The p_s for α, β, δ and δ' can be evaluated as described in the last subsection but a different treatment is required for γ. The interval for the τ_n is estimated as described previously.

Procedure for choosing the p_s for γ

Since $\breve{\gamma}$ can take positive and negative values, $\breve{\gamma}^*$ is not necessarily a monotonic function of p. If $\breve{\gamma}^*(p)$ oscillates then the p_s should be chosen so that they model the oscillations. Therefore, a proper algorithm is required to check if there are oscillations and to identify the values of p_n where the sign of the slope of $\breve{\gamma}^*(p)$ changes. This is first accomplished by checking if there are values of p_n for which the slope of $\breve{\gamma}^*$ is equal to zero. The homogenisation solution does not compute this quantity and therefore it must be calculated numerically. In addition, the value of p for which the slope is equal to zero must be positive (since the curve fit is carried out on the positive p axis). So, if we introduce $p = x^2$, then we seek x so that:

$$\frac{\partial\breve{\gamma}^*}{\partial x}(x^2) = 0 \approx \frac{\breve{\gamma}^*(x^2+\epsilon) - \breve{\gamma}^*(x^2-\epsilon)}{2\epsilon} \tag{4.56}$$

where the Jacobian

$$\frac{\partial^2\breve{\gamma}^*}{\partial x\partial x}(x^2) \approx 2x\frac{\breve{\gamma}^*(x^2+\epsilon) + \breve{\gamma}^*(x^2-\epsilon) - 2\breve{\gamma}^*(x^2)}{\epsilon^2} \tag{4.57}$$

[1]This extracts the components of a second order tensor which are in the plane perpendicular to the axis of transverse isotropy.

where $\epsilon \ll 1$. The first step is to find a value p_{lim} above which there are no oscillations. This can be accomplished by evaluating $\breve{\gamma}^*$ at successive increasingly large values of p until consecutive values of $\breve{\gamma}^*$ are close to $\breve{\gamma}^*(\infty)$ and consecutive slopes of $\breve{\gamma}^*$ are of the same sign. Then, use a Newton-Raphson technique to solve equation (4.56) with different starting points. If a solution leads to $p > p_{\text{lim}}$ or to a point where the slope has the same left and right sign, this point is rejected. These K different points are ordered. Then, the set of p_s is evaluated as follows:

$$\begin{gathered}\breve{\gamma}^*(p_s) = \breve{\gamma}^*(p_{k-1}) + \frac{s-(k-1)Z}{Z}\left[\breve{\gamma}^*(p_k) - \breve{\gamma}^*(p_{k-1})\right] \\ \text{for} \quad k = 1, \ldots, K \quad \text{and} \quad s = 1, \ldots, KZ\end{gathered} \tag{4.58}$$

where Z is the number of p_s in a given interval $[p_{k-1}, p_k]$. p_K should be chosen so that it is the closest point to p_{lim} that meets $\breve{\gamma}^*(p_K) = (1 \pm \epsilon)\breve{\gamma}^*(\infty)$, if $\breve{\gamma}^*(\infty)$ is approached from above or below. For the cases we have simulated, we have used $K = 25$ so that there are at least 50 p_s. Of course, if there are no oscillations, the p_s are calculated as was done in the case of isotropy or cubic symmetry.

Determination of approximate function

$\{\hat{\delta}, \hat{\delta}'\}$ can be identified separately by solving problem (4.49). If thermodynamic stability is not required, $\{\hat{\alpha}, \hat{\beta}, \hat{\delta}, \hat{\delta}'\}$ are solutions of (4.49) and $\hat{\gamma}$ is chosen so that it minimises:

$$E^2 = \sum_{s=1}^{S}\left[\breve{\gamma}^*(p_s) - \sum_{n=1}^{N}\frac{\bar{\gamma}^n p_s \tau_n}{1 + p_s\tau_n}\right]^2 - \lambda\left[\sum_{n=1}^{N}\bar{\gamma}^n - \breve{\gamma}^*(\infty)\right] \tag{4.59}$$

When thermodynamic stability is required, $\hat{\gamma} \in \left[-\sqrt{\hat{\alpha}\hat{\beta}}, \sqrt{\hat{\alpha}\hat{\beta}}\right]$ for all t. A relationship exists between $\{\alpha, \beta, \gamma\}$ which can be considered as a constraint in the optimisation problem. The problem is then one of finding $\{\hat{\alpha}, \hat{\beta}, \hat{\gamma}\}$ which *simultaneously* minimises the difference between these approximate functions and the real function in the LC space, subject to the constraints imposed by thermodynamics. Introduce $\bar{\alpha}^n = (x^n)^2$, $\bar{\beta}^n = (y^n)^2$, $\bar{\gamma}^n = \sqrt{(x^n)^2(y^n)^2}\sin v^n$ and:

$$R_\alpha^2 = 1 - \frac{\nu}{\text{SSE}_\alpha}\sum_{s=1}^{S}\left[\breve{\alpha}^*(p_s) - \sum_{n=1}^{N}\frac{(x^n)^2 p_s\tau_n}{1 + p_s\tau_n}\right]^2 \tag{4.60a}$$

$$R_\beta^2 = 1 - \frac{\nu}{\mathrm{SSE}_\beta} \sum_{s=1}^{S} \left[\breve{\beta}^*(p_s) - \sum_{n=1}^{N} \frac{(y^n)^2 p_s \tau_n}{1 + p_s \tau_n} \right]^2 \tag{4.60b}$$

$$R_\gamma^2 = 1 - \frac{\nu}{\mathrm{SSE}_\gamma} \sum_{s=1}^{S} \left[\breve{\gamma}^*(p_s) - \sum_{n=1}^{N} \frac{\sqrt{(x^n)^2 (y^n)^2} \sin v^n p_s \tau_n}{1 + p_s \tau_n} \right]^2 \tag{4.60c}$$

We then define the new problem as:

$$\begin{gathered} \sup_{x^n, y^n, v^n} R_\alpha^2 + R_\gamma^2 + R_\gamma^2 \quad \text{with} \quad \sum_{n=1}^{N} \bar{\alpha}^n = \breve{\alpha}^*(\infty), \\ \sum_{n=1}^{N} \bar{\beta}^n = \breve{\beta}^*(\infty) \quad \text{and} \quad \sum_{n=1}^{N} \bar{\gamma}^n = \breve{\gamma}^*(\infty) \end{gathered} \tag{4.61}$$

The Lagrange multiplier technique is not efficient for solving such a problem. As a feasibility study, this problem has been numerically solved using the Nelder-Mead simplex algorithm implemented in Mathematica and the constraints were enforced by a penalty function. Other, more refined techniques, could be used.

4.3.4 General anisotropy

As in the other cases of symmetry, the same procedure is used for determining and refining the τ_n. The p_s associated with the diagonal terms are calculated similarly to those in the case of isotropy or cubic symmetry while the p_s for the off diagonal terms are calculated in the same way as those of $\hat{\gamma}$ in the case of transverse isotropy. If the solution does not need to meet thermodynamic requirements, the inversion can be carried out on the 21 independent coefficients of $\mathbf{G}$ separately.

Meeting the thermodynamic conditions in the case of general anisotropy is more involved. $\hat{\mathbf{G}}$ consists of a series of positive semi-definite matrices (multiplying a decaying exponential) which simultaneously minimise the square of the error between $\hat{\mathrm{G}}_{ij}^*(p)$ and $\breve{\mathrm{G}}_{ij}^*(p)$ for all independent ij component.

A definite semi-positive matrix is a matrix for which all the eigenvalues are greater than or equal to zero. We recall that any symmetric positive semi-definite matrix in a given base can be expressed as: $\mathbf{A} = \mathbf{B}^{\mathrm{T}}\mathbf{D}\mathbf{B}$ where $\mathbf{D}$ is a diagonal matrix containing the eigenvalues of $\mathbf{A}$ and $\mathbf{B}$ is an orthogonal matrix containing the eigenvectors of $\mathbf{A}$. $\mathbf{B}$ is a rotation matrix, which in our case, has 6 dimensions. It can be shown in n dimensions that a general rotation matrix can be given as a sequence of simple rotations in a plane.

For example,

$$\mathbf{B}(\theta_1) = \begin{pmatrix} \cos\theta_1 & \sin\theta_1 & 0 & 0 & 0 & 0 \\ -\sin\theta_1 & \cos\theta_1 & 0 & 0 & 0 & 0 \\ 0 & 0 & 1 & 0 & 0 & 0 \\ 0 & 0 & 0 & 1 & 0 & 0 \\ 0 & 0 & 0 & 0 & 1 & 0 \\ 0 & 0 & 0 & 0 & 0 & 1 \end{pmatrix} \tag{4.62}$$

is a rotation in the $1-2$ plane. In 6 dimensions, there can be 15 plane rotations and the general rotation matrix is given by:

$$\mathbf{B} = \prod_{n=1}^{15} \mathbf{B}(\theta_n) \tag{4.63}$$

Therefore, $\mathbf{A}$ can be defined by 21 independent constants: 15 rotation angles and 6 eigenvalues. If we define $\mathrm{D}_{ii}^{+} = \mathrm{D}_{ii}^{2}$ (so that all the eigenvalues are greater than or equal to zero), then:

$$\hat{\mathbf{G}}(t) = \sum_{n=1}^{N} \mathbf{B}_n^{\mathrm{T}} \mathbf{D}_n^{+} \mathbf{B}_n \exp\left[-t\tau_n\right] = \sum_{n=1}^{N} \bar{\mathbf{G}}^{\mathbf{n}} \exp\left[-t\tau_n\right] \tag{4.64}$$

If w denotes one of the 21 independent components of $\mathbf{G}$, n one of the terms in $\hat{\mathbf{G}}$, D_{ii}^{n+} one of the 6 components of $\mathbf{D}^{+}$ for a given n, and θ_v^n one of the 15 angles of the rotation matrix associated with a given n, then the problem becomes:

$$\begin{gathered} \sup_{\mathrm{D}_{ii}^{n+},\theta_v^n} \sum_{w=1}^{21} R_w^2 \quad \text{with} \quad \sum_{n=1}^{N} \bar{\mathrm{G}}_w^n = \mathrm{G}_w^*(\infty) \\ \text{for} \quad i = 1,\ldots,6 \quad v = 1,\ldots,15 \quad n = 1,\ldots,N \end{gathered} \tag{4.65}$$

Problem (4.65) is a maximisation problem with $21 \times N$ variables. For $N = 15$ this problem has been solved with the Nelder-Mead simplex algorithm in Mathematica and the constraints were introduced by using a penalty function.

4.3.5 Validation for selected cases

The algorithm has been validated using cases where it has been possible to invert the analytical symbolic stiffness or compliance. Such solutions are usually simple and limited to materials exhibiting symmetry. Therefore, for the general anisotropic material, a form of $\mathrm{d}\check{\mathbf{G}}(\tau)$ was assumed. The various

S_i defined in section 1.3.1 were tested (i.e., we tried using our algorithm to generate an inversion of a particular S_i). In most cases, the results of the inversion were very good and it was impossible to visually distinguish the approximate and real curves on a graph. For conciseness, such plots are not reported here.

Validation against analytical solutions

Consider a composite material made of long fibres aligned along the x axis. Assume that the matrix is isotropic and obeys a Zener behaviour, while the fibres are linear elastic, isotropic and incompressible. The overall behaviour of such a composite is transversely isotropic. The elastic solutions for such a composite, homogenised according to the Mori-Tanaka scheme are given by Wang and Weng [99]. The transient homogenised properties of this material are given by:

$$\begin{aligned}
\alpha(t) &= (\alpha_1 + \alpha_2 t)\exp[-\tau_1 t] + (\alpha_3 + \alpha_4 t)\exp[-\tau_2 t] \\
&\quad + \alpha_5 \exp[-\tau_3 t] + \alpha_6 \exp[-\tau_4 t] \\
\beta(t) &= \beta_1 \exp[-\tau_3 t] + \beta_2 \exp[-\tau_4 t] \\
\gamma(t) &= \gamma_1 \exp[-\tau_1 t] + \gamma_2 \exp[-\tau_2 t] + \gamma_3 \exp[-\tau_3 t] + \gamma_4 \exp[-\tau_4 t] \\
\delta(t) &= \delta_1 \exp[-\tau_5 t] + \delta_2 \exp[-\tau_6 t] + \delta_3 \exp[-\tau_7 t] \\
\delta'(t) &= \delta'_1 \exp[-\tau_4 t] + \delta'_2 \exp[-\tau_8 t]
\end{aligned} \tag{4.66}$$

Figure 4.5 shows a typical plot for $\gamma(t)$ where the approximate and analytical curves can be distinguished graphically. It can be observed that the quality of the inversion is satisfactory. Consider now the case of two isotropic distributions of isotropic and incompressible Maxwell phases homogenised using the Self-Consistent scheme. The resulting material is isotropic and incompressible. Rougier [82] has shown that the transient part of the shear relaxation modulus for such a material is given by:

$$\begin{aligned}
\mu(t) = \int_0^\infty \exp\left[-\frac{t}{\tau}\right] \Big[& \mu_1 \delta(t-\varphi_1) + \mu_2 \delta(t-\varphi_2) \\
& + \frac{k_c \varphi_1 \varphi_2}{\pi\sqrt{\theta_1\theta_2}} \frac{\sqrt{(\tau-\theta_1)(\theta_2-\tau)}}{\tau(\tau-\varphi_1)(\varphi_2-\tau)} \left[H(\tau-\varphi_1) - H(\tau-\varphi_2)\right] \Big] \mathrm{d}\tau
\end{aligned} \tag{4.67}$$

The algorithm we suggest has been successfully applied to this type of behaviour and the exact and approximate solutions were visually identical when graphed.

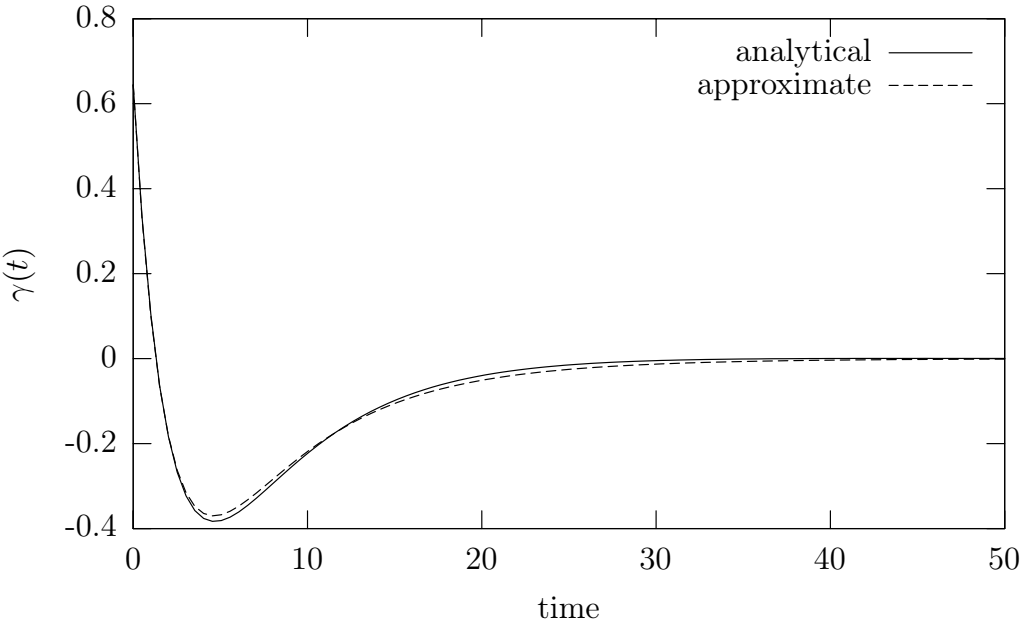


Figure 4.5: Inverse Laplace-Carson transform of γ^* for long elastic incompressible fibres embedded in an isotropic matrix which obeys a Zener behaviour law. The resulting material is transversely isotropic.

Validation against general behaviour laws

The general forms of behaviour calculated in Section 1.3.1 (i.e., the S_i functions) are useful to check if the approximate function we have chosen can predict some generalised behaviour. We have applied our algorithm to all the S_i functions. The quality of the approximation was excellent for all cases, except for $S_4(t) = at^\alpha$ and $S_6(t) = a\log(1+bt)$. This is not surprising since the behaviour at infinity of such functions is quite different from that of decaying exponentials. The capacity of the algorithm to perform a relevant inversion can be numerically checked by evaluating the behaviour of the transient part at infinity. For a creep compliance, this means checking if $\int_0^\infty \mathrm{d}\check{\mathbf{S}}(\tau) < +\infty$ and for a relaxation modulus if $\mathbf{C}^*(0)$ is finite. If these conditions are not met, then the algorithm will fail to provide an appropriate inversion. For those cases, a different approximate function should be used.

4.3.6 Numerical inversion of Laplace – Carson Transforms for the homogenisation tensors

So far, we have presented an algorithm for numerical inversion of the homogenised properties, namely the homogenised creep compliance $\tilde{\mathbf{S}}(t)$ and

the homogenised relaxation modulus $\tilde{\mathbf{C}}(t)$. However, these are not the only results which are required to solve the whole homogenisation problem. For example, equations (3.20,3.21) show that computation of the global response required knowledge of $\mathbf{B_0}(t)$ and $\mathbf{R}_0(t)$. It would be tempting to use the algorithm we have developed previously to carry out the inversion of the LCT of these quantities. However, the nature of these tensor functions is quite different to those of the homogenised properties.

Consider the Mori-Tanaka solutions for the tensors listed at equations (3.14,3.16). In the LC space, the spherical and deviatoric parts of the tensors will be positive since the LCT of the constituent materials are positive for all p. Therefore, these tensors are definite semi-positive for all p in the LC space. There is no guarantee, however, that their time domain expressions correspond to linear viscoelastic behaviour laws. If we denote by α the deviatoric or spherical part of such tenors, it is possible that $\alpha(s)$ starts at zero, increases up to a certain value and decreases towards a positive asymptote. Trying to approximate such a function with a mathematical function that is similar to a creep compliance or a relaxation modulus will fail since the nature of the two curves is different. We have observed such oscillatory behaviour in the cases we have simulated. Of all the oscillating cases we have observed the function only had one oscillation. The conditions under oscillations occur were not studied in this work.

The algorithm we have used for these tensors is quite similar to those we have presented in the previous section. We have only considered the case of isotropic tensors and hence treated the deviatoric and spherical parts of these tensors separately. Again, the procedure for choosing the τ_n is the same as the one described in section 4.3.2. The procedure to determine the set of p_s is the same as the one used for γ in the case of transverse isotropy. The optimisation problem solved to obtain the inversion is simply:

$$\inf_{\bar{\alpha}^n} \sum_{s=1}^{S} \left[\hat{\alpha}^*(p_s) - \breve{\alpha}^*(p_s)\right]^2 \quad \text{with} \quad \sum_{n=1}^{N} \bar{\alpha}^n = \breve{\alpha}^*(\infty) \tag{4.68}$$

which is solved with the Lagrange multiplier technique and leads to the alternative optimisation problem:

$$\inf_{\bar{\alpha}^n} \sum_{s=1}^{S} \left[\breve{\alpha}^*(p_s) - \sum_{n=1}^{N} \frac{\bar{\alpha}^n p_s \tau_n}{1 + p_s \tau_n}\right]^2 - \lambda \left[\sum_{n=1}^{N} \bar{\alpha}^n - \breve{\alpha}^*(\infty)\right] \tag{4.69}$$

Again the solution was considered acceptable when $R^2 > 0.999$. The same refinement algorithm as used previously was implemented if an acceptable solution was not reached within ten attempts. For all the cases we have simulated, an acceptable solution was obtained.

4.4 Simulations and comparison of the two models

The objectives of this last section is to test the complete numerical implementation which has been described and to compare the two models we have developed. We recall that the comparison between finite elements and experimental data is done in Chapter Five.

We have run many simulations and varied the following parameters in order to explore the general trends of the two models:

1. The volume fraction of reinforcements was varied from 0 to 30%.

2. The difference in the mechanical properties of the constituents was considered. Glass is much stiffer than the nonlinear viscoelastic matrix. In order to explore the opposite tendency, we have simulated a material where the glass beads were replaced by spherical voids.

3. The influence of the loading rate was examined.

4. Variations of the loading path were analysed. We have simulated monotonic as well as loading-unloading stress histories. In addition, we have applied radial as well as non radial load histories.

5. Different types of loadings were considered. We have simulated uniaxial tension, hydrostatic pressure, pure shear, biaxial traction, traction on one plane in combination with compression on another plane, and combined shear and tension[2].

6. The nonlinearity in the model was varied. In order to accomplish that, we have modified our constitutive theory. We have set that $g_2(h) = 1$ for $100 \times h \in [0, 1.4]$ and $g_2(h) = 1 + \zeta 0.8(h - 1.4)$ for $100 \times h \in [1.4, 12.5]$ where ζ is a parameter which controls the nonlinearity in the model. We have studied the cases where $\zeta = 1, 3$ and 5.

We have observed consistent tendencies over these simulations. Therefore, rather than showing all the plots, we only present the results for unixial tension for conciseness. In general, it was found that the secant model needed fewer iterations at each step than the affine model.

[2]It should be noted that for pure hydrostatic and shear loadings, we applied a small loading on the other component. For example, if we applied macroscopic shear, we also applied a very small hydrostatic pressure. This ensured that the average stress in the matrix had a deviatoric as well as a hydrostatic component, so that all the parameters of the linearised material could be identified.

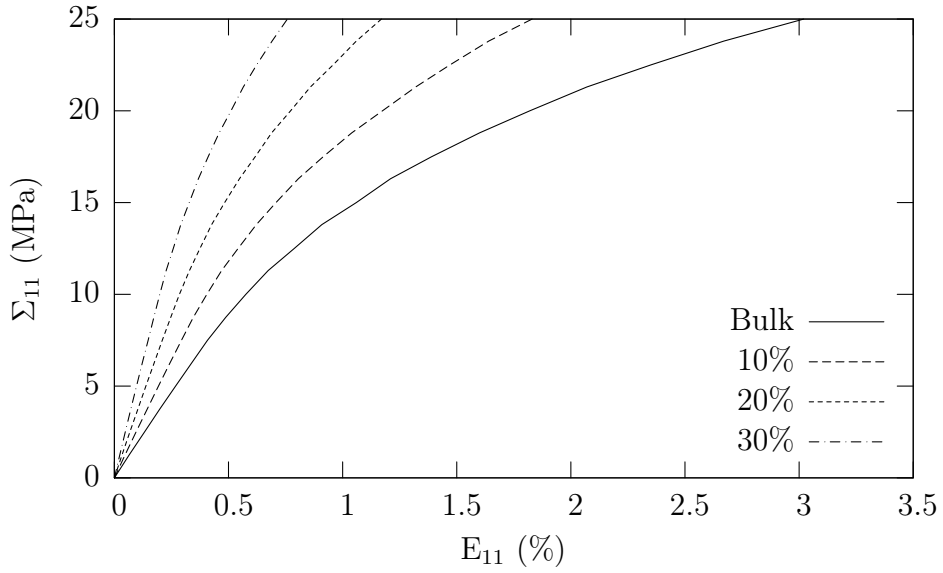


Figure 4.6: Stress-strain curves obtained for the nonlinear viscoelastic composite material for various volume fractions of glass beads during a tensile test at a constant stress rate of $\frac{25\text{MPa}}{7000\text{s}}$ for the secant model.

For certain loading paths and nonlinearities, it was not possible to obtain the whole solution with the affine model for the number of iterations we allowed at each step. Decreasing the step size did not improve the convergence and it was not possible to compare the two models for all the cases. The cases where a solution was not obtained did not follow any definite pattern (for example, for a certain volume fraction, nonlinearity, etc.).

Unless otherwise specified, the plots are for a tensile stress history where $\sigma_{11}(t) = \frac{25\text{MPa}}{7000\text{s}}t$. We plot the stress/strain curves.

4.4.1 Variation of the glass beads volume fraction

Figure 4.6 shows the tensile response of the nonlinear viscoelastic material under tensile loading for volume fractions of glass beads ranging from 0 to 30% for the secant model. As expected, as the volume fraction of glass beads increases, the material stiffens and the nonlinearity is less severe.

4.4.2 Variation of the volume fraction of spherical voids

Figure 4.7 shows the tensile response of the nonlinear viscoelastic material under tensile loading for volume fractions of spherical voids ranging from 0 to 30% for the secant model. As expected, as the volume fraction of voids

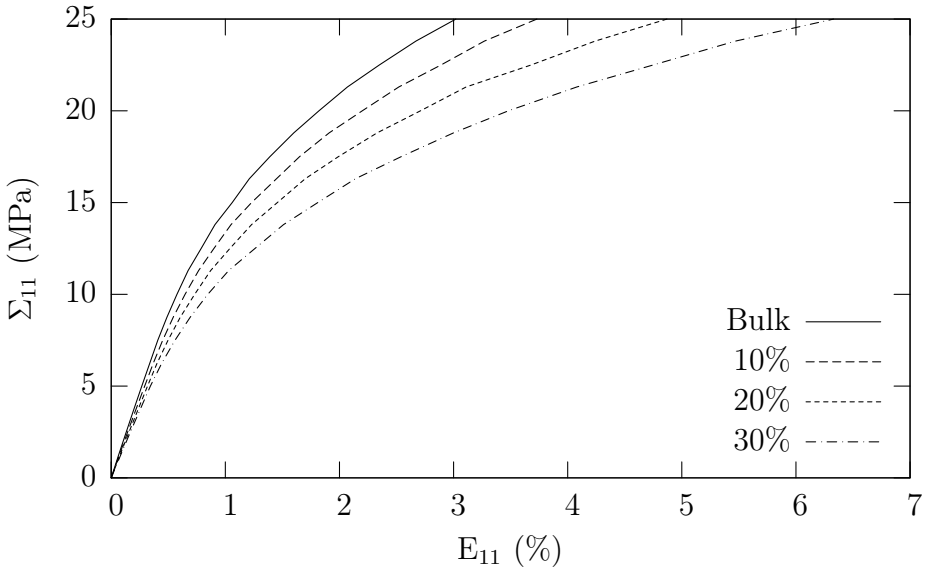


Figure 4.7: Stress-strain curves obtained for the nonlinear viscoelastic composite material for various volume fractions of spherical voids during a tensile test at a constant stress rate of $\frac{25\text{MPa}}{7000\text{s}}$ for the secant model.

increases, the material softens.

4.4.3 Variation of the loading rate

Figure 4.8 shows the influence of stress rate on the tensile response of the nonlinear viscoelastic composite with a volume fraction of 20% of glass beads for the secant model. As expected, as the stress rate increases, the material becomes stiffer.

4.4.4 Simulation of loading-unloading

Figure 4.9 shows the stress-strain curves for the nonlinear viscoelastic material for 20% of glass beads during a loading-unloading test at a constant stress rate, for the secant model. Unlike its non hereditary analogue, our secant model can be used to predict loading-unloadings.

4.4.5 Variation of the nonlinearity and comparison of the affine and secant models

For the load cases we have simulated, the responses of the two models were very close when $\zeta = 1$. However, when this parameter is increased, there

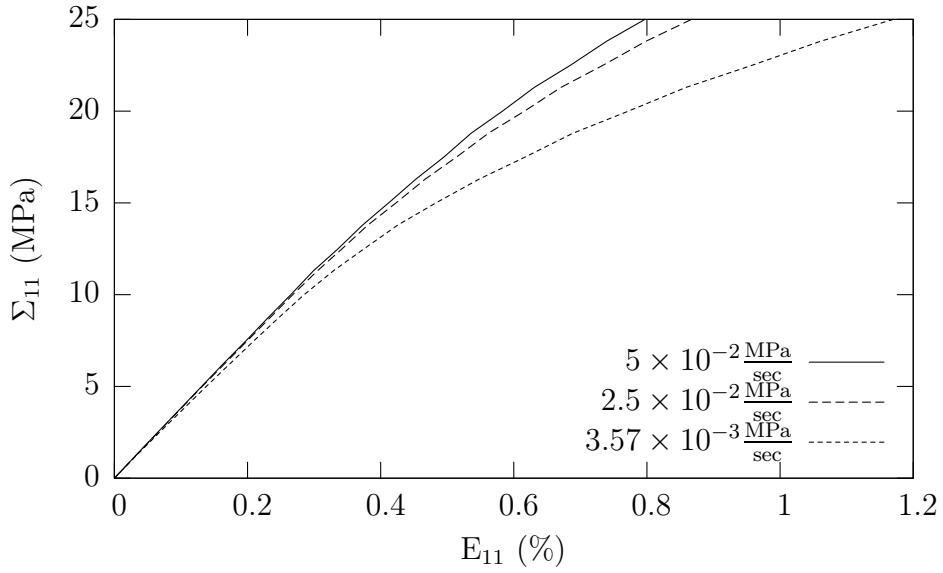


Figure 4.8: Stress-strain curves obtained for the nonlinear viscoelastic composite material for 20% of glass beads during a tensile test at various constant stress rates for the secant model.

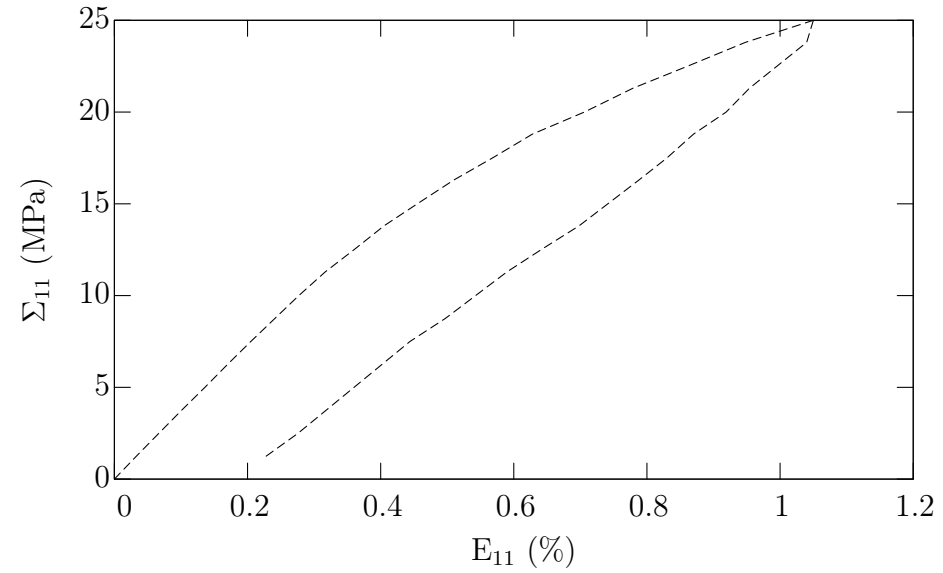


Figure 4.9: Stress-strain curves obtained for the nonlinear viscoelastic composite material for 20% of glass beads for a tensile loading-unloading test at a constant stress rate for the secant model.

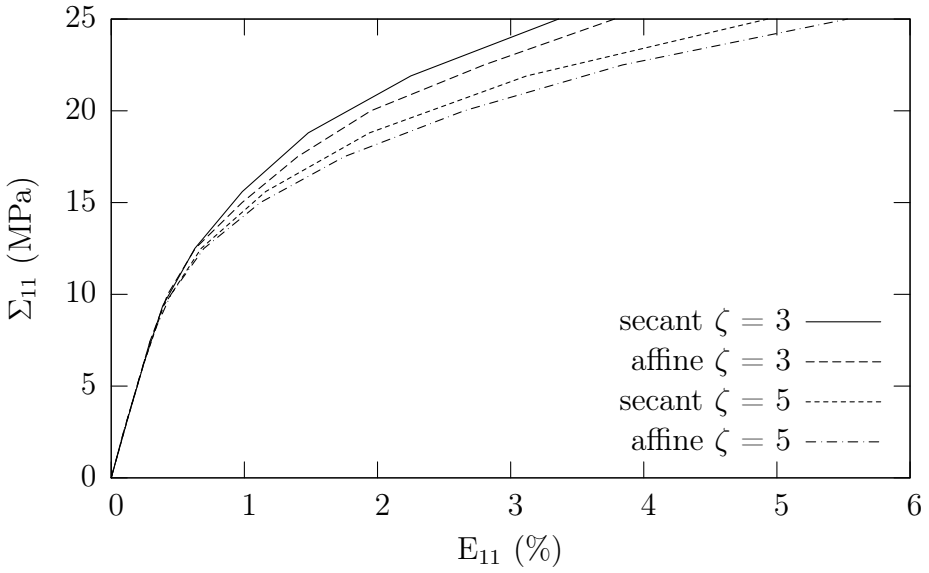


Figure 4.10: Stress-strain curves obtained for the nonlinear viscoelastic composite material for 10% of glass beads for a tensile test at a constant stress rate for various level of nonlinearity and for the secant and affine models.

is a noticeable difference. We have noticed, that as the volume fraction of glass beads increases, this difference becomes less important. This is mainly due to the facts that i) the average stress in the matrix (in the sense of our h) decreases as the volume fraction of glass beads increases and ii) the glass beads are linear elastic. Figure 4.10 shows the comparison between the affine and secant models for $\zeta = 3$ and 5 for a tensile loading at a constant stress rate. The figure first shows that the initial response of the two models are identical. This is due to the fact that, initially, the material is linearly viscoelastic. Then, as the nonlinearity of the matrix becomes apparent, the predictions of the two models begin to diverge. We can see from the figure that the affine model leads to softer estimates than the secant model. In addition, this discrepancy seems to be more important as the degree of nonlinearity increases.

4.5 Conclusion

In conclusion, we have partially reached our objective of implementing and comparing the simulations of our affine and secant models, since it was not possible to obtain a complete simulation for the affine model in all cases.

The solution scheme we have used was adequate for the secant model since it led to a solution for every simulation in a few iterations at each step. On the other hand, more difficulties were encountered with the affine model and it was not possible to solve them.

In this study, we restricted ourselves to isotropic linearised materials as well as a simple microstructure for which a simple analytical solution was known. We expect that using a general anisotropic linear viscoelastic comparison material would lead to better approximations of the exact tangent/secant materials. However, as we have seen when developing algorithms for the inversion of Laplace-Carson transforms, imposing the positive semi-definitiveness of a general anisotropic material is numerically involved. This would require developing an efficient minimisation procedure adapted to this specific problem. Since the linearised material would be anisotropic, this would also require developing a numerical calculation of Eshelby's tensor (for computing the homogenisation tensors) and using a LCT inversion algorithm for general anisotropic materials. Even if we reached this point, there is no guarantee that the procedure would lead to numerically stable models. We have seen, in our simplified case, that our approximate treatment of the tangent material did not allow us to obtain simulations for all the load cases we have simulated.

However, for our constitutive law, it was possible to generate a secant model and a relevant approximation for radial loadings. On the other hand, if we apply a radial macroscopic loading $\mathbf{\Sigma}$ there is no guarantee that the average stress in the matrix is also radial, unless the glass beads are replaced by voids. However, when the reinforcements were made of glass beads, we observed that the average stress in the matrix was almost radial. For these load cases, we believe that our secant models are a relevant approximation to the exact secant models.

It is interesting to note that, for the cases shown here, the affine model seems to lead to softer estimates than the secant model, as is observed for non hereditary materials. This observation should be interpreted with caution since our approximate secant materials matched the exact secant materials more closely than did our approximate tangent materials. It is not possible, *a priori*, to predict the response of our affine model if the tangent condition should be met with the same accuracy as the secant model.

Chapter 5

Comparison of the Secant and Affine Predictions with Finite Element Simulations and Experimental Data

The objective of this final chapter is to compare the predictions of the secant and affine models implemented in the previous chapter with finite element simulations and experimental data. The finite element technique has been chosen to generate estimations of the homogenised properties for our composite material since they rely on the same hypotheses as the homogenisation model regarding the behaviour of the constituent phases. This way, we can assess the relevance of our linearisation/homogenisation schemes. The experimental data has been included in order to validate our hypotheses regarding the behaviour law of the constituents and the microstructure.

The first part of this chapter deals with the Finite Element (FE) simulations. We present the meshes we have used as well as the implementation of our constitutive law in the commercial software ABAQUS. Then, we compare the predictions of the homogenisation models with FE simulations and finally, with experimental data.

The finite elements simulations were carried out on a 2.4 GHz Intel Pentium IV personal computer with 1 GB of RAM.

5.1 Generation of the FE meshes

5.1.1 3D FE meshes of the microstructure

The finite element technique has been used initially to predict the behaviour of periodic microstructures. The advantage of such microstructures is that, due to their periodic nature, meshing is required of only one unit cell to predict the overall mechanical properties of the material, which leads to relatively small meshes. Using periodic microstructures requires imposing periodic boundary conditions on the unit cell. Anthoine [2] and Michel *et al.* [61] first showed how these boundary conditions are applied and implemented. With the improved development of computers, non periodic microstructures could be modelled.

One of the key issues in this approach is to define a proper Representative Volume Element (RVE). Mishnaevsky and Schmauder [63] reviewed of some techniques used so far. As pointed out by Kanit *et al.* [43], the RVE has been given many qualitative definitions. For example, it could be defined as a volume sufficiently large so that it is statistically representative of the heterogeneous material. With this definition, one can imagine choosing two different large volumes of material and comparing their overall properties. Since these two volumes are different, it is very likely that the homogenised response would be different, in absolute terms (i.e., maybe to the tenth digit, but still different). However, if many such volumes are studied, one can measure the mean value and the scatter in the overall properties thus obtained. Following this line of thought, Kanit *et al.* [43] have given a statistical sense to the representativeness of the RVE. They define the RVE as the volume required to identify one average mechanical property, for a given confidence interval and for a given number of realisations (i.e., number of different microstructures representing the material which are tested numerically or experimentally). So, for the same material, for the same accuracy on the mean value of the overall property and for the same number of realisations, it is possible that the size of the RVE would be different for different mechanical properties. They also point out that using RVEs which are too small would introduce a bias in the calculation of the overall properties. They conjecture that there is a minimum size for a RVE for which the mean value of the overall properties, for a very large number of realisations, converges to the "real" overall mechanical property of the material. It should be noted that their developments were made for the case of linear elasticity.

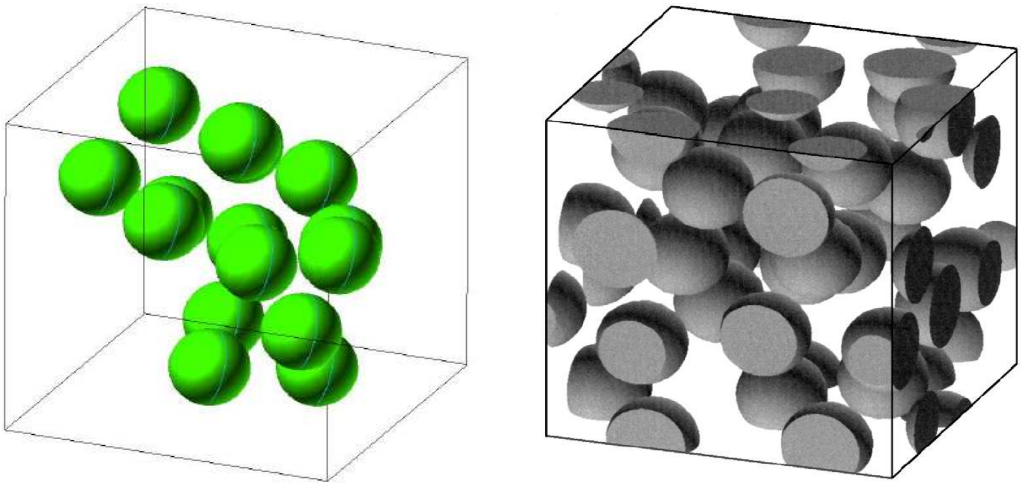
The other issue concerns the generation of the meshes which represent the microstructure. One approach could be to take a physical volume of material and try to mesh the structure exactly. For example, Horgan and

Gilchrist [39] have developed FE meshes of the human skull and brain using information obtained from CT scans. Such an approach requires significant development and is beyond the scope of this work. One other approach would be to generate and subsequently mesh random geometries. This is the approach which was used to generate our 3D meshes. We recall that our microstructure consists of glass beads randomly distributed in a homogeneous matrix. This configuration has been studied in detail by many investigators (see Gusev [32], Segurado and LLorca [94] and Mishnaevsky [62], for example) due to its relative geometric simplicity. With spherical particles, the only random variable is their centre position. A different reinforcement geometry would require considering the orientation and ensuring that two different reinforcements would not penetrate each other can become quite involved. The 3D meshes used in this study were supplied by Mishnaevsky [62].

In this study, we have used particles of the same size and the radius of which was calculated as a function of the volume fraction sought and the number of particles inside the FE mesh. The particles were located in a cubic volume of dimensions $10 \times 10 \times 10\,\text{mm}$. We used microstructures with 10 and 15 particles for a volume fraction of 10%. Due to memory limitations, it was not possible to mesh more than 15 particles, since a greater number of particles required more elements. Each particle was meshed with approximately the same number of elements. The coordinates of the first particle were generated by a uniform random number generator with the condition that the minimum distance between the particle and the sides of the cube was no less than $0.05R_p$, where R_p is the particle radius. Then, the positions of the subsequent particles were generated randomly and independently. If the distance between this particle and any other particle was not greater than $0.1R_p$, then a new coordinate was generated randomly until this and the previous conditions were met. These two conditions were imposed to ensure that there was enough space to generate elements with good aspect ratios. Once the centre position of the particles were calculated, the meshes were generated by the free mesh algorithm implemented in MSC/PATRAN. The microstructures were meshed with ten-noded tetrahedral[1] elements. Figure 5.1(a) shows a typical 15 particles mesh.

It can be argued that such a mesh generation approach is biased in the sense that it is not a fully random "window" in the material. For example, it is possible that two particles would touch each other or that some particles would be cut by the sides of the box. The case of two touching particles is a problem since it is very difficult to obtain elements with good aspect ratios near the contact points of the spheres. However, authors such as Segurado

[1]The interpolation functions are quadratic.



(a) FE mesh where the particles do not intersect with the cube sides

(b) FE mesh where the particles intersect with the cube sides with a periodic continuity [94]

Figure 5.1: Comparison of two different mesh types for a spherical particles in a homogeneous matrix configuration

and LLorca [94] have developed algorithms where particles can intersect with the sides. Such a mesh is illustrated in figure 5.1(b). In order to keep the volume fraction constant, a periodic representation was used for the particles intersecting the sides. For example, if $\frac{1}{3}$ of a particle intersects with the side having its normal in the positive x axis, then $\frac{2}{3}$ of the particle will be placed on the side having its normal along the negative x axis. This restriction also leads to a bias in the microstructure generation. One other alternative would be to generate particles randomly and not complete those intersecting with the sides. Continue in this manner until the volume fraction is reached. However, such a technique has the disadvantage that there is no guarantee that the resulting volume fraction is exactly that being sought. Of course, using more particles leads to more accuracy regarding the resulting volume fraction, but at the expense of computational time.

It should be noted that generating the particle centres independently might not be the most efficient way of generating microstructures. As the number of beads and the volume fraction increases, it is difficult to meet all the conditions regarding the distance between the particles within a reasonable number of iterations. To avoid such difficulty, Segurado and LLorca [94] designed an algorithm which allowed moving the other particles so as to insert the next particles.

It should further be noted that Moulinec and Suquet [67] have developed a

computationally efficient algorithm based on Fourier Transforms which allows the overall mechanical response of a complex microstructure to be predicted. The method uses photographs of the microstructure and does not require any meshing. This is a significant advantage and it facilitates simulating larger RVEs for a smaller computational cost, when compared with FE.

5.1.2 Boundary conditions

The other issue to address is the type of boundary conditions applied on our RVE. For example, we could apply a uniform displacement on the boundaries of the cube and calculate the spatial average of the stress field, or conversely, apply a uniform pressure on the sides and calculate the average of the strain field. It is well known that applying either $\mathbf{\Sigma}$ or $\mathbf{E}$ leads to different results, depending on the size of the RVE[2] (see for example chapter 2 in Bornert *et al.* [8]) although these converge to the same result as the RVE tends towards infinity. In addition, for a finite size of RVE, Huet [42] has shown that the exact effective properties of heterogeneous linear elastic materials are bounded by those obtained with uniform displacement or pressure conditions. For random microstructures, Kanit *et al.* [43] have observed that applying periodic boundary conditions converges faster, in terms of RVE size, to the mean overall mechanical property than by applying uniform $\mathbf{\Sigma}$ or $\mathbf{E}$. Figure 5.2 shows an example obtained for the overall shear modulus of a polycrystal. This figure has been obtained by first generating RVE meshes of different sizes (i.e., the number of grains). Then, for each RVE size, 433 different meshes were created and the three different boundary conditions were applied to evaluate the overall shear modulus. Then, for each RVE size, the mean value and a "confidence interval" computed with two standard deviations of the overall shear modulus are plotted[3]. It can be observed that for approximately 15 grains the periodic boundary condition leads to a constant mean value of the overall shear modulus while no such value has been obtained for the other boundary conditions, even for more than 1000 grains. However, the scatter in the data is more important with the periodic boundary condition, which

[2]The size of a RVE for a periodic microstructure should be interpreted here as the number of repetitions of the unit cell.

[3]If we assume that the shear modulus measured by such process is normally distributed, a confidence interval on the mean value of this shear modulus is given by: $\bar{\mu} \pm t_\alpha \frac{s}{\sqrt{N}}$, where t is the Student distribution of $N-1$ degrees of freedom for a confidence level of α, s is the experimental standard deviation and N is the number of observations (see for example Mendenhall and Sincich [60]). For a two tailed 95% confidence interval for 422 degrees of freedom, $t_\alpha \approx 2$. Since two standard deviations are plotted on figure 5.2 the confidence interval for the mean value of μ would be $\frac{1}{\sqrt{433}} \approx \frac{1}{20}$ times smaller than the interval plotted.

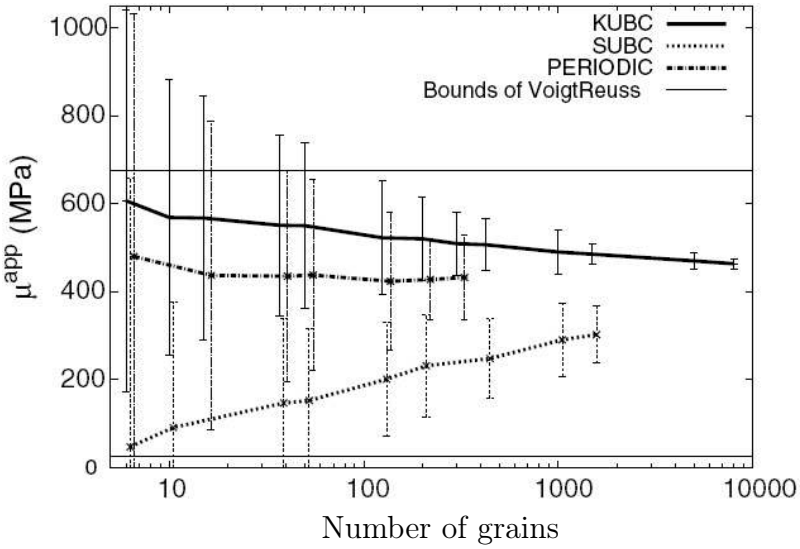


Figure 5.2: Evolution of averaged shear modulus of a linear elastic polycrystal as a function of the number of grains simulated in the RVE, for various boundary conditions [43]. KUBC refers to a homogeneous displacement boundary condition, SUBC refers to homogeneous stress boundary conditions and PERIODIC refers to periodic boundary conditions. The error bars represent the confidence interval on the average value of the overall shear modulus within two standard deviations. 433 realisations were carried out per RVE size.

means that more realisations are required than with the other boundary conditions in order to estimate the overall properties of the heterogeneous material. In our case, it was not possible to produce large FE meshes due to software/hardware limitations. We assumed that the same result applied to our material and applied periodic boundary conditions on our meshes. Such an approach has been also used by González *et al.* [28] for a similar composite material where the matrix was elasto-plastic.

A periodic displacement field can be decomposed as [61]:

$$\boldsymbol{u}(\boldsymbol{x}) = \mathbf{E} \cdot \boldsymbol{x} + \boldsymbol{u}^*(\boldsymbol{x}) \tag{5.1}$$

where $\mathbf{E}$ is again the uniform overall strain and where $\boldsymbol{u}^*(\boldsymbol{x})$ takes identical values on the opposite faces of our cube. If we develop this equation, we obtain:

$$\begin{aligned} \boldsymbol{u}(0, x_2, x_3) + \mathbf{E} \cdot (L, x_2, x_3) &= \boldsymbol{u}(L, x_2, x_3) \\ \boldsymbol{u}(x_1, 0, x_3) + \mathbf{E} \cdot (x_1, L, x_3) &= \boldsymbol{u}(x_1, L, x_3) \\ \boldsymbol{u}(x_1, x_2, 0) + \mathbf{E} \cdot (x_1, x_2, L) &= \boldsymbol{u}(x_1, x_2, L) \end{aligned} \tag{5.2}$$

where L is the length of a cube side. If we develop equations (5.2), we can express the components of $\mathbf{E}$ as a function of the displacements. For example, if we set $\boldsymbol{u}(\mathbf{0}) = \mathbf{0}$ to prevent rigid body motions, we have (for example):

$$\begin{aligned} \frac{u_1(L,0,0)}{L} &= \mathrm{E}_{11}, \quad \frac{u_2(L,0,0)}{L} = \mathrm{E}_{12}, \quad \frac{u_3(L,0,0)}{L} = \mathrm{E}_{13}, \\ \frac{u_2(0,L,0)}{L} &= \mathrm{E}_{22}, \quad \frac{u_3(0,L,0)}{L} = \mathrm{E}_{23}, \quad \frac{u_3(0,0,L)}{L} = \mathrm{E}_{33} \end{aligned} \tag{5.3}$$

So, when equations (5.3) are inserted into equations (5.2) a relationship can be established between points on opposing faces. Practically, in a commercial FE code like ABAQUS, such constraints are applied with Multiple Point Constraints (MPC). This requires, however, that the nodes forming two opposite surfaces are the mirror image of each other. Then, the MPC are applied according to relations (5.2) to the degrees of freedom on the right hand side of the equation which are not involved in equations (5.3). A periodic stress field is defined as (for our cube):

$$\begin{aligned} \boldsymbol{\sigma}(0,x_2,x_3)\cdot\boldsymbol{n}(0,x_2,x_3) &= -\boldsymbol{\sigma}(L,x_2,x_3)\cdot\boldsymbol{n}(L,x_2,x_3) \\ \boldsymbol{\sigma}(x_1,0,x_3)\cdot\boldsymbol{n}(x_1,0,x_3) &= -\boldsymbol{\sigma}(x_1,L,x_3)\cdot\boldsymbol{n}(x_1,L,x_3) \\ \boldsymbol{\sigma}(x_1,x_2,0)\cdot\boldsymbol{n}(x_1,x_2,0) &= -\boldsymbol{\sigma}(x_1,x_2,L)\cdot\boldsymbol{n}(x_1,x_2,L) \end{aligned} \tag{5.4}$$

where $\boldsymbol{n}$ is the vector normal to a cube side. In addition, the stress field must be in equilibrium (i.e., $\operatorname{div}\boldsymbol{\sigma} = 0$).

The meshes that were supplied to us did not meet the requirements to apply periodic boundary conditions since the nodes forming two opposite faces were not exact mirror images of each other. To avoid this such difficulty but still impose periodic boundary conditions, we introduce a simplifying hypothesis. We assume that the real material exhibits periodicity with unit cells having three planes of symmetry. It that case, our unit cell (i.e., our cube with the randomly distributed particles) represents $\frac{1}{8}$ of the unit cell. The load case we have simulated (pure tension) is a symmetric load case. We applied a uniformly distributed pressure on one cube side and the symmetry boundary conditions ensured that the stress field is periodic. For this load case, the displacement periodic boundary as well as the symmetry boundary conditions are [7, 61]:

$$\begin{gathered} u_1(0,x_2,x_3) = 0, \quad u_2(x_1,0,x_3) = 0, \quad u_3(x_1,x_2,0) = 0, \\ u_1(L,x_2,x_3) = u_1(L,0,0), \quad u_2(x_1,L,x_3) = u_2(0,L,0), \\ u_3(x_1,x_2,L) = u_3(0,0,L) \end{gathered} \tag{5.5}$$

This implies that the sides of the cube remain planar. These constraints are

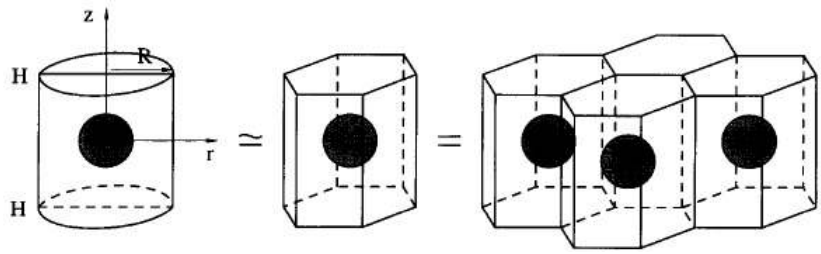


Figure 5.3: Circular base cylinder approximation of a hexagonal base cylinder periodic unit cell [61]

easily applied with MPCs. In that case, the macroscopic strain is given by:

$$\mathrm{E}_{11} = \frac{u_1(L,0,0)}{L}, \quad \mathrm{E}_{22} = \frac{u_2(0,L,0)}{L}, \quad \mathrm{E}_{33} = \frac{u_3(0,0,L)}{L}, \qquad (5.6)$$
$$\mathrm{E}_{12} = \mathrm{E}_{13} = \mathrm{E}_{23} = 0$$

5.1.3 Axisymmetric meshes

We recall that we had 3D meshes for a glass beads volume fraction of 10%. In order to estimate the responses of the other volume fractions, we have assumed that our beads are periodically distributed in a hexagonal array, so that the unit cell is a cylinder with a hexagonal base. We have approximated this unit cell with a circular base cylinder of the same volume, as is classically done. Figure 5.3 illustrates this approximation. The dimensions of the cylinder are chosen so that they lead to the same volume as the exact hexagonal unit cell. We have used $H = R$ (see figure 5.3). We have used an axisymmetric mesh of this unit cell where the elements were eight noded shell elements. The unit cell on figure 5.3, in addition to being axisymmetric, has a plane of symmetry. Therefore, we meshed only one half of the unit cell and imposed symmetry boundary conditions on the plane of symmetry. The other boundary conditions applied were periodic boundary conditions. Figure 5.4 illustrates these boundary conditions. It should be noted that a hexagonal array of particles does not lead to an isotropic material.

5.2 Implementation of the nonlinear viscoelastic constitutive law

Schapery's constitutive law has been implemented in FE packages by many investigators. See for example Henriksen [36], Lai and Bakker [49], Zhang

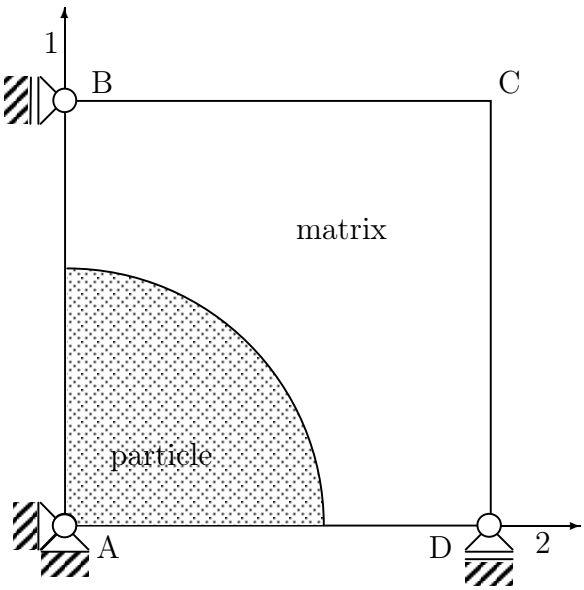


Figure 5.4: Illustration of the symmetry and periodic boundary conditions on the axisymmetric approximation of an hexagonal periodic unit cell. Symmetry conditions are applied on the sides AB and AD while periodic boundary conditions are applied on the sides BC and CD. The periodic boundary conditions impose that u_1 is equal for all points on the line BC and that u_2 is equal for all points on the CD line.

et al. [104] and Haj-Ali and Muliana [33]. We recall that the authors implemented constitutive theories that are generalisations of the one-dimensional Schapery's constitutive law and it was not checked whether such theories met thermodynamic requirements. These works suggest using the recurrence relation for the integral of the behaviour law we have developed in the previous chapter. We use this relation in our specific implementation, which we detail below.

The constitutive theory was implemented in ABAQUS by using the UMAT subroutine. Since the material is nonlinear, the solution is reached by a series of time increments and the code computes, in our situation, the stress and strain increments during a time increment. The UMAT subroutine requires the user to calculate two quantities [37]:

1. The stress increment at the end of the time increment,
2. The Jacobian matrix $\frac{\partial \boldsymbol{\Delta\sigma}}{\partial \boldsymbol{\Delta\varepsilon}}$.

Computation of these two quantities requires to computing $\boldsymbol{\Delta\sigma}$ when $\boldsymbol{\Delta\varepsilon}$ is applied. However, our constitutive theory can be arranged so that it expresses $\boldsymbol{\Delta\varepsilon} = \boldsymbol{\Upsilon}(\boldsymbol{\Delta\sigma})$. Therefore, we need to develop a procedure to calculate $\boldsymbol{\Delta\sigma}$ when a given $\boldsymbol{\Delta\varepsilon}^{\mathbf{app}}$ is applied. The nonlinear system of equations to be solved can then be expressed as:

$$\boldsymbol{\Upsilon}(\boldsymbol{\Delta\sigma}) - \boldsymbol{\Delta\varepsilon}^{\mathbf{app}} = \boldsymbol{\Theta}(\boldsymbol{\Delta\sigma}) = \mathbf{0} \tag{5.7}$$

where the unknown is $\boldsymbol{\Delta\sigma}$. We have solved this system of equations with the Newton method which requires calculating the Jacobian:

$$\mathbf{N} = \frac{\partial \boldsymbol{\Upsilon}(\boldsymbol{\Delta\sigma})}{\partial \boldsymbol{\Delta\sigma}} \tag{5.8}$$

We present first the computation of the quantities described at equations (5.7,5.8). Then, we show how we have calculated the stress at the end of the increment as well as $\frac{\partial \boldsymbol{\Delta\sigma}}{\partial \boldsymbol{\Delta\varepsilon}}$. Finally, we show how we have implemented the whole process in ABAQUS.

5.2.1 Definition and computation of $\boldsymbol{\Delta\varepsilon}$

If we define t_i and t_{i+1} respectively as the times at the beginning and end of a given increment, then the strain increment $\boldsymbol{\Delta\varepsilon}$ becomes:

$$\boldsymbol{\Delta\varepsilon} = \boldsymbol{\varepsilon}(t_{i+1}) - \boldsymbol{\varepsilon}(t_i) \tag{5.9}$$

which is explicitly (with our constitutive law):

$$\begin{aligned}
\boldsymbol{\Delta\varepsilon} &= \mathbf{Q} : \boldsymbol{\Delta\sigma} \\
&\quad + \mathbf{Q} : \sum_{m=1}^{3} \left[\int_0^{t_{i+1}} \alpha_m \lambda_m \exp[-\lambda_m (t_{i+1} - \tau)] g_2(\tau) \boldsymbol{\sigma}(\tau) \mathrm{d}\tau \right] \\
&\quad - \mathbf{Q} : \sum_{m=1}^{3} \left[\int_0^{t_i} \alpha_m \lambda_m \exp[-\lambda_m (t_i - \tau)] g_2(\tau) \boldsymbol{\sigma}(\tau) \mathrm{d}\tau \right] \\
&= \mathbf{Q} : \boldsymbol{\Delta\sigma} + \mathbf{Q} : \sum_{m=1}^{3} \left[\left(\exp[-\lambda_m \Delta t] - 1 \right) \boldsymbol{\rho}_m(t_i) \right] \\
&\quad + \mathbf{Q} : \sum_{m=1}^{3} \left[\int_{t_i}^{t_{i+1}} \alpha_m \lambda_m \exp[-\lambda_m (t_{i+1} - \tau)] g_2(\tau) \boldsymbol{\sigma}(\tau) \mathrm{d}\tau \right]
\end{aligned} \tag{5.10}$$

where again:

$$\boldsymbol{\rho}_m(t_i) = \int_0^{t_i} \alpha_m \lambda_m \exp[-\lambda_m (t_i - \tau)] g_2 \boldsymbol{\sigma}(\tau) \mathrm{d}\tau \tag{5.11}$$

can be seen as a constant during the time increment. In addition, $g_2(\tau)$ is to be interpreted as $g_2(h(\boldsymbol{\sigma}(\tau)))$. We now need to introduce $\boldsymbol{\Delta\sigma}$ in the last integral of equation (5.10). From t_i to t_{i+1}, we assume that $\boldsymbol{\sigma}$ varies linearly. Therefore, we can write that:

$$\boldsymbol{\sigma}(t) = \boldsymbol{\sigma}(t_i) + \frac{t - t_i}{\Delta t} \boldsymbol{\Delta\sigma} = \boldsymbol{\sigma}(t_i) + \beta(t) \boldsymbol{\Delta\sigma} \quad \text{for} \quad t \in [t_i, t_{i+1}] \tag{5.12}$$

where $\Delta t = t_{i+1} - t_i$. We also recall that g_2 varies linearly as a function of:

$$h(t) = \frac{1}{2} \boldsymbol{\sigma}(t) : \mathbf{Q} : \boldsymbol{\sigma}(t) \tag{5.13}$$

so that:

$$g_2(h(t)) = g_2(h(t_i)) + \gamma[h(t) - h(t_i)] = g_{2_i} + \gamma[h - h_i] \tag{5.14}$$

where we have made the assumption that γ is constant within a time increment. When definition (5.12) is used in (5.13) and equation (5.14) is used, we obtain:

$$\begin{aligned}
g_2(t)\boldsymbol{\sigma}(t) &= g_{2_i} \boldsymbol{\sigma}(t_i) + g_{2_i} \beta(t) \boldsymbol{\Delta\sigma} + \gamma\beta(t) \left(\boldsymbol{\sigma}(t_i) : \mathbf{Q} : \boldsymbol{\Delta\sigma} \right) \boldsymbol{\sigma}(t_i) \\
&\quad + \frac{\gamma\beta(t)^2}{2} \left(\boldsymbol{\Delta\sigma} : \mathbf{Q} : \boldsymbol{\Delta\sigma} \right) \boldsymbol{\sigma}(t_i) \\
&\quad + \gamma\beta(t)^2 \left(\boldsymbol{\sigma}(t_i) : \mathbf{Q} : \boldsymbol{\Delta\sigma} \right) \boldsymbol{\Delta\sigma} \\
&\quad + \frac{\gamma\beta(t)^3}{2} \left(\boldsymbol{\Delta\sigma} : \mathbf{Q} : \boldsymbol{\Delta\sigma} \right) \boldsymbol{\Delta\sigma} \\
&= \boldsymbol{\kappa}_1 + \boldsymbol{\kappa}_2 \beta(t) + \boldsymbol{\kappa}_3 \beta(t)^2 + \boldsymbol{\kappa}_4 \beta(t)^3
\end{aligned} \tag{5.15}$$

where the $\boldsymbol{\kappa}_i$ are constant with respect to time and explicit functions of the $\boldsymbol{\Delta\sigma}$. Then, one m integral of the last term of equation (5.10), denoted by $\boldsymbol{\omega}_m$, becomes:

$$\boldsymbol{\omega}_m = \int_{t_i}^{t_{i+1}} \alpha_m \lambda_m \exp[-\lambda_m(t_{i+1}-\tau)] \\ \left(\boldsymbol{\kappa}_1 + \boldsymbol{\kappa}_2\beta(\tau) + \boldsymbol{\kappa}_3\beta(\tau)^2 + \boldsymbol{\kappa}_4\beta(\tau)^3\right)\mathrm{d}\tau \quad (5.16)$$

When integration is carried out, it simply becomes:

$$\boldsymbol{\omega}_m = \sum_{s=1}^{4} \boldsymbol{\kappa}_s \zeta_{sm} \quad (5.17)$$

where:

$$\begin{aligned} \zeta_{1m} &= (1-\exp[-\lambda_m\Delta t])\alpha_m \\ \zeta_{2m} &= \frac{(\exp[-\lambda\Delta t]-1+\lambda_m\Delta t)\alpha_m}{\lambda_m\Delta t} \\ \zeta_{3m} &= \frac{\left[2-2\exp[-\lambda_m\Delta t]-\lambda_m\Delta t(2-\lambda_m\Delta t)\right]\alpha_m}{(\lambda_m\Delta t)^2} \\ \zeta_{4m} &= -\frac{\left[6-6\exp[-\lambda_m\Delta t]-\lambda_m\Delta t[6-\lambda_m\Delta t(3-\lambda_m\Delta t)]\right]\alpha_m}{(\lambda_m\Delta t)^3} \end{aligned} \quad (5.18)$$

Then we have that $\boldsymbol{\Delta\varepsilon}$ is simply:

$$\boldsymbol{\Delta\varepsilon} = \mathbf{Q} : \left(\boldsymbol{\Delta\sigma} + \sum_{m=1}^{3}\left[(\exp[-\lambda_m\Delta t - 1)\,\boldsymbol{\rho}_m(t_i) + \sum_{s=1}^{4}\boldsymbol{\kappa}_s\zeta_{sm}\right]\right) \quad (5.19)$$

So when $\boldsymbol{\Delta\sigma}$ is supplied, we can compute $\boldsymbol{\Delta\varepsilon} = \boldsymbol{\Upsilon}(\boldsymbol{\Delta\sigma})$ and therefore $\boldsymbol{\Theta}(\boldsymbol{\Delta\sigma})$ (see equation (5.7)).

5.2.2 Computation of the Jacobian N

Equation (5.19) allows a straightforward computation of the Jacobian:

$$\frac{\partial\boldsymbol{\Delta\varepsilon}}{\partial\boldsymbol{\Delta\sigma}} = \mathbf{Q} : \left(\mathbf{I} + \sum_{m=1}^{3}\sum_{s=1}^{4}\frac{\partial\boldsymbol{\kappa}_s}{\partial\boldsymbol{\Delta\sigma}}\zeta_{sm}\right) \quad (5.20)$$

where:

$$\begin{aligned}
\frac{\partial \boldsymbol{\kappa}_1}{\partial \boldsymbol{\Delta\sigma}} &= \mathbf{0} \\
\frac{\partial \boldsymbol{\kappa}_2}{\partial \boldsymbol{\Delta\sigma}} &= \gamma \mathbf{Q} : \boldsymbol{\sigma}(t_i) \otimes \boldsymbol{\sigma}(t_i) + g_{2_i} \mathbf{I} \\
\frac{\partial \boldsymbol{\kappa}_3}{\partial \boldsymbol{\Delta\sigma}} &= \gamma \left(\mathbf{Q} : \boldsymbol{\Delta\sigma} \otimes \boldsymbol{\sigma}(t_n) + \mathbf{Q} : \boldsymbol{\sigma}(t_i) \otimes \boldsymbol{\Delta\sigma} + (\boldsymbol{\sigma}(t_i) : \mathbf{Q} : \boldsymbol{\Delta\sigma}) \mathbf{I} \right) \\
\frac{\partial \boldsymbol{\kappa}_4}{\partial \boldsymbol{\Delta\sigma}} &= \gamma \mathbf{Q} : \boldsymbol{\Delta\sigma} \otimes \boldsymbol{\Delta\sigma} + \frac{\gamma}{2} (\boldsymbol{\Delta\sigma} : \mathbf{Q} : \boldsymbol{\Delta\sigma}) \mathbf{I}
\end{aligned} \tag{5.21}$$

and $\mathbf{I}$ is the fourth order identity tensor. During an increment, the ζ_{sm} are calculated only once since the unknown is the stress increment. Therefore, computation of the exact gradient required very few operations and can be computed quite rapidly.

5.2.3 Computation of the quantities required by the UMAT subroutine

Computation of the stress at the end of the increment

The stress at the end of the increment is computed by: $\boldsymbol{\sigma}(t_{i+1}) = \boldsymbol{\sigma}(t_i) + \boldsymbol{\Delta\sigma}$, where $\boldsymbol{\sigma}(t_i)$ is supplied by the UMAT subroutine. The subroutine also supplies $\boldsymbol{\Delta\varepsilon}^{\mathbf{app}}$. Then, the nonlinear system of equations described in (5.7) is solved with the Newton technique and $\boldsymbol{\sigma}(t_{i+1})$ is calculated with the $\boldsymbol{\Delta\sigma}$ thus obtained.

In order to accept or reject a solution, we defined the following norm:

$$\vartheta = \sqrt{\boldsymbol{\Theta}(\boldsymbol{\Delta\sigma}) : \boldsymbol{\Theta}(\boldsymbol{\Delta\sigma})} \tag{5.22}$$

The solution was accepted when $\vartheta \leq 1 \times 10^{-10}$.

Computation of the Jacobian $\frac{\partial \boldsymbol{\Delta\sigma}}{\partial \boldsymbol{\Delta\varepsilon}}$

This Jacobian has been calculated numerically with a centered difference by:

$$\frac{\partial \Delta\sigma_I}{\partial \Delta\varepsilon_J} \approx \frac{\Delta\sigma(\boldsymbol{\Delta\varepsilon}^{\mathbf{app}} + \boldsymbol{\delta\varepsilon})_I - \Delta\sigma(\boldsymbol{\Delta\varepsilon}^{\mathbf{app}} - \boldsymbol{\delta\varepsilon})_I}{2\delta\varepsilon_J} \tag{5.23}$$

where the non zero component of $\boldsymbol{\delta\varepsilon}$ is $\delta\varepsilon_P = \epsilon$ for $P = J$. We have used $\epsilon = 1 \times 10^{-4}$. This required solving the nonlinear system of equations $\boldsymbol{\Upsilon}(\boldsymbol{\Delta\sigma}) - \boldsymbol{\Delta\varepsilon}^{\mathbf{app}} \pm \boldsymbol{\delta\varepsilon} = \mathbf{0}$ 12 times by the Newton method.

Note on the conventions used by ABAQUS

It should be noted that ABAQUS uses the classical Voigt notation. We had to transform $\boldsymbol{\sigma}(t_i)$ and $\boldsymbol{\Delta\varepsilon}^{\mathbf{app}}$ supplied by the UMAT subroutine to the modified Voigt notation, next perform our calculations, and then express the result using the classical Voigt notation.

5.2.4 Execution procedure

As mentioned earlier, the load history is applied incrementally. For each integration point of each element, the UMAT subroutine is calculated a number of times, depending on the number of iterations required to achieve the solution within a given time increment. We have seen that $\boldsymbol{\rho}_m(t_i)$ (see equation (5.11)) is required to compute the stress increment $\boldsymbol{\Delta\sigma}$. Since the subroutine is called at all the integration points in the model, $\boldsymbol{\rho}_m(t_i)$ must be known for all these points at the beginning of the increment. Therefore, we need a global variable which is accessible by the UMAT subroutine where this information is stored. Since the subroutines of ABAQUS are coded in FORTRAN, this is accomplished with the COMMON statement.

By definition, $\boldsymbol{\rho}_m(t_i)$ must be updated at the beginning of each increment. As was done previously, it can be updated by the following recurrence relation:

$$\boldsymbol{\rho}_m(t_{i+1}) = \exp[-\lambda_m \Delta t]\boldsymbol{\rho}_m(t_i) + \boldsymbol{\omega}_m \tag{5.24}$$

where $\boldsymbol{\omega}_m$ is defined at equation (5.17). $\boldsymbol{\rho}_m(t_{i+1})$ was obtained by using the UEXTERNALDB subroutine of ABAQUS that can be called at the end of an increment. For all the integration points, the $\boldsymbol{\Delta\sigma}$ computed by the UMAT was stored in a global variable. Then, with the COMMON statement, this variable is available in the UEXTERNALDB subroutine and $\boldsymbol{\omega}_m$ can be evaluated. Finally, $\boldsymbol{\rho}_m(t_{i+1})$ is computed as described in the last equation. Then, $\boldsymbol{\rho}_m(t_{i+1})$ is saved in a COMMON block and is available for the UMAT subroutine at the beginning of the next increment.

For almost all the cases we have simulated, this procedure led to convergence within 1-4 iterations per increment. For all simulations, we have checked that the number of increments was sufficient so that the solution did not change significantly as the number of increments was increased. The implementation was tested on a small cube consisting of 4 brick elements under various simple load histories. The FE simulations and the theoretical predictions were very close and the implementation was judged satisfactory.

5.3 Comparison of the predictions of the homogenisation model against finite element simulations

To illustrate the performances of our homogenisation model, we present here the comparisons we have obtained for tensile loadings at a constant stress rate. We have studied the case of spherical glass reinforcements, spherical voids and spherical glass reinforcements for a more important nonlinearity. We have studied these topics for 10%, 20% and 30% volume fractions of glass beads/voids. We recall that under radial loading, our approximate secant linear viscoelastic comparison material is a relevant approximation of the exact secant material. We present first the results obtained for a volume fraction of 10% of glass beads/voids since we had 3D meshes of such microstructures and it was possible to run many simulations in order to verify that the RVEs we have used were sufficiently large. Then, we present the results obtained with the axisymmetric meshes for volume fractions of 20% and 30% of reinforcements/voids.

In all the cases, the tensile load was applied by a uniform pressure on one side of the cube/axisymmetric cell. The tensile loading was applied at a constant stress rate of $\frac{25\,\mathrm{MPa}}{7000\,\mathrm{sec}} \approx 3.57 \times 10^{-3} \frac{\mathrm{MPa}}{\mathrm{sec}}$.

5.3.1 Comparisons for 10% of glass beads/voids

Study of the RVE size

We have performed 9 simulations for 10 and 15 beads/voids for the three configurations: i)glass beads; ii)voids and iii)glass beads for a nonlinearity factor $\zeta = 3$ (see section 4.4.5). For illustration purposes, figure 5.5 shows typical curves obtained for a mesh containing 10 glass beads for the nonlinearity factor of $\zeta = 1$. We recall that we have performed the simulation of the same loading for 9 different meshes containing 10 glass beads. The "softest" curve corresponds to the softest response observed amongst these 9 simulations while the curve "stiffest" represents the stiffest response. This gives a graphical idea of the scatter in the simulations. The curve "average" represents the average curve of the 9 simulations and the "axisymmetric" curve represents the predictions of the periodic hexagonal cell approximation.

In order to assess the representativeness of our RVE, we prefer to present the data using a different form. Since we deal with a nonlinear heterogeneous material, we have to define a "mechanical property", as was done in Kanit *et al.* [43]. In our case, we are interested in knowing the axial strain at 25 MPa

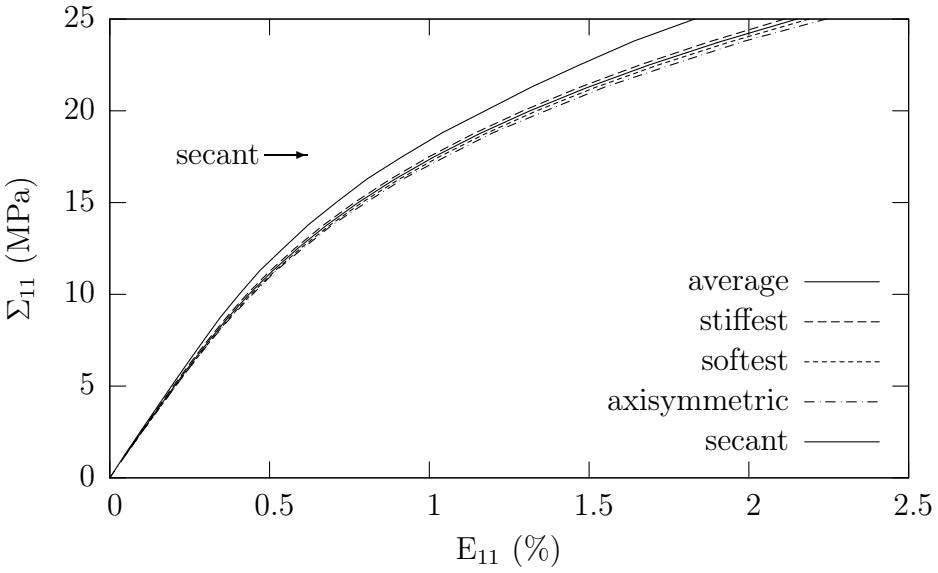


Figure 5.5: Comparison of the simulations of the secant model with the finite element simulations for a glass beads reinforced composite (10% volume fraction) under macroscopic tensile loading. The curve "softest" refers to the most compliant curve obtained with the 10 particles models and "stiffest" refers to the stiffest curve for the same type of meshes. "Average" refers to the average stress/strain curve obtained for the 10 particles models and "axisymmetric" refers to the simulation of axisymmetric mesh.

which we denote by E_{11}^{25}. So, we assume that E_{11}^{25} is distributed normally and we calculate a confidence interval for $\bar{E}_{11}^{25}$, which is the average of E_{11}^{25}. The confidence intervals are calculated for a confidence level of 95%. In addition, we also plot E_{11}^{25} calculated with the approximate hexagonal cell in order to assess the quality of this approximation of the real microstructure. Figures 5.6, 5.7 and 5.8 present these plots.

We can observe from these figures that the confidence intervals for $\bar{E}_{11}^{25}$ for each number of particles overlap each other. Therefore, we cannot infer that, with a confidence level of 95%, any $\bar{E}_{11}^{25}$ (for the same composite material) is different from the other. If we assume that the standard deviation remains approximately constant, performing more simulations might show that there is a difference, since the confidence interval decreases approximately with $\frac{1}{\sqrt{N}}$, where N is the number of observations [60]. In that respect we cannot determine if we have reached the critical RVE size since we cannot see the evolution of $\bar{E}_{11}^{25}$ as a function of the number of particles.

On the other hand, it can be observed from figures 5.6, 5.7 and 5.8 that the bounds of the confidence intervals are relatively small with respect to the

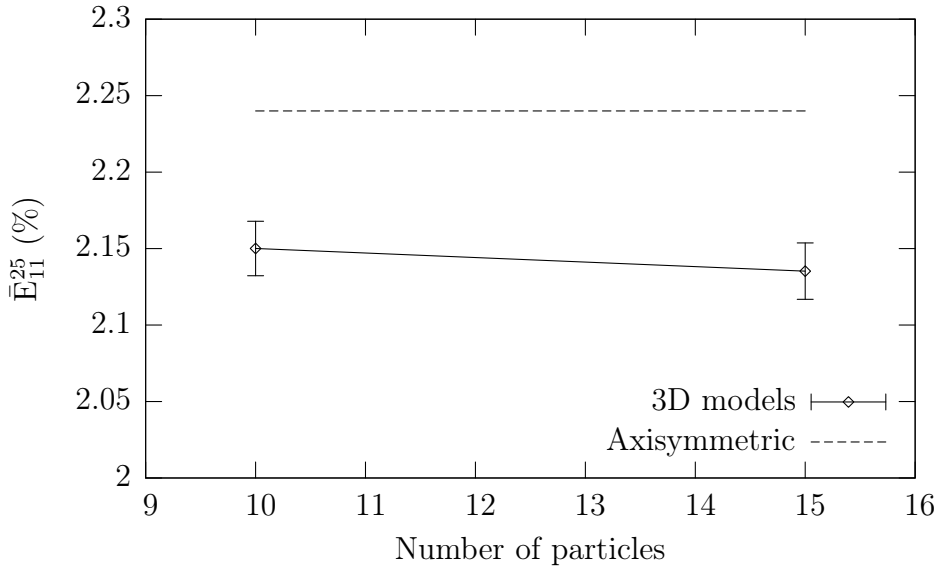


Figure 5.6: Mean value and 95% confidence interval for the macroscopic strain at 25 MPa $\bar{E}_{11}^{25}$ as a function of the number of glass beads (10%) in the 3D meshes for a constant stress rate tensile loading.

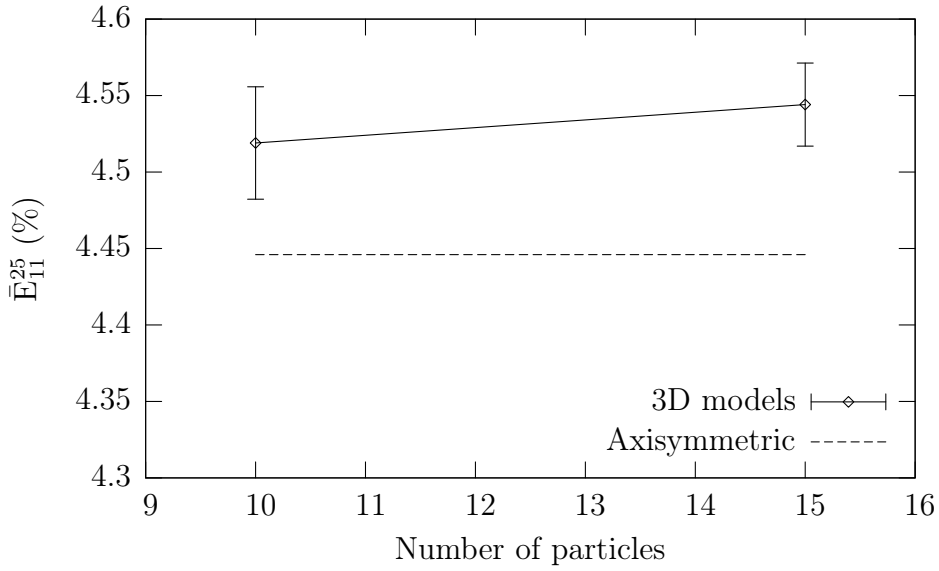


Figure 5.7: Mean value and 95% confidence interval for the macroscopic strain at 25 MPa $\bar{E}_{11}^{25}$ as a function of the number of spherical voids (10%) in the 3D meshes for a constant stress rate tensile loading.

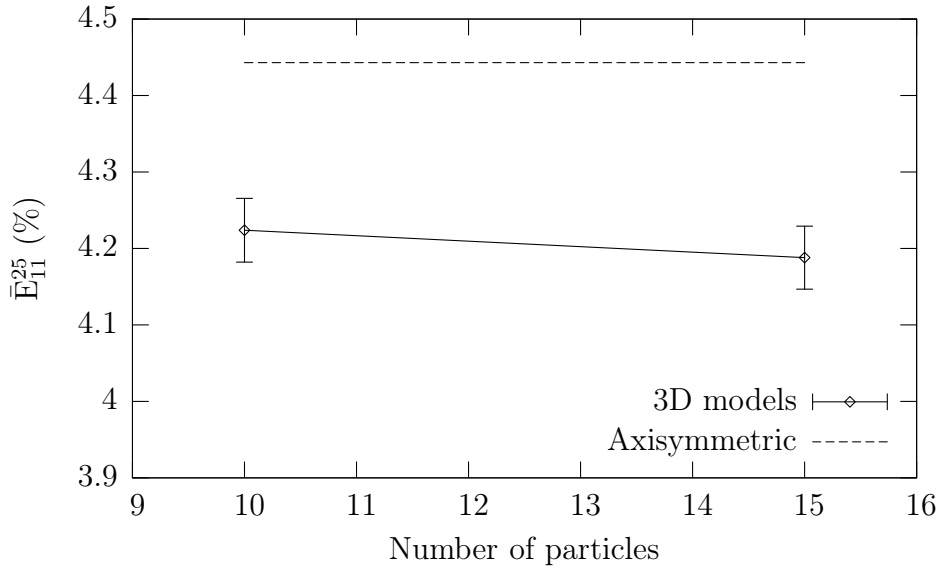


Figure 5.8: Mean value and 95% confidence interval for the macroscopic strain at 25 MPa $\bar{E}_{11}^{25}$ as a function of the number of glass beads (10%) in the 3D meshes for a constant stress rate tensile loading and a nonlinearity factor $\zeta = 3$.

value of $\bar{E}_{11}^{25}$. In both cases, the upper or lower bound lies within 1% of $\bar{E}_{11}^{25}$. In addition, the $\bar{E}_{11}^{25}$ has relatively small variations for one particle number to the next. It would therefore seem reasonable to assume that 15 particles is sufficiently adequate to model the axial response of these materials when subjected to a uniaxial tensile load.

It is interesting to observe that the predictions of the axysymmetric meshes are different from those obtained for the 3D meshes. For a material reinforced with glass beads, the axysimmetric meshes led to a more compliant response, while for the voided material they led to a stiffer response. This shows that it is not possible to determine if the estimations of the axisymmetric meshes are systematically below or above the estimations of the 3D meshes. In any case, the predictions of these models are within 6% of the predictions given by the 3D meshes with 15 particles. This is a relatively good approximation, considering the degree of simplification of these FE models.

Comparison of the homogenisation models with FE simulations

We have plotted on figure 5.5 the predictions of the secant model for a composite reinforced with glass beads. Figures 5.9 and 5.10 present the com-

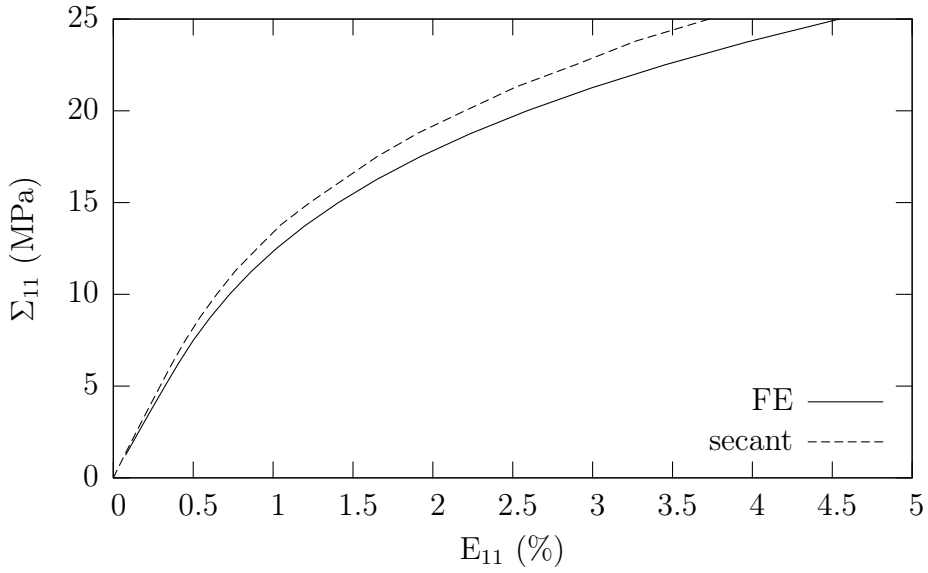


Figure 5.9: Comparison of the secant model and the FE simulations for a volume fraction of 10% of spherical voids

parisons between the homogenisation models and the FE simulations for spherical voids and glass beads with a nonlinearity factor $\zeta = 3$. These figures suggest that our secant and affine models (when available) led to responses which are stiffer than those predicted with FE simulations. For the glass beads composites, the difference in the E_{11}^{25} between the secant and the FE simulations is 14.3% and 19.6% for the nonlinearity factors $\zeta = 1$ and $\zeta = 3$ respectively. For the voided material, the discrepancy is 17.9%. These discrepancies are more important than the confidence intervals we have calculated for $\bar{E}_{11}^{25}$.

For an elasto-plastic matrix, González *et al.* [28] compared the predictions of the classical secant model of Berveiller and Zaoui [5], and the modified secant model of Suquet [95] with FE simulations. For the cases they have simulated, they observed that the classical secant formulation led to a stiffer response than the FE simulations while the modified secant model led to predictions which were in very good agreement with the FE simulations. This suggests that the predictions of our models could be improved by using the history of the second moments of the stress field when calculating the linear viscoelastic comparison material.

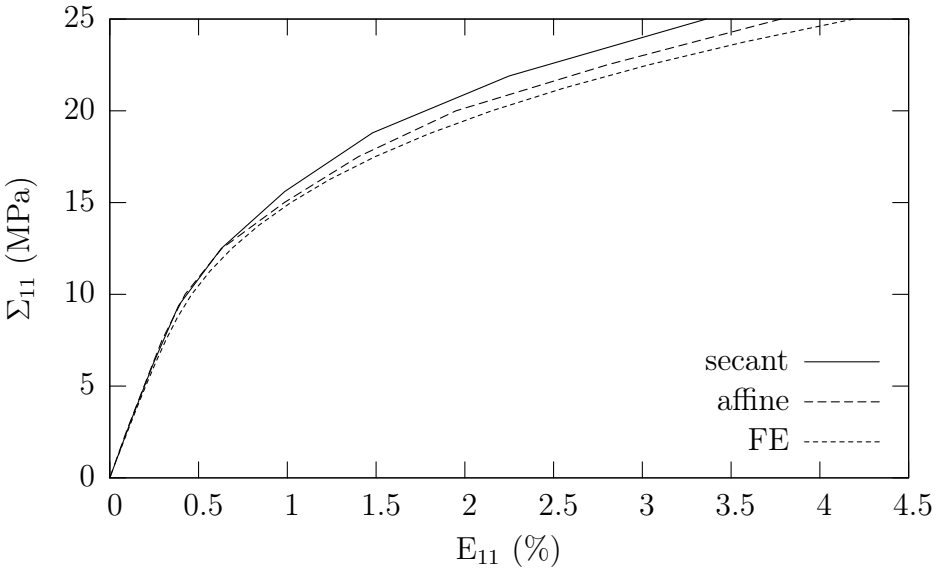


Figure 5.10: Comparison of the affine and secant models with FE simulations for a composite reinforced with glass beads and for a matrix with a nonlinearity factor $\zeta = 3$.

5.3.2 Comparison for the 20% and 30% volume fractions of glass beads/spherical voids

As mentioned previously, we did not have 3D meshes for these volume fractions. We have seen that our axisymmetric meshes are a relatively good approximation of the real material for 10% of glass beads/spherical voids. We assume that this result holds for the higher volume fractions.

Figures 5.11, 5.12 and 5.13 show the comparison between the predictions of the secant model and the axisymmetric FE meshes for volume fractions of 20% and 30% of glass beads/spherical voids. We can observe the same tendencies from these plots as those observed for the 10% volume fractions of glass beads/spherical voids. In all cases, the secant model leads to a stiffer response than the one predicted by the FE simulations. In addition, the discrepancies between the FE and secant model simulations are more important than those observed between the 3D and the axisymmetric meshes for a glass beads volume fraction of 10%. This also strongly suggests that our secant model leads to overstiff estimates than the real material response. It should be noted that the FE simulations were done with finite displacements (i.e. FE accounted for geometrical nonlinearities). We can see that for the spherical voids, the macroscopic strain is quite important and the hypothesis of small strains might not be relevant in that case.

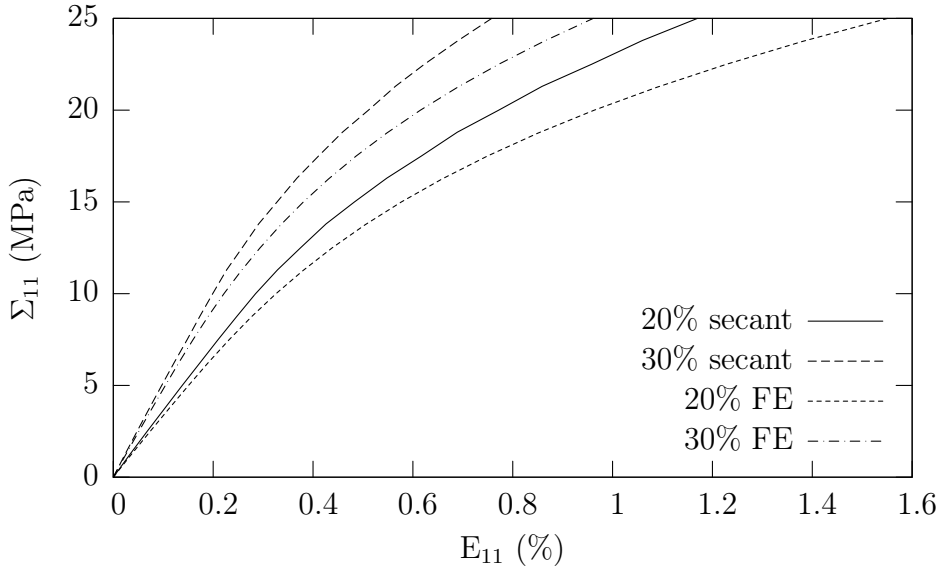


Figure 5.11: Comparison of the predictions of the secant model with FE simulations for 20% and 30% volume fraction of glass beads

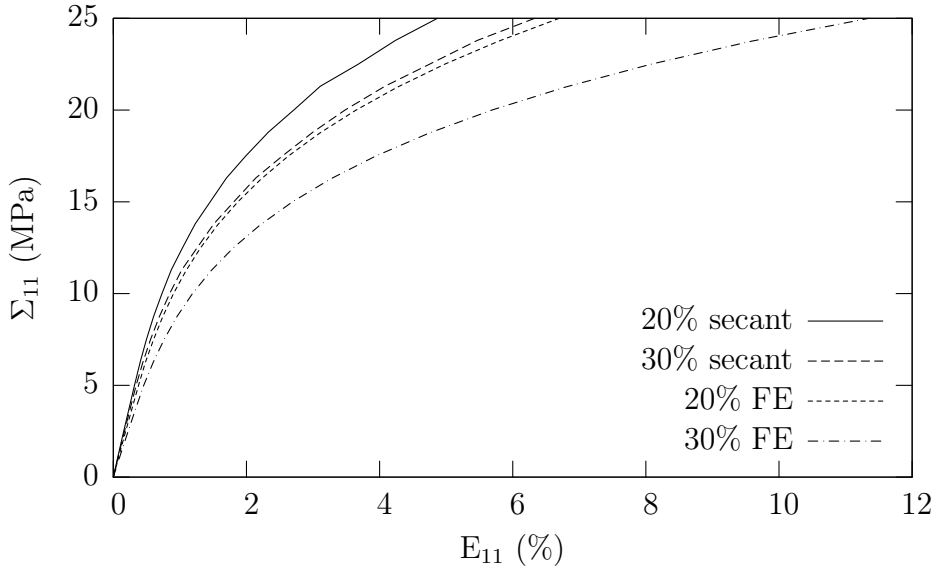


Figure 5.12: Comparison of the predictions of the secant model with FE similuations for 20% and 30% volume fraction spherical voids

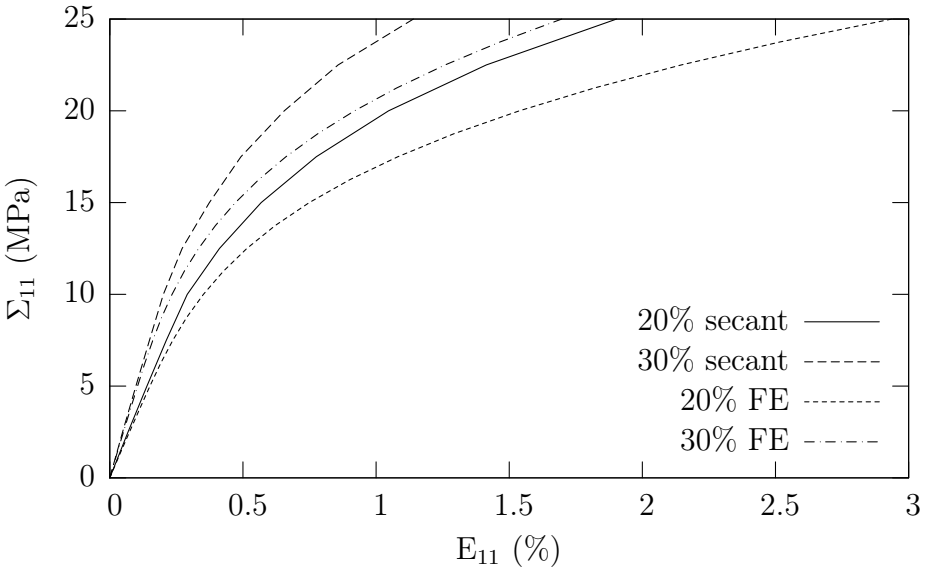


Figure 5.13: Comparison of the predictions of the secant model with FE similuations for 20% and 30% volume fraction glass beads for a nonlinearity factor $\zeta = 3$

5.4 Comparisons with experimental data

We have performed tensile tests at a nominal stress rate of $\frac{20\,\mathrm{MPa}}{5600\,\mathrm{sec}}$ for the bulk polypropylene and the 10% and 20% volume fraction glass beads reinforced composite. The axial strain was measured by a knife edged extensometer. Figure 5.14 reports the results. It can clearly be observed from the figure that the composite material is more compliant than the bulk polypropylene. This can be due to many factors, which might be cumulative:

1. We identified the behaviour law using one dimensional tests. It might be possible that the three dimensional behaviour of the matrix is not modelled well by our constitutive law.

2. We have identified our constitutive law up to 20 MPa, or for $100 \times h = 10$. It is possible that locally, the value of $100 \times h$ is greater than 10 so that the material enters a regime which is outside the validity domain of our constitutive law. This can lead to damage in the matrix (crazing, microcracks, etc.) or plasticity. Such phenomena were not included in our constitutive law.

3. It is possible that the in-situ and bulk polypropylene are not identical materials. The specimens which we had were processed under the same

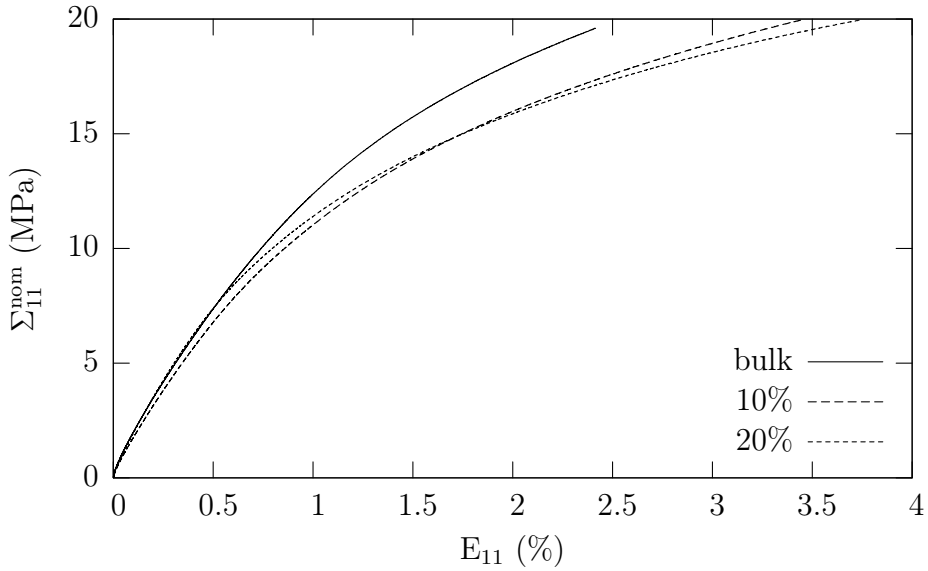


Figure 5.14: Stress/strain curves for a tensile test at a constant nominal stress rate of $\frac{20\,\mathrm{MPa}}{5600\,\mathrm{sec}}$ for the bulk polypropylene as well as the 10% and 20% glass beads reinforced material.

conditions as the bulk polypropylene. It is possible, however, that during the manufacturing process the presence of glass reinforcements modifies the heat transfer and the formation of microstructure (size of the spherulites, crystallinity, etc.). As an indication, we have measured the crystallinity of bulk polypropylene and the composite material with Differential Scanning Calorimetry. It was found that the crystallinity of the two materials were very close (within 2%).

4. There is no adhesion between the glass beads and the matrix, which means that the glass beads do not support any load and the material is approximately voided.

We have conducted in-situ tensile tests in order to investigate these phenomena. The in-situ tensile tests consisted of performing a tensile test inside the chamber of a Scanning Electron Microscope (SEM). We used miniature dog bone specimens where one surface is polished in order to see some glass beads. Then, this surface is coated with gold and the specimen is tested in the SEM chamber.

The displacement of the machine jaws was measured with a LVTD and the force was measured by a load cell attached to the tensile machine. It was not possible to control the applied force with this equipment. We performed the tests at a very low displacement rate. The test was stopped many times

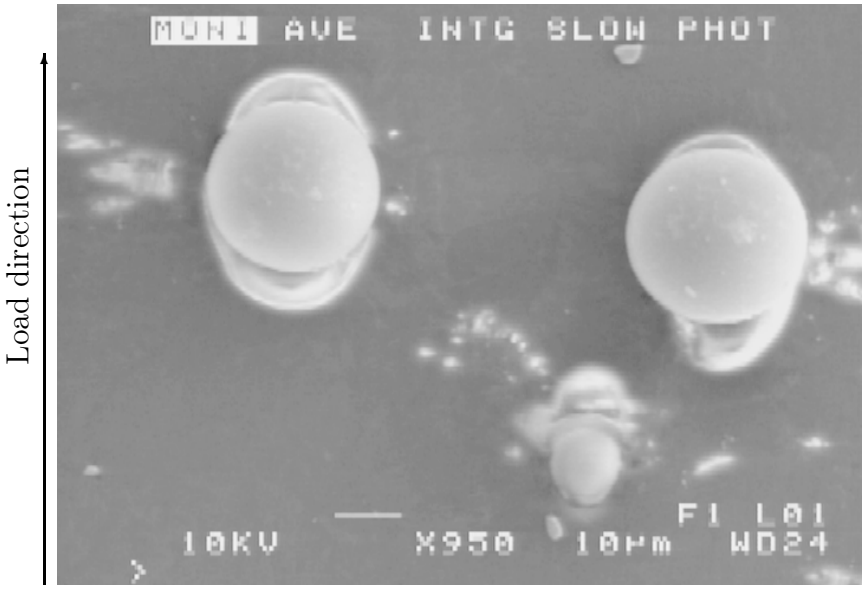


Figure 5.15: Illustration of the particle debonding for a glass bead volume fraction of 10% during an in-situ tensile test. The picture is taken for $\Sigma_{11} \approx 6\,\text{MPa}$.

in order to take photographs. In other words, it was not possible to apply the same load history as in the macroscopic tensile tests. Since the load histories are different, the observations we present here are given as indications of the evolving microstructure. The results we present here were obtained for a composite reinforced with a 10% volume fraction of glass beads.

We have observed that the glass beads debond at a relatively low macroscopic stress level. Figure 5.15 illustrates the cavity growth around a glass bead for $\Sigma_{11} \approx 6\,\text{MPa}$. We have observed that, as the loading increases, the volume of the cavities increases. Figure 5.16 shows the same microstructure at a higher stress $\Sigma_{11} \approx 10$ MPa. We can observe on the top right corner the size of the cavities around the glass beads. In addition, we can also observe some crazing in the middle of the picture. On the bottom left corner, we can see that cracks are initiating between two particles. As the load increases, a network of such cracks appears between neighbouring glass beads. So, we can see that there is damage in the matrix and there is very poor adhesion between the glass beads and the matrix.

We have also performed tensile tests in the SEM chamber on the bulk polypropylene. On these tests, we observed very little crazing for $\Sigma_{11} = 20$ and none for $\Sigma_{11} = 10\,\text{MPa}$. If we assume that the glass beads do not support any load, for $\Sigma_{11} \approx 10\,\text{MPa}$, the average stress field in the matrix is approximately $\Sigma_{11} = 11.1\,\text{MPa}$. Since the material has a low volume fraction

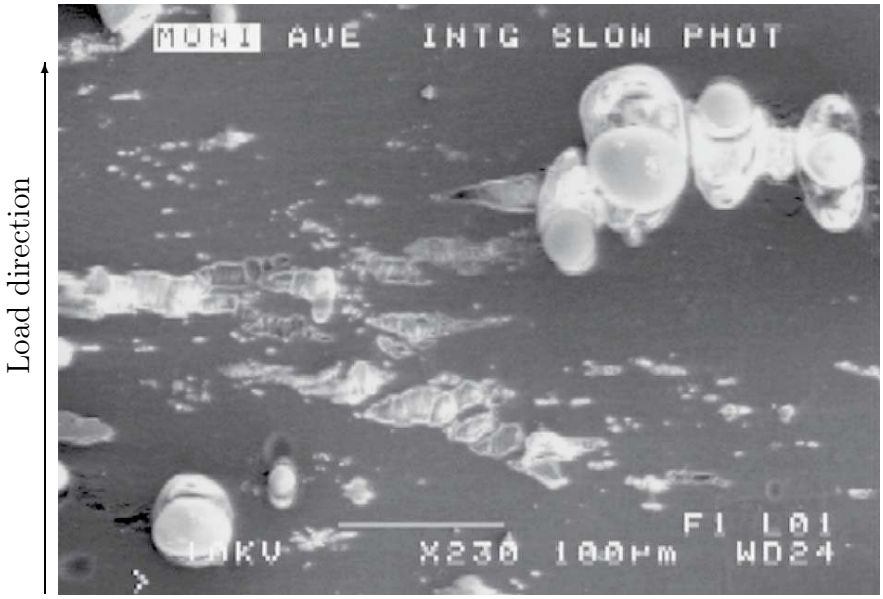


Figure 5.16: Illustration of the particle debonding and crazing for a glass bead volume fraction of 10% during an in-situ tensile test. The picture is taken for $\Sigma_{11} \approx 10\,\text{MPa}$.

of porosities, it is reasonable to assume that the stress field remote from any particle is uniform to a first approximation and should be below the mean value of the stress field in the matrix. This is due to the fact that the porosities induce stress concentrations and since the spatial average of the stress field in the matrix must be equal to the applied stress, the intensity of the stress field must be below the average value somewhere in the matrix. So, to a first approximation we can assume that the stress field remote from the voids is uniaxial tension of approximately $\Sigma_{11} \approx 11.1\,\text{MPa}$. If we assume that the bulk and in-situ polypropylene have the same mechanical properties, it is surprising to observe some crazing in the composite material for this load level. It is possible then that the in-situ and bulk polypropylene used in this study have different mechanical properties.

In addition, as the load increases, the volume fraction of the cavities increases and can take large proportions, as illustrated in figure 5.16. So, if the initial volume fraction of porosities was 10%, for $\Sigma_{11} = 20\,\text{MPa}$ it is possible that this volume fraction of porosities is much greater.

Figure 5.17 plots the theoretical predictions of the secant model and the 3D FE meshes for glass beads and spherical voids as well as the experimental data for the tensile test on the composite material reinforced with 10% of glass beads. The figure shows that even at a low stress level the spherical voids

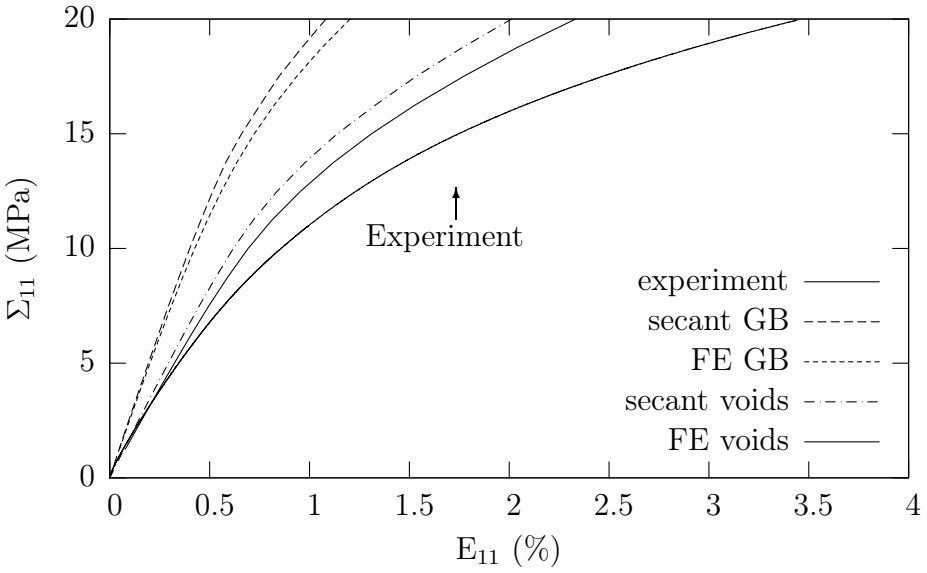


Figure 5.17: Comparison of the predictions of the secant model and the 3D FE mesh for composites with a volume fraction of 10% of glass beads (GB) and voids with experimental data for a tensile test at a uniform stress rate.

models are in good agreement with the experimental data. This suggests that before applying any load, there is poor adhesion between the matrix and the glass beads. However, as the load increases, the theoretical models lead to a stiffer response than the experimental data.

In the development of our theoretical models, we assumed that the matrix remained undamaged and that there was perfect adhesion between the particles and the matrix. We also assumed that the in-situ matrix in the composite had the same mechanical properties as the bulk matrix. The experimental observations we have made suggest that these hypotheses are most likely erroneous. In addition, all the phenomena described previously have the effect of decreasing the mechanical properties of the composite, which is what we have observed. It is not possible at this stage to evaluate the importance of each phenomenon. This would require a more detailed study.

It should be noted that these surface observations are an indication of the deformation process inside the material. The stress field on the surface is different to that inside the material due to edge effects. In addition, it is possible that the polishing process damages the beads/matrix interface and causes the damage initiation.

5.5 Conclusion

This chapter allowed us to first compare the performance of our homogenisation models when compared with a solution which is close to the "exact" response of the composite material and which is based on the same hypotheses. Then, the experimental investigation allowed us to validate the hypotheses on which the theoretical models are based.

The comparison of the predictions of our homogenisation models against finite element simulations suggest that the classical secant and affine models lead to overstiff estimates of the material response. We recall that we have used the average of the stress field to calculate the linear viscoelastic comparison material. In the real material, we can expect that there are stress concentrations around the glass beads/spherical voids. Since the material is nonlinear and the matrix becomes "softer" as the stress increases, such stress concentrations lead to a more important macroscopic strain. Using field fluctuations to compute the linear thermoviscoelastic comparison material should improve the quality of the predictions. However, to our knowledge, it has not been formally shown that the correspondence principle can be invoked to compute the second moment of the stress/strain field history, as was done for the homogenisation of linear viscoelastic materials with the self-consistent scheme (see Laws and McLaughlin [51]). In the opinion of the author, it would be worthwhile to undertake such theoretical work.

Our experimental investigation has shown that the hypotheses on which the homogenisation and the FE models are based are most certainly false. There is very poor adhesion between the glass beads and the matrix, the matrix is damaged as the load increases and locally we expect that the stress field leads to a value of h which lies outside the validity domain of the constitutive law we have identified. The problem of cavity growth in (non)linear viscoelastic materials is a challenging topic. Figure 5.17 shows that the discrepancies between the theoretical models are less important than the discrepancies between the FE simulations and the experimental data. This suggests that there is an urgent need for more realistic three-dimensional behaviour laws for semi-crystalline polymers which incorporates viscoelasticity, plasticity, crazing, etc. It should be noted that refining the constitutive law would not change our linearisation scheme: in essence, the comparison material is a linear viscoelastic material, regardless of the constitutive law it linearises. The literature survey we have done in Chapter One suggests that a considerable amount of work is required before realistic constitutive laws are developed, identified and used intensively so that a certain level of confidence in their predictive capacities can be obtained.

Conclusion

The principal objective of this thesis has been to predict the mechanical behaviour of a thermoplastic composite material by a homogenisation approach. The composite material was a polypropylene reinforced with linear elastic glass beads. The first logical step was to find a proper constitutive law for our thermoplastic matrix. Our literature survey has shown that there are no well established three-dimensional constitutive laws for our material. Consequently, we restricted ourselves to nonlinear viscoelasticity and adapted Schapery's constitutive theory to our specific material. Next, we developed a methodology to identify such constitutive theory. The resulting constitutive law expresses the strains as a functional of the stress history.

Our task was then to build a homogenisation model for this nonlinear viscoelastic composite material. We have used an empirical approach where the nonlinear matrix is linearised by a linear thermo-viscoelastic material. Literature which has been surveyed has shown that there are major practical difficulties associated with the use of behaviour laws expressed as functionals of the load histories. The first one is that it is difficult to define, for example, a tangent or secant linear viscoelastic material, as opposed to non hereditary materials where a tangent or a secant material can be given an unambiguous definition. Using functional analysis and the results of Pouya and Zaoui [78], it was possible to generate classical and modified secant and affine models. In addition, for our constitutive theory, it was possible to give a systematic definition of a secant material. However, the second difficulty is that these theoretical linearised materials are not linear viscoelastic materials. Therefore, the correspondence principle cannot be used to solve the homogenisation problem with such materials. This meant that we had to make an approximation of such materials. It was not possible to generate a systematic approximation of these exact secant or affine materials which ensured that the resulting material would be a linear viscoelastic material meeting the requirements of thermodynamics. Faced with such difficulty, we generated an isotropic approximation of the exact secant and affine materials. This approximation is calculated so that for any case, it leads to a linear

viscoelastic material. We have seen that this approximation is relevant under radial loadings and for the secant model (for our constitutive law). We have also obtained simulations for the secant model for non radial load histories. However, for the affine model, it was not possible to complete the simulations in all cases, which shows the limitations of this approach.

Finally, we have compared the simulations of the secant and affine models (when available) with finite element simulations. It was shown that these models led to overstiff predictions of the composite behaviour. We believe that this is due to the fact that the linearisation was carried around the average stress field. Incorporating field fluctuations should improve the predictions of the models. We have also compared the theoretical results with experimental data. It was observed that there was no adhesion between the glass beads and the matrix and there was significant damage in the matrix. Therefore, the hypotheses on which the homogenisation model relied were wrong. In addition, the discrepancy between the homogenisation models and the finite element simulations were less important than the discrepancies observed between the finite element simulations and the experimental data.

So, in conclusion, we can list as follows the contributions of this work:

1. A general methodology for identifying the parameters and functions of a nonlinear viscoelastic constitutive law. The methodology enforces that the nonlinear constitutive law thus obtained is both physically reasonable as well as thermodynamically admissible. In addition, by comparison to the existing methods, our proposition relies on a more controllable and reliable experimental protocol. The validation of the constitutive law against a complex load history showed good agreement.

2. A general methodology to generate linear viscoelastic comparison materials to carry out the homogenisation of nonlinear viscoelastic materials. The theoretical methodology allows empirical models developed for non hereditary materials to be translated to hereditary materials. The numerical methodology allows a thermodynamically admissible linear viscoelastic material which best matches the theoretical linearisation to be computed.

3. Numerical Laplace–Carson inversion algorithms for the homogenised properties of linear viscoelastic heterogeneous materials. The algorithms lead to linear viscoelastic materials which meet the requirements of thermodynamics. In addition, the precision of the method, when compared to the classical collocation method [84], can be controlled

and led to very accurate inversions. For isotropic materials, such algorithms lead to very good results for a reasonable computational time. In other cases, the algorithm requires more computational power.

It is the opinion of the author that, as far as nonlinear viscoelasticity is concerned, this constitutive law identification methodology should be extended to more complex stress/strain fields than those obtained in a classical tensile test. This would allow behaviour in two or three dimensions to be validated for various stress/strain states. Such experiments could be achieved, for example, by designing tensile specimens of complex geometry. This way, a conventional tensile machine could be used to introduce the loading. On the other hand, this would require using strain field measurement techniques (digital image correlation, grid techniques, etc.). Then, we could imagine, for example, using the finite element technique to determine the material parameters which fit best these strain fields *histories*. In our methodology we have fixed the space aspect of the problem (by using a pure tension strain field) but explored the time or history sensitivity of the constitutive theory. What is suggested for future investigation is that the space sensitivity of the constitutive law is explored in conjunction with its time sensitivity.

We have also seen that a better prediction of the mechanical behaviour of thermoplastics is urgently needed if accurate homogenisation models are sought. In our particular case, we have seen that damage, and possibly plasticity, can initiate in the polymer matrix. Such phenomena should be introduced in a subsequent constitutive law, as was done by Schapery [92] for example, and identified experimentally. Such refined constitutive laws should not pose any theoretical difficulties as far as the homogenisation model is concerned since ultimately we perform a linearisation of the constitutive law, no matter if it is viscoelastic, viscoplastic, etc.

The numerical Laplace–Carson inversion algorithms we have introduced led to very good results for isotropic creep compliances and relaxation moduli. However, for anisotropic materials, we only explored the feasibility of such algorithms. One further step would be to implement more refined minimisation algorithms than those used in this study with anisotropic materials. In addition, we have seen that the other tensors involved in homogenisation are not necessarily in the form of a creep compliance or a relaxation modulus. It would be worthwhile to determine the general shape of such linear viscoelastic tensor functions so that a more suitable approximation function is obtained for these quantities.

The chronology of the events leading to this thesis followed approximately the order in which the chapters are presented. When we initiated the work, it made perfect sense to identify a constitutive theory which represents ade-

quately our polymer matrix and then build or adapt a homogenisation model for this particular constitutive law. We have seen that there are major difficulties with constitutive laws expressed as functionals. On the other hand, the recent work of Lahellec and Suquet [46], dealing also with nonlinear viscoelasticity, shows that predictions of a remarkable accuracy can be obtained when the constitutive law is expressed by potentials and pseudo-potentials. We have also seen that, even if there are restrictions imposed by thermodynamics, there is a wide range of nonlinear viscoelastic constitutive laws that can be generated. In light of our limited experience, it would seem worthwhile to explore the development of constitutive theories which are compatible with variational approaches or linearisation schemes already existing or anticipated. After all, these constitutive theories are an approximation of reality and a constitutive theory compatible with homogenisation techniques could be a relevant approximation. Such approaches would avoid the difficulties we encountered with our functional constitutive theory.

Nevertheless, if the use of functional representations of nonlinear viscoelasticity is to be pursued, considerable modifications will be required for the classical tools used to solve of the homogenisation problem. For example, we have seen that the secant and affine models can be interpreted as ageing linear viscoelastic materials and different correspondence principles could be imagined. Such considerations are left for another time...

Appendix A

Conventions

A.1 Tensor, vectors and scalars

In this thesis, we represent a fourth order tensor by a bold capital Roman letter, for example $\mathbf{A}$. We denote a second order tensor by a Greek bold letter, both lower or upper case, for example $\boldsymbol{\sigma}$, $\boldsymbol{\Sigma}$. We denote a vector by a lower case Roman bold letter, for example, $\boldsymbol{x}$. A scalar is represented by any normal character, for example a, α_n, G, Φ.

A.2 Modified Voigt notation

For the tensors representing mechanical quantities, we have used the modified Voigt notation for the calculations. Bornert *et al.* [9] give a detailed presentation of this notation. We present here the principal results.

The second and fourth order tensors involved in mechanics usually exhibit major and minor symmetries. Such symmetries allow the second order tensors as vectors and fourth order tensors to be written as matrices. So, a second order tensor $\boldsymbol{\alpha}$ can be represented as:

$$[\boldsymbol{\alpha}] = \begin{bmatrix} \alpha_{11} \\ \alpha_{22} \\ \alpha_{33} \\ \sqrt{2}\alpha_{23} \\ \sqrt{2}\alpha_{31} \\ \sqrt{2}\alpha_{12} \end{bmatrix} \tag{A.1}$$

A fourth order tensor $\mathbf{A}$ is represented as:

$$[\mathbf{A}] = \begin{bmatrix} \mathrm{A}_{1111} & \mathrm{A}_{1122} & \mathrm{A}_{1133} & \sqrt{2}\mathrm{A}_{1123} & \sqrt{2}\mathrm{A}_{1131} & \sqrt{2}\mathrm{A}_{1112} \\ \mathrm{A}_{2211} & \mathrm{A}_{2222} & \mathrm{A}_{2233} & \sqrt{2}\mathrm{A}_{2223} & \sqrt{2}\mathrm{A}_{2231} & \sqrt{2}\mathrm{A}_{2212} \\ \mathrm{A}_{3311} & \mathrm{A}_{3322} & \mathrm{A}_{3333} & \sqrt{2}\mathrm{A}_{3323} & \sqrt{2}\mathrm{A}_{3331} & \sqrt{2}\mathrm{A}_{3312} \\ \sqrt{2}\mathrm{A}_{2311} & \sqrt{2}\mathrm{A}_{2322} & \sqrt{2}\mathrm{A}_{2333} & 2\mathrm{A}_{2323} & 2\mathrm{A}_{2331} & 2\mathrm{A}_{2312} \\ \sqrt{2}\mathrm{A}_{3111} & \sqrt{2}\mathrm{A}_{3122} & \sqrt{2}\mathrm{A}_{3133} & 2\mathrm{A}_{3123} & 2\mathrm{A}_{3131} & 2\mathrm{A}_{3112} \\ \sqrt{2}\mathrm{A}_{1211} & \sqrt{2}\mathrm{A}_{1222} & \sqrt{2}\mathrm{A}_{1233} & 2\mathrm{A}_{1223} & 2\mathrm{A}_{1231} & 2\mathrm{A}_{1212} \end{bmatrix} \tag{A.2}$$

This notation allows the doubly contracted product to be computed as a matrix product. For example, $[\mathbf{A} : \boldsymbol{\alpha}] = [\mathbf{A}] \cdot [\boldsymbol{\alpha}]$, $[\mathbf{A} : \mathbf{B}] = [\mathbf{A}] \cdot [\mathbf{B}]$ and $[\boldsymbol{\alpha} : \boldsymbol{\beta}] = [\boldsymbol{\alpha}]^{\mathrm{T}} \cdot [\boldsymbol{\beta}]$ where the centered dot ($\cdot$) represents the classical matrix product. In addition, we denote by $\otimes$ the tensor product which is, for example $\mathbf{A} = \boldsymbol{\alpha} \otimes \boldsymbol{\alpha} = \mathrm{A}_{ijkl} = \alpha_{ij}\alpha_{kl} = \mathrm{A}_{IJ} = \alpha_I \alpha_J$ where I and J are the components of the matrix representation of the tensor.

Of interest are the fourth and second order identity tensors. The fourth order identity tensor $\mathbf{I}$ is given by (for the tensorial symmetries involved in mechanics): $\mathrm{I}_{IJ} = \delta_{IJ}$ where δ is Kronecker's delta. The second order identity tensor $\boldsymbol{i}$ is given by δ_{ij}, which leads to $i_1 = i_2 = i_3 = 1$ and $i_4 = i_5 = i_6 = 0$.

A.3 Short hand notation

It is possible to represent tensors with a high degree of symmetry (isotropy, cubic symmetry and transverse isotropy) in a very convenient notation. For isotropy, we can define:

$$\mathbf{J} = \frac{1}{3}\boldsymbol{i} \otimes \boldsymbol{i} \quad \text{and} \quad \mathbf{K} = \mathbf{I} - \mathbf{J} \tag{A.3}$$

where $\mathbf{J}$ and $\mathbf{K}$ are referred to as spherical/hydrostatic and deviatoric projection tensors. For example, we have that:

$$\mathbf{J} : \boldsymbol{\alpha} = \frac{1}{3}\mathrm{tr}(\boldsymbol{\alpha})\boldsymbol{i} \quad \text{and} \quad \mathbf{K} : \boldsymbol{\alpha} = \mathrm{dev}(\boldsymbol{\alpha}) = \boldsymbol{\alpha} - \frac{1}{3}\mathrm{tr}(\boldsymbol{\alpha})\boldsymbol{i} \tag{A.4}$$

Then, with these tensors, any isotropic tensor can be expressed as: $\mathbf{A} = \alpha\mathbf{J} + \beta\mathbf{K}$, which is simply denoted by $\{\alpha, \beta\}$. Due to the properties of $\mathbf{J}$ and $\mathbf{K}$, simple calculation rules follow from this notation. For example $\mathbf{A} + \mathbf{B} = \{\alpha + \alpha', \beta + \beta'\}$, $\mathbf{A} : \mathbf{B} = \{\alpha\alpha', \beta\beta'\}$ and $\mathbf{A}^{-1} = \{\frac{1}{\alpha}, \frac{1}{\beta}\}$, where $\mathbf{B} = \{\alpha', \beta'\}$. Other short hand notations can be found in [9].

Appendix B

Explicit expressions for the tensors associated with the Mori-Tanaka scheme in thermoelasticity

The results we present here are those given in the thesis of Bourgeois [12]. In the present developments we assume that we have a composite material composed of a matrix phase and R reinforcement phases. The matrix phase is referred to by a subscript 0 while any phase is referred to by the subscript r. We denote by $\mathbf{S}_\mathbf{r}^{\mathrm{E}}$ the Eshelby tensor associated with phase $r \neq 0$. Expressions for Eshelby's tensor can be found in the book by Mura [68]. We denote by $\mathbf{C}$ an elastic stiffness and by $\mathbf{S}$ an elastic compliance.

The overall response of the heterogeneous material is given by:

$$\begin{aligned}\mathbf{E} &= \tilde{\mathbf{S}} : \boldsymbol{\Sigma} + \mathbf{E^0} \\ &= \langle \mathbf{B}(\boldsymbol{x}) : \mathbf{S}(\boldsymbol{x}) \rangle : \boldsymbol{\Sigma} + \left\langle \mathbf{B}^{\mathrm{T}}(\boldsymbol{x}) : \boldsymbol{\varepsilon}^{\mathbf{0}}(\boldsymbol{x}) \right\rangle \\ &= \left(\sum_{r=0}^{R} c_r \mathbf{B_r} : \mathbf{S_r} \right) : \boldsymbol{\Sigma} + \sum_{r=0}^{R} c_r {\mathbf{B_r}}^{\mathrm{T}} : \boldsymbol{\varepsilon}_{\boldsymbol{r}}^{\mathbf{0}}\end{aligned} \tag{B.1}$$

where $\mathbf{E}$ and $\boldsymbol{\Sigma}$ are the overall strain and stress and $\boldsymbol{\varepsilon}_{\boldsymbol{r}}^{\mathbf{0}}$ is the uniform stress free strain induced by the temperature variation. We introduce:

$$\mathbf{T_r} = \left[\mathbf{I} + \mathbf{S}_\mathbf{r}^{\mathrm{E}} : {\mathbf{C_0}}^{-1} : (\mathbf{C_r} - \mathbf{C_0}) \right]^{-1} \tag{B.2}$$

Then we have that the strain localisation tensor is given by:

$$\mathbf{A_r} = \mathbf{T_r} : \left[\sum_{r=0}^{R} c_r \mathbf{T_r} \right]^{-1} \tag{B.3}$$

where c_r is the volume fraction of phase r. The stress concentration tensor is given by:

$$\mathbf{B_r} = \mathbf{C_r} : \mathbf{T_r} : \left[\sum_{r=0}^{R} c_r \mathbf{C_r} : \mathbf{T_r}\right]^{-1} \tag{B.4}$$

and we recall that the homogenised compliance and stiffness are:

$$\tilde{\mathbf{C}} = \sum_{r=0}^{R} c_r \mathbf{A_r} : \mathbf{C_r} \tag{B.5}$$

$$\tilde{\mathbf{S}} = \sum_{r=0}^{R} c_r \mathbf{B_r} : \mathbf{S_r} \tag{B.6}$$

It is of interest is to calculate the average stress induced in phase r by the presence of the $\boldsymbol{\varepsilon}^{\mathbf{0}}_{\boldsymbol{r}}$. We introduce:

$$\mathbf{D_r} = \left[\mathbf{I} - \mathbf{C_0} : (\mathbf{S}^{\mathrm{E}}_{\mathbf{r}} - \mathbf{I}) : (\mathbf{S_r} - \mathbf{S_0})\right]^{-1} : \mathbf{C_0} : (\mathbf{S}^{\mathrm{E}}_{\mathbf{r}} - \mathbf{I}) \tag{B.7}$$

Then the average residual stress is expressed as:

$$\hat{\boldsymbol{\sigma}}_{\boldsymbol{r}} = \mathbf{D_r} : (\boldsymbol{\varepsilon}^{\mathbf{0}}_{\boldsymbol{r}} - \boldsymbol{\varepsilon}^{\mathbf{0}}_{\mathbf{0}}) - \mathbf{B_r} : \left[\sum_{r=0}^{R} c_r \mathbf{D_r} : (\boldsymbol{\varepsilon}^{\mathbf{0}}_{\boldsymbol{r}} - \boldsymbol{\varepsilon}^{\mathbf{0}}_{\mathbf{0}})\right] \tag{B.8}$$

When there is a coupled thermal and mechanical loading, the average stress in a phase r is simply:

$$\bar{\boldsymbol{\sigma}}_{\boldsymbol{r}} = \mathbf{B_r} : \boldsymbol{\Sigma} + \hat{\boldsymbol{\sigma}}_{\boldsymbol{r}} \tag{B.9}$$

List of Figures

2.1 Schematic representation of the uniaxial strain evolution during a creep – recovery test 24
2.2 Values of $\frac{1}{g_3}$ calculed by Lai and Bakker [48] for creep–recovery tests treated individually 26
2.3 Typical stress history used to identify the constitutive law . . 29
2.4 Examples of absolutely increasing g_i as a function of h 32
2.5 Stress histories and material responses used to determine the linear viscoelasticity domain of the polypropylene 36
2.6 Stress history ($\sigma(t)$) and material's response ($\varepsilon_1(t)$ and $\varepsilon_2(t)$) used for the identification of the material's parameters 37
2.7 Experimental data and theoretical predictions of the constitutive law 38
2.8 g_2 as a function of h for our material 38
2.9 Validation of the identified behaviour law for a load history different than the one used for the identification. 39

3.1 Eshelby's ellipsoidal inclusion problem 48
3.2 Homogenised shear compliance of a Maxwell matrix reinforced by Maxwell reinforcements 55
3.3 Schematic representation of the various empirical linearisation procedures 63
3.4 Comparison between a typical Bernstein function and the pseudo creep compliance $\tilde{S}$ 73
3.5 Comparison of the approximate and exact secant conditions for the shear compliance of the linear viscoelastic comparison material 80
3.6 Comparison of the homogenised creep compliances of the linear viscoelastic comparison materials calculated in figure 3.5 . 80
3.7 General solution algorithm 85

4.1 Hydrostatic component of strain associated with the secant condition for the linearised secant and nonlinear material . . . 98
4.2 Hydrostatic component of strain associated with the tangent condition for the linearised affine and nonlinear material . . . 99
4.3 Hydrostatic components of the creep compliances and the stress free strains for the approximate secant and affine models . . . 100
4.4 Comparison between some components of the strain history of the exact and approximate secant materials when subjected to the same non radial stress history 101
4.5 Inverse Laplace-Carson transform of γ^* for long elastic incompressible fibres embedded in an isotropic matrix which obeys a Zener behaviour law 115
4.6 Stress-strain curves obtained for the nonlinear viscoelastic composite material for various volume fractions of glass beads during a tensile test at a constant stress rate of $\frac{25\text{MPa}}{7000\text{s}}$ for the secant model. 118
4.7 Stress-strain curves obtained for the nonlinear viscoelastic composite material for various volume fractions of spherical voids during a tensile test at a constant stress rate of $\frac{25\text{MPa}}{7000\text{s}}$ for the secant model. 119
4.8 Stress-strain curves obtained for the nonlinear viscoelastic composite material for 20% of glass beads during a tensile test at various constant stress rates for the secant model. 120
4.9 Stress-strain curves obtained for the nonlinear viscoelastic composite material for 20% of glass beads for a tensile loading-unloading test at a constant stress rate for the secant model. . 120
4.10 Stress-strain curves obtained for the nonlinear viscoelastic composite material for 10% of glass beads for a tensile test at a constant stress rate for various level of nonlinearity and for the secant and affine models. 121

5.1 Comparison of two different mesh types for a spherical particles in a homogeneous matrix configuration 126
5.2 Evolution of averaged shear modulus of a linear elastic polycrystal as a function of the number of grains simulated in the RVE, for various boundary conditions 128
5.3 Circular base cylinder approximation of a hexagonal base cylinder periodic unit cell [61] 130
5.4 Illustration of the symmetry and periodic boundary conditions on the axisymmetric approximation of an hexagonal periodic unit cell 131

5.5 Comparison of the simulations of the secant model with the finite element simulations for a glass beads reinforced composite (10% volume fraction) under macroscopic tensile loading . . . 138
5.6 Mean value and 95% confidence interval for the macroscopic strain at 25 MPa $\bar{E}_{11}^{25}$ as a function of the number of glass beads (10%) in the 3D meshes for a constant stress rate tensile loading. 139
5.7 Mean value and 95% confidence interval for the macroscopic strain at 25 MPa $\bar{E}_{11}^{25}$ as a function of the number of spherical voids (10%) in the 3D meshes for a constant stress rate tensile loading. 139
5.8 Mean value and 95% confidence interval for the macroscopic strain at 25 MPa $\bar{E}_{11}^{25}$ as a function of the number of glass beads (10%) in the 3D meshes for a constant stress rate tensile loading and a nonlinearity factor $\zeta = 3$. 140
5.9 Comparison of the secant model and the FE simulations for a volume fraction of 10% of spherical voids 141
5.10 Comparison of the affine and secant models with FE simulations for a composite reinforced with glass beads and for a matrix with a nonlinearity factor $\zeta = 3$. 142
5.11 Comparison of the predictions of the secant model with FE simulations for 20% and 30% volume fraction of glass beads . 143
5.12 Comparison of the predictions of the secant model with FE similuations for 20% and 30% volume fraction spherical voids . 143
5.13 Comparison of the predictions of the secant model with FE similuations for 20% and 30% volume fraction glass beads for a nonlinearity factor $\zeta = 3$ 144
5.14 Stress/strain curves for a tensile test at a constant nominal stress rate of $\frac{20\,\mathrm{MPa}}{5600\,\mathrm{sec}}$ for the bulk polypropylene as well as the 10% and 20% glass beads reinforced material. 145
5.15 Illustration of the particle debonding for a glass bead volume fraction of 10% during an in-situ tensile test. The picture is taken for $\Sigma_{11} \approx 6\,\mathrm{MPa}$. 146
5.16 Illustration of the particle debonding and crazing for a glass bead volume fraction of 10% during an in-situ tensile test. The picture is taken for $\Sigma_{11} \approx 10\,\mathrm{MPa}$. 147
5.17 Comparison of the predictions of the secant model and the 3D FE mesh for composites with a volume fraction of 10% of glass beads (GB) and voids with experimental data for a tensile test at a uniform stress rate. 148

List of Tables

2.1 Numerical values of the various material's properties 38

Bibliography

[1] D. H. Allen, J. A. Holmberg, M. Ericson, L. Lans, N. Svensson, and S. Holmberg. Modeling the viscoelastic response of GMT structural components. *Composites Science and Technology*, 61:503 – 515, 2001.

[2] A. Anthoine. Derivation of the in-plane elastic characteristics of masonery through homogenization theory. *International Journal of Solids and Structures*, 32(2):137 – 163, 1995.

[3] S.G. Bardenhagen, M.G. Stout, and G.T. Gray. Three-dimensional, finite deformation, viscoplastic constitutive models for polymeric materials. *Mechanics of Materials*, 25:235 – 253, 1997.

[4] Y. Benveniste. A new approach to the application of Mori-Tanaka's theory in composite materials. *Mechanics of Materials*, 6:147 – 157, 1987.

[5] M. Berveiller and A. Zaoui. An extension of the self-consistent scheme to plastically-flowing polycrystals. *Journal of the Mechanics and Physics of Solids*, 26:325 – 344, 1979.

[6] M.A. Biot. Theory of stress-strain relations in anisotropic viscoelasticity and relaxation phenomena. *Journal of Applied Physics*, 25(1):1385 – 1391, 1954.

[7] H.J. Böhm. A short introduction to basic aspects of continuum micromechanics. CDL-FMD - Report 3, Christian-Doppler-Laboratorium – Funktionsorientiertes Wekstoff-Design, 1998.

[8] M. Bornert, T. Bretheau, and P. Gilormini. *Homogénéisation en mécanique des matériaux 1 - Matériaux aléatoires élastiques et périodiques.* Hermès Science Publications, Paris, 2001.

[9] M. Bornert, T. Bretheau, and P. Gilormini. *Homogénéisation en mécanique des matériaux 2 - Comportements non linéaires et problèmes ouverts.* Hermès Science Publications, Paris, 2001.

[10] N. Bouleau. Interprétation probabiliste de la viscoélasticité linéaire. *Mechanics Research Communications*, 19:16 – 20, 1991.

[11] N. Bouleau. Viscoélasticité et processus de lévy. *Journal of Potential Analysis*, 11(3):289 – 302, 1999.

[12] N. Bourgeois. *Caractérisation et modélisation micromécanique du comportement et de l'endommagement d'un composite à matrice métallique: Al/SiCp*. PhD thesis, Ecole Centrale de Paris, 1994.

[13] R. Brenner. *Influence de la microstructure sur le comportement en fluage thermique d'alliages de zirconium: Analyse expérimentale et mise en oeuvre de méthodes d'homogénéisation*. PhD thesis, Université Paris XIII, 2001.

[14] R. Brenner, O. Castelneau, and P. Gilormini. A modified affine theory for the overall properties of nonlinear composites. *Comptes Rendus de l'Académie des Sciences*, t. 329(Série II b):649 – 654, 2001.

[15] R. Brenner, R. Masson, O. Castelneau, and A. Zaoui. A "quasi-elastic" affine formulation for the homogenised behaviour of nonlinear viscoelastic polycrystals and composites. *European Journal of Mechanics A/Solids*, 21:943 – 960, 2002.

[16] L.C. Brinson and W.S. Lin. Comparison of micromechanics methods for effective properties of multiphase viscoelastic composites. *Composites Structures*, 41:353 – 367, 1998.

[17] C.P. Buckley. Multiaxial nonlinear viscoelasticity in solid polymers. *Polymer Engineering and Science*, 27(2):155 – 164, 1987.

[18] R.M. Christensen. Viscoelastic properties of heterogeneous media. *Journal of the Mechanics and Physics of Solids*, 17:23 – 41, 1969.

[19] R.M. Christensen. Restrictions upon viscoelastic relaxation functions and complex moduli. *Transactions of the Society of Rheology*, 16(4):603 – 614, 1972.

[20] R.M. Christensen. *Mechanics of Composite Materials*. John Wiley and sons, New York, 1980.

[21] C. Cunat. The DNLR approach and relaxation phenomena. Part I – Historical account and DNLR formalism. *Mechanics of Time-Dependent Materials*, 5(1):39 – 65, 2001.

[22] B. Davies and B. Martin. Review - Numerical inversion of the laplace transform: A survey and comparison of methods. *Journal of Computational Physics*, 33:1 – 32, 1979.

[23] K. Derrien, D. Baptiste, D. Guedra-Degeorges, and J. Foulquier. Multiscale modeling of the damaged plastic behaviour and failure of Al/SiCp composites. *International Journal of Plasticity*, 15:667 – 685, 1999.

[24] A. D. Drozdov. A constitutive model for nonlinear viscoelastic media. *International Journal of Solids and Structures*, 34(21):2685 – 2707, 1997.

[25] A.D. Drozdov, A. Al-Mulla, and R.K. Gupta. A constitutive model for the viscoplastic behaviour of rubbery polymers at finite strains. *Acta Mechanica*, 164:139 – 160, 2003.

[26] G.G. Duffy. On the numerical inversion of laplace transforms: Comparison of three new methods on characteristic problems from applications. *ACM Transactions of Mathematical Software*, 19(3):333 – 359, 1993.

[27] J.D. Eshelby. The determination of the elastic field of an ellipsoidal inclusion and related ploblems. *Proceedings of the Royal Society of London, Serie A.*, 241:376 – 396, 1957.

[28] C. González, J. Segurado, and J. LLorca. Numerical simulation of elasto-plastic deformation of composites: evolution of stress microfields and implications for homogenization models. *Journal of the Mechanics and Physics of Solids*, 52:1573 – 1593, 2004.

[29] A.E. Green and R.S. Rivlin. The mechanics of nonlinear materials with memory. *Archive for Rational Mechanics and Analysis*, 1:1 – 21, 1957.

[30] A.E. Green and R.S. Rivlin. The mechanics of nonlinear materials with memory - Part III. *Archive for Rational Mechanics and Analysis*, 4:387 – 404, 1960.

[31] A.E. Green, R.S. Rivlin, and A.J.S. Spencer. The mechanics of nonlinear materials with memory - Part II. *Archive for Rational Mechanics and Analysis*, 3:82 – 90, 1959.

[32] A. Gusev. Representative volume element size for elastic composites: A numerical study. *Journal of the Mechanics and Physics of Solids*, 45(9):1449 – 1459, 1997.

[33] R.M. Haj-Ali and A. H. Muliana. Numerical finite element formulation of the Schapery non-linear viscoelastic material model. *International Journal of Numerical Methods in Engineering*, 59:25 – 45, 2004.

[34] Z. Hashin. Viscoelastic fibre reinforced materials. *AIAA Journal*, 4(8):1411 – 1417, 1966.

[35] Z. Hashin. Complex moduli of viscoelastic composites - II Fibre reinforced materials. *International Journal of Solids and Structures*, 6:797 – 807, 1970.

[36] M. Henriksen. Nonlinear viscoelastic stress analysis - A finite element approach. *Computers and Structures*, 18(1):133 – 139, 1984.

[37] Hibbitt, Karlsson, and Sorensen Inc. *ABAQUS/Standard User's Manual, version 6.2*. HKS, 2001.

[38] R. Hill. Continuum micro-mechanics of elastoplastic polycrystals. *Journal of the Mechanics and Physics of Solids*, 13:89 – 101, 1965.

[39] T. Horgan and M. D. Gilchrist. The creation of three-dimensional finite element models for simulating head impact biomechanics. *International Journal of Crashworthiness*, 8(4):353 – 366, 2003.

[40] G. Hu. A method of plasticity for general aligned spheroidal voids or fibre-reinforced composites. *International Journal of Plasticity*, 12(4):439 – 449, 1996.

[41] Y. Hu, F. Ellyin, and Z. Xia. An experimental investigation of normal and shear stress interaction of an epoxy resin and model predictions. *Polymer Engineering and Science*, 41(11):2047 – 2060, 2001.

[42] C. Huet. Application of variational concepts to size effects in elastic heterogeneous bodies. *Journal of the Mechanics and Physics of Solids*, 38:813 – 841, 1990.

[43] T. Kanit, S. Forest, I. Galliet, V. Mounoury, and D. Jeulin. Determination of the size of the representative volume element for random composites : Statistical and numerical approach. *International Journal of Solids and Structures*, 40:3647 – 3679, 2003.

[44] W. G. Knauss. Perspectives in experimental solid mechanics. *International Journal of Solids and Structures*, 37:251 – 266, 2000.

[45] W. G. Knauss and I. Emri. Volume change and the nonlinearly thermo-viscoelastic constitution of polymers. *Polymer Engineering and Science*, 27(1):86 – 100, 1987.

[46] N. Lahellec and P. Suquet. Composites non linéaires à deux potentiels: Estimations affine et du second-ordre. In M. Potier-Ferry, M. Bonnet, and A. Bignonnet, editors, *6ème Colloque National en Calcul des Structures. Tome 3.*, pages 49–56. CSMA, 2003.

[47] N. Lahellec and P. Suquet. Nonlinear composites: A linearization procedure, exact to second-order in contrast and for which the strain-energy and the affine formulations coincide. *Comptes Rendus de l'Académie des Sciences:*, t. 332(Série II b):693–700, 2004.

[48] J. Lai and A. Bakker. An integral constitutive equation for nonlinear plasto-viscoelastic behavior of High-Density polyethylene. *Polymer Engineering and Science*, 35(17):1339 – 1347, 1995.

[49] J. Lai and A. Bakker. 3-D Schapery representation for non-linear viscoelasticity and finite element implementation. *Computational Mechanics*, 18:182 – 191, 1996.

[50] R. S. Lakes and W.J. Drugan. Dramatically stiffer elastic composite materials due to negative stiffness phase ? *Journal of the Mechanics and Physics of solids*, 50:979 – 1009, 2002.

[51] N. Laws and R. McLaughlin. Self-consistent estimates for the viscoelastic creep compliances of composite materials. *Proceedings of the Royal Society of London A*, 359:251 – 273, 1978.

[52] S. Lee and W.G. Knauss. A note of the determination of relaxation and creep data from ramp tests. *Mechanics of Time-Dependent Materials*, 4:1 – 7, 2000.

[53] J Lemaitre and J.-L. Chaboche. *Mécanique des milieux solides*. Dunod, 1998.

[54] J. Li and G.J. Weng. A secant-viscosity approach to the time-dependent creep of an elastic-viscoplastic composite. *Journal of the Mechanics and Physics of Solids*, 45(7):1069 – 1083, 1997.

[55] F.J. Lockett. Creep and stress-relaxation experiments for non-linear materials. *International Journal of Engineering Science*, 3:59 – 75, 1965.

[56] Y. C. Lou and R.A. Schapery. Viscoelastic characterisation of a nonlinear fibre-reinforced plastic. *Journal of Composite Materials*, 5:208 – 234, 1971.

[57] R. Masson. *Estimations non linéaires du comportement global de matériaux hétérogènes en formulation affine : Application aux alliages de zirconium*. PhD thesis, Ecole Polytechnique - Paris, 1998.

[58] R. Masson, M. Bornert, P. Suquet, and A. Zaoui. An affine formulation for the prediction of the effective properties of nonlinear composites and polycrystals. *Journal of the Mechanics and Physics of Solids*, 48:1203 – 1227, 2000.

[59] R. Masson and A. Zaoui. Self-consistent estimates for the rate dependent elastoplastic behaviour of polycrystalline materials. *Journal of the Mechanics and Physics of Solids*, 47:1543 – 1568, 1999.

[60] W. Mendenhall and T. Sincich. *Statistics for engineering and the sciences*. Prentice Hall, United States of America, 1994.

[61] J. C. Michel, H. Moulinec, and P. Suquet. Effective properties of composite materials with periodic microstructure: A computational approach. *Computer Methods in Applied Mechanics and Engineering*, 172:109 – 143, 1999.

[62] L. Jr. Mishnaevsky. Three-dimensional numerical testing of microstructures of particle reiforced composites. *Acta Materialia*, 52(14):4177 – 4188, 2004.

[63] L. Jr. Mishnaevsky and S. Schmauder. Continuum mesomechanical finite element modeling in materials development: A state-of-the-art review. *Applied Mechanics Reviews*, 54(1):1203 – 1227, 2001.

[64] R. Mohan and D.F. Adams. Nonlinear creep-recovery response of a polymer matrix and its composites. *Experimental Mechanics*, 25(4):262 – 271, 1985.

[65] A. Molinari, G. Canova, and S. Ahzi. A self-consistent approach of the large deformation polycrystal viscoplasticity. *Acta Metallurgica*, 35(12):2983 – 2994, 1987.

[66] T. Mori and K. Tanaka. Average stress in matrix and average elastic energy of materials with misfitting inclusions. *Acta Metallurgica et Materialia*, 21:597 – 629, 1973.

[67] H. Moulinec and P. Suquet. A numerical method for computing the overall response of nonlinear composites with complex microstructure. *Computer Methods in Applied Mechanics and Engineering*, 157:69 – 94, 1998.

[68] T. Mura. *Micromechanics of defects in solids, Second revised edition.* Martinus Nijhoff Publishers, 1987.

[69] G.C. Papanicolaou, S.P. Zaoutsos, and A.H. Cardon. Further development of a data reduction method for the nonlinear viscoelastic characterization of FRP. *Composites part A: Applied science and manufacturing*, 30:839 – 848, 1999.

[70] A. Paquin. *Modélisation micromécanique du comportement élastoviscoplastique des matériaux hétérogènes.* PhD thesis, Université de Metz, 1998.

[71] A. Paquin, H. Sabar, and M. Berveiller. Integral formulation and self-consistent modelling of elastoviscoplastic behaviour of heterogeneous materials. *Archives of Applied Mechanics*, 69(1):14 – 35, 1999.

[72] A. Pasricha, M. E. Tuttle, and A. F. Emry. Time-dependent response of IM7/5260 composites subjected to cyclic thermo-mechanical loading. *Composites Science and Technology*, 56:55 – 62, 1996.

[73] P. Ponte Castañeda. The effective mechanical properties of nonlinear isotropic composites. *Journal of the Mechanics and Physics of Solids*, 39:45 – 71, 1991.

[74] P. Ponte Castañeda. Exact second-order estimates for the effective mechanical properties of nonlinear composite materials. *Journal of the Mechanics and Physics of Solids*, 44:827 – 862, 1996.

[75] P. Ponte Castañeda. Second-order homogenization estimates for nonlinear composites incorporating field fluctuations: I – Theory. *Journal of the Mechanics and Physics of Solids*, 50:737 – 757, 2002.

[76] P. Ponte Castañeda and P. Suquet. Nonlinear composites. *Advances in Applied Mechanics*, 34:172 – 302, 1998.

[77] P. Ponte Castañeda and J.R. Willis. Variational second-order estimates for nonlinear composites. *Proceedings of the Royal Society of London A.*, 455:1799 – 1811, 1999.

[78] A. Pouya and A. Zaoui. Linéarisation et homogénéisation en viscoélasticité. *Comptes Rendus de l'Académie des Sciences*, t. 326(Série II b):365 – 370, 1999.

[79] W. H. Press, S. A. Teukolsky, W. T. Vetterling, and B. P. Flannery. *Numerical Recipes in Fortran 77 : The art of scientific Computing*. Cambridge University Press, United States of America, 2001.

[80] Y.P. Qui and G.J. Weng. A theory of plasticity for porous materials and particle-reinforced composites. *Journal of Applied Mechanics*, 59:261 – 268, 1992.

[81] Y. Rougier. *Etude du comportement sous irradiation: Modélisation Micromécanique de l'élastoviscoplasticité*. PhD thesis, Ecole Polytechnique - Paris, 1994.

[82] Y. Rougier, C. Stolz, and A. Zaoui. Représentation spectrale en viscoélasticité linéaire des matériaux hétérogènes. *Comptes Rendus de l'Académie des Sciences*, t. 316(Série II b):1517 – 1522, 1993.

[83] Y. Rougier, C. Stolz, and A. Zaoui. Self-consisten modelling of elastoviscoplastic polycrystals. *Comptes Rendus de l'Académie des Sciences*, t. 318(Série II b):145 – 151, 1994.

[84] R. A. Schapery. Approximate methods of transform inversion for viscoelastic stress analysis. *Proceedings of the 4th US National Congress on Applied Mechanics*, 2:1075 – 1085, 1962.

[85] R. A. Schapery. Application of thermodynamics to thermomechanical, fracture, and berefringent phenomena in viscoelastic media. *Journal of Applied Physiscs*, 35(5):1451 – 1465, 1964.

[86] R. A. Schapery. Stress analysis of viscoelastic composite materials. *Journal of Composite Materials*, 1:228 – 267, 1967.

[87] R. A. Schapery. On a thermodynamic constitutive theory and its application to various nonlinear materials. *Proceedings of IUTAM Symposium*, pages 259 – 285, 1968.

[88] R. A. Schapery. *Further development of a thermodynamic constitutive theory : stress formulation*. Purdue University, School of Aeronautics, 1969.

[89] R. A. Schapery. On the characterization of nonlinear viscoelastic materials. *Polymer Engineering and Science*, 9(4):295 – 310, 1969.

[90] R. A. Schapery. Viscoelastic behavior and analysis of composite materials. In G.P. Sendeckyj, editor, *Mechanics of composite materials*, pages 85 – 168. Academic Press, New York, 1974.

[91] R. A. Schapery. Nonlinear viscoelastic and viscoplastic constitutive equations based on thermodynamics. *Mechanics of Time-Dependent Materials*, 1:209 – 240, 1997.

[92] R. A. Schapery. Nonlinear viscoelastic and viscoplastic constitutive equations with growing damage. *International Journal of Fracture*, 97:33 – 66, 1999.

[93] R. A. Schapery. Nonlinear viscoelastic solids. *International Journal of Solids and Structures*, 37:359 – 366, 2000.

[94] J. Segurado and J. LLorca. A numerical approximation to the elastic properties of sphere-reinforced composites. *Journal of the Mechanics and Physics of Solids*, 50:2107 – 2121, 2002.

[95] P. Suquet. Overall properties of nonlinear composites: a modified secant moduli theory and its link with Ponte Castañeda's nonlinear variational procedure. *Comptes Rendus de l'Académie des Sciences*, 320(Série II b):563 – 571, 1995.

[96] O. Taiwo, J. Schultz, and V. Krebs. A comparison of two methods for the numerical inversion of the laplace transforms. *Computers and Chemical Engineering*, 19(3):303 – 308, 1995.

[97] C.L. III Tucker and E. Lian. Stiffness predictions for unidirectional short-fiber composites : Review and evaluation. *Composites Science and Technology*, 59:655 – 671, 1999.

[98] P.A. Turner and C.N. Tomé. Self-consistent modeling of visco-elastic polycrystals: application to irradiation creep and growth. *Journal of the Mechanics and Physis of Solids*, 41(7):1191 – 1211, 1993.

[99] Y.M. Wang and G.J. Weng. The influence of inclusion shape on the overall viscoelastic behavior of composites. *Journal of Applied Mechanics*, 59:510 – 518, 1992.

[100] G. J. Weng. Self-consistent determination of time dependent behavior of metals. *Journal of Applied Mechanics*, 48:41 – 46, 1981.

[101] S.P. Zaoutsos, G.C. Papanicolaou, and A.H. Cardon. On the nonlinear viscoelastic characterization of polymer matrix composites. *Composites Science and Technology*, 58(6):883 – 889, 1998.

[102] L.J. Zapas and J.M. Crissman. Creep and recovery behaviour of ultra-high molecular weight polyethylene in the region of small uniaxial deformations. *Polymer*, 25:57 – 62, 1983.

[103] L. Zhang, L.J Ernst, and H.R. Brouwer. A study of nonlinear viscoelasticity of an unsaturated polyester resin. Part 1. Uniaxial model. *Mechanics of Materials*, 26:141 – 166, 1997.

[104] L. Zhang, L.J Ernst, and H.R. Brouwer. A study of nonlinear viscoelasticity of an unsaturated polyester resin. Part 2. 3D Model. *Mechanics of Materials*, 26:167 – 195, 1997.

MODÉLISATION DU COMPORTEMENT MÉCANIQUE DE MATÉRIAUX COMPOSITES VISCOÉLASTIQUES NON LINÉAIRES PAR UNE APPROCHE D'HOMOGÉNÉISATION

RESUME: L'objectif principal de ce travail de thèse est d'établir un modèle, s'appuyant sur l'homogénéisation, permettant la prédiction du comportement mécanique de matériaux composites viscoélastiques non linéaires. L'approche est appliquée à un polypropylène renforcé de billes de verre réparties aléatoirement. La première partie du document est consacrée à l'écriture et l'identification d'une loi de comportement viscoélastique non linéaire pouvant être appliquée au polypropylène. La deuxième partie traite de l'établissement du modèle ainsi que de son implémentation numérique. Le modèle d'homogénéisation est développé au troisième chapitre. L'approche proposée permet de transposer certains modèles existants pour des matériaux ne dépendant pas de l'histoire de chargement à des comportements viscoélastiques non linéaires. La méthodologie permet donc de ramener le problème viscoélastique non linéaire à un problème viscoélastique linéaire à histoire de déformations libres. Ce nouveau problème est résolu à l'aide du principe de correspondance viscoélastique linéaire et des transformées de Laplace-Carson. Le quatrième chapitre est dédié à l'implémentation numérique du modèle. On insiste notamment sur le fait que le matériau viscoélastique linéaire de comparaison rencontre les exigences de la thermodynamique des milieux continus. De plus, nous proposons un algorithme conduisant à une inversion précise des transformées de Laplace-Carson. Finalement, la dernière partie de la thèse est consacrée à la validation des modèles proposés. Des modèles éléments finis de la microstructure et l'implémentation de la loi de comportement viscoélastique non linéaire sont réalisés au chapitre cinq. Ce chapitre présente aussi la comparaison, pour des chargements de traction, entre les simulations issues du modèle d'homogénéisation, des éléments finis ainsi que des résultats expérimentaux.

Mots-clés: *homogénéisation, matériaux composites, viscoélasticité non linéaire*

MECHANICAL BEHAVIOUR MODELLING OF NONLINEAR VISCOELASTIC COMPOSITE MATERIALS BY A HOMOGENISATION APPROACH

ABSTRACT: The main objective of this thesis is to develop a model, based on homogenisation, for predicting the mechanical response of nonlinear viscoelastic composites. The model is applied to a glass beads reinforced polypropylene in which the beads are randomly distributed. The initial part of the thesis is concerned with the development of a three dimensional nonlinear viscoelastic constitutive law that can be applied to this polypropylene composite. The second stage of the thesis deals with the development and identification of the homogenisation model while this theoretical model is presented in Chapter Three. This approach allows material models, for which the response does not depend on the load history, to be applied to nonlinear viscoelastic materials. The approach involves transforming the initial nonlinear viscoelastic problem into one which is linear viscoelastic with a history of stress-free deformations. This problem is solved with the linear viscoelastic correspondence principle and Laplace-Carson transforms. Chapter Four deals with the numerical implementation of such a model. The implementation is achieved in such a way that the comparison materials, which represent the new linear viscoelastic problem, satisfy all thermodynamic requirements. Moreover, a new algorithm has been developed to numerically invert the Laplace-Carson transforms with good accuracy. The final part of the thesis validates the theoretical model through means of finite element models of typical microstructures and the numerical implementation of the nonlinear viscoelastic constitutive law. Comparisons are also presented between the predictions of the homogenisation model, the finite element simulations and results of experimental tensile tests.

Keywords: *homogenisation, composite materials, nonlinear viscoelasticity*

